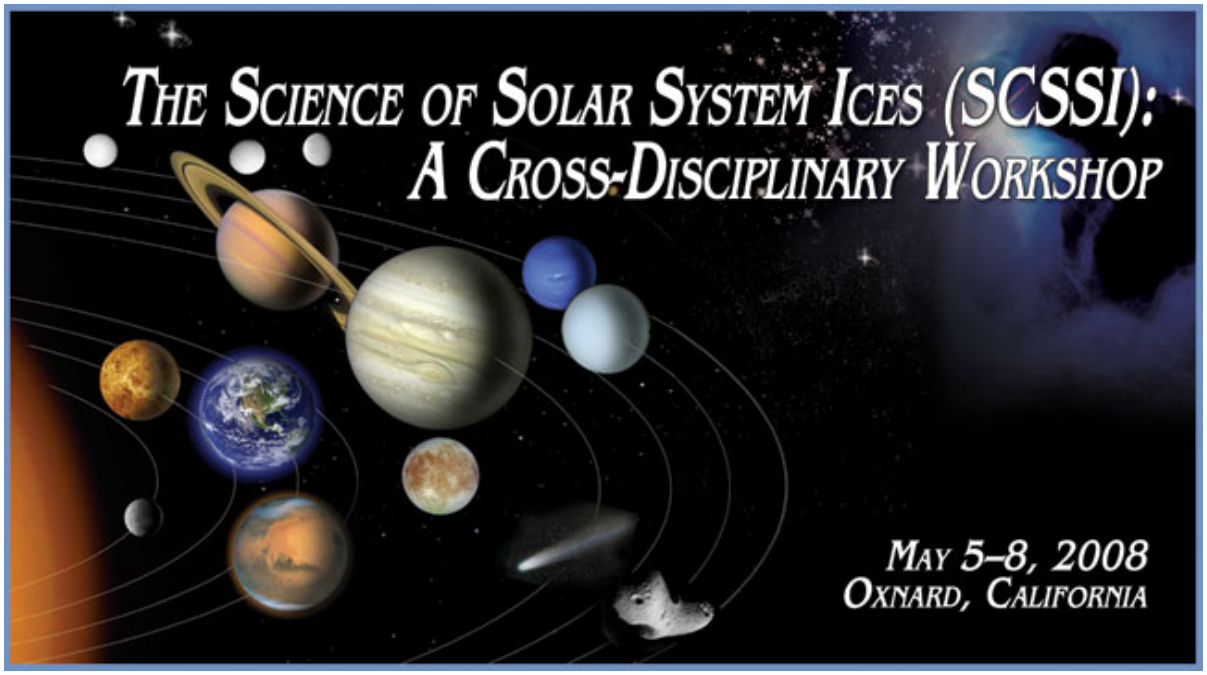

PROGRAM AND ABSTRACTS

LUNAR AND PLANETARY INSTITUTE

LPI Contribution No. 1406

THE SCIENCE OF SOLAR SYSTEM ICES (SCSSI): A CROSS-DISCIPLINARY WORKSHOP

May 5–8, 2008
Oxnard, California

SPONSORS

Lunar and Planetary Institute
Jet Propulsion Laboratory, California Institute of Technology
National Aeronautics and Space Administration
Ball Aerospace and Technologies Corporation
Kurt J. Lesker Company
Thermo Fisher Scientific
Varian Incorporated

ORGANIZERS

Murthy Gudipati, *Jet Propulsion Laboratory*
Bob Pappalardo, *Jet Propulsion Laboratory*
Julie Castillo, *Jet Propulsion Laboratory*

INTERNATIONAL ORGANIZING COMMITTEE

Lou Allamandola, *NASA Ames Research Center*
Akiva Bar-Nun, *Tel Aviv University*
Pat Beauchamp, *Jet Propulsion Laboratory*
Mike Brown, *California Institute of Technology*
Bonnie Buratti, *Jet Propulsion Laboratory*
Razvan Caracas, *Universität Bayreuth*
Julie Castillo, *Jet Propulsion Laboratory*
Brad Dalton, *Jet Propulsion Laboratory*
Paul Duval, *Centre National de la Recherche Scientifique*
Andrew Fortes, *University College London*
Murthy Gudipati, *Jet Propulsion Laboratory*
Bob Johnson, *University of Virginia*
Isik Kanik, *Jet Propulsion Laboratory*
Jeff Kargel, *University of Arizona*
Steve Kirby, *U.S. Geological Survey*
Lonne Lane, *Jet Propulsion Laboratory*
Bob Pappalardo, *Jet Propulsion Laboratory*
Olga Prieto-Ballesteros, *Instituto Nacional de Tecnica Aerospacial*
Giovanni Strazzulla, *INAF Catania Astrophysical Observatory*

Lunar and Planetary Institute 3600 Bay Area Boulevard Houston TX 77058-1113

LPI Contribution No. 1406

Compiled in 2008 by
LUNAR AND PLANETARY INSTITUTE

Abstracts in this volume may be cited as

Author A. B. (2008) Title of abstract. In The *Science of Solar System Ices (ScSSI): A Cross-Disciplinary Workshop,* p. XX. LPI Contribution No. 1406, Lunar and Planetary Institute, Houston.

This volume is distributed by

ORDER DEPARTMENT
Lunar and Planetary Institute
3600 Bay Area Boulevard
Houston TX 77058-1113, USA
Phone: 281-486-2172
Fax: 281-486-2186
E-mail: order@lpi.usra.edu

Mail orders requestors will be invoiced for the cost of shipping and handling.

ISSN No. 0161-5297

PREFACE

This volume contains abstracts that have been accepted for presentation at The Science of Solar System Ices (ScSSI): A Cross-Disciplinary Workshop, May 5–8, 2008, Oxnard, California.

Administration and publications support for this meeting were provided by the staff of the Publications and Program Services Department at the Lunar and Planetary Institute.

CONTENTS

Program 1

The Solar Ice-Salt Sheets
P. Aftabi 13

Ice In and On Cometary Nuclei
M. F. A'Hearn 15

Impact Experiments on Snow: The Effect of Sintering on the Formation of Crater
M. Arakawa 16

Radiation Effects in Water Ice in the Solar System
R. A. Baragiola, M. Famá, M. J. Loeffler, U. Raut, J. Shi, and B. D. Teolis 18

The Mechanism of Gas Trapping and Release in Solar System Water Ice
A. Bar-Nun, D. Laufer, G. Notesco, and Y. Pat-EL 19

Mobile Lid Convection Beneath Enceladus' South Polar Terrain
A. C. Barr 20

Large-Grained Dust in the Coma of 174P/Echeclus
J. M. Bauer, Y-J. Choi, P. R. Weissman, J. A. Stansberry, Y. R. Fernández, H. G. Roe, B. J. Buratti, and H-I. Sung 22

The Locations of Mini-Outbursts on the Nucleus of 9P/Tempel 1: The Case for Cometary Cryo-Volcanism
M. J. S. Belton 23

The Structure of Planetary Ices: How Laboratory Diffraction Methods can Support Astronomical Observations
D. F. Blake 24

Ice Properties Relevant to Radar Sounding of Icy Moons: Lessons from Earth Applied to Europa
D. D. Blankenship and D. A. Young 25

Thermoelastic Properties of Mirabilite and Meridianite Determined Using Experimental and Computational Techniques
H. E. A. Brand, A. D. Fortes, K. S. Knight, I. G. Wood, and L. Vočadlo 27

Ephemeral Ices Associated With the Martian South Polar Recession
A. J. Brown 29

Observations of Irradiation Chemistry in the Kuiper Belt
M. E. Brown 31

Ion Irradiation and the Colors of TNOs
R. Brunetto and G. Strazzulla 32

Photometry of Icy Satellites
B. J. Buratti 33

Nitrogen in Intermediate Pressure Range
R. Caracas and R. J. Hemley 34

Stability of H_2O Ice Polymorphs at High Pressure
R. Caracas and R. J. Hemley 35

Experimental Studies of the Sputtering of Mixed Ices: Europa's Surface Composition and Detection of Trace Species by Surface Sputtering
R. W. Carlson and K. P. Hand 36

Ice Response to Cyclic Loading for Low Stresses and Frequencies — Application to Icy Satellites
J. C. Castillo-Rogez, F. Zhong, M. Barmatz, M. Choukroun, H. Engelhardt, and C. Sotin 37

Sublimation Kinetics of CO_2 Ice on the Surface of Mars
V. F. Chevrier, L. A. Roe, K. F. White, K. Bryson, and D. G. Blackburn 39

New Growth Setup of Planetary Clathrate Hydrates Analogs for Physical Properties Measurements
M. Choukroun, M. Barmatz, and C. Sotin 41

Spectroscopic Remote Sensing of Solar System Ices: Laboratory Research and Applications for Mapping Compounds
R. N. Clark 43

Laboratory Investigations Relevant to the Erosion of Ice on Titan
G. C. Collins, L. S. Sklar, B. Zygielbaum, and P. Polito 44

The Synthesis and Direct Detection of O-Atoms in Water Ice
P. D. Cooper, M. H. Moore, and R. L. Hudson 46

Near-Infrared Laboratory Spectroscopy of CH_4/N_2 Ice Mixtures: Implications for Icy Dwarf Planets
D. M. Cornelison, S. C. Tegler, W. Grundy, and M. Abernathy 48

Electrical Properties of Amorphous and Crystalline Ices
J. P. Cowin and M. J. Iedema 49

Cryogenic Infrared Reflectance Spectroscopy of Acetylene and Cyanoacetylene
J. M. Curchin, R. N. Clark, C. Shaffer, R. J. McMahon, and T. M. Hoefen 50

A Summary of Mission-Critical Cryogenic Laboratory Spectral Measurements for Determination of Icy Satellite Surface Composition from Orbital Spacecraft Observations
J. B. Dalton III 51

Signatures of Ices in Spectra of TNOs and Centaurs: Peculiarities and Problems in Their Interpretation
C. de Bergh, M. A. Barucci, F. Merlin, and A. Guilbert 53

Numerical Simulations of the Deformation of Icy-Satellite Lithospheres
A. J. Dombard 54

The Viscous Behavior of Glacier Ice; Effect of Impurities, Grain Size and Liquid Phase
P. Duval and M. Montagnat 56

Reflectances of Icy Solar System Bodies as $\lambda > 2.5$ μm
J. P. Emery, C. M. Dalle Ore, D. P. Cruikshank, Y. R. Fernandez, D. E. Trilling, and J. A. Stansberry 57

Sputtering of Ice by Low Energy Ions: Effects on Ice Grains and Icy Satellites in Saturn's Inner Magnetosphere
M. Famá, R. E. Johnson, J. Shi, R. A. Baragiola, M. Liu, E. C. Sittler Jr., and H. T. Smith 59

Ab Initio Approaches to the Physical Properties of Planetary Ices
A. D. Fortes, J. P. Brodholt, and L. Vocadlo 61

The Rheological Properties of Ice — Where We Are and Wither We Are Tending
D. L. Goldsby 63

A Thermodynamic Model for Water and High-Pressure Ices: A Way to Investigate the Stability of Water Compounds in Planetological Conditions
O. Grasset, M. Choukroun, G. Tobie, and C. Sotin 65

Electrical Properties of Saline Ices, Salt Hydrates, and Ice-Silicate Mixtures: Applications to Solar-System Exploration
R. E. Grimm and D. E. Stillman 67

Experimental Rheology of Planetary Ices: Triaxial Deformation Tests on $MgSO_4 \bullet 11H_2O$ (Meridianiite)
P. M. Grindrod, A. D. Fortes, I. G. Wood, P. R. Sammonds, D. P. Dobson, C. A. Middleton, and L. Vocadlo 69

Amorphous Versus Crystalline Water Ice
W. M. Grundy 71

Understanding the Radiation Chemistry of Pure and Impure Solar System Water Ices — The Role of Laboratory Studies
M. S. Gudipati 73

Near-Infrared Spectra of TNOs: First Results of the New ESO-Large Program and Implications
A. Guilbert, M. A. Barucci, A. Alvarez-Candal, F. Merlin, A. Coradini, C. de Bergh, C. Dumas, and O. R. Hainaut 75

Laboratory Experiments Toward Distinguishing Abiotic Radiolytic Chemistry from Radiolytically Modified Biological Material on Icy Worlds
K. P. Hand and R. W. Carlson 76

Flavors of Amorphous Surface Ice on Europa: A Broader Peak on the TrailingSide
G. B. Hansen 78

Titan's Surface Composition: Constraints from Laboratory Experiments and Cassini/VIMS Observations
P. Hayne, T. B. McCord, C. Sotin, M. Barmatz, J.-Ph. Combe, and G. B. Hansen 80

UV Spectra of the Icy Moons of Jupiter and Saturn
A. R. Hendrix 82

Volatiles, but not Ices, from Icy Satellites to Our Moon
C. A. Hibbitts 84

Sublimation, Deposition and UV Photochemistry of Enceladus Plume Mixtures
R. Hodyss, P. V. Johnson, J. D. Goguen, J. V. Stern, C. F. Campbell, and I. Kanik 86

Thermal and Surface Implications of Ices in the Outer Solar System
D. Jewitt 88

Radiation Effects on the Icy Satellites and Ring Particles
R. E. Johnson, A. R. Hendrix, and T. A. Cassidy 89

Thermal Conductivity and Melting Properties of Materials Forming Icy Satellite Crusts
J. S. Kargel 90

Investigating Gas Clathrate Hydrate Structure, Formation and Decomposition
C. A. Koh, K. C. Hester, J. Lachance, H. Ohno, L. J. Rovetto, T. A. Strobel, S. F. Dec, and E. D. Sloan 92

H_2O Ice Formation from the Reaction of Cold H Atoms with Solid O_2 at 10 K
A. Kouchi, N. Miyauchi, H. Hidaka, T. Chigai, A. Nagaoka, and N. Watanabe 93

Thermo-Physical Modeling of Cometary Nuclei with Moving Ice Boundaries
E. Kuehrt, N. Gortsas, and U. Motschmann 94

Interpreting the Basal and Prism Native Surface of Ice I_h with Sum Frequency Generation Spectroscopy
I. Li, H. Groenzin, and M. J. Shultz 95

Spectral Measurements for Improved Studies of the Role of Water Ice in Solar System Formation and Evolution
C. M. Lisse, C. A. Hibbitts, and R. E. Peale 97

Irradiation of Ammonia-Water Mixtures at 20 K and 120 K: A Complement to Previous Laboratory Studies.
M. J. Loeffler, U. Raut, and R. A. Baragiola 99

Influence of NaCl on Ice VI and Ice VII Phase Relations and Properties: Implications for Solar System Ices
C. E. Manning and I. Daniel 101

Optical Properties of Amorphous and Crystalline H_2O-Ices
R. M. Mastrapa, M. P. Bernstein, S. A. Sandford, T. L. Roush, D. P. Cruikshank, and C. M. Dalle Ore 103

Binding Energies of CH_4 and H_2O-Ice Systems
R. M. Mastrapa, T. Cadarette, and S. A. Sandford 105

Ice Rheology and the Evolution of Icy Satellites: Ten Propositions
W. B. McKinnon 107

Activity of Comets at Large Heliocentric Distances
K. J. Meech, O. R. Hainaut, S. C. Lowry, J. Pittichova, A. Bar-Nun, G. Notesco, and D. Laufer 108

The Rheology of Ice-Rock Mixtures — Application to the Satellites of the Outer Solar System
C. A. Middleton, P. R. Sammonds, P. M. Grindrod, A. D. Fortes, and L. Vočadlo 110

Liquid Interfacial Water in Planetary Ices: Presence and Consequences
D. Möhlmann 112

Formation of Complex Molecules in Planetary Ice Analogs
M. H. Moore and R. L. Hudson 113

Tidal-Convective Equilibrium at Europa and Enceladus
W. B. Moore 114

Tidal Dissipation and Faulting
F. Nimmo 116

Ultraviolet Spectra of Icy Satellites
K. S. Noll 118

Combining New Laboratory Studies and Cassini CIRS Data Analysis to Determine the Composition and Texture of Saturn's Rings
C. R. Nugent, M. S. Gudipati, L. J. Spilker, S. G. Edgington, S. H. Pilorz, C. Leyrat, N. Altobelli, and C. T. Russell 120

The Roles of Energy Localization and Buried Interfaces in Electronic Sputtering of Pristine and Mixed Low-Temperature Ices
T. M. Orlando and G. A. Greives 122

Mixed Guest Clathrates and Planetary Dynamics: Continuous vs. Episodic Events
J. P. Osegovic and M. D. Max 123

Radar Properties of the Icy Satellites of Jupiter and Saturn
S. J. Ostro 125

Surface Weathering in Different Radiation Environments
C. Paranicas, D. G. Mitchell, S. M. Krimigis, D. C. Hamilton, E. Roussos, N. Krupp, G. H. Jones, R. E. Johnson, J. F. Cooper, and T. P. Armstrong 127

Impact Gardening on Europa
C. B. Phillips and L. Grossman 128

Differentiation of Gas-rich Briny Cryomagmas in Icy Satellites. Simulation Experiments at High Pressure
O. Prieto-Ballesteros, J. S. Kargel, J. A. Rodriguez-Manfredi, F. Gómez, and V. García-Baonza 130

Compaction of Porous Solar System Ices by Ion Irradiation: Laboratory Studies
U. Raut, M. Fama, M. J. Loeffler, and R. A. Baragiola 132

Volatile Ices in the Kuiper Belt: Theory and Observations
E. L. Schaller and M. E. Brown 134

Cratering on Ice — A Cold Laboratory
P. M. Schenk 135

Friction and Fracture of Ice I_h
E. M. Schulson 136

On Frozen Volatiles in Comets, and Their Sublimation
R. Schulz 137

Laboratory Measurements on Water Ice Under Simulated Mars' Conditions
D. W. G. Sears, V. Chevrier, R. Ulrich, L. A. Roe, and K. Bryson 139

Ion Irradiation Induced Electrostatic Charging Effects on Solar Ices
J. Shi, M. Fama, and R. A. Baragiola 141

Abrasion Susceptibility of Ultra-Cold Water Ice: Preliminary Measurements of Abrasion Rate, Tensile Strength and Elastic Modulus
L. S. Sklar, P. Polito, B. Zygielbaum, and G. C. Collins 143

Convection in Icy Satellites: Models and Constraints from Laboratory Experiments
C. Sotin, G. Tobie, and P. Duval 145

Ganymede's Impact Crater Melkart: An Example for a Combination of High-Resolution Spectral and Geological Analyses in the Outer Solar System
K. Stephan, R. Wagner, C. A. Hibbitts, G. B. Hansen, and R. Jaumann 147

What We Want to Know About Ices for Understanding the Structure and Evolution of Ice-rich Bodies
D. J. Stevenson 149

Advances in Modeling Collisions on Icy Bodies
S. T. Stewart and L. E. Senft 150

Ion Implantation and the Origin of Minor Species on the Surfaces of Icy Satellites
G. Strazzulla 152

Phase Properties and Types of Earth's Water Ice and Space Ices
P. K. Thakur and A. Velumurgan 153

Ammonia Hydrate on Tethys' Trailing Hemisphere
A. J. Verbiscer, D. E. Peterson, M. F. Skrutskie, M. Cushing, P. Helfenstein, M. J. Nelson, J. D. Smith, and J. C. Wilson 155

Erosional Processes on Callisto: Galileo SSI Results, Open Questions, and Requirements for New Camera Data
R. J. Wagner and G. Neukum 157

Gas Inclusion, Adsorption, and Diffusion in Ices
C. Wittig, H. Reisler, S. Malyk, and O. Rebolledo 159

CO_2 in Comets Beyond 5 AU
L. M. Woodney, Y. R. Fernandez, and C. M. Lisse 160

Near Infrared Spectroscopy on the Outburst Comet 17P/Holmes
B. Yang, D. Jewitt, and S. J. Bus 161

Experimental Study on the Rheology of Ice-Silica Beads Mixtures: Effects of Silica Content and Temperature on the Flow Law
M. Yasui and M. Arakawa 162

Spatial Distribution and Evolution of Nitrogen Ice on Triton
L. A. Young, W. M. Grundy, J. A. Stansberry, and M. W. Buie 164

New Technique for Measuring Thermal Conductivity of Icy Materials Under Pressure
F. Zhong, M. Barmatz, and H. Englehardt 166

PROGRAM

Monday, May 5, 2008

VOLATILES IN ICES
8:00 a.m. Ballroom

Chairs: **R. A. Baragiola**
M. H. Moore

8:00 a.m. Introduction

8:15 a.m. Thakur P. K. * Velumurgan A.
Phase Properties and Types of Earth's Water Ice and Space Ices **[#9014]**

8:30 a.m. Bar-Nun A. * Laufer D. Notesco G. Pat-EL Y.
The Mechanism of Gas Trapping and Release in Solar System Water Ice **[#9036]**

9:00 a.m. Hodyss R. * Johnson P. V. Goguen J. D. Stern J. V. Campbell C. F. Kanik I.
Sublimation, Deposition and UV Photochemistry of Enceladus Plume Mixtures **[#9065]**

9:15 a.m. Wittig C. * Reisler H. Malyk S. Rebolledo O.
Gas Inclusion, Adsorption, and Diffusion in Ices **[#9096]**

9:45 a.m. BREAK

10:15 a.m. A'Hearn M. F. *
Ice In and On Cometary Nuclei **[#9031]**

10:45 a.m. Belton M. J. S. *
The Locations of Mini-Outbursts on the Nucleus of 9P/Tempel 1: The Case for Cometary Cryo-Volcanism **[#9003]**

11:00 a.m. Meech K. J. * Hainaut O. R. Lowry S. C. Pittichova J. Bar-Nun A. Notesco G. Laufer D.
Activity of Comets at Large Heliocentric Distances **[#9047]**

11:15 a.m. Schulz R. *
On Frozen Volatiles in Comets, and Their Sublimation **[#9004]**

11:30 a.m. Young L. A. * Grundy W. M. Stansberry J. A. Buie M. W.
Spatial Distribution and Evolution of Nitrogen Ice on Triton **[#9048]**

11:45 a.m. Jewitt D. *
Thermal and Surface Implications of Ices in the Outer Solar System **[#9045]**

12:15 p.m. LUNCH

* *Denotes speaker*

1:45 p.m. Brown A. J. *
Ephemeral Ices Associated with the Martian South Polar Recession **[#9046]**

2:00 p.m. Sears D. W. G. Chevrier V. Ulrich R. Roe L. A. Bryson K. *
Laboratory Measurements on Water Ice Under Simulated Mars' Conditions **[#9063]**

2:15 p.m. Chevrier V. F. * Roe L. A. White K. F. Bryson K. Blackburn D. G.
Sublimation Kinetics of CO_2 Ice on the Surface of Mars **[#9067]**

2:30 p.m. GENERAL DISCUSSION
Discussion Chair: M. J. S. Belton
Co-Chairs: M. P. Bernstein and P. V. Johnson

Monday, May 5, 2008 *(continued)*

ICE SURFACE CHEMISTRY
2:45 p.m. Ballroom

Chairs: **W. M. Grundy**
M. S. Gudipati

2:45 p.m. Johnson R. E. * Hendrix A. R. Cassidy T. A.
Radiation Effects on the Icy Satellites and Ring Particles **[#9084]**

3:15 p.m. Baragiola R. A. * Famá M. Loeffler M. J. Raut U. Shi J. Teolis B. D.
Radiation Effects in Water Ice in the Solar System **[#9043]**

3:45 p.m. BREAK

4:15 p.m. Gudipati M. S. *
Understanding the Radiation Chemistry of Pure and Impure Solar System Water Ices — The Role of Laboratory Studies **[#9038]**

4:30 p.m. Brown M. E. *
Observations of Irradiation Chemistry in the Kuiper Belt **[#9058]**

5:00 p.m. Orlando T. M. * Greives G. A.
The Roles of Energy Localization and Buried Interfaces in Electronic Sputtering of Pristine and Mixed Low-Temperature Ices **[#9081]**

5:30 p.m. Cowin J. P. *
Electrical Properties of Amorphous and Crystalline Ices **[#9098]**

5:45 p.m. Moore M. H. * Hudson R. L.
Formation of Complex Molecules in Planetary Ice Analogs **[#9078]**

Tuesday, May 6, 2008

ICE SURFACE CHEMISTRY (*continued*)
8:00 a.m. Ballroom

Chairs: **W. M. Grundy**
M. S. Gudipati

8:00 a.m. Strazzulla G. *
Ion Implantation and the Origin of Minor Species on the Surfaces of Icy Satellites **[#9008]**

8:30 a.m. Möhlmann D. *
Liquid Interfacial Water in Planetary Ices: Presence and Consequences **[#9099]**

8:45 a.m. Carlson R. W. * Hand K. P.
Experimental Studies of the Sputtering of Mixed Ices: Europa's Surface Composition and Detection of Trace Species by Surface Sputtering **[#9033]**

9:15 a.m. Hand K. P. * Carlson R. W.
Laboratory Experiments Toward Distinguishing Abiotic Radiolytic Chemistry from Radiolytically Modified Biological Material on Icy World **[#9082]**

9:30 a.m. GENERAL DISCUSSION
Discussion Chair: M. E. Brown
Co-Chairs: J. B. Dalton and K. P. Hand

9:45 a.m. BREAK

Tuesday, May 6, 2008 *(continued)*

SURFACE ICE CHARACTERIZATION
10:15 a.m. Ballroom

Chairs: **D. L. Goldsby**
T. A. Cassidy

10:15 a.m. Buratti B. J. *
Photometry of Icy Satellites **[#9039]**

10:45 a.m. Hayne P. * McCord T. B. Sotin C. Barmatz M. Combe J.-Ph. Hansen G. B.
Titan's Surface Composition: Constraints from Laboratory Experiments and Cassini/VIMS Observations **[#9093]**

11:00 a.m. Clark R. N. *
Spectroscopic Remote Sensing of Solar System Ices: Laboratory Research and Applications for Mapping Compounds **[#9066]**

11:30 a.m. Noll K. S. *
Ultraviolet Spectra of Icy Satellites **[#9085]**

12:00 p.m. Hendrix A. R. *
UV Spectra of the Icy Moons of Jupiter and Saturn **[#9088]**

12:15 p.m. LUNCH

1:45 p.m. Ostro S. J. *
Radar Properties of the Icy Satellites of Jupiter and Saturn **[#9041]**

2:15 p.m. POSTER SUMMARY I

2:30 p.m. Blake D. F. *
The Structure of Planetary Ices: How Laboratory Diffraction Methods can Support Astronomical Observations **[#9026]**

3:00 p.m. Grundy W. M. *
Amorphous Versus Crystalline Water Ice **[#9072]**

3:30 p.m. Mastrapa R. M. * Bernstein M. P. Sandford S. A. Roush T. L.
Cruikshank D. P. Dalle Ore C. M.
Optical Properties of Amorphous and Crystalline H_2O-Ices **[#9010]**

3:45 p.m. Hibbitts C. A. *
Volatiles, but not Ices, from Icy Satellites to Our Moon **[#9077]**

4:00 p.m. GENERAL DISCUSSION
Discussion Chair: B. J. Buratti
Co-Chairs: P. Hayne and A. R. Hendrix

Tuesday, May 6, 2008 *(continued)*

POSTER SESSION
4:15 – 6:30 p.m.

Chairs: **J. D. Dalton**
M. S. Gudipati

Bauer J. M. Choi Y-J. Weissman P. R. Stansberry J. A. Fernández Y. R. Roe H. G. Buratti B. J. Sung H-I.
Large-Grained Dust in the Coma of 174P/Echeclus **[#9061]**

Brand H. E. A. Fortes A. D. Knight K. S. Wood I. G. Vočadlo L.
Thermoelastic Properties of Mirabilite and Meridianite Determined Using Experimental and Computational Techniques **[#9021]**

Brunetto R. Strazzulla G.
Ion Irradiation and the Colors of TNOs **[#9009]**

Caracas R. Hemley R. J.
Nitrogen in Intermediate Pressure Range **[#9090]**

Choukroun M. Barmatz M. Sotin C.
New Growth Setup of Planetary Clathrate Hydrates Analogs for Physical Properties Measurements **[#9080]**

Cooper P. D. Moore M. H. Hudson R. L.
The Synthesis and Direct Detection of O-Atoms in Water Ice **[#9069]**

Cornelison D. M. Tegler S. C. Grundy W. Abernathy M.
Near-Infrared Laboratory Spectroscopy of CH_4/N_2 Ice Mixtures:Implications for Icy Dwarf Planets **[#9089]**

Curchin J. M. Clark R. N. Shaffer C. McMahon R. J. Hoefen T. M.
Cryogenic Infrared Reflectance Spectroscopy of Acetylene and Cyanoacetylene **[#9074]**

Dalton J. B. III
A Summary of Mission-Critical Cryogenic Laboratory Spectral Measurements for Determination of Icy Satellite Surface Composition from Orbital Spacecraft Observations **[#9028]**

de Bergh C. Barucci M. A. Merlin F. Guilbert A.
Signatures of Ices in Spectra of TNOs and Centaurs: Peculiarities and Problems in their Interpretation **[#9022]**

Duval P. Montagnat M.
The Viscous Behavior of Glacier Ice; Effect of Impurities, Grain Size and Liquid Phase **[#9013]**

Emery J. P. Dalle Ore C. M. Cruikshank D. P. Fernandez Y. R. Trilling D. E. Stansberry J. A.
Reflectances of Icy Solar System Bodies as $\lambda > 2.5$ μm **[#9068]**

Famá M. Johnson R. E. Shi J. Baragiola R. A. Liu M. Sittler E. C. Jr. Smith H. T.
Sputtering of Ice by Low Energy Ions: Effects on Ice Grains and Icy Satellites in Saturn's Inner Magnetosphere **[#9001]**

Grindrod P. M. Fortes A. D. Wood I. G. Sammonds P. R. Dobson D. P. Middleton C. A. Vocadlo L.
Experimental Rheology of Planetary Ices: Triaxial Deformation Tests on $MgSO_4 \cdot 11H_2O$ (Meridianiite) **[#9030]**

Guilbert A. Barucci M. A. Alvarez-Candal A. Merlin F. Coradini A. DeBergh C. Dumas C. Hainaut O. R.
Near-Infrared Spectra of TNOs: First Results of the New ESO-Large Program and Implications **[#9018]**

Hansen G. B.
Flavors of Amorphous Surface Ice on Europa: A Broader Peak on the TrailingSide **[#9070]**

Kimmel G. A. Petrik N. G.
Electron-stimulated Production of O_2 in Amorphous Solid Water: Precursor Transport Through the Hydrogen Bonding Network **[#9097]**

Kouchi A. Miyauchi N. Hidaka H. Chigai T. Nagaoka A. Watanabe N.
H_2O Ice Formation from the Reaction of Cold H Atoms with Solid O_2 at 10 K **[#9006]**

Li I. Groenzin H. Shultz M. J.
Interpreting the Basal and Prism Native Surface of Ice I_h with Sum Frequency Generation Spectroscopy **[#9005]**

Lisse C. M. Hibbitts C. A. Peale R. E.
Spectral Measurements for Improved Studies of the Role of Water Ice in Solar System Formation and Evolution **[#9059]**

Loeffler M. J. Raut U. Baragiola R. A.
Irradiation of Ammonia-Water Mixtures at 20 K and 120 K: A Complement to Previous Laboratory Studies **[#9051]**

Mastrapa R. M. Cadarette T. Sandford S. A.
Binding Energies of CH_4 and H_2O-Ice Systems **[#9012]**

Middleton C. A. Sammonds P. R. Grindrod P. M. Fortes A. D. Vočadlo L.
The Rheology of Ice-Rock Mixtures — Application to the Satellites of the Outer Solar System **[#9032]**

Nugent C. R. Gudipati M. S. Spilker L. J. Edgington S. G. Pilorz S. H. Leyrat C. Altobelli N. Russell C. T.
Combining New Laboratory Studies and Cassini CIRS Data Analysis to Determine the Composition and Texture of Saturn's Rings **[#9071]**

Osegovic J. P. Max M. D.
Mixed Guest Clathrates and Planetary Dynamics: Continuous vs. Episodic Events **[#9037]**

Phillips C. B. Grossman L.
Impact Gardening on Europa **[#9035]**

Prieto-Ballesteros O. Kargel J. S. Rodriguez-Manfredi J. A. Gómez F. García-Baonza V.
Differentiation of Gas-rich Briny Cryomagmas in Icy Satellites. Simulation Experiments at High Pressure **[#9050]**

Raut U. Fama M. Loeffler M. J. Baragiola R. A.
Compaction of Porous Solar System Ices by Ion Irradiation: Laboratory Studies **[#9049]**

Schaller E. L. Brown M. E.
Volatile Ices in the Kuiper Belt: Theory and Observations **[#9056]**

Shi J. Fama M. Baragiola R. A.
Ion Irradiation Induced Electrostatic Charging Effects on Solar Ices **[#9054]**

Sklar L. S. Polito P. Zygielbaum B. Collins G. C.
Abrasion Susceptibility of Ultra-Cold Water Ice: Preliminary Measurements of Abrasion Rate, Tensile Strength and Elastic Modulus **[#9076]**

Stephan K. Wagner R. Hibbitts C. A. Hansen G. B. Jaumann R.
Ganymede's Impact Crater Melkart: An Example for a Combination of High-Resolution Spectral and Geological Analyses in the Outer Solar System **[#9060]**

Stewart S. T. Senft L. E.
Advances in Modeling Collisions on Icy Bodies **[#9052]**

Verbiscer A. J. Peterson D. E. Skrutskie M. F. Cushing M. Helfenstein P. Nelson M. J.
Smith J. D. Wilson J. C.
Ammonia Hydrate on Tethys' Trailing Hemisphere **[#9064]**

Woodney L. M. Fernandez Y. R. Lisse C. M.
CO_2 in Comets Beyond 5 AU **[#9024]**

Yang B. Jewitt D. Bus S. J.
Near Infrared Spectroscopy on the Outburst Comet 17P/Holmes **[#9017]**

Yasui M. Arakawa M.
Experimental Study on the Rheology of Ice-Silica Beads Mixtures: Effects of Silica Content and Temperature on the Flow Law **[#9016]**

Zhong F. Barmatz M. Englehardt H.
New Technique for Measuring Thermal Conductivity of Icy Materials Under Pressure **[#9083]**

Wednesday, May 7, 2008

GEOPHYSICS OF ICES I
8:00 a.m. Ballroom

Chair: **C. Sotin**
W. B. Moore

8:00 a.m. Grimm R. E. * Stillman D. E.
Electrical Properties of Saline Ices, Salt Hydrates, and Ice-Silicate Mixtures: Applications to Solar-System Exploration **[#9062]**

8:15 a.m. Blankenship D. D. * Young D. A.
Ice Properties Relevant to Radar Sounding of Icy Moons: Lessons from Earth Applied to Europa **[#9075]**

8:45 a.m. McKinnon W. B. *
Ice Rheology and the Evolution of Icy Satellites: Ten Propositions **[#9079]**

9:15 a.m. POSTER SUMMARY II

9:45 a.m. BREAK

10:15 a.m. Koh C. A. * Hester K. C. Lachance J. Ohno H. Rovetto L. J. Strobel T. A. Dec S. F. Sloan E. D.
Investigating Gas Clathrate Hydrate Structure, Formation and Decomposition **[#9025]**

10:45 a.m. Grasset O. * Choukroun M. Tobie G. Sotin C.
A Thermodynamic Model for Water and High-Pressure Ices: A Way to Investigate the Stability of Water Compounds in Planetological Conditions **[#9027]**

11:00 a.m. Fortes A. D. * Brodholt J. P. Vocadlo L.
Ab Initio Approaches to the Physical Properties of Planetary Ices **[#9029]**

11:15 a.m. Kargel J. S. *
Thermal Conductivity and Melting Properties of Materials Forming Icy Satellite Crusts **[#9057]**

11:45 a.m. Schulson E. M. *
Friction and Fracture of Ice Ih **[#9040]**

12:15 p.m. GENERAL DISCUSSION
Discussion Chair: W. B. McKinnon
Co-Chairs: J. C. Castillo-Rogez and A. D. Fortes

12:30 p.m. LUNCH

Wednesday, May 7, 2008

GEOPHYSICS OF ICES II
2:00 p.m. Ballroom

Chairs: **W. B. McKinnon**
J. C. Castillo-Rogez

2:00 p.m. POSTER SUMMARY III

2:30 p.m. Goldsby D. L. *
The Rheological Properties of Ice — Where We Are and Whither We Are Tending **[#9087]**

3:00 p.m. Sotin C. * Tobie G. Duval P.
Convection in Icy Satellites: Models and Constraints from Laboratory Experiments **[#9092]**

3:30 p.m. Moore W. B. *
Tidal-Convective Equilibrium at Europa and Enceladus **[#9086]**

4:00 p.m. Kargel J. S. * Schenk P. Mithcell K. L. Lopes R. Pappalardo R. T.
Zolotov M. Castillo-Rogez J. C.
Cryovolcanism: Where Does Geology, Cosmochemistry, and Physical Chemisty Converge?

Wednesday, May 7, 2008
POSTER SESSION *(continued)*
4:15 – 6:30 p.m.

The abstracts included in the poster session are listed on pages 6 through 8 in this program booklet.

Thursday, May 8, 2008

GEOPHYSICS OF ICES II (*continued*)
8:00 a.m. Ballroom

Chairs: **J. C. Castillo-Rogez**
W. B. McKinnon

8:00 a.m. Nimmo F. *
Tidal Dissipation and Faulting **[#9007]**

8:30 a.m. Castillo-Rogez J. C. * Zhong F. Barmatz M. Choukroun M. Engelhardt H. Sotin C.
Ice Response to Cyclic Loading for Low Stresses and Frequencies — Application to Icy Satellites **[#9073]**

8:45 a.m. Collins G. C. * Sklar L. S. Zygielbaum B. Polito P.
Laboratory Investigations Relevant to the Erosion of Ice on Titan **[#9020]**

9:00 a.m. Wagner R. J. * Neukum G.
Erosional Processes on Callisto: Galileo SSI Results, Open Questions, and Requirements for New Camera Data **[#9055]**

9:15 a.m. Manning C. E. * Daniel I.
Influence of NaCl on Ice VI and Ice VII Phase Relations and Properties: Implications for Solar System Ices **[#9042]**

9:30 a.m. Caracas R. * Hemley R. J.
Stability of H_2O Ice Polymorphs at High Pressure **[#9091]**

9:45 a.m. Kuehrt E. * Gortsas N. Motschmann U.
Thermo-Physical Modeling of Cometary Nuclei with Moving Ice Boundaries **[#9053]**

10:00 a.m. Schenk P. M. *
Cratering on Ice — A Cold Laboratory **[#9095]**

10:30 a.m. BREAK

11:00 a.m. Dombard A. J. *
Numerical Simulations of the Deformation of Icy-Satellite Lithospheres **[#9015]**

11:30 a.m. Arakawa M. *
Impact Experiments on Snow: The Effect of Sintering on the Formation of Crater **[#9019]**

11:45 a.m. Stevenson D. J. *
What We Want to Know About Ices for Understanding the Structure and Evolution of Ice-rich Bodies **[#9094]**

12:15 p.m. GENERAL DISCUSSION
Discussion Chair: D. J. Stevenson
Co-Chairs: F. Nimmo and P. M. Schenk

12:30 p.m. CONCLUSION AND SYNTHESIS

1:00 p.m. MEETING ADJORNED

The Solar Ice-Salt Sheets

Pedram Aftabi*

The ice(CO_2+H_2O) occurs in the polar caps on Mars and in the red planet's soils[1,2,3,4,5,6,7&9]with huge outflow channels[8,9]. NASA[9] also prepared pictures which show frozen surfaces on Titan ,Jupiter's moon Europa[10]Callisto and Ganymede[9] . A type of different (hot)snows of salt may exist in top of the mountains on Venus(see pictures in [9]). The salt is as old as the Solar System, so the water trapped inside the salt is also ancient[11]. Both sulfate and chloride contaminants are plausible constituents of icy shells[12].The ice in solar system is as rock consist of ice,salt,minerals and rocky fragements.All the mixtures of ice and rocks flow but in different rates[14,15], although the ice flow slowly in cold conditions in compare to Earth[13]. Rock salt is unusually soft [19] and is probably close to the extreme in natural solid state rock flow[16,17&18]and flow elastically or elastic plastic and plastically during minutes,days,month and years[20,21,17].PDMS 36 is the best material for simulation the structures in most flowing situations[22,21, 17,13,18,14,15,23]. Rectangular sheets of PDMS used to understanding the steady state flow in a horizontal surface [22,21,17,13,18,14,15&23]as following the Ramberg's methods[24]. For unsteady flow used the prototype materials[23].Different roles played by viscous forces and viscous stresses, the differences in behavior of stagnation pressure and stagnation enthalpy , and the role of viscous stresses on the boundary in creating these behaviors in author's ice models. The ice can move by steady laminar flow or transitional flow, but it may turbulent in the deeper part when the ice is warmer. The ice in the polar areas(e.g. Mars) mostly considered that feed from above[25,7&26].The ice in all planets can flow sideways as viscous material(Fig1[13]) from a conical shape(Fig3) or rectangular shape to a droplet(Fig1). Planar passive markers that begin parallel to flow trajectories remain planar as they are carried by slow steady flows (Fig1). The roll over folds are developed as a result of trajectories of steady 3D flows crossing passive planar markers(Figs1&2).The evolution of vertical and horizontal markers during and steady flow of ice sheets shown in Figs 1&2.The pushed from top happened in the sheets , when the material inserted from top(Fig2). The down sinking sheets in below flow sideways as thick sheets and with medium rates(Fig2b,c) but the sheets in the load steady flow but in high rate. The weight of upper sheets creates a thin layer of liquid water that lubricates them and makes gliding possible(Figs2b,c). The sheets then stick together and progressive as larger scales(Fig2c).The ice propagates further during time(Figs1,2) to form the tank track folds[24,21]. In the case of changing atmospheric temperature/pressure and the ice sheet content, and also other articles(e.g. salt), polar ices generated compositional layering(Fig2c) , with multi roll over folds and ,oscillatory refolded folds. (Figs1).

*Tectonics, Geological Survey of Iran, PO Box 13185-1494,Tehran,Iran,Ped_Aftabi@yahoo.com

When the supply from top decreased or finished ,as well in the predominant atmospheric temperature and pressure, the liquefaction of the ice and the thermal contraction-expansion generated joints and fractures in ice and ice-salt mixtures , which the ice flow upward as liquid-solid material to generate pit like features(Fig1d).

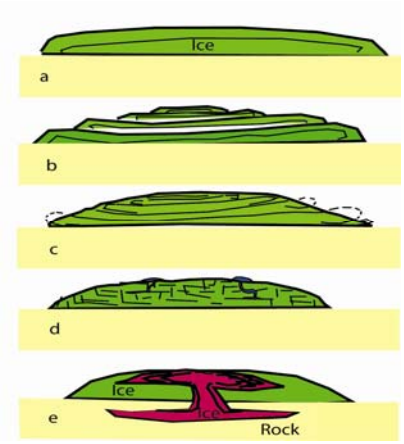

Fig1

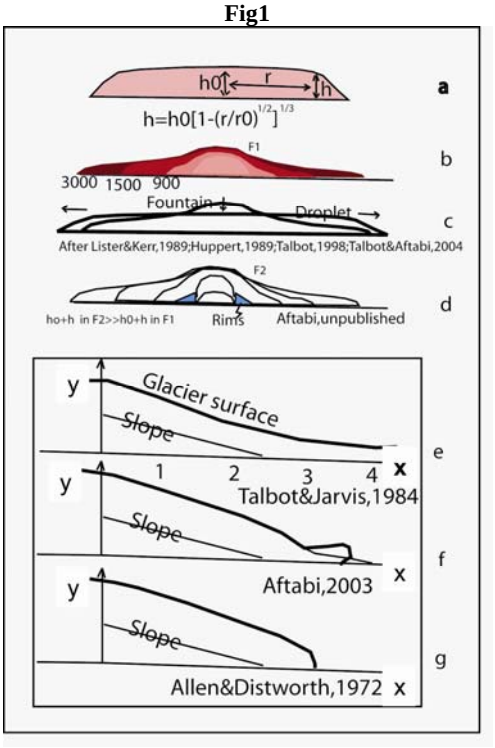

Fig2

Some of the pit shape structures may generated by convectional movements and rising(Fig1d) of ice or high content brines(e.g. on Mars). However the ice feeding from top may lead to loading of the older ice –salt sheets(e.g. on Mars) and formed rising ice- salt sheet , which injected to the new sheets(Fig1e)and spread sideways into it.

The layers thinned by fast steady flow and the folds change to tight, but in the slow flow layers be thicker. Three types of external structures simulated in the plastic, viscous and granular materials[21].The viscous materials in nature considered in two type structure[27,21].The fountain model[28] and the droplet models[29]later evolved to several sub-types[30].These forms also models in analytical methods([31,32]Figs 2e,g).However the natural salt glaciers under slope generated a taper, when the erosion is too low, or very gentle slop semi parallel to the main rock slope in below(Fig2f).In nature Viscous fluids flow down pressure gradients under the influence of boundary conditions[20,27].For example the external shape of the Southern polar cap of Mars probably show a viscous droplet , but the Martian Northern pole is as plastic conical shape. This means that the water may rise in the Northern pole. It is possible that the rate of spreading(or rise) in N and S is different. The rising water in the Northern pole may is higher than the southern polar cap, but it may start to flow sideways, even more rapidly. The experiments show that all viscous materials (without supply)flow sideways and changed the shapes from a plastic shape to a droplet viscous shape(Figs 3&4). The experiments(Fig3)are applicable for all Solar system ice caps.

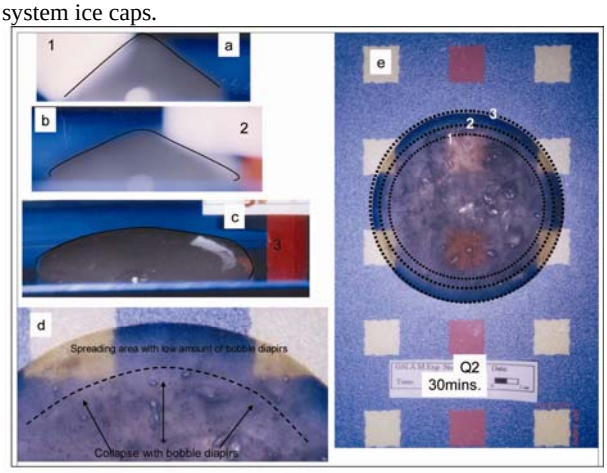

Fig3

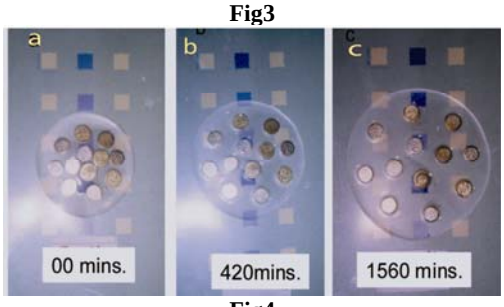

Fig4

They are granular(Fig3a) if the inserted ices from above are more than spreading ice-salt sideways. This shape also occurs when the rate of rise of the brine is so high and the freezing happened at the same time(like processes in volcanoes or ice volcanoes on Earth). However the ice or salt glaciers flow down slop base on analytical models, physical models and also natural models(Figs3e,f,&g).The ice acted as viscous-plastic material, which are changing together in external structures in the solar system(Fig3).However many inclusions(rocks) in the spreading sheets(like duricrusts) propagate sideways(Fig4),but sink during flow. The sinking rock articles in ice may leads to the injection of fresh water up(Fig1d) and then sideways. The inclusions, loading changes, competence contrast of layers, pre-existing joints-faults[21] and ice thin skin deformation[14,15,and 20] in the viscous sheets on Earth operated on the steady flow and generated folds(Fig5)by changes in the flow rate. They sink into the base and slow the spreading rate in termini, but fast the flow rate in back(Fig5[20]).The changes from steady state flow to variable flow (fast or slow)changed the shaping of tank track folds in nature([20];Fig5).The models here can be use for ice, salt and other viscous material elsewhere in solar system, to understanding flow laws. The shaping and rate of spreading in ice sheets and other viscous sheets like salt can help us to understanding brines material properties in the icy crusts and water explorations elsewhere in the solar system.

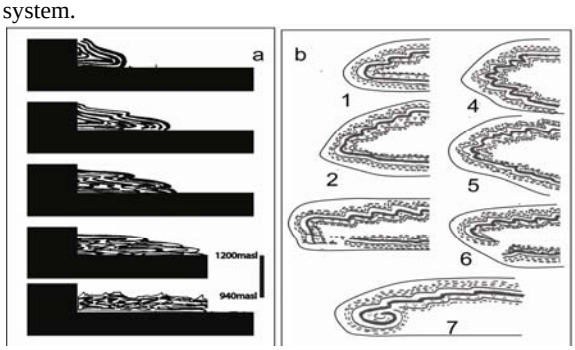

Fig5

References:

[20]Aftabi, P., 2000, Salt Tectonics of Central Iran, MSC thesis, Institute for Earth Science Research and Hans Ramberg Tectonic Laboratory, Tehran-uppsala,321pp, In English.

[30]Aftabi,P.2003,GSI,Potash structures and explorations, Report of investigation no3,50pp.

[17]Aftabi, P. et al.,2005, Radar , Houston, Texas,LPI,2pp.

[13]Aftabi,P.,2006(1),Polar,Davos,Switzerland,LPI, PDF1323,8059,2pp.

[18]Aftabi,P.,2006(2),EGU,Vol.8,7962,2pp

[14]Aftabi,p.,2007(1),Phobos&Deimos,LPI,NASA Ames,7030,1pp.

[15]Aftabi,P.,2007(2),Phobos&Deimos ,LPI,NASA Ames, 7047,1pp.

[23]Aftabi,p.,2008,MartianGullies,Theories&tests,Texas,LPI ,P8014,2pp.

[32]Allen Jr,T.,&Ditsworth,R.L.,Fluid Mechanics, McGraw-Hill B.C,415pp.

[2]Boynton, W. V. et al., 2002, Science 297:81-85.

[7]Byrne,S.,&Zuber,M.T.,2006,Polar,Davos,LPI,8035,2pp.

[4]Dout,S.,et al.,2006,Polar,Davos,LPI,8030,2pp.

[9]http://www.nasa.gov/.

[29]Huppert,H.E,1982,JFM,121,43-58.

[19]Jackson,M.P.A.,&Talbot,C.J.,1989,Continental Deformation,Hancock,P.(ed.),p.159-179.

[25]James, P. B., et al.,1992, University of Arizona Press, Tucson pp, 934–968.

[10]Kivelson,M.G.,2000,Science 289, n. 5483, pp. 1340 – 1343.

[28]Lister,J.R.,&Kerr,R.C.,1989,JFM,203,215-249.

[26]Magalhães, J.A. et al., 1999,J. Geophys. Res. 104 (E4), 8943–8956.

[8]Malin, M. C. & Edgett, K. S.,2000,.Science 288, 2330- 2335.

[12]McCord, T.B. et al. 1999. J. Geophys. Res.104, 11827.

[3]Mitrofanov, I. et al.., 2002, Science 297, pp.78-81.

[24]Ramberg, H., 1981, Gravity,Deformation and the Earth's crust, Academic Press, London.

[21]Talbot, C.J., &Aftabi, P., 2004, GSL,V.161, p.321-334.

[31]Talbot, C.J. &Jarvis, R.J., 1984, JSG, 6,521-533.

[27]Talbot, C.J., 1998, GSL, 143,315-334.

[16]Talbot, C.J. et al., 2000, Salt Tectonics, G I Alsop; Derek J Blundell; Ian Davison (eds.); GSL.

[5]Thomas et al., 2000, Nature, 404,161-164.

[6]Thomas et al., 2005, Icarus, 174(2), 535-559.

[1]Vaniman, D.T., & Others, 2004, Nature, Vol. 431, pp. 663-665. pp.311-325.

[22]Weijermars, R., 1986, Naturwissenschaften, Vol.73, S, p.33.

[11]Zolensky et al. (1999) Science 285, 1377.

Ice In and On Cometary Nuclei. Michael F. A'Hearn[1] (Department of Astronomy, University of Maryland, College Park MD 20742)

Introduction: Although frozen water is almost surely the single most abundant "mineral" in cometary nuclei, there are remarkably few direct observations to constrain our ideas about its structure and form. Thus most theories are based on indirect observations.

Theoretical Ideas: Theoretical models have been developed based on a variety of assumptions. One of the topics on which there is considerable disagreement is whether there is amorphous ice or whether it is all crystalline. There are also arguments about whether the ice is at the surface or deep below the surface.

Observations: There have been a very few reports of an ice absorption feature in the near-infrared region from comets at large heliocentric distance but it is not clear whether this is from icy grains in the coma or from ice on the nucleus.

Recent observations from Deep Impact have shown that there is highly localized, crystalline ice on the surface. The observations have also shown that the bulk of the ice that is responsible for the gaseous water in the coma is buried at very shallow depths below the surface.

What does this tell us about the nature of ice in cometary nuclei? Stay tuned for the talk.

IMPACT EXPERIMENTS ON SNOW: THE EFFECT OF SINTERING ON THE FORMATION OF CRATER. Masahiko Arakawa, Graduate School of Environmental Studies, Nagoya University (Chikusa-ku, Furo-cho, Nagoya, 464-8601, Japan: arak@eps.nagoya-u.ac.jp)

Introduction: Recent planetary explorations for small bodies revealed that they have large craters compared to their seizes. These small bodies could be a mixture of silicates and ices. The important mechanism to give the strength in porous small bodies could be a sintering of the dusts. Sirono and Yamamoto (1997) studied the porosity evolution by sintering and the thermal history in small icy bodies for the implication to comets [1]. They showed that the mechanical structure of the strength developed by sintering in the process of the thermal evolution. Therefore, we studied the contribution of sintering to the mechanical strength of icy bodies and the effect of sintering on the formation of impact craters made on snow.

Experimental method: Impact experiments on snow were conducted to make clear the formation mechanism of crater and the disruption mechanism of the sintered porous materials [2,3,4]. The target was made of ice particles with the size of about 500 microns. The ice particles were put in a cylindrical container with the diameter of 13.5cm and the height of 10cm for the cratering experiments. The target porosity was between 35 % to 45 % and the target was set in a cold room for sintering from 3 minutes to 60 hours. We used the projectile made of ice and snow with the porosity of about 30%. The projectile was a cylinder with the diameter of 7mm and launched by a He-gas gun at the impact velocity less than 150 m/s. Every impact experiment was conducted in a large cold room at the temperature of -5 to –18°C. In order to compare these results obtained by low velocity impacts with the craters formed by high velocity impacts, the craterig experiments were conducted by using a two stage light gas gun set in a cold room. The nylon projectile was launched at the velocity from 2 to 3 km/s and it was impacted on the snow target with the porosity of about 40%, which was sintered for 24 hrs at -10°C. The crater found on the recovered target was measured and the thin section near the crater area was made to analyze the melting region.

Results: In the low velocity impact experiments made by snow and ice projectile, we have found that the crater size clearly increased with increasing the impact velocities at -10°C. The snow projectile was recovered intact at the impact velocity lower than 70m/s, but it was broken completely at the velocity higher than 70m/s and the relic of impact point was observed as ring-like structure. At lower temperatures, the crater size became larger at the same impact velocity. In contrast, the crater size became smaller at higher temperatures. The relationship between the crater volume (V_{cr}) and the projectile kinetic energy (E_k) was fit by power law equations for each temperature and projectile. The power law index derived from the fitting for each data was about 0.5 irrespective of the temperatures. The V_c of the lower temperatures becomes larger at the same E_k because of the effect of sintering. The V_{cr} at –18°C is noted to be three times larger than that at –5°C (Fig.1).

In the high velocity impact experiments made by nyron projectiles, the recovered crater had a spherical

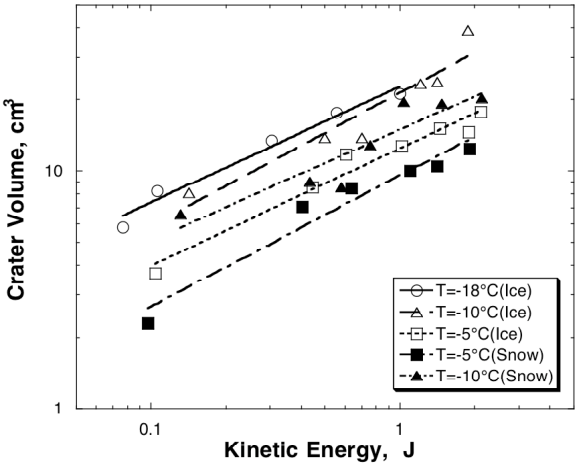

Fig.1 Crater volume vs. Kinetic energy of the projectiles

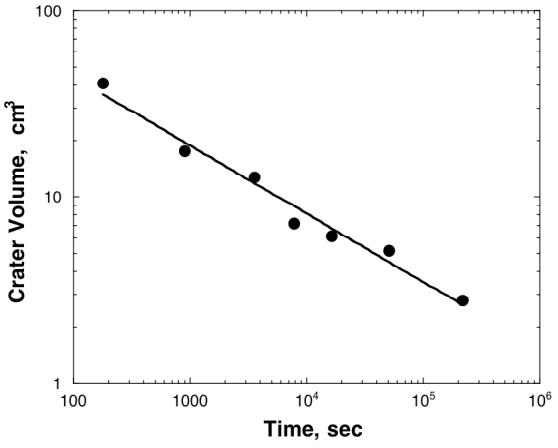

Fig.2 Crater volumes made on the snow with different degree of sintering

pit and a concentric spall area surrounding the pit. The pit radius was about 10mm and the center of the pit was about 9mm below the surface. The wall of the spherical pit was covered with a thin ice layer about the thickness of 0.5mm, which was observed in the thin section under a microscope. This ice layer could be a refrozen snow target melted by the impact. This melt evidence and the spall area observed aroud the pit were characteristics of the high velocity impact. We never observed them in the low velocity impacts.

We also found that the crater size simply decreased with time from 3min. to 60 hrs. at –10°C. Figure 2 shows the crater volume for the targets sintered at different duration. The target was sintered at –10°C, and the crater was formed at the impact velocity of 100m/s. The crater volume decreases with increasing sintering duration. The empirical relationship between V_{cr} and t_s is as follows,

$$V_{cr}[\mathrm{cm}^3] = 236 \cdot t_s^{-0.37}[\mathrm{sec}]. \quad (1)$$

Because the target strength should increase with increasing the duration by sintering, we can expect that the above power law relationship can be explained by the strength variation with time.

In order to measure the mechanical strength of sintered snow at -10°C, the impact test by dropping the metal weight was conducted and the impact acceleration of the weight was measured to evaluate the snow dynamic strength. We define the snow dynamic strength by the maximum stress. We recognize that the strength (Y) increases with the duration according to the following power law relationship,

$$Y[\mathrm{kPa}] = 5.75 \cdot t_s^{0.28}[\mathrm{sec}]. \quad (2)$$

Now we can rewrite the equation (1) by using equation (2) to represent the strength dependence of the crater volume.

$$V_{cr}[\mathrm{cm}^3] = 1852 \cdot Y^{-1.3}[\mathrm{kPa}]. \quad (3)$$

The above empirical equation shows the effect of strength on the crater formation. The important property discovered in this experiment is that the volume is inversely proportional to the material strength for the porous sintered target.

Discussion: According to a simple theoretical consideration on the impact crater formed on weak targets, we propose a scaling parameter of P_0/Y for the scaling law of a sintered snow, where P_0 is an initial impact pressure, and Y is a strength of sintered snow. All of our resuts shown in Fig.1 were reanalyzed to plot them by using P_0/Y and a crater volume normalized by the projectile volume. Figure 3 shows the relationship between the normalized crater volume and P_0/Y for all of our results with different tempetratures and projectiles. The difference among the results observed in Fig.1 was reduced and all of the data were fit by one line described by the following equation,

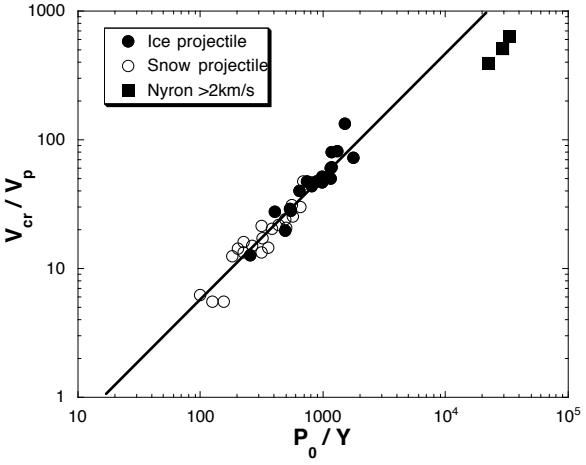

Fig.3 Normalize crater volume vs. Normalized impact pressure for snow targets with the porosity of 40% impacted at the velocity from 10m/s to 3km/s.

$$V_{cr}/V_p = 0.07(P_0/Y)^{0.95}, \quad (4)$$

where V_p is a projectile volume. This equation can be suitable for the data obtained by not only snow projectiles but also ice projectiles. We also pot the results derived from the high velocity impact. They are slightly lower than the fitted line: the craterig efficiency was less than that derived from the low velocity impacts. This difference might be caused by the impact melting because the impact energy was consumed by the latent heat to reduce the crater volume.

References: [1]Sirono and Yamamoto (1997) *Planet. Space. Sci*., *45*, 827-834. [2] Arakawa et al. (2002) *Icarus*, 158, 516-531. [3] Arakawa and Tomizuka (2004) *Icarus*, 170, 193-201. [4] Burchell et al. (2005) *Icarus*, 179, 274-288.

RADIATION EFFECTS IN WATER ICE IN THE SOLAR SYSTEM. R. A. Baragiola, M. Famá, M. J. Loeffler, U. Raut, J. Shi and B. D. Teolis, University of Virginia, Laboratory for Atomic and Surface Physics, Thornton Hall, Charlottesville, VA 22904, USA. E-mail: raul at virginia.edu.

Introduction: This presentation will describe the physical and chemical effects that occur in water ice at low temperatures (< 160K) as a result of irradiation with energetic ions, electrons, and UV photons in different regions of the solar system. This will be an update on the properties of vapor-deposited, low-temperature ice and radiation effects reviewed a few years ago [1]. After a brief description of basic phenomena we will give an update of experimental findings and applications to solar system objects. The presentation will include the following topics:

1) Energy deposition and transfer – differences between exciting particles: light and heavy ions, electrons and UV photons.
2) Production of radiolytic species and comparative effects of different particles. Effect of excitation density on molecular formation (O_2, H_2O_2) [2-5].
3) Ion implantation, trapping and formation of new species that include the projectiles [5] and their thermal desorption [6,7].
4) Photodesorption and sputtering of water, H_2 and O_2 molecules as source of exospheres [5,8-10].
5) Synergistic effects of concurrent impacts of particles and atmospheric gases: enhanced trapping, production of ozone from ice [11].
6) Irradiation induced phase changes, compaction and their implications [12,13].
7) Radiolysis of mixed water:ammonia ices [7].
8) Electrostatic charging and surface potentials [14].

Within each topic, we will illustrate, with examples, how laboratory studies help understand specific instances of astronomical phenomena that have been captured by remote sensing.

The presentation will include published data from our laboratory as well as yet unpublished results of our recent experiments, some of which will be presented as posters.

References: [1] Baragiola, R.A. (2003) *Planet. Sp. Sci*. 51, 953-961. [2] Loeffler, M.J. and Baragiola, R. A. (2005), *GRL* 32, L172023. [3] Loeffler, M.J. et al (2006) *Icarus* 180, 265-273. [4] Loeffler, M.J. et al (2006) *J. Chem. Phys.* 124, 104702. [5] Teolis, B.D. et al (2005) *Phys. Rev.* B 72, 245422. [6] M. J. Loeffler, Teolis, B.D. and Baragiola, R.A. (2006) *Astrophys. Journal Lett* 639, L103-L106. [7] Loeffler, M.J., Raut, U. and Baragiola, R.A., *Astrophys. J. Letters* 649, L133–L136 [8] Baragiola, R.A. et al. (2003) *Nucl. Instr. Meth. Phys. Res*. B 209, 294-303. [9] Vidal, R.A., Teolis, B.D. and Baragiola, R.A. (2005) *Surface Sci.* 588, 1-5. [10] Famá, M., Shi, J. and Baragiola, R.A. *Surface Sci.* 602, 156. [11] Teolis, B.D. et al., (2006) *Astrophys. J. Letters* 644, L141-L144. [12] Baragiola, R.A. et al (2005) *Rad. Phys. Chem.* 72, 187-191. [13] Raut, U. et al (2007) *J. Chem. Phys.* 126, 244511. [14] Shi, J., Fama, M. and Baragiola, R.A. (2008) – this conference

THE MECHANISM OF GAS TRAPPING AND RELEASE IN SOLAR SYSTEM WATER ICE

Akiva Bar-Nun,Diana Laufer,Gila Notesco and Yigal Pat-EL
Dept.of Geophysics and Planetary Sci.
Tel Aviv University,Tel Aviv,Israel
akivab@post.tau.ac.il

Water ice,deposited from the vapor below 130K,is amorphous and has many pores.If the deposition is carried out in the presence of gas,the gas molecules enter the pores and stick to the ice walls by van der Waals forces.When another layer of ice forms above the pores,the gas is trapped inside.Upon warming up,the water molecules in the ice move,opening some of the pores and some of the gas can escape.Preferences in trapping efficiencies among various gases will be discussed,as well as grain ejection and collapse during massive gas release.The experimental findings will be used to predict and explain phenomenae on comets and icy satellites.

MOBILE LID CONVECTION BENEATH ENCELADUS' SOUTH POLAR TERRAIN. Amy C. Barr, Department of Space Studies, Southwest Research Insititue. (Southwest Research Institute, 1050 Walnut St., Suite 300, Boulder, CO 80302; amy@boulder.swri.edu).

Introduction: Observations of Enceladus by the *Cassini* spacecraft indicate that this tiny satellite is geologically active, wth plumes of water vapor, dust, and other materials erupting from a region centered near its south pole dubbed the "south polar terrain" (SPT) [1,2]. Enceladus' plumes are spatially associated with a region of increased heat flux, with a total power output of 5.8 ± 1.9 GW spread over a region ~70,000 km^2 [1,2]. The total power output corresponds to a heat flux F=55 to 110 mW m^{-2}. The active region at the south pole is bounded by cycloidal arcs, with wedge-shaped regions of intense folding at their cusps [3]. The CIRS data provide a unique opportunity to observe the heat flux from the surface of an icy satellite at the time of active resurfacing. The heat flux estimates can be used to argue for or against certain types of convective behavior, can clarify the relationship between convection and resurfacing on Enceladus, and may provide insight into convective-driven resurfacing on other icy satellites.

The high brightness temperatures observed within the tiger stripes [2] led Nimmo et al., [4] to suggest that shear heating due to cyclical strike-slip motion along fault zones within the stripes could be a dominant source of heat generation within the SPT. Another possibility is that Enceladus' ice shell is heated from within by tidal dissipation and is vigorously convecting [5,6]. However, prior predictions of the heat flux carried by stagnant lid convection and tidal dissipation using nominal parameters for the rheology of ice are a factor of 3-4 lower than the CIRS estimate [5,6,7].

Here, I suggest that the high heat flux and increased cryovolcanic and tectonic activity in the region suggest that near-surface ice near the south pole has become rheologically and mechanically weakened enough to permit convective plumes to reach close to the surface [7]. In this case, convection occurs in the "mobile lid" regime, characterized by high heat fluxes and horizontal spreading of near-surface ice. If this style of convection is occurring within the SPT, ice atop the region should be spreading horizontally with velocities ~O(1-10) mm yr^{-1} and should be resurfaced in ~0.1 to 10 Myr, providing a means by which this idea can be tested with *Cassini* data.

Mobile Lid Regime: The heat flux from a convecting planetary mantle (or ice I shell on an icy satellite) is controlled in part by the ratio between the viscosity of the ice at the satellite's cold surface (η_0) and the viscosity at the warm base of the ice shell (η_1), $\Delta\eta=\eta_0/\eta_1$. A basic requirement for mobile lid behavior is $\Delta\eta <$ exp $(4(n+1))$, where n~1-4 is the stress exponent in the material flow law [8]. Values of $\Delta\eta$ for water ice in the outer solar system are ~ 10^{20} or greater [7,9]. Like any planetary mantle, the cold near-surface ice in a convecting ice shell on Enceladus is expected to exhibit a brittle/elastic behavior, with true viscous behavior dominating only at high temperatures or at depth. One way of mimicking the effects of a brittle lithosphere in a purely viscous convection model is to limit the viscosity of the near-surface ice to a value $\eta_0 \sim \sigma_Y/\dot{\varepsilon}_{II}$, the ratio between the yield stress of ice and the second invariant of the strain rate tensor, effectively decreasing $\Delta\eta$ [10,11,12].

Heat Flux. To constrain the relationship between convective heat flux and rheological parameters for ice in the mobile lid regime, I performed numerical simulations of convection (using CITCOM [13]) in a basally heated ice shell with $10^2 < \Delta\eta < 10^{3.25}$ [7]. A Newtonian rheology with temperature dependence of form $\eta=\exp(-\gamma T)$, where $\gamma=\theta/\Delta T$ and $\theta=\ln(\Delta\eta)$. The convective heat flux in the mobile lid regime is related to θ as [7],

$$F_{conv} = 0.32\left(\frac{\rho g \alpha \Delta T^4 k^3}{\kappa}\right)^{1/3} \frac{\exp(\theta/19)}{\eta_0^{1/3}}, \quad (1)$$

where ρ=920 kg m^{-3}, g=0.13 m s^{-2}, α=1.7x10^{-4} K^{-1}, ΔT=(273-70) K, k=2.27 W m^{-2} K^{-1} s^{-1}, κ=1.23 x10^{-6} m^2 s^{-1}. Similar to the stagnant lid regime, F_{conv} does not depend on the thickness of the ice shell. Effective near-surface viscosities η_0~10^{16} to 10^{17} Pa s and basal ice viscosities 10^{13} to 10^{15} Pa s give F_{conv} comparable to the regional heat flux observed by CIRS.

Surface Velocities. As its name implies, convection in the mobile lid regime is characterized by large horizontal velocities in the near-surface ice. If mobile lid convection is responsible for crustal recycling in the SPT, the SPT should have a younger surface than the rest of Enceladus, and the age of the surface should be related to the horizontal velocity of the surface ice. The velocity of the near-surface ice is related to the thermal and physical parameters of the ice shell and ice shell thickness D as [7],

$$\max\left(\left|v_{x,sf}\right|\right) = 0.08\frac{\kappa}{D}\left(\frac{\rho g \alpha \Delta T D^3}{\kappa}\right)^{0.8} \eta_0^{-0.8}, \quad (2)$$

or,

$$\max\left(\left|v_{x,sf}\right|\right) = 25 \text{ mm yr}^{-1} \left(\frac{10^{17} \text{ Pa s}}{\eta_0}\right)^{0.8} \left(\frac{D}{30 \text{ km}}\right)^{1.4}. \quad (3)$$

For a circular SPT with an area 70,000 km^2, the equivalent radius is R_{spt}~150 km. The age of the SPT is related to the ice shell thickness and effective surface viscosity as [7],

$$\tau_{spt} \sim 6 \text{ Myr} \left(\frac{\eta_0}{10^{17} \text{ Pa s}}\right)^{0.8} \left(\frac{30 \text{ km}}{D}\right)^{1.4}. \quad (4)$$

For the range of effective surface viscosities that give F_{conv} close to the heat flux observed by CIRS, the predicted age of the SPT is between 0.2 and 7 Myr, depending on the ice shell thickness.

Tidal Heating: In the mobile lid regime, the low viscosity of near-surface ice permits more tidal deformation in the model ice shells than predicted for the stagnant lid regime. However, estimates of tidal heat using the standard model of dissipation in a Maxwell viscoelastic solid also fall short of the convective heat flux- and heat flux observed by CIRS [7]. For a broad range of plausible ice shell viscosities, the tidal heat generation in an ice shell with a *globally low* $\Delta\eta$ (which may not be physically realistic) falls short of the convective heat flux by a factor of ~10 or more.

Conditions for Mobile Lid Convection: The most straightforward method of lowering the effective viscosity contrast of the ice shell is to suppose that h_0 is limited by the finite yield stress of the near-surface ice. Recently, Solomatov [11] has developed a general criterion for the critical yield strength for lid mobilization based on the rheology of the convecting fluid layer. For convection to occur in the mobile lid regime, stresses built up in the lithosphere from the underlying convection have to be comparable to the yield strength of the lithosphere, or [11],

$$\sigma_y < 13 \frac{\alpha \rho g}{\Delta T} \left(\frac{R_G T_i^2}{Q^*}\right)^2 l_h, \quad (5)$$

where R_G=8.134 J mol^{-1} K^{-1} is the gas constant, Q^* is the activation energy in the ice flow law, T_i~200 K is the characteristic temperature in the well-mixed convecting interior of the ice shell, l_h~O(D) is the horizontal length scale over which stress accumulates in the lithosphere. In Enceladus' ice shell, convective deformation is likely accommodated by volume diffusion [5], Q^*=59.4 kJ mol^{-1}; this implies that the yield strength of the lithosphere must be lass than $\sigma_y \sim 10^{-3}$ MPa for mobile lid convection to occur.

Discussion: Laboratory studies in two areas can shed light upon the behavior of ice relevant to Enceladus' SPT.

1. Fracture and Failure in Cold, Cyclically Deformed Ice. Field characterization of fracture in the Ross Ice Shelf suggest that the yield stress of ice at terrestrial conditions is ~0.1 MPa; much larger than σ_Y required for mobile lid convection on Enceladus. Terrestrial field estimates for σ_y may not be directly be applicable to the surfaces of icy satellites because the microphysical processes responsible for fracture (e.g., grain boundary sliding and dislocation pile-ups [14]) are thermally driven [15] and may not be responsible for fracture in ice at temperatures relevant to Enceladus' lithosphere. Further characterization of fracture in ice at extremely low temperatures, and modes of failure in cold ice deformed cyclically at enceladean frequencies are needed to shed light upon the style of convection on Enceladus and other icy bodies.

2. Cyclical Deformation in Pure Water Ice. The amount of tidal heating generated in a mobile lid ice shell falls short of the amount of heat transported by mobile lid convection. Shear heating due to strike-slip motion along fault zones within the tiger stripes likely contribute to the regional heat flux in the SPT; observations of the heat flux in parts of the SPT *away from* the tiger stripes may shed light upon how tidal dissipation is partitioned between shear heating and viscous dissipation in the ice shell [7]. Another possibility is that Newtonian volume diffusion does not accommodate diurnal tidal strain in Enceladus' ice shell; if another processes such as grain boundary sliding or primary creep accommodated tidal deformation, the effective viscosity over *tidal* time scales would be different than over *convective* time scales. Very little is known about the micro- and possibly macro-scale processes responsible for attenuation in cyclically flexed ice. Such information is critically needed to clarify the relationship between tidal flexing and activity at the SPT.

Acknowledgements: This work is supported by NASA CDAP Grant NNX07AE80G.

References: [1] Porco C. C. et al. (2006) *Science 311*, 1393-1401. [2] Spencer J. R. et al. (2006) *Science 311*, 1401-1405. [3] Helfenstein, P. et al., (2006) *LPSC XXXVII* #2182. [4] Nimmo, F. et al., *Nature* 447, 289-291 (2007). [5] Barr A. C. and McKinnon W.B. (2007) *GRL*, v.24, L09202. [6] Roberts, J. and F. Nimmo (2008) *Icarus* in press. [7] Barr, A. C., *JGR* submitted (2008). [8] Solomatov, V. S. (1995) *Phys. Fluids* 7 266-274. [9] Showman, A. P. and L. Han (2004) *Icarus* 177 425-437. [10] Moresi, L.-N. and V. S. Solomatov (1998) *GJI* 133, 669-682., [11] Solomatov, V. S., (2004) *JGR* v. 109, B01412. [12] Showman, A. P. and L. Han (2005) *Icarus* v. 177, 425-43. [13] Moresi, L.-N. and V. S. Solomatov (1995) *Phys. Fluids* 7 2154-2162. [14] Frost, H. J. (2001) Eng. Fracture Mech. 68, 1823-1837. [15] Sinha, N. K. (1991), in *Ice-Structure Interaction*, Jones et al., eds., Springer-Verlag, pp. 69-87.

LARGE-GRAINED DUST IN THE COMA OF 174P/ECHECLUS. J. M. Bauer[1], Y-J. Choi[1,5], P. R. Weissman[1], J. A. Stansberry[2], Y. R. Fernández[3], H. G. Roe[4], B. J. Buratti[1], and H-I. Sung[5], [1]Jet Propulsion Laboratory, California Institute of Technology, 4800 Oak Grove Drive, MS 183-501, Pasadena, CA, USA 91109 (correspondence: *bauer@scn.jpl.nasa.gov*), [2] University of Arizona, Steward Observatory, 933 N. Cherry Ave., Tuscon AZ 85721, [3] University of Central Florida, Dept. of Physics, P.O. Box 162385, Orlando, FL 32816-2385, [4] Lowell Observatory, 1400 W. Mars Hill Road, Flagstaff, AZ 86001, [5]Korea Astronomy and Space Science Institute 61-1 Hwaam-dong, Yuseong-gu, Daejon 305-348, South Korea.

Introduction: On December 30, 2005, Choi and Weissman[1] discovered that the formerly dormant Centaur 2000 EC98 was in strong outburst. Previous observations spanning a 3-year period indicated a lack of coma down to the 27 mag/sq. arcsec level[2]. We present Spitzer Space Telescope MIPS observations of this newly active Centaur - now known as 174P/Echeclus (2000 EC98) or 60558 Echeclus - taken in late February 2006, and the final results of their analyses[3].

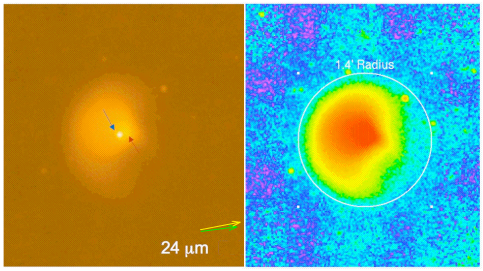

Figure 1: 24μm Spitzer image obtained on Feb 24 at 6" resolution, in low-contrast (left) and false-color high contrast (right). Left Panel: The central condensation of the coma (red arrow) is barely resolved apart from the Centaur (blue arrow), while the Sun-Comet sky-plane vector (yellow arrow) is offset only ~3° from the sky-plane motion (green arrow). The upper bound on the extent of the coma is demarcated by the white circle in the right panel.

MIPS Observations: The images show strong signal at both the 24 and 70 μm bands, and reveal an extended coma about 2 arcmin in diameter. Analyses yield estimates of the coma signal contribution that are in excess of 90% of the total signal in the 24-μm band.

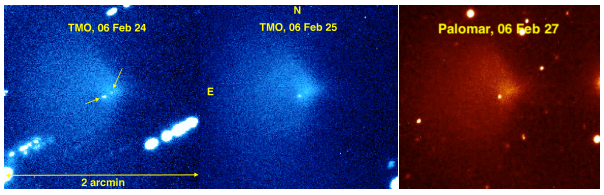

Figure 2: R-band image from TMO's 0.6m telescope taken simultaneously with the SST MIPS observations (left and center), and an RI-band image (right panel) from the Palomar 200-inch telescope taken 2 nights after the observations (similar scales and orientations).

Ground-Based Data: Simultaneous visible-wavelength observations were also obtained with Palomar Observatory's 200-inch telescope, the 1.8-m Vatican Advanced Technology Telescope, the Bohyunsan Optical Astronomy Observatory(BOAO) 1.8-m telescope, and Table Mountain Observatory's 0.6-m telescope, revealing a coma morphology nearly identical to the mid-IR observations. Dust production estimates ranging from 1.7-4.2 × 10^2 kg/s are on the order of 30 times that seen in other Centaurs, assuming grain densities onteh order of water-ice.

Discussion: Combined ground-based and SST photometry reveals several characteristics of Echelus' activity. The nucleus and coma were resolved in the visual and IR data sets. Separation between the nucleus and coma brightness peaks was ~6 arcsec on the plane of the sky. The coma extended out ~ 1 arcmin or greater in our visual and IR images, more than 500,000 km in projected distance from Echeclus' nucleus; this extent is approximately constant over timescales of weeks in February 2006 and over a large range of wavelengths. The surface brightness profiles suggest that the coma is generated by steady-state, isotropic, or nearly isotropic, outflow. In both of the observed IR bands, the coma accounts for > 90% of the observed signal.

Visual and IR dust production estimates indicate a dust particle size distribution similar to that generated by typical cometary activity, as seen by the Stardust spacecraft,'s encounter with 81P/Wild 2, for example. The particle size distribution is far less comparable to that generated by an impactor, as implied by the fluxes seen at varying wavelengths from the Deep Impact encounter with 9P/Tempel 1. The grain size distribution derived from the data yields a log particle mass power-law with a slope that is consistent with steady cometary activity, such as that observed during the Startdust spacecraft's encounter at 81P/Wild 2, and not with an impact-driven event, such as that caused by the Deep Impact experiment. Estimates of mass loss exceed production estimates of other Centaurs and Jupiter family comets.

References:[1] Choi & Weissman (2006) *IAU Circ. 8656,* 1151–1154. [2] Rousselot et al. (2005) *Icarus 176*, 478–491. [3] Bauer et al. (2008) *PASP, in press.*

Acknowledgements: This research was funded in part by the General Observer program of the SST. This work was also supported to completion in part by the NASA Planetary Astronomy and Discovery Data Analysis Programs.

THE LOCATIONS OF MINI-OUTBURSTS ON THE NUCLEUS 9P/TEMPEL 1: THE CASE FOR COMETARY CRYO-VOLCANISM

M. J. S. Belton, Tucson AZ (michaelbelton@beltonspace.com)

Abstract

Data on the UT 2005 June 14 mini-outburst of comet 9P/Tempel 1 taken from different viewpoints (HST, Deep Impact, and Calar Alto, Spain) has been examined for morphological and parallax differences. The outburst source region was found to be located near 218+/-6E, 6+/-5N on the shape model of Thomas *et al*. (2007). The outburst occurred in the afternoon at ~1 pm local solar time. The distribution of light in the outburst is similar to that expected for an optically thin inverted cone-like sheet of material (presumably an ejecta curtain) suggesting a localized source.

We have also computed tracks of possible source regions for nine other mini-outbursts seen from DI. We find that five of these tracks converge on the same region where the June 14 event occurred. Three of the tracks converge at a second location near (60E, 20S). These two locations coincide with the regions of lowest surface gravity on the nucleus, *i.e.,* at places where the principal axis of minimum moment of inertia cut the surface. These results are consistent with the hypothesis that multiple outbursts occur at each location emanating from a single source or from a few sources in close proximity. Given this hypothesis, the outbursts are found to occur both during the day and night indicating at most weak, or no, control by direct sunlight. The times of outburst appear to be non-random with a preference for early afternoon, dusk and near midnight. None of the outbursts occurred near dawn when the surface temperature is rising. The region responsible for the strongest outbursts lies adjacent to a portion of the surface that was imaged at moderate resolution during the DI encounter that is characterized by circular depressions, the source regions of smooth flows, and by water – rich ice patches. There is no imaging information for the second location but it is possible that NExT may soon provide such information.

To explain these results we consider active cryo-volcanism in the interior of the nucleus as a cause of the outbursts. Our concept is based on aspects of surface morphology revealed in the DI images, the ideas of Prialnik *et al*. (2004) for a source of high pressure gas in the interior of the nucleus, and an interior structure based on the talps hypothesis (Belton, M.J.S. *et al*., 2007) that could allow spatially localized traps of high pressure gas to form. Providing the interface between talps layers has less permeability to gas diffusion than the material in the bulk of the layers themselves a qualitative explanation can be achieved.

THE STRUCTURE OF PLANETARY ICES: HOW LABORATORY DIFFRATION METHODS CAN SUPPORT ASTRONOMICAL OBSERVATIONS. D.F. Blake[1], [1]MS 239-4, NASA Ames Research Center, Moffet Field, CA (dblake@mail.arc.nasa.gov).

Introduction: Solar system ices – water ice, water ice clathrates and frozen gases – are major players in the physical and chemical processes that occur in and on outer solar system bodies. An understanding of the physical chemistry (including such things as condensation and volatilization temperatures, structure states and stability, extent of solid solution with other elements and compounds) of outer solar system ices is key to unraveling the past, present and future behavior of these bodies. Remote observations of outer solar system ices, in particular of highly processed bodies such as Kuiper Belt Objects are extremely difficult to make because of their great distance from Earth and their low albedo. Occasionally, one sees dramatic brightening of a cometary apparition due to anomalous outgassing of (presumably) a solid icy material, but the underlying cause of the outgassing remains speculative. Likewise, direct observation of meteoritic materials (including interplanetary dust) may suggest the prior presence and action of frozen volatiles or of water ice, but only indirectly. In such cases, it is abundantly clear that laboratory simulation and analysis of solar system ice analogs will help our understanding.

With regard to condensed phases, it is well known in mineral chemistry that the structure of a crystalline material controls all other observed characteristics. Thus, the study of the sructure of a solid ice and its transitions – amorphous to amorphous, amorphous to crystalline and of one crystalline phase to another, will control all other detected or predicted properties.

Caveats for Laboratory Analog Studies: It is tempting to suggest that laboratory analog investigations are a panacea for planetary ice studies. However, as usual there are limitations to each technique (no one knows this better than the experimentalist!). What does one need to be aware of in order to properly study the behavior of an icy material in the laboratory?

- It is important to know the phase diagram of the material (this of course doesn't apply to amorphous materials). This is especially true for low-temperature studies in which a material approaches stability sluggishly or not at all. One can arrive at the wrong conclusion, if laboratory data are extrapolated to solar system time scales without knowing the phase relationships!
- One must be sure that the experimental protocol (mode of observation, method of growth of the ice, geometry or scale length of the experiment, etc.) is not influencing the structure or properties of the ice. For example, is the electron or photon beam processing the material in some unknown way? Will bulk ice behave in a similar fashion to the thin film that is being measured? There is never any completely satisfactory way to validate a laboratory experiment that is intended to be analogous to a planetary satellite-sized body.
- Experiments in pure end-member systems may not be representative of the dilute solutions or mixed chemistries that exist in nature; in fact, they probably aren't.

Adventures with Laboratory Analogs: Despite the caveats, many noble souls choose to enter into the labyrinth of experimental laboratory ice studies. It is implicit in any laboratory study that those experimentalists who conduct them and those astronomers who who read and apply them to observations of solar system ices, understand the value (and the limitations) of laboratory results. Experimentalists should explicitly state the limitations of their results, and observationalists should read and understand the minutia of the experiments that could limit or invalidate the experimental result for their particular application.

A case study of the structure of water ice: Some rather dated experiments by the author on the structure of vapor-deposited water ice and dilute water solutions will be shown as a case study.[1-4] Results will be shown of a transmission electron microscope study of vapor-deposited water ice and dilute water ice solutions from 10-170K in controlled warming experiments in vacuum. Comparisions will be made with IR experiments, and molecular dynamics / montecarlo simulations of ices deposited and warmed under similar conditions.

References:

1. Blake, D., L. Allamandola, S. Sandford, D. Hudgins and F. Freund. 1991. "Clathrate hydrate formation in amorphous cometary ice analogs in vacuo. " *Science*, 254:548–552.
2. Jenniskens, P. and David F. Blake. 1994. "Structural transitions in amorphous water ice and astrophysical implications." *Science* 265:753–756.
3. Wilson, M.A., A. Pohorille, Peter Jenniskens and David F. Blake. 1995. "Probing the structure of cometary ice." Origins of Life and Evolution of the Biosphere **25**:3-19 (1995).
4. Jenniskens, P. and D.F. Blake. 1996. "Crystallization of amorphous water ice in the solar system." Astrophysical Journal, **473**, Nol. 2, Pt. 1, pp. 1104-1113.

ICE PROPERTIES RELEVANT TO RADAR SOUNDING OF ICY MOONS: LESSONS FROM EARTH APPLIED TO EUROPA. D. D. Blankenship[1] and D. A.Young[1], [1]Institute for Geophysics, John A. and Katherine G. Jackson School of Geosciences, The University of Texas at Austin, 10100 Burnet Road (R2200), Austin, TX, 78758 (blank@ig.utexas.edu).

Introduction: Earth's ice sheets and ice shelves could be viewed as poor analogs for understanding the physical character and processes within icy moons because the formation of Earth's ice is dominated by atmospheric processes. However, below the top few tens of meters, the atmosphere ceases to dominate processes within Earth's large ice masses so they become increasingly relevant as analogs for icy moons. These analogs are particularly useful in the case where the icy shell overlies an ocean; the most robust example being Europa.

Our intent is to examine the thermal and compositional properties of Earth's ice sheets and ice shelves that are relevant to radar sounding. We will then examine the governing processes on Earth that give rise to these properties and then relate these processes to those hypothesized for Europa. Our ultimate goal is to identify physical states within Europa's icy shell that may be observable through orbital radar sounding and to prioritize the laboratory measurements of the dielectric properties of ice (as a function of its thermal, compositional and possibly structural state) needed to interpret these observations.

Thermal Character: The absorption of electromagnetic energy in ice at radar sounding frequencies (1-100 MHz) is highly non-linear in temperature and is significantly higher at warmer temperatures.

Earth's polar ice sheets in East Antarctica, West Antarctica and Greenland are up to five km in thickness and have surface temperatures ranging from 213 – 273 K. In many cases, their internal temperature profiles are nearly isothermal in the upper half, where vertical advection of cold material from above (snow) dominates, and linearly increasing with depth in the lower half where upward conduction of geothermal and latent heat dominates. Strain heating, horizontal advection and spatially- or temporally-varying boundary conditions all contribute to deviations from this simplified description.

A significant deviation from this temperature structure exists for polythermal ice caps (e.g., Svalbard) where significant thicknesses of temperate ice (isothermal at the pressure melting point) are found at the base, overlain by a linearly-varying layer. These profiles generally result from the vertical advection of heat by surface melt draining through the colder upper layer of these ice caps. The temperature profiles for ice shelves are widely varied as the profile inherited from the present ice sheet continues to be modified by downward advection of accumulating material and melt/freeze processes become dominant at the base. Advected heat either from surface melt or ocean infiltration can substantially modify these profiles.

Many processes analogous to those responsible for the thermal state of Earth's ice sheets and ice shelves have been proposed for Europa's icy shell. These include an overlying kilometers-thick brittle shell where thermal conduction is thought to dominate but with added tidally driven strain heating or possibly substantial melting and freezing at depth. In addition, the vertical advection of heat by the redistribution of surface material by sputtering (frost) and gardening, downslope motion or the draining of brines may be thermally analogous. Finally, it should be noted that there are no known Earth analogs for thermal convection within a deep warm ductile layer that has been proposed for Europa although the thermal processes in Earth's polythermal glaciers may yet prove analogous.

Obviously, a thorough understanding of the electromagnetic absorption of ice at radar sounding frequencies over a temperature range from a few tens of K to its pressure melting point will be critical to using orbital radar sounding to elucidate processes within Europa's icy shell (or that of any other icy moon).

Compositional Character: The absorption of electromagnetic waves in ice is also a function of both soluble and insoluble impurities with the soluble impurities (in particular chlorine, ammonia and acids) dominating. Under terrestrial conditions, the temperature dependence of the absorption due to impurities is less than that of pure water; understanding these absorption trends in the much greater temperature range of the outer solar system will be important for interpreting radar sounding results.

The compositional state of Earth's ice sheets and ice shelves is dominated by subtle debris and impurity layering. The process driving the layering is surface deposition and vertical advection of material resulting from transient events. The material may be transported atmospherically (e.g., volcanic ash) or through the process of mass wasting (debris fall).

The other primary compositional states are represented by units of impure ice found both at the base of and within ice shelves. The process causing these bodies is associated with freezing of sea water either in the low temperature gradient at the ice-water interface (so-called marine-ice units) or in the sharper temperature gradients within cracks that penetrate a substantial portion of the ice shelf. The steepness of the temperature gradient modulates the rate of impurity rejection as the ice freezes.

An ice shelf dominated by marine ice formation is the Filchner-Ronne ice shelf of West Antarctica; crack-

fill is associated both with tidal flexure at grounding lines and ice berg calving. Often, sub-ice cracks extend into the upper regions of the ice shelf allowing sea water to infiltrate the poorly compacted material and migrate laterally giving horizontally extensive bodies of very impure ice well above any marine ice layer.

Processes on Europa that may be analogous to those described above include the modulation of the deposition of sputtering by-products by transient gardening and mass wasting events resulting in layering of impurities (somewhat analogous to density layering processes described below). A slow freezing of sub-ice sea water is commonly proposed in association with the infilling of transient melt zones for spot/chaos formation as well as crack infilling for ridge/band formation. Analogous to Earth, a likely implication of these crack infilling hypotheses for Europa would be laterally extensive units of impure ice at the base of any zone of porous regolith penetrated by a water filled crack.

Laboratory measurements of the electromagnetic absorption of ice contaminated by the full range of hypothesized insoluble and, in particular, soluble impurities must be undertaken to utilize radar sounding to test virtually any contemporary hypothesis for the exchange of materials between the surface, subsurface and any ocean on Europa or any other icy moon. Particular emphasis should be given to measurements both at the coldest estimated temperatures and as the temperature warms toward the eutectic for each of these impurities.

A Note on Structural Character: The dielectric constant for the near-surface of any icy moon will be a function of the percentage of void space which will decrease as the firn-like upper layer densifies with depth. Density layering in the upper few tens of meters of Earth's ice sheets and ice shelves is pervasive. This is because ice sheet surfaces on Earth are continually generated by deposition and densification processes that vary temporally but on independent timescales. Analogous structural processes on Europa may include vertical density variations in the shallow subsurface caused by the interplay between deposition of sputtering byproducts (e.g., frost) and deposition/erosion associated with gardening/mass-wasting. Because of this, any laboratory measurements of the dielectric properties of the electromagnetic properties of candidate ice mixtures should be made over a broad range of density.

THERMOELASTIC PROPERTIES OF MIRABILITE AND MERIDIANIITE DETERMINED USING EXPERIMENTAL AND COMPUTATIONAL TECHNIQUES. H. E. A. Brand[1], A. D. Fortes[1], K. S. Knight[2, 3] I. G. Wood[1] and L. Vočadlo[1]. [1]Centre for Planetary Sciences, Department of Earth Sciences, University College London, Gower Street. London, WC1E 6BT, U.K. [2]ISIS facility, Rutherford Appleton Laboratory, Chilton, Didcot, Oxfordshire, OX11 0LA, U.K. [3]The Natural History Museum, Cromwell Road, London, SW7 5BD, U.K (email; helen.brand@ucl.ac.uk).

Introduction: The presence of soluble salts such as $MgSO_4$ and Na_2SO_4 in chondritic meteorites has led to the suggestion that hydrated salts such as mirabilite ($Na_2SO_4{\cdot}10H_2O$) and meridianiite ($MgSO_4{\cdot}11H_2O$) may be major rock-forming minerals in the mantles of large icy moons [1], in addition to pure water ice. Evidence for hydrated alkali salts on the jovian satellites has been observed by the Near Infrared Mapping Spectrometer (NIMS) instrument aboard the Galileo space-craft [2][3]. To interpret the observed surface morphologies of the icy moons and to understand their thermal evolution, geophysical models of their interiors must be constructed. To do this we need to know the phase behaviour, thermoelastic, and transport properties of the constituent materials under the appropriate pressure and temperature conditions, i.e. up to ~ 5 GPa, and from 100 – 300 K. We are therefore engaged in a program of cross-disciplinary research to determine these properties of planetary ices and hydrates using both computational and experimental methods (see contributions by Fortes *et al*., Middleton *et al.,* and Grindrod *et al*., this volume).

Both mirabilite and meridianiite pose experimental and computational challenges by virtue of their crystallography: mirabilite is monoclinic, has a large and complex unit-cell, and exhibits hydrogen-bond disorder; meridianiite is a triclinic crystal (the only symmetry is an inversion centre), and its structural and thermoelastic properties are dominated by weak hydrogen-bonding. Difficulties with the formation and handling of phase-pure specimens means that application of computational mineral physics is the only way to reliably obtain certain material properties. Here we describe combined time-of-flight neutron powder diffraction studies and quantum mechanical calculations of the thermoelastic properties of mirabilite and meridianiite.

Experimental method: Deuterated crystals of mirabilite and meridianiite were grown from supersaturated aqueous solutions of D_2O and ground to a powder. Neutron diffraction data from these powders were collected on the HRPD instrument at the ISIS neutron spallation source, Rutherford Appleton laboratory. Highly accurate lattice parameters obtained from these data as a function of temperature allow determination of the molar volume and full thermal expansion tensor, as well as yielding crystal structures which are used to provide insight into the origin of the behaviour of the bulk elastic properties of the crystal.

Computational method: Quantum mechanical (first principles or *ab initio*) calculations were done using VASP (Vienna *Ab initio* Simulation Package) with PW91 GGA functional, known to produce good results with hydrogen-bonded systems. For each structure, we calculate the total energy of the crystal as a function of molar volume (e.g., Fig. 2) and obtain the relevant material parameters by fitting equations of state. Integrated forms of the well-known 3rd-order Birch-Murnaghan equation of state (BMEOS3) [4] and of the 4th-order logarithmic equation of state (LNEOS4) [5] are fitted to the E(V) points to determine the zero-pressure volume, V_0, the zero-pressure bulk modulus, K_0, its first pressure derivative, $(dK/dP)_0$ or K_0', and in the case of LNEOS4, the second pressure derivative, K_0".

Experimental results: Figure 1 shows the volume thermal expansivity of mirabilite [6] and meridianiite [7] as determined by fitting the neutron data with Debye and Einstein models of the crystals' internal energy. The volume thermal expansion of both phases is similar to that of epsomite [8], and considerably smaller than that of ice Ih [9].

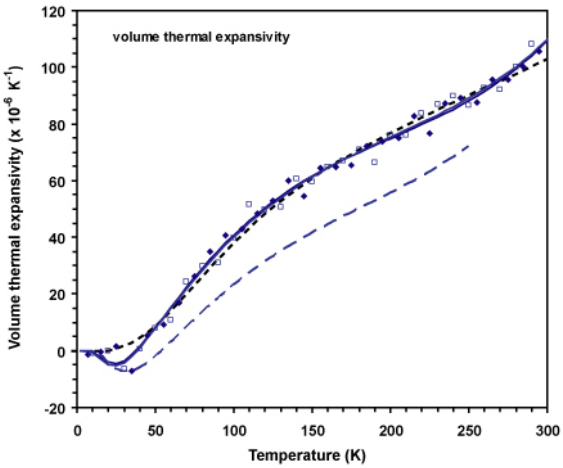

Figure 1. Comparison of the volume thermal expansion coefficient α_V, for deuterated mirabilite from Debye (solid line) and Einstein (dotted line) models. The dashed line shows the volume thermal expansion of meridianiite [7] for comparison.

Our analysis of the thermal expansion in relation to structural elements in both crystals reveals that hydro-

gen-bonding is responsible for the magnitude and orientation of the expansion tensors as a function of temperature (and, in all probability, pressure as well). In mirabilite, the two interstitial water molecules appear to dominate, and in meridianiite it is the bifurcated interlayer hydrogen bond. Although we intend to explore the thermoelastic behaviour using high-pressure neutron diffraction during 2008, we have already acquired a detailed understanding of how these hydrogen-bonds affect the bulk crystal properties using quantum mechanical calculations.

Computational results: Figure 2 shows the calculated E(V) curve for mirabilite, fitted with equations of state; parameters obtained from these fits (for both mirabilite and meridianiite) are given in Table 1. In both cases the difference between the calculated and measured V_0 is ~ 3 %, which is typical of these types of calculations.

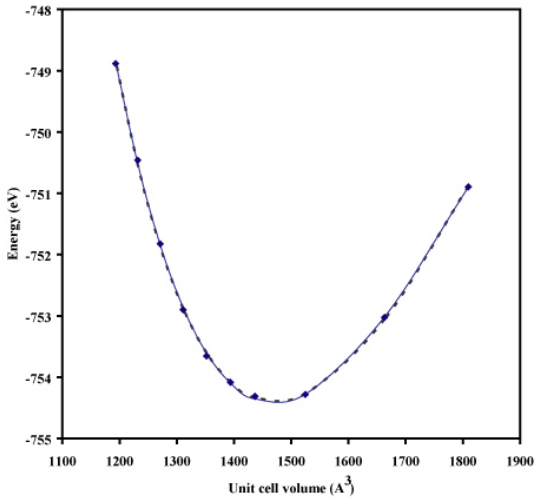

Figure 2. The *ab initio* E(V) curve for mirabilite. The points are the calculations, the solid line is a LNEOS4 fit and the dotted line a BMEOS3 fit. The fit parameters are given in Table 1.

It is of some interest to note that the calculated bulk moduli of mirabilite, meridianiite, and epsomite [8] are all identical (within errors), despite major differences in intermolecular bonding. Both mirabilite and meridianiite exhibit major discontinuities in their elastic properties at high pressure (~ 5 GPa) which are the result of very small changes in the hydrogen-bond network. In the case of meridianiite, we find that changes in the bifurcated h-bond result in rotation of the $Mg(H_2O)_6$ octahedra, such that a *single* hydrogen-bond donated to a sulfate tetrahedron breaks, and reforms to a $Mg(H_2O)_6$ octahedron. Such small structural changes would be a challenge to observe experimentally at present, illustrating the value and complementarity of computational mineral physics in the study of planetary ices.

Summary: The evolution and dynamics of the icy satellites are governed by the behaviour of the consituent materials of the satellites. Modelling of these planetary bodies requires a combination of experimental and computational techniques to obtain the necessary thermoelastic properties and polymorphic phase behaviour. Quantum mechanical calculations make a significant contribution to this effort, allowing the rapid determination of physical properties for the kinds of complex low-symmetry salt hydrates that may comprise such moons. The results we have obtained here give us the confidence to tackle much more difficult problems, using the *ab initio* method, such as calculation of diffusion coefficients as a route to understanding diffusion creep processes in these crystals.

References: [1] Kargel, J. S. (1991) *Icarus* **94**, 368. [2] Dalton *et al.* (2005) *Icarus* **177**, 472. [3] Orlando *et al.* (2005) *Icarus* **177**, 528. [4] Birch, F. (1952) *J. Geophys. Res*. **57**, 227 [5] Poirier, J.P. and A.Tarantola (1998) *Phys. Earth Planet. Int.* **109,** 1. [6] Brand *et al., submitted.* [7] Fortes *et al.* (2008) *Phys. Chem. Min*., doi:10.1007/s00269-008-0214-x [8] Fortes *et al.* (2006) *Eur. J. Min*. **18**, 449 [9] Röttger *et al.*, (1994) *Acta Cryst. B* **50**, 644.

Acknowledgements: The authors wish to thank the STFC ISIS facility for beam time, and technical support staff for invaluable assistance. HEAB is funded by a postgraduate studentship from the Natural Environment Research Council; ADF is funded by a fellowship from the Science and Technology Facilities Council.

Table 1. Fitted thermoelastic parameters for mirabilite and meridianiite from *ab initio* simulation.

	Mirabilite		**Meridianiite**	
	BMEOS3	LNEOS4	BMEOS3	LNEOS4
V_0 (Å³)	1471(2)	1470(2)	722.0(3)	722.1(3)
E_0 (eV per unit cell)	-754.392(2)	-754.411(3)	-403.667(2)	-403.667(2)
K_0 (GPa)	22.1(2)	23.3(8)	23.1(1)	22.8(6)
K’	5.2(3)	5.1(2)	2.9(3)	2.9(3)
K” (GPa^{-1})	-	0.7 (3)	-	0.4(12)

EPHEMERAL ICES ASSOCIATED WITH THE MARTIAN SOUTH POLAR RECESSION. A. J. Brown[1], [1]SETI Institute, 515 N. Whisman Rd, Mountain View, CA 94043, email: abrown@seti.org, web: http://abrown.seti.org.

Introduction: From February to August 2007, Mars went through spring in the Martian southern hemisphere. During this period, the seasonal cap of carbon dioxide sublimed into the atmosphere gradually as temperatures at the surface rose.

The Compact Reconnaissance Imaging Spectrometer carried out observations of this process and we have put together a mosaic of the south pole every two Earth weeks (one MRO programming cycle) [1]. Here we present some of the mosaic sequences and suggest laboratory work that might be applicable to understanding the process of springtime recessions on Mars.

Compact Reconnaissance Imaging Spectrometer for Mars (CRISM): CRISM is a visible-infrared (0.4-3.9μm) imaging spectrometer that is now in orbit around Mars [2] and has been collecting data since November 2006. CRISM takes measurements with 544 channels. CRISM has many modes of operation, including Full Resolution Targeted (FRT), Half Resolution Long (HRL) and Half Resolution Short (HRS) observation.

Observations: The mosaics were constructed from CRISM Multispectral (MSP) mapping observations and hence have 55 bands covering the 1-4 micron region of the spectrum, with a pixel size of ~185m across. Each mosaic covers all regions poleward of 55ºS. Mosaics are presented in polar stereographic projection, constructed from MSP strips that are ~12km across on the surface. The number of strips in each mosaic varied between 56 and 475, depending on the number of observations that were taken over each fortnight. As such, it was not possible to cover the entire pole each fortnight.

We present 'ice maps' that have been constructed using absorption features of CO_2 and H_2O ice, in a manner similar to the OMEGA team [3]. We used the 1.5 micron band of H_2O ice and the sharp 1.4 micron of CO_2 ice to determine wether these ices were present, putting each pixel into a 'CO_2', 'H_2O', 'CO_2 and H_2O mixture', or 'No ice' category (Figure 1-2). All processing was carried out by the MR PRISM software package for CRISM analysis [4].

At this stage of our analysis, we have not separated atmospheric from surface effects, though this work is ongoing [5]. Early spring observations indicate a large amount of water ice is present over most of the cap, possibly in the form of clouds (Figure 3). As springtime proceeds, more interesting juxtapositions of ice form, particularly in the 'Cryptic region', which shows spatial mixtures of water and CO_2 ice as well as no ice at all in places (Figure 4). Higher resolution images suggest that the water ice at these times is most likely on the surface in the form of a lag. The high spatial reolution of CRISM enables this process to be revealed in detail. The last vestiges of water ice are detected at around L_s=251 (Figure 5). The asymmetric recession of the south polar cap is captured after L_s=270 (Figure 6). At this point, no water ice is detected by CRISM.

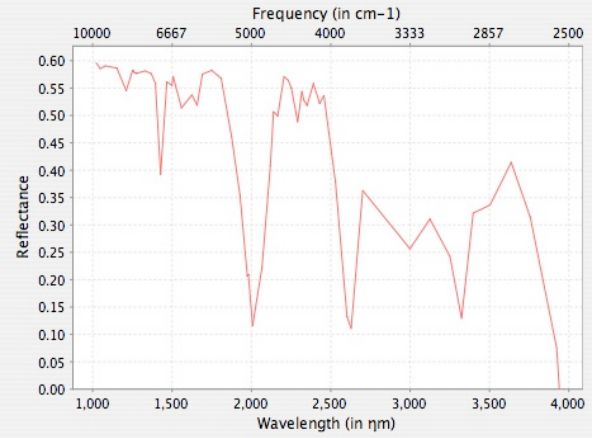

Figure 1. Example CRISM 'L channel' (1-4 micron) spectrum of 'pure' CO_2 ice. Note sharp 1.4 micron band and no overlapping broad 1.5 micron water ice band. Note strong 3.3 micron CO_2 ice band.

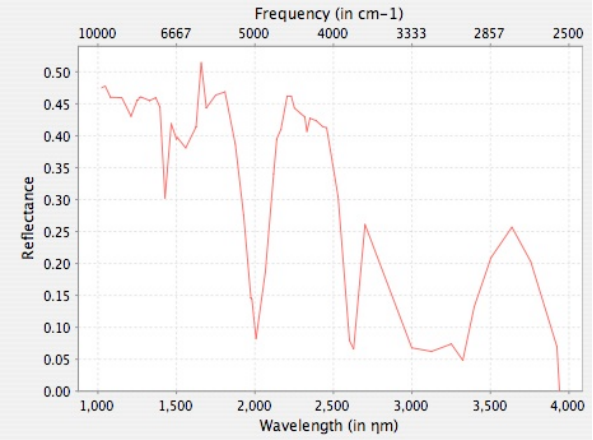

Figure 2. Example CRISM 'L channel' (1-4 micron) spectrum of CO_2 and H_2O ice mixture. Note overlapping broad 1.5 micron water ice band has been superimposed on CO_2 1.4 micron band. Note the 3.3 micron CO_2 ice band is subdued.

Laboratory work: The challenges of replicating the Mars polar regions, with temperatures at 145K and pressures of 6 mbar, have meant only a limited number of studies have been carried out in this area. A couple of ideas for future work relevant to the CRISM observations include:

Studies of H_2O and CO_2 mixtures. Water and carbon dioxide ices have only received limited attention (e.g. [6]). The coexistence of these ices in the Martian polar caps (particularly in the north) opens up a wide field of laboratory work possibilities to explore the properties of these mixtures and test them against CRISM observations.

Annealing of CO_2 ice in Martian polar conditions. Theoretical models of the development of CO_2 ice have suggested that it may form an 'annealed polycrystalline layer' [7], which has been invoked to explain cold CO_2 jets in the south polar regions [8]. This has been suggested to be at odds with observations [9]. Laboratory simulations of CO_2 annealing in Martian polar conditions may offer a fascinating test of this theory and throw light on these observations.

References: [1] Brown, A.J. et al. (2007) *AGU* #P33A-1016 [2] Murchie, S. et al. (2007) *JGR* 112 [3] Langevin Y. et al. (2007) JGR 112 10.1029/2006JE002841 [4] Brown, A.J. and Storrie-Lombardi, M.C. (2006) *SPIE Optics and Photonics* doi:10.1117/12.677107 [5] Brown A.J. et al. (2008) *LPS XXXIX*, #2140. [6] Bernstein M. P. et al. (2005) *Icarus, 179*, 527-534. [7] Elusciewicz J. (1993) *Icarus*, 103, 43-48. [8] Kieffer, H. et al. (2006) *Nature* 442 793-796 [9] Langevin, Y. et al. (2006) *Nature*, 442, 790-792.

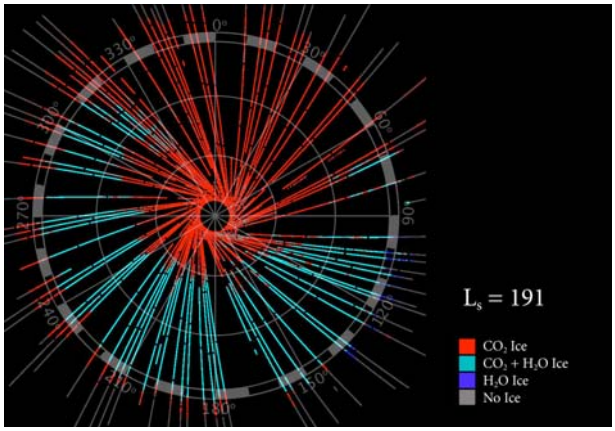

Figure 3. Example mosaic for CRISM observations from February 2007 (Ls=191 on Mars). See text for discussion.

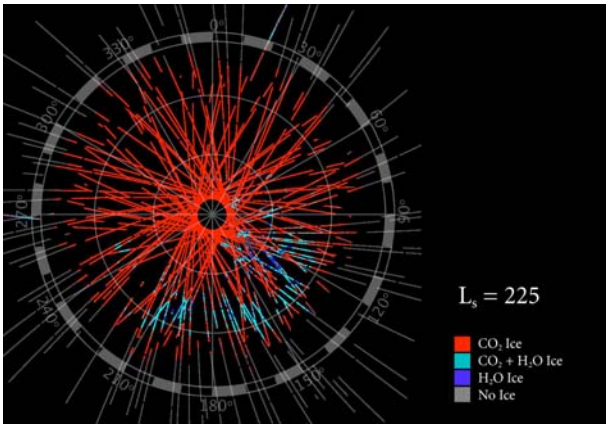

Figure 4. Example mosaic for CRISM observations from March 2007 (Ls=225 on Mars). See text for discussion.

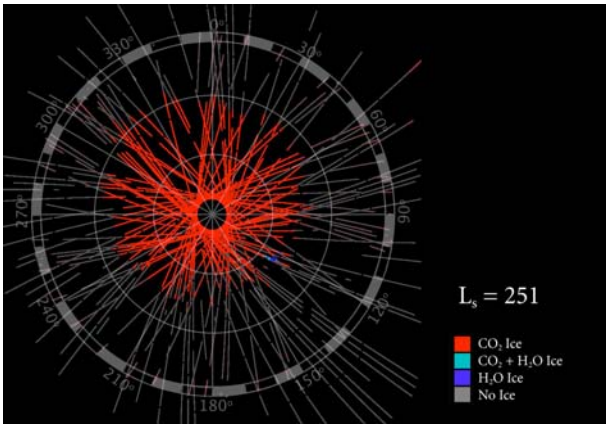

Figure 5. Example mosaic for CRISM observations from April 2007 (Ls=251 on Mars). See text for discussion.

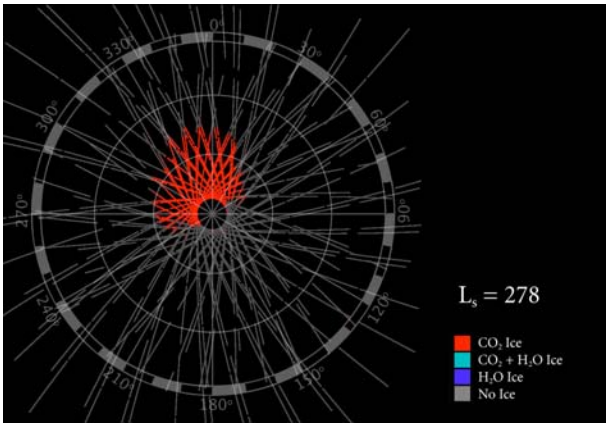

Figure 6. Example mosaic for CRISM observations from June 2007 (Ls=278 on Mars). See text for discussion.

Acknowledgements: Thanks go the CRISM Science and Operations team at JHU APL for their dedication in bringing this dataset to realization.

OBSERVATIONS OF IRRADIATION CHEMISTRY IN THE KUIPER BELT. M.E. Brown[1]
[1]Division of Geological and Planetary Sciences, Caltech, Pasadena, CA, 91125, (mbrown@caltech.edu)

For many years there has been an observational disconnect between laboratory and telescopic observations of irradiation chemistry in the outer solar system. Laboratory studies have found an array of hydrocarbons that should be created, but objects in the outer solar system have mostly been observed to have pure methane and/or red surfaces often interpreted as complex fully irradiated hydrocarbons, with no intermediate irradiation products observed.

The large Kuiper belt object 2005 FY9 is the first body to finally show a full range of irradiation products. While on bodies such as Pluto and Triton much of the methane is locked in low concentration solutions with nitrogen, on 2005 FY9 the methane is essentially pure. This purity allows irradiation processing to proceed, and a host of hydrocarbon compounds have now been detected on the surface.

Additional objects in the Kuiper belt are now also known to have essentially pure methane which supports rapid irradiation processing, and irradiation products have also now been seen on these bodies.

I'll discuss what we now know about irradiation processing in the Kuiper belt in light of the studies of the surface of 2005 FY9 and other Kuiper belt objects, and I'll highlight terrestrial laboratory studies that are needed for interpretation of observations of this Kuiper belt laboratory.

ION IRRADIATION AND THE COLORS OF TNOS. R. Brunetto[1,2], and G. Strazzulla[1], [1]INAF-Osservatorio Astrofisico di Catania, Italy, [2]Institut d'Astrophysique Spatiale, CNRS, University of Paris-Sud, Orsay, France

Solar wind and cosmic ion irradiation affects the surface properties of airless bodies. Effects such as chemical and structural modifications have been investigated in the laboratory, as well as the induced changes in the spectral slope of frozen gases. Visible and near-infrared reflectance spectra of trans-Neptunian objects and Centaurs revealed a great variety of colors that are believed to be the result of a competition between aging (e.g., cosmic ion irradiation) and rejuvenating (e.g., impacts with space debris, cryovolcanism, etc.) processes [1,2].

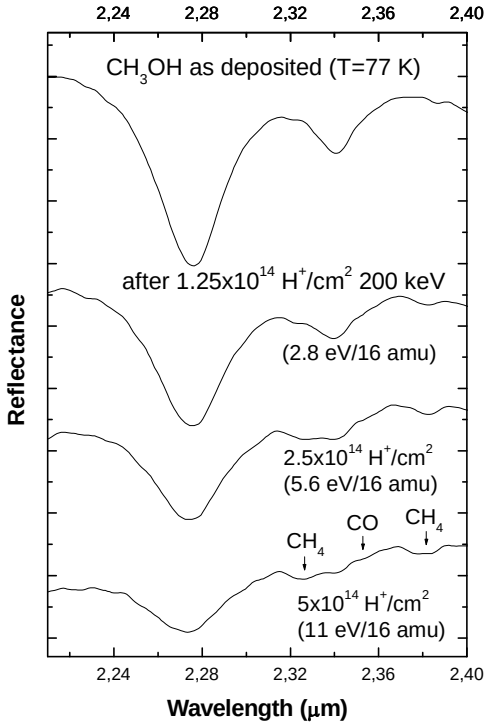

Figure 1: Reflectance spectra (2.2-2.4 μm) showing the formation of CH_4 and CO after irradiation of frozen (77K) methanol with 200 keV protons.

Here we present the results of ion irradiation experiments performed by irradiating frozen C-rich targets with 100's keV H and Ar ions. We evidence the formation of new molecular species. An example is given in Figure 1 that shows the formation of CH_4 and CO after 200 keV H^+ irradiation of frozen methanol [3].

Irradiation of frozen (16–80 K) methanol (CH_3OH), methane (CH_4), and benzene (C_6H_6), with 200 keV H^+ and Ar^+ ions, and 400 keV Ar^{++} ions, up to a dose released to target molecule of about 350 eV per 16 amu, evidences a strong reddening and darkening of the spectra (see e.g. Figure 2), due to the formation of an organic (C-rich) refractory residue [4].

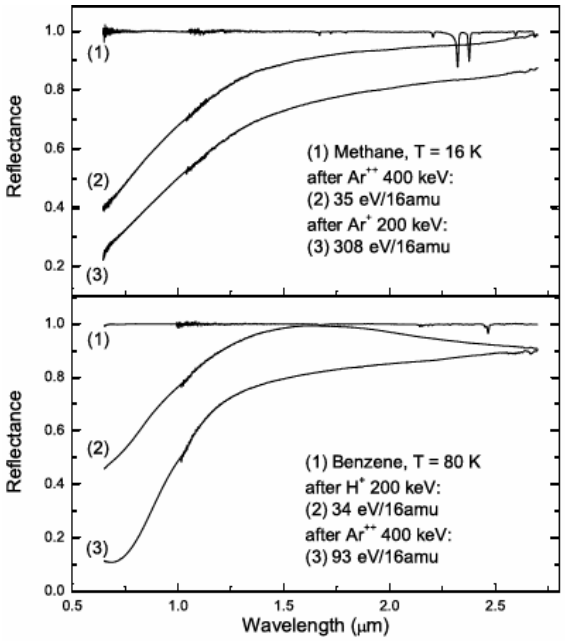

Figure 2. Absolute reflectance of as-deposited and ion irradiated methane at 16 K, and benzene at 80 K.

The laboratory spectra are compared with the spectra of some Centaurs and TNOs: we find that the colors of many icy objects in the outer Solar System are reproduced by laboratory spectra. Those objects could have grown an irradiation mantle.

References:

[1] Doressoundiram A. et al. (2002) AJ 124, 2279-2296. [2] Peixinho N. et al. (2004) Icarus, 170, 153-166. [3] Brunetto R. et al. (2005) Icarus 175, 226-232. [4] Brunetto R. et al. (2006) ApJ, 644, 646-650.

PHOTOMETRY OF ICY SATELLITES. B. J. Buratti [1]NASA Jet Propulsion Laboratory, California Inst. Of Technology, 4800 Oak Grove Dr. 183-501, Pasadena CA 91109. bonnie.buratti@jpl.nasa.gov

Introduction: Photometry of satellites offers clues on the physical nature of their surfaces. For example, the steepness of the solar phase curve (the function that expresses how the brightness of a celestial body changes with solar phase angle) at large phase angles reveals the roughness of a planetary surface. The compaction state can be derived from studying near-opposition observations. Often, the character of the surface below the resolution limit of a spacecraft camera can be studied by fitting observations to photometric models. Unusual surface texture that could indicate geology activity often exhibits itself first as a photometric clue.

Physical Properties: The Table summarizes the physical parameters that are studied in photometric measurements and modeling. Details of specific models that characterize and fit these parameters are given in [1,2,3,4,5,6,]

Table - Photometric parameters

Parameter	Meaning
Single-scattering albedo	Characterization of fraction of light scattered
Width and amplitude of the opposition surge	Measure of the compaction state of upper regolith and surface particle size
Single particle phase function	Function of the particle size, morphology and indices of refraction
Mean slope angle	Measure of the macroscopic roughness, and thus geologic history

Each of these parameters holds important clues to the current state and past evolution of icy planetary bodies. For example, loose, fluffy surfaces that exhibit large opposition surges are thought to result from a history of sustained meteoritic bombardment or volcanic deposition (as in the case of Io). A high degree of macroscopic roughness (as in the case of the Saturnian satellite Phoebe) is evidence for a history of intense bombardment with large impactors.

Fundamental Photometric Quantities: In addition to these physical parameters, there are important photometric quantities that characterize the energy balance on a planetary surface. For icy bodies, they are especially important to derive because they direct the nature of volatile transport. One such quantity is the phase integral, which expresses the directional scattering properties of a planetary body. When multiplied by the geometric albedo, this quantity yields the Bond albedo. Integrated over all wavelengths, the bolometric Bond albedo is a measure of the total energy balance on a planetary body.

Observations: Both spacecraft imaging and spectroscopic data and groundbased telescopic measurements of a wide range of icy bodies have been fit to photometric models. One important result that has emerged over two decades of work is that icy and rocky bodies exhibit remarkable similarities in their photometric properties. This case is believed to result from the similar mechanical behavior exhibited by rock and ice at low temperatures.

But important differences that indicate disparate geologic histories have emerged. For example, icy satellites that have experienced recent geology or resurfacing tend to have much lower macroscopic roughness [5,7,8]. Different opposition surges on the two hemispheres of Callisto suggest more intense meteoritic bombardment on the leading side [6].

Often photometric observations yield the first clue that something is unusual on a planetary body. For example, observations of Europa by the *New Horizons* spacecraft during its late February encounter with the Jovian system provided key data at solar phase angles that were not attained by *Voyager* [9]. Analysis of these images reveals that the solar phase curve of Europa is remarkable, showing a decrease in brightness between opposition and 70 degrees that is even less than that exhibited by Enceladus. These results imply that the surface of Europa may be covered with a substance or features that tend to scatter in an isotropic fashion, such as snow or deposits from outgassing. The morphology of this material is below the resolution limit of the camera systems that have imaged its surface so far.

References: [1] Horak, H. (1950) *Ap.J. 112,* 449-463. [2] Hapke, B. (1981) *JGR 86,* 3039-3054. [3] Hapke, B. (1984) *Icarus 59,* 49-59. [4] Hapke, B. (1986) *Icarus 67,* 264-280. [5] Buratti, B. (1985) *Icarus 61,* 208-217. [6] Buratti, B. (1995) *JGR 100,* 19061-19066. [7] Helfenstein, P. et al. (1992). *Science 255,* 824-826. [8]. Domingue, D. et al. (1995) *Icarus 115,* 228-249. [9] Grundy, W. et al. (2007) *Science 318,* 234.

Acknowlegement: This work was carried out at the Jet Propulsion Laboratory, California Institute of Technology, under contract to the National Aeronautics and Space Administration.

NITROGEN IN INTERMEDIATE PRESSURE RANGE. R. Caracas[1] and R.J. Hemley[2], [1]Laboratoire de Sciences de la Terre CNRS UMR5570, Ecole Normale Supérieure de Lyon, 46, allée d'Italie, 69364 Lyon cedex 07, France, razvan.caracas@ens-lyon.fr, [2]Geophysical Laboratory, Carnegie Institution of Washington, 5251 Broad Brnach Rd., NW, Washington DC 20015, USA, rhemley@ciw.edu

We predict the existence of new structures of molecular nitrogen in the intermediate pressure regime from first-principles density-functional calculations. First we start from experimental observations on analogous system. A series of structures was examined, from which a structure with Immm orthorhombic symmetry is stable relative to the epsilon and cubic gauche phases in LDA, whereas GGA shows the epsilon and the new orthorhombic structure are energetically competitive [1]. This structure is dynamically stable at least from ambient pressure up to 90 GPa and thus may be observed as a stable or metastable polynitrogen phase prior to the transition to the atomic phases of nitrogen. Second we base our findings on lattice dynamical analysis of experimental data obtained for nitrogen [2]. Unstable optical phonon modes in zone-center of a Pbam structure lead to metastable structures with different orthorhombic symmetries. Some of these structures might be stabilized thermally or kinetically and may appear as intermediate steps on the transition path between molecular and atomic nitrogen.

References: [1] R. Caracas and R.J. Hemley, Chem. Phys. Lett., 442, 65 (2007). [2] E. Gregoryanz et al., J. Chem. Phys., 126, 184505 (2007).

STABILITY OF H_2O ICE POLYMORPHS AT HIGH PRESSURE. R. Caracas[1] and R.J. Hemley[2], [1]Laboratoire de Sciences de la Terre CNRS UMR5570, Ecole Normale Supérieure de Lyon, 46, allée d'Italie, 69364 Lyon cedex 07, France, razvan.caracas@ens-lyon.fr, [2]Geophysical Laboratory, Carnegie Institution of Washington, 5251 Broad Brnach Rd., NW, Washington DC 20015, USA, rhemley@ciw.edu

We employ density functional theory as implemented in the ABINIT package [1] to investigate the high-pressure behavior of H_2O ice. We find that at low temperatures ice VII can transform in a metastable tetragonal structure in the same stability field as ice VIII [2]. Ice VIII is thermodynamically stable to at least up 60 GPa. In the 60-120 GPa pressure range we show based on static (0K) and dynamical calculations that disordered ice X is more stable than ice VIII. In this pressure range ice X is characterized by one unstable flat phonon band, which leads to the disordering of the structure. Ice X is dynamically stable above 120 GPa and up to about 400 GPa pressure. In this range, with compression ice X shows a softening of the lowest phonon mode in M (=1/2 1/2 0), which becomes unstable above 400 GPa. The instability corresponds to collective displacements of the hydrogen and oxygen atoms on (110) planes that induce the bending of the O-H-O angle. The structure that results after the lock-in of this unstable mode is the Pbcm orthorhombic structure obtained from molecular-dynamics calculations [3]. Consequently we propose a high-pressure low-temperature phase-transition sequence as ice VIII – disordered ice X - ice X - ice Pbcm.

References: [1] Gonze et al., Comp. Mat. Sci. 25, 478 (2002); Z. Kristall. 220, 558 (2005). [2] Maddury et al., J. Chem. Phys., 2007. [3] Benoit et al., Phys. Rev. Lett., 76, 2934, 1996.

EXPERIMENTAL STUDIES OF THE SPUTTERING OF MIXED ICES: EUROPA'S SURFACE COMPOSITION AND DETECTION OF TRACE SPECIES BY SURFACE SPUTTERING

R. W. Carlson[1] and K. P. Hand[1], [1]Jet Propulsion Laboratory, California Institute of Technology, Pasadena, CA 91109 (Robert.W.Carlson@jpl.nasa.gov)

Introduction. Nature's ubiquitous high-energy radiation serves conflicting roles in our search for life beyond Earth. While generally considered harmful, radiation may also be beneficial, producing the organic compounds that sparked life and producing chemicals that may support microorganisms. Similarly, our search for life on other worlds may be complicated by radiolytic modification of biomolecules, but that same radiation could also provide a means – by sputtering - for biosignature detection from orbit.

Sputtering and Detection of Surface Material. Europa's surface may contain material upwelled from the ocean below, and if there is extant life within Europa's ocean, then diagnostic biomarkers may exist on Europa's surface. Naturally occurring intense ion bombardment constantly ejects these molecules by a process known as sputtering and can be used to infer surface composition, as first pointed out by Johnson et al in 1998 [1]. They suggested that Europa's surface molecules, including large whole organic molecules, could be investigated by detecting molecules sputtered from the surface that are subsequently photoionized and observable using an orbiting ion mass spectrometer. One can also envision detecting the more plentiful neutral sputter products with a neutral mass spectrometer or by remote sensing of the sputtered atmosphere through mm-wave rotational line spectroscopy, for example. The latter method allows detection of large molecules that do not reach orbital altitudes.

A New Experimental Program. Although there have been many studies of sputtering multi-component metals, there have been few studies of the sputtering of molecules mixed in ice, particularly for those biomolecules of astrobiological interest. Theoretical estimates for the yields indicate different low-cascade density, high-cascade density, and thermal pulse sputtering. Furthermore, the velocity profiles of each ejected species are unknown and must be determined in order predict their altitude distribution and thereby relate a local or column measurement to the surface composition.

Our newly started experimental program determines the yields, molecular fractionation patterns, and velocity distributions of sputtered biosignature molecules in ice. Our current experiments are being performed with a 5-keV pulsed ion gun (Hiden !G20) with time-resolved positive ion, negative ion, and neutral sputter-product determinations employing a quadrupole mass spectrometer (Hiden IDP) and multichannel scalar. Both unirradiated and electron-irradiated biosignature molecules in ice ([2], simulating Europa's surface and radiation environment) are being studied, and results will presented.

[1] Johnson, R. E., et al., 1998. *Geophys. Res. Lett.* **25,** 3257-3260. [2] Hand, K. P. and Carlson, R. W., this Conference

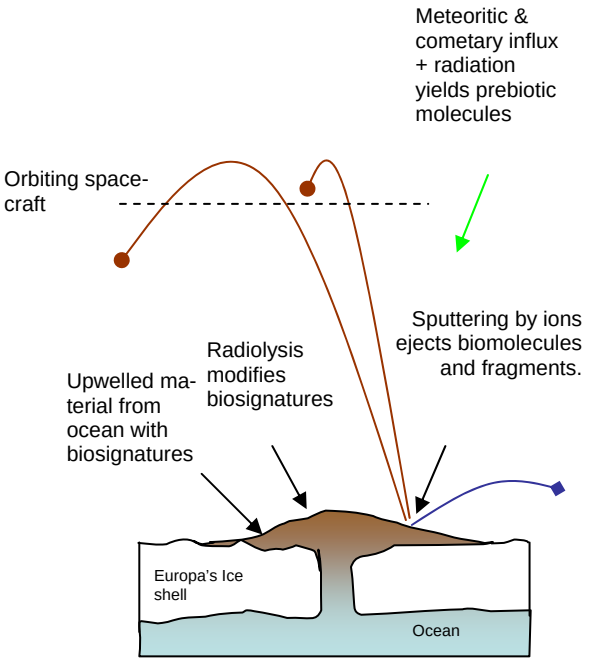

ICE RESPONSE TO CYCLIC LOADING FOR LOW STRESSES AND FREQUENCIES - APPLICATION TO ICY SATELLITES. J. C. Castillo-Rogez[1], F. Zhong[1], M. Barmatz.[1], M. Choukroun[1], H. Engelhardt[2], and C. Sotin[1], [1]Jet Propulsion Laboratory, California Institute of Technology, 4800 Oak Grove Drive, Pasadena, CA 91109 (e-mail address: Julie.C.Castillo@jpl.nasa.gov), [2]California Institute of Technology, 1200 E California Blvd, Pasadena, CA 91125.

Introduction: Tidal heating is considered to be an important energy source controlling the interior dynamics, thermal evolution, and orbital characteristics of icy satellites like Europa, Enceladus or Titan. However the attenuation properties of ices at stresses and frequencies relevant to these icy bodies are still missing. In an effort to determine these characteristics, we have set up an experimental laboratory where ice samples are synthetized, deformed and analyzed. Here we report on the first cycling loading experiments that have been performed on single crystals in order to compare our results to previous results [e. g. 1]. We have started performing a series of tests for temperatures between 150 K and 270 K on single ice crystals and are planning similar tests on polycrystalline water ice samples. We present the experimental setup, sample preparation, preliminary results, and future projects.

Experiments: *Setup:* Measurements were obtained at ambient pressure with an *Instron* compression system equipped with an environmental chamber that can achieve temperatures from 80 K to ambient temperature with a thermal control of 0.2 ºC. The temperature is also controlled just outside the top and bottom of the chamber. We are working on improving the thermal insulation of the whole system in order to limit the impact of diurnal variations within the laboratory. This is especially important when we perform cyclic loading measurements at frequencies lower than 5×10^{-4} Hz over several days.

Samples: We present results obtained for single-crystal water ice. These crystals were grown and characterized in the Mars Simulation and Ice Laboratory at Caltech. Using a single crystal seed, the water was frozen from the bottom to the top of a cylindrical mold in a cold room at -15 ºC at a rate slower than 10^{-6} m/s with air constantly flowing at a slow rate in the remaining water. This method guarantees freezing excluding bubbles and cracks that leads to the production of perfect single ice crystals. Thermal stressing of the samples was avoided during transportation to the measurement system using common water ice at a temperature of -15 ºC.

Measurements: Samples were inserted into the environmental chamber at a temperature of -15 ºC. After thermal equilibrium was achieved, a load was applied to the sample corresponding to a mean stress of 1 MPa. The system was automated and controlled with *LabVIEW*. The measurements proceed as follows: the sample creep under constant load was measured for several hours, followed by a cyclic loading sequence that ranged over ten frequencies from 0.1 Hz down to 6×10^{-6} Hz for stress amplitudes between 0.1 and 0.25 MPa. This range is comparable to the amplitude of tidal stress acting on outer planet satellites. It is important to note the capability of the system to perform accurate position measurements (accuracy better than 2 microns), at strain rates as low as 1×10^{-10} s^{-1}, and stress lower than 1 MPa.

For each temperature we perform an independent measurement of the *Instron* system compliance needed for correcting the measurements obtained on icy samples.

Data Processing: An example of a 69 hr. cyclic loading test is presented in Fig. 1 for a single ice crystal sample tested at -30 ºC, for a mean stress of 1 MPa and stress amplitude of 0.25 MPa. Using the compliance test we can correct the total response from the response of the system. The sharp strain evolution happening during the first three hours is mostly driven by the response of the Instron system to the cooling of the environmental chamber.

At this stage we are still working on characterizing the creep behavior of the sample, whose amplitude is affected by the diurnal variations in temperature. We expect this problem to have a negligible effect on the phase lag, since the maximum thermal variations undergone by the system for the test in Fig. 1 was 5 ^{o}C over 24 hrs (while the longest cycles applied during the test are 3 hrs long). The attenuation of the sample can be inferred from measuring the phase lag between stress and strain, similarly to [1]. The phase lag δ is directly related to the attenuation coefficient (or dissipation factor) Q by $Q^{-1} = \tan\delta$. The phase lag is inferred from signal processing methods (Fourier transform), and by direct visualization of the waves (Figure 3). For the measurements at a frequency of 10^{-4} Hz presented in Figs. 2, we can clearly see the time lag between stress and strain, which is about 420 s in the example displayed in Figure 3, after correction from the attenuation of the system at that frequency inferred from the compliance test. From these initial measurements we estimate a dissipation factor $Q \sim 3\text{-}4$ for a cyclic loading frequency of 10^{-4} Hz.

Analysis of the sample properties for frequencies from 0.1 to 10^{-4} Hz shows a decrease of the attenuation factor from about 60 to about 3. After performing cyclic loading a first time over the range 0.1 to 10^{-4} Hz, we performed another cyclic loading test on the same sample. The results show a difference in the phase lag measured at 10^{-4} Hz, by about 10%, which illustrates the effect of ice history on its attenuation behavior.

Future Activities: We have just started acquiring research-grade data with this new system. Cyclic loading measurements on single ice crystals and polycrystalline ice for various temperatures and stress amplitudes are planned in the near future.

Samples will be characterized using optical polarizing microscopy and cryo-ESEM techniques.

Acknowledgements: Part of this work was performed at JPL under contract to NASA. Part of this work was also carried out in the Mars and Ice Simulation Laboratory at Caltech.

References: [1] Tatibouet Tatibouet, J., Perez, J. and Vassoille, R., 1981, J. Physique. Coll. 42 (C5) 541. [2] McCarthy C. *et al.* (2007) AGU *Fall meet.*, #MR11A-07.

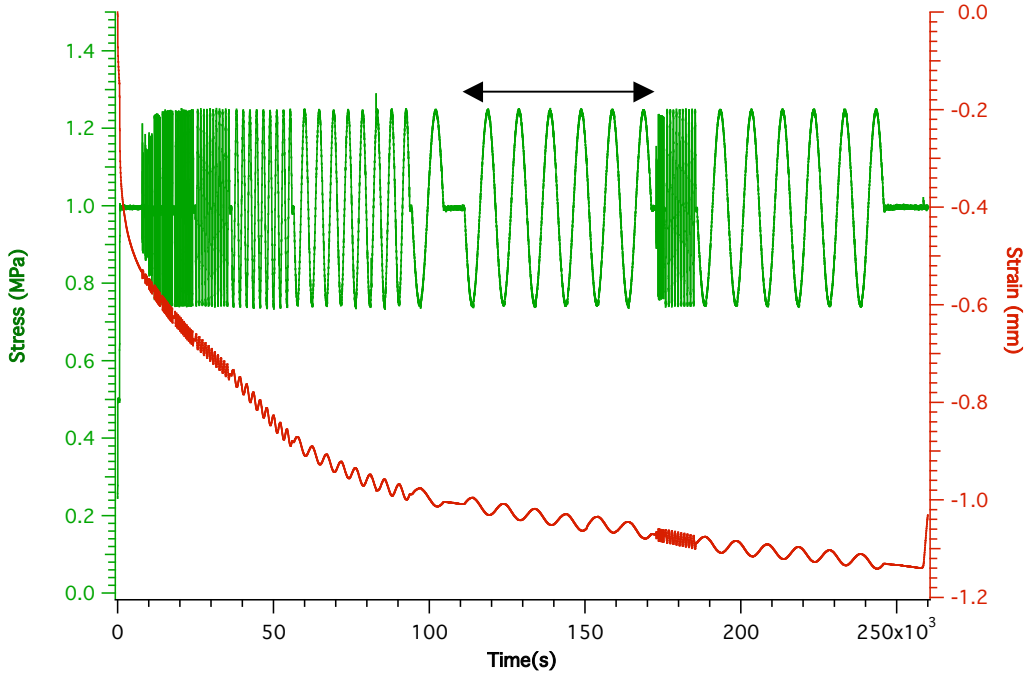

Figure 1. *Stress and strain measured over the full duration of the test on a single ice crystal at -30 °C.*

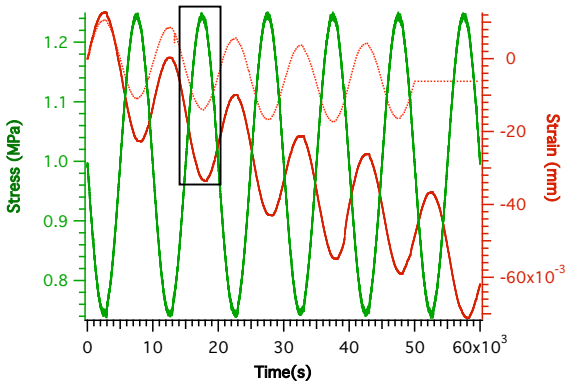

Figure 2. D*etail of the measurements obtained at a frequency of 10^{-4} Hz, shown in Fig. 1 by the horizontal arrows. The plain red line correspond to the measurements obtained on the sample and the dashed red line to the compliance test.*

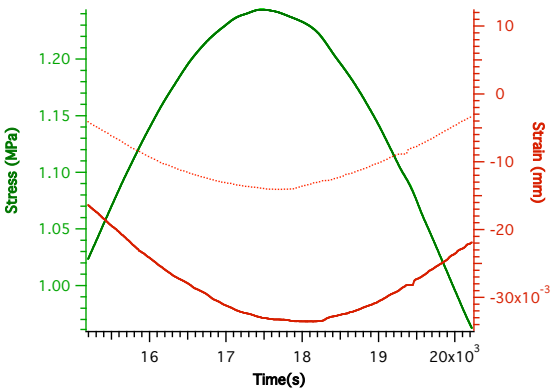

Figure 3. *Zoom of the strain of the sample and of the system obtained during the compliance test for the data highlighted in the box in Figure 2.*

SUBLIMATION KINETICS OF CO_2 ICE ON THE SURFACE OF MARS V. F. Chevrier[1], L. A. Roe[1], K. F. White[2], K. Bryson[1] and D. G. Blackburn[1], [1]Arkansas Center for Space and Planetary Science, University of Arkansas, Fayetteville, AR 72701, USA, [2]Department of Physics & Astronomy, Ball State University, Muncie, IN 47306, USA <vchevrie@uark.edu>.

Introduction: The martian polar caps are in majority composed of CO_2 ice [1-3]. Early modeling of the polar caps suggested that they were in equilibrium with the ~6 mbar CO_2 atmosphere [2], and various observations have shown a ciclicity of growth and retreat, following martian seasons [4]. However, other studies show that CO_2 ice constitutes only a thin veneer on the surface of a probably much thicker ice layer [5]. This veneer is too small for the caps to be in equilibrium with the atmosphere [6,7]. This would also suggest that the polar caps are very young [8]. Therefore, there must be a much larger unidentified CO_2 reservoir in the martian subsurface, possibly adsorbed CO_2 in the regolith [9,10], to buffer the much larger atmosphere, or it means the total budget of CO_2 is present in the atmosphere, and that Mars has today much less CO_2 than other telluric planets.

However, the majority of dynamic models of the polar caps are based on CO_2 ice sublimation, lacking laboratory confirmation. Most studies use thermal modeling [2] or geomorphic observations [7] to study sublimating CO_2, but the details of CO_2 sublimation in a CO_2 atmosphere remain unknown, and could have deep implications for the dynamics of the polar caps on the martian surface. We report here the experimentally measured sublimation rate of pure CO_2 ice under simulated martian conditions, as done previously for H_2O [11,12].

Methods: Dry ice was packed into a beaker with a thermocouple above surface of the dry ice and, in later experiments, a second thermocouple placed inside the dry ice. Our planetary environmental chamber was evacuated to less than 0.09 mbar, filled with dry gaseous CO_2 (g) to atmospheric pressure, and cooled to between 0 and -10ºC. Once stable, the chamber was opened and the sample was placed on a top loading analytical balance inside the chamber. The platform supporting the balance and the sample was then lowered into the chamber. The chamber was then evacuated to 7 mbar. Experiments lasted ~1 hour and mass, pressure, and temperature were recorded every minute. Pressure and atmospheric temperature were maintained between 6.5 and 7.5 mbar and -11 to -1ºC, respectively. Before and after each experiment the height and diameter of the dry ice was measured.

Results: The mass loss of CO_2 is extremely linear, with R^2 coefficients systematically above 0.99 (Fig. 1). The mass loss in g min^{-1} is converted into sublimation rate E_S in mm h^{-1} using the density and the surface area of the sample. Results are summarized in Table 1 and show remarkably constant values, validating the reproducibility of our experiments. The average value for CO_2 ice is 1.20 ± 0.27 mm h^{-1}. These results are less than one order of magnitude higher than *in situ* measurements of polar caps retreat showing 0.13-0.19 mm h^{-1} [4] and 0.36 mm h^{-1} [6]. This suggests a common process for the sublimation mechanism on Mars and in our chamber.

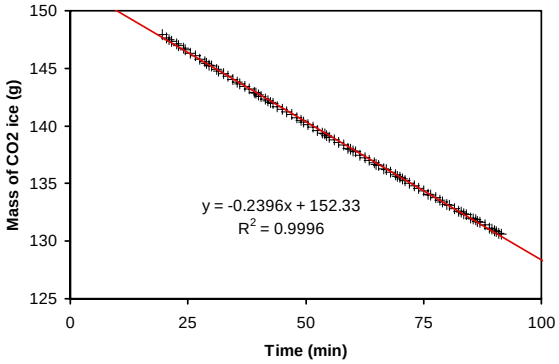

Figure 1. Mass of CO_2 ice as a function of time (sample #3 in Table 1).

Table 1. Sublimation rates E_S for the 10 samples studied in our chamber.

#	Texture	Mass loss (g min^{-1})	E_S (mm h^{-1})
1	Gravel	0.46	1.06
2	Solid block	0.24	1.01
3	Solid block	0.24	0.99
4	Powder	0.34	1.36
5	Powder	0.37	1.63
6	Powder	0.34	1.68
7	Loose powder	0.47	1.22
8	Loose powder	0.43	1.09
9	Packed powder	0.33	0.91
10	Packed powder	0.36	1.04

Discussion: It has been shown previously that surface temperature controls the sublimation rate of water ice [11,13]. We measured the temperature profiles inside the sample, a about 3 mm above the surface and 20 cm above the sample (Fig. 2). The temperature of the atmosphere remains very constant during the experiments, as well as the sample temperature at 148–153K, which corresponds to the equilibrium temperature of CO_2 at 7 mbar. This is exactly what is observed on the surface of Mars, where the polar caps are usually at the temperature 150K, thus in thermal equilibrium with the atmospheric pressure. The temperature a few mm above the surface is higher, 30 to 60K, as a result of the strong gradient between the

surface and the atmosphere. The sudden increase in the sample temperature at t = 18 min (Fig. 2) results from the fact that the thermocouple reaches the surface when the ice is recessing due to sublimation. The temperature then converges towards the temperature a few mm above the surface.

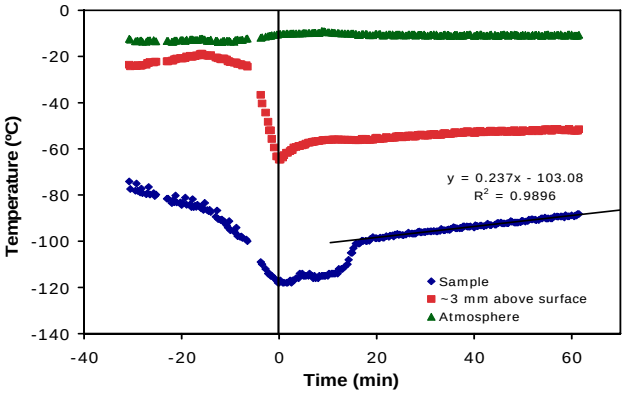

Figure 2. Thermal profiles of the atmosphere, 20 cm above the sample (green), 20 mm above the surface (red) and inside the sample (blue), obtained during sublimation of CO_2 ice at 7 mbar.

The CO_2 sublimation process is governed by heat transfer between the chamber and the ice, and by diffusion of the sublimated molecules from the surface. There are three possible heat transfer processes: conduction from the ice surface into the ice interior, heat transfer from the warmer atmosphere to the cooler ice surface, and radiation from the chamber walls to the ice surface.

At the beginning of the experiment, the thermocouple below the ice surface reads ~150K, indicating that conduction has caused the ice to reach internal thermal equilibrium during the approximately 30 min pump-down. As a result, the surface and interior of the ice are at the same temperature, eliminating conduction into the ice as a heat transfer model. At this point, the ice surface has reached the solid - vapor equilibrium temperature associated with chamber pressure (7 mbar, 150K, Fig. 2). Therefore sublimation occurs because the atmosphere is too warm compared to the cold ice surface (263K against 150K, Fig. 2).

Thermal conduction in the CO_2 atmosphere is too low to be an efficient process in the chamber. Since the ice surface is considerably colder than the atmosphere, there are no buoyancy effects creating free convection, and there is no wind to create forced convection. Therefore, sublimation of CO_2 ice is controlled by radiation from the walls. We therefore use the following equation to describe CO_2 ice sublimation:

$$E_S = \frac{\Delta E_{rad}}{\rho_{ice} \Delta H^{sub}_{298K,1bar}} \qquad (1)$$

where ΔE_{rad} is the energy absorbed by the surface (W m^{-2}), ρ_{ice} is the CO_2 ice density (1562 kg m^{-3}) and $\Delta H^{sub}_{298K,1bar}$ is the latent heat of sublimation (571.3 × 10^3 J kg^{-1}). Our calculations show that radiative energy from the walls at 263K is about 220 W m^{-2}, giving a sublimation rate of 0.89 mm hr^{-1}, a value close to experimental results (1.2 mm hr^{-1}). Including the conduction from the atmosphere (~20 W m^{-2}) raises the sublimation rate to 0.97 mm hr^{-1}.

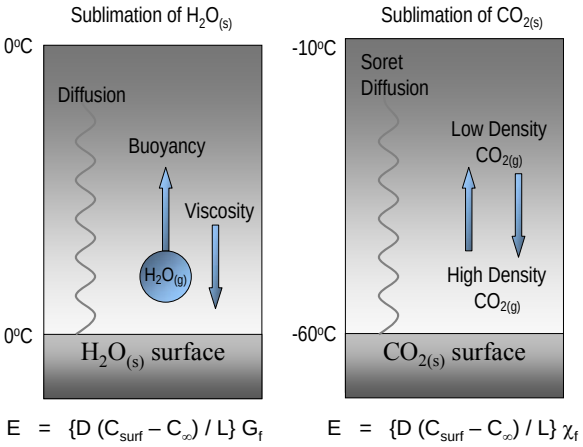

Figure 3. Comparison between sublimation processes of H_2O and CO_2 ice on Mars. Water ice sublimation is mostly driven by diffusion and buoyancy into the heavier CO_2 atmosphere [13]. In the case of CO_2, the density gradient is reversed since the atmosphere is less dense than the surface. This situation simplifies the heat transfer to radiation from the walls only (no possible convection, and very low conduction from the gas phase).

Conclusions: Our experimental results suggest that radiative transfer is controlling sublimation. Interestingly, our radiative energy value is very close to the highest values calculated for martian polar caps (about 250 W m-2 at 85ºN). This explains the strong similarity between our measured sublimation rate and values measured from polar caps recession [4,6].

References : [1] Langevin Y. et al. (2005) *Science* 307, 1581-1584. [2] Leighton R. B., B. C. Murray (1966) *Science* 153, 136-144. [3] Murray B. C., M. C. Malin (1973) *Science* 182, 437-443. [4] Smith D. E. et al. (2001) *Science* 294, 2141-2146. [5] Bibring J. P. et al. (2004) *Nature* 428, 627-630. [6] Malin M. C. et al. (2001) *Science* 294, 2146-2148. [7] Byrne S., A. P. Ingersoll (2003) *Science* 299, 1051-1053. [8] Fishbaugh K. E., J. W. Head III (2001) *Icarus* 154, 145-161. [9] Fanale F. P. et al. (1982) *J. Geophys. Res.* 87, 10215-10225. [10] Fanale F. P., W. A. Cannon (1971) *Nature* 230, 502-504. [11] Chevrier V. et al. (2007) *Geophys. Res. Lett.* 34. [12] Sears D. W. G., S. R. Moore (2005) *Geophys. Res. Lett.* 32. [13] Ingersoll A. P. (1970) *Science* 168, 972-973.

NEW GROWTH SETUP OF PLANETARY CLATHRATE HYDRATES ANALOGS FOR PHYSICAL PROPERTIES MEASUREMENTS. M. Choukroun, M. Barmatz, and C. Sotin, NASA Jet Propulsion Laboratory, California Institute of Technology, 4800 Oak Grove Dr, Mail Stop 79-24, Pasadena, CA, 91109, E-mail: mathieu.choukroun@jpl.nasa.gov.

Introduction: Clathrate hydrates are inclusion compounds, with an ice-like structure that consists in an arrangement of ice cages in which guest gas molecules are trapped individually. These structures are stabilized by van der Waals interactions between the gas and the cages [e.g. 1]. Their potential ubiquitous occurence in the Solar System [e.g. 2] has strong implications in various domains: quest for future energy resources [3], climatology of the Earth [4] and Mars [5], astrophysics [6] and outer planets and icy satellites compositions [7]. Clathrate hydrates could especially play a significant role on the evolution and in the dynamic processes occurring on icy satellites, such as methane outgassing from the interior on Titan [e.g. 8,9]. Addressing the physical properties (mechanical behavior, thermal conductivity, density) of these compounds is essential to improve our current understanding of geophysical properties of icy satellites. We present a new high-pressure apparatus for the generation of clathrate hydrates with relevant compositions to icy satellites. Expected results on clathrate hydrates thermo-physical properties from measurements conducted on these samples are also presented.

Clathrate hydrates and implications for the behavior of volatiles in icy satellites: Clathrate hydrates are thought of as a likely trap for volatiles in the outer presolar nebula, prior to planets and satellites accretion [e.g. 7,10]. These icy structures can contain up to 14 percents of gas, these significant amounts being compatible to some extent with planetary abundances expected on giant planets and their moons. Particularly, large amounts of N_2, CH_4, CO_2, and noble gases (Ar, Xe) may have been accreted in planetesimals and satellitesimals and could thus have contributed significantly to the volatile budget of icy satellites [10].

Influence on the thermal evolution of icy satellites: The density contrast between clathrate hydrates and other species (ammonia hydrates, salt hydrates, high-pressure phases of ice, etc) within the H_2O-dominated interior of icy satellites could have led to the early formation of a segregated layer of clathrate hydrates. Density, but also stability and thermal conductivity of clathrate hydrate depend highly on the nature of the guest gas, or of the gas mixture in equilibrium with clathrate hydrates. As an example, the density of clathrate hydrates varies from 0.92 (methane clathrate) to 1.25 or more (CO_2 clathrate). Therefore, segregated layers of clathrate hydrates can exist above or below the primordial ocean in the icy moons of Jupiter and Saturn. A recent study [9] has shown that the heat release of Titan through time decreases drastically if an outer clathrate hydrate shell is present, thus delaying crystallization of the internal ocean. As the thermal conductivity of clathrate hydrates is up to five times smaller than that of ice [e.g. 1 and references therein], even the presence of small amounts of clathrate hydrates within an icy shell would have a significant impact on the thermal behavior of the crust. Furthermore, tidal heating is a key issue in the development of convective plumes within the icy shells [e.g. 11]. Therefore, good knowledge of the mechanical properties of clathrate hydrates is also essential to understand the dynamics of icy satellites and their thermal evolution.

Role in volatile release from the interior via cryovolcanism: Observation of potentially cryovolcanic features on Titan [12,13], as well as measurements of large amounts of CH_4 and CO_2 in Enceladus' plume [14] by the instruments onboard the Cassini spacecraft, raise the problem of volatile outgassing from the interior in icy satellites. Methane clathrate hydrates dissociation at depth has long been a hypothesis for Titan's atmospheric methane replenishment [e.g. 15]. Recent experimental [8,16] and numerical [9] studies have shown that such dissociation can only occur at a local scale and through a succession of events involving reaction with ammonia-water cryomagmas at shallow depth [16]. Dissociation of clathrate hydrates containing a gas mixture (CO_2, CH_4, N_2) has also been proposed as the source of Enceladus plume volatiles [17]. However, these studies only focused on the dissociation at equilibrium. Experimentally, dissociation of methane clathrate hydrates has been observed within their stability field during mechanical measurements [18]. Understanding the mechanical behavior of clathrate hydrates and its potential impact on the stability of these structures can thus bring new constraints on cryovolcanic processes and the release of volatiles on the icy moons of Jupiter and Saturn.

Experimental setup for clathrate hydrates generation: The apparatus under development for clathrate hydrates generation consists of a high-pressure vessel, cooled by a refrigerated circulator. Indeed, generation of clathrate hydrates is much easier to achieve under pressure, and reaction kinetics is improved.

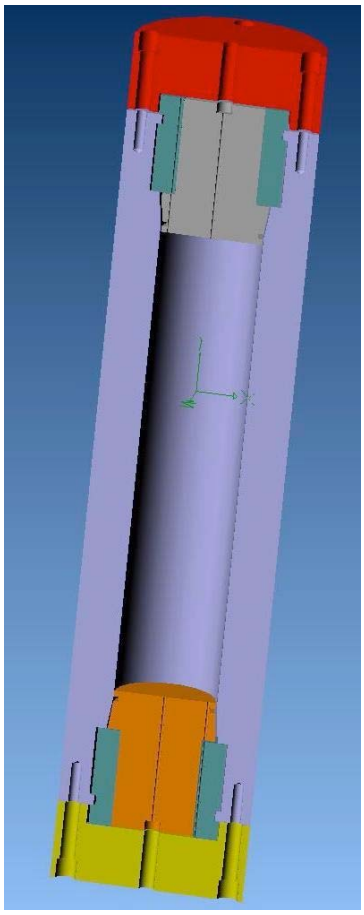

Figure 1. Preliminary design for the high-pressure autoclave. An O-ring type closure system with two lids and a bolted cover will be used for rapid access to the samples after formation.

High-pressure vessel: The high-pressure vessel is a custom-built autoclave, developed with Autoclave Engineers. A 3D view of the item ordered is presented in Fig. 1. The 1-liter autoclave has a maximum allowable working pressure of 200 bars, with a 316-type stainless steel body that can sustain temperatures down to 240 K under pressure. It is equipped with two inlet/outlet valves, for pressurizing the system with sample gas (CO_2, CH_4, N_2). Internal dimensions of the vessel are 2.5 in. diameter and 12 in. length. A Pt100 probe will be placed in the allocated thermowell to provide an external temperature control to the Lauda RP-855 C that will be used to cool the system.

Procedure: Due to the slow kinetics of clathrate hydrates formation, the programming capabilities of the RP-855C circulator will be used to perform temperature cycles around the dissociation curve of clathrate hydrates with corresponding composition. Growth of the crystals will be controlled by the temperature ramping and initial size. The procedure followed will be similar to that described in [1].

Expected results: Pure clathrate hydrates of CH_4, CO_2, and N_2, will be generated with this apparatus. Preservation of the samples will be ensured by transport in a liquid nitrogen-cooled container. The initial large clathrate sample will be cut to appropriate size for several types of measurements with the facilities available at the JPL Cryoices Lab [19]: *1)* thin sections will be observed within an Instec cryostage placed under a microscope, for characterization and structural analysis of the grains; *2)* samples with a length of 2 in. will be used for mechanical measurements using an Instron 5848 system; *3)* samples with a length of 0.25 in. will be used for thermal conductivity measurement following the method described by [20].

Mechanical measurements to be conducted with the Instron 5848 System at cryogenic temperatures include determination of the Young's modulus, creep properties, stability under differential stress, and cyclic loading at icy satellites conditions [21]. These new results, combined with thermal conductivity measurements, will help constrain the mechanical and thermal state of a mixed ice-clathrate crust on icy satellites, with implications on their evolution and the cryovolcanic processes that can take place.

Acknowledgments: This work has been conducted at Jet Propulsion Laboratory, under contract with NASA. MC is supported by a NASA Postdoctoral Program Fellowship, administered by Oak Ridge Associated Universities.

References: [1] Sloan E. D. Jr (1998), Marcel Dekker, New York, NJ. [2] Miller S. L. (1961), Proc. Natl. Acad. Sc. **8**, 1798-1808. [3] Kvenvolden K. A. (1999), Proc. Natl. Acad. Sc. **96**, 3420-3426. [4] Jacobsen S. B. (2001), *Nature* **412**, 691-693. [5] Pellenbarg R. E. et al. (2003), *J. Geophys. Res.* **108** (E4), 8042. [6] Lunine J. I. and Stevenson D. J. (1985), Astrophys. J. Suppl. Series **58**, 493-451. [7] Gautier D. amd Hersant F. (2005), Space Sci. Rev. **116**, 25-52. [8] Loveday J. S. et al. (2001), Nature **410**, 661-663. [9] Tobie G. et al. (2006), Nature **440**, 61-64. [10] Hersant F. et al. (2008), Icarus, in press. [11] Tobie G. et al. (2005), Icarus **175**, 496-502. [12] Sotin C. et al. (2005), Nature **435**, 786-789. [13] Lopes R. M. C. et al. (2007), Icarus **186**, 395-412. [14] Porco C. et al. (2005), Science **311** (5766), 1393-1401. [15] Lunine J. I. and Stevenson D. J. (1987), Icarus **70**, 61-77. [16] Choukroun M. et al. (2008), Lunar Planet. Sci. Conf. XXXIX Abstracts, #1837. [17] Fortes A. D. (2007), Icarus **191**, 743-748. [18] Durham W. B. et al. (2003), J. Geophys. Res., 108 (B4), doi:10.1029/2002JB001872. [19] Barmatz M. et al. (2008), Lunar Planet. Sci. Conf. XXXIX Abstracts, #1950. [20] Zhong F. et al. (2008), Lunar Planet. Sci. Conf. XXXIX Abstracts, #2343. [21] Barmatz M. B. et al. (2008), Lunar Planet. Sci. Conf. XXXIX Abstracts, #2281.

SPECTROSCOPIC REMOTE SENSING OF SOLAR SYSTEM ICES: LABORATORY RESEARCH AND APPLICATIONS FOR MAPPING COMPOUNDS. Roger N. Clark, U. S. Geological Survey, Mail Stop 964, Box 25046 Federal Center, Denver, CO, 80225, USA, rclark@usgs.gov.

Introduction: Spectroscopic remote sensing is the dominant method for studying surface composition of solid surfaces in the solar system, from Earth-based telescopes, spacecraft, and from landers. Chemical composition is a key component to understanding the origin and evolution of planetary surfaces.

Many spectrometers and imaging spectrometers have flown, are currently flying/orbiting and will soon be encountering solar system bodies. We currently have huge data banks of imaging spectroscopy data for the Earth, Mars, Jupiter and Saturn systems, as well as some asteroids, comets, and soon Pluto.

Spectroscopy: Imaging spectrometers acquire data with enough spectral range, resolution and sampling at every pixel in a raster image so that individual absorption features can be identified and spatially mapped. Further, with such sampling, the information in the spectral data are inherently self-verifying in many cases using known information in the remote scene [1]. This verification allows refinement and monitoring of spectral wavelength calibration (e.g., using known absorptions) as well as surface reflectance (e.g., spikes and offsets are "non-physical"). Imaging spectrometers are being used to map many minerals, amorphous materials, man-made materials (on the Earth), and sample solids, liquids and gases.

However, interpretation of solar system of solid surfaces spectroscopic data remains a challenge. Presently, we have no theoretical models that can generate spectra of molecular solids, and the radiative transfer models currently in use have deficiencies. While modeling is important for understanding compositional details, those models must employ basic spectroscopic data derived from laboratory measurements. With tens of thousands of compounds, plus complexities of elemental substitutions into lattices causing shifting of absorption band positions, combined with temperature and pressure effects, radiation damage/modification, and grain size effects, decades of laboratory research has only scratched the surface of what is needed to rapidly interpret exotic planetary surfaces. In some cases, even basic compounds have yet to be measured with spectroscopy. In other cases, measurements have only been made of thin films in transmittance whereas remote observations are made in reflectance or emittance. Sometimes measurements have been made at room temperature and applied to outer solar surfaces without knowing that temperature radically changes the spectrum of the material. Limited a wavelength ranges or poor spectral resolution in either the observed or laboratory data can lead to identifications of compounds not supported by other wavelength ranges/resolutions. New absorption features are discovered in planetary data for which there are currently no known compounds that match, thus driving the need for expanding current spectral databases. Some laboratory data only exists in one wavelength region (e.g. mid-infrared transmittance), when the preponderance of remotely-sensed spectra of solar system ices is from the UV to near infrared (reflected solar radiation wavelength range, ~0.1 to ~5 microns).

Discussion: This talk will review some of the applications that have already been accomplished, current problems, topics that might be addressed in the near future, and it will discuss some of the difficulties in advancing the science of mapping chemistry of solar system ices. Historical examples will be shown as well as recent results from current missions such as Cassini.

References:

[1] Clark, R. N., G. A. Swayze, K. E. Livo, R. F. Kokaly, S. J. Sutley, J. B. Dalton, R. R. McDougal, and C. A. Gent, Imaging spectroscopy: Earth and planetary remote sensing with the USGS Tetracorder and expert systems, *J. Geophys. Res.*, 108(E12), 5131, doi:10.1029/2002JE001847, pages 5-1 to 5-44, December, 2003.

LABORATORY INVESTIGATIONS RELEVANT TO THE EROSION OF ICE ON TITAN. Geoffrey C. Collins[1], Leonard S. Sklar[2], Beth Zygielbaum[2], and Peter Polito[2], [1]Physics and Astronomy Dept., Wheaton College, Norton MA 02766, [2]Dept. of Geosciences, San Francisco State University, San Francisco CA 94132. gcollins@wheatoncollege.edu

Introduction: As images of Titan's surface have been returned over the past few years, it has become abundantly clear that erosion is a dominant geological process on Titan. Vast "sand seas" of dunes imaged by the Cassini RADAR [1] and the rounded gravel and cobbles on the surface imaged by the Huygens probe [2] both point to the mobility and processing of sediment on the surface. Branching, sinuous valley networks observed in many areas of Titan [2, 3] point to fluvial erosion as an important process modifying Titan's surface. The paucity of impact craters on the surface [4] makes the question of the rate of erosion on Titan especially interesting.

Titan is the only icy satellite to display such Earth-like surface processes. As we begin to investigate the detailed physical mechanisms that control these processes, we are currently hampered by a lack of knowledge about some of the relevant physical properties of ice. Here we discuss some of our efforts to fill this gap, and mention other studies that could be undertaken to further our understanding of geological processes on Titan's surface.

Erosion of bedrock stream channels: The central process likely to be setting the overall erosion rate on Titan is the incision of stream channels into the ice "bedrock" that composes the core of topographic features such as mountain chains and crater rims. The dark materials seen in the bottoms of the stream channels at the Huygens landing site are probably exposures of this water ice-rich material [5]. The physical mechanisms by which stream channels are incised into bedrock is currently a subject of active terrestrial research (e.g. as reviewed in [6]). On Titan one of the most effective mechanisms of fluvial incision [7] is likely to be wear of the streambed by saltating bedload.

Sklar and Dietrich [8] have developed a model of the physical mechanisms that control wear by saltating bedload, confirmed by experimental work on various rock samples. This model accounts for enough of the underlying physics that it can be applied directly to the Titan environment, explicitly accounting for the different gravity, fluid, and material parameters [7]. However, there is one unknown material property that controls the rate at which ice will be eroded.

Bedrock at the bottom of a stream channel is slowly chipped away by low-velocity impacts as sediment particles hop and roll along the streambed. The rate at which these chips are detached from the bedrock is proportional to the kinetic energy of the impacts and the capacity of the material to store elastic energy, as defined by $\sigma^2 / 2E$ where σ is the tensile yield strength and E is Young's modulus [8]. The nondimensional constant of proportionality that controls the rate is called the abrasion susceptibility coefficient, and it needs to be determined experimentally.

Abrasion susceptibility of water ice: Initial, crude attempts to measure the abrasion susceptibility of water ice at Titan temperatures were attempted by repeatedly dropping small weights onto ice disks cooled with liquid nitrogen [7]. These experiments showed ice to be about two orders of magnitude more susceptible to abrasion than most rocks. With lower gravity and less dense sediments on Titan, there is less kinetic energy delivered to a streambed by sediment impacts. If water ice is as weak as these experiments showed, the two factors cancel out and we should expect the rate of incision on Titan to be very similar to that on Earth [7]. However, these initial experiments were flawed by imprecise control of the input energy and ambient temperature, and lack of facilities for precisely measuring the wear rate.

We are currently running a new set of experiments to determine the abrasion susceptibility of polycrystalline water ice under better-controlled conditions and with better measurement facilities. Details of the experimental methods are described in a companion abstract [9]. Since the wear rate is a function of both the abrasion susceptibility and the tensile strength, the first step is to firmly nail down the tensile strength of our experimental

samples. We are currently exploring the dependence of ice tensile strength on temperature, and testing the hypothesis that below a temperature of about 220 K tensile strength becomes insensitive to further reductions in temperature.

Other relevant parameters: Though it is one of the dominant factors controlling erosion, understanding the incision of fluvial channels into ice bedrock is only part of the full picture. In particular, there are several aspects of Titan hydrology and regolith processes that must be explored in order to build a more accurate picture of stream flow on Titan. To make progress in understanding Titan surface processes, we suggest that other studies should be undertaken in the future to investigate the following:

• *Coating organics onto ice grains:* How do organics in Titan's cold surface environment interact with water ice on the surface? When looking at sediments on the surface, are ice particles likely to be separated from solid organic particles, or can organics form surface coatings on the ice particles? This is important for understanding the range of possibilities for Titan regolith mixtures. It is also important for interpreting the spectral data from Titan's surface [5].

• *Infiltration of liquid methane into ice-based regolith:* What are the wetting properties of liquid methane in a porous water ice matrix, and what flow rates would be predicted through ice regolith? How would these be affected by the presence of organics in the regolith, either as separate particles or as surface coatings on the ice? This is important for understanding the subsurface hydrology on Titan, including aquifer holding capacity, discharge rates from springs, and the relationship between precipitation and runoff.

• *Mechanical properties of saturated ice regolith:* How does the saturation of ice-based regolith with liquid methane affect its mechanical properties, and how much fluid is needed to reach its liquid limit? How does the presence of organic particles or coatings change these mechanical properties? This is important for understanding hillslope processes, sediment supply into streams, and the role of landslides in modifying Titan's landscape.

Conclusion: In the coming months we will be measuring abrasion rates, ice tensile strength, and elastic modulus across a range of temperatures representative of conditions on Titan and other planetary surfaces. These measurements will provide a good quantitative description of the abrasion suscpetability of ice, including its possible dependence on temperature. Once we have measured this key parameter we will have a much more solid understanding of the efficacy of fluvial abrasion on Titan. This will lay the groundwork for investigating the rates of landscape evolution on Titan, and for understanding the surface geology of this strangely Earth-like icy satellite.

References: [1] Lorenz et al. (2006) *Science* 312, 724-727; [2] Tomasko et al. (2005) *Nature* 438, 765-778; [3] Elachi et al. (2005) *Science* 308, 970-974; [4] Wood et al. (2008) *LPSC XXXIX*, #1990; [5] Soderblom et al. (2007) *Planet. Space Sci.* 55, 2025-2036; [6] Whipple et al. (2000) *GSA Bull.* 112, 490-503; [7] Collins (2005) *Geophys. Res. Lett.* 32, L22202; [8] Sklar and Dietrich (2001) *Geology* 29, 1087-1090; Sklar and Dietrich (2004) *Water Resour. Res.* 40, W06301; [9] Sklar et al. (2008) this meeting.

Acknowledgements: This work is supported by grant NNX07AL26G from the Outer Planets Research Program.

THE SYNTHESIS AND DIRECT DETECTION OF O-ATOMS IN WATER ICE. P. D. Cooper[1], M. H. Moore[2] and R. L. Hudson[3], [1]Department of Chemistry and Biochemistry, MS 3E2, George Mason University, 4400 Universtry Drive, Fairfax, VA 22030, pcooper6@gmu.edu [2]NASA/Goddard Space Flight Center, Astrochemistry Branch, Code 691, Greenbelt, MD 20771, Marla.H.Moore@nasa.gov [3]Department of Chemistry, Eckerd College, 4200 54th Avenue South, St. Petersburg, FL 33711, hudsonrl@eckerd.edu

Introduction: There have been several recent laboratory investigations of the formation of molecular oxygen from irradiated water ice [1-3]. This is of particular interest in the formation of O_2 on the surface of the icy Galilean satellites [4-5] and also an O_2 atmosphere associated with Saturn's rings [6-7]. Both sources of O_2 are postulated to be formed from the radiolytic and/or photolytic destruction of H_2O molecules in the ice grains of these objects.

Experimental: In brief, we prepare gaseous mixtures of H_2O + $^{18}O_2$ (6:1) in a vacuum manifold. Millipore water was freeze-pump-thaw cycled multiple times to remove dissolved atmospheric gases. The $^{18}O_2$ (Isotec; purity of >97%) was used without further purification. Blank experiments on irradiated pure $^{18}O_2$ produced $^{18}O_3$ and no other detectable isotopologues. The H_2O + $^{18}O_2$ gaseous mixtures were then deposited onto an aluminum mirror, cooled to 10 K by a closed-cycle helium refrigerator. The samples are then warmed to 80 K at ~2 K/min. An increase in the vacuum chamber base pressure at ~30 K indicates that some of the O_2 sublimes out of the ice. This is consistent with previous work [8]. Due to the sublimation of some of the O_2, the exact H_2O to O_2 ratio is unknown. The samples are then irradiated with 0.8 MeV protons generated from a Van de Graaff accelerator. IR spectra are measured using a Nicolet 6700 Nexus spectrometer at 4 cm^{-1} spectral resolution.

Results: The figure below shows spectra of a

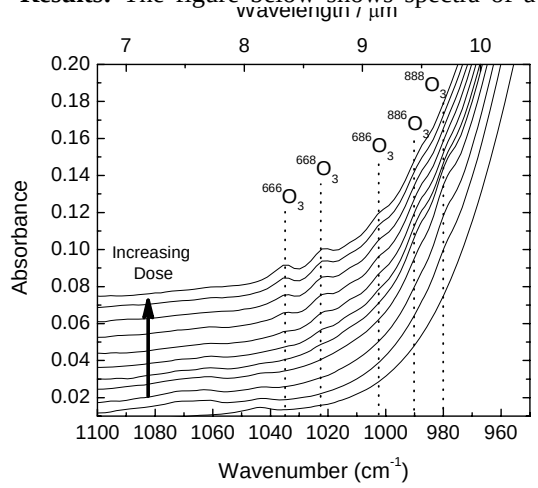

6:1 H_2O + $^{18}O_2$ sample with increasing radiation dose. As the dose increases a broad but shallow absorption band appears at 980 and 990 cm^{-1} associated with the formation of the 888 and 886 isotopologues, where 8 represents an ^{18}O atom and 6 represents a ^{16}O atom. The 888 is produced from residually trapped $^{18}O_2$ molecules that are nearest neighbors. The irradiation of pure $^{18}O_2$ did not yield any measurable ozone isotopolgues containing ^{16}O and there is no measurable amount of CO_2 atmospheric contaminant in our sample. The ^{16}O atom in the 886 must originate from H_2O. The 888 species is gradually destroyed with increasing dose by the replacement of ^{18}O by radiolytically-produced ^{16}O to form 886.

We have considered the possibility that the source of ^{16}O in these experiments could be from ^{16}OH formed in the radiolytic destruction of H_2O. An ozone molecule containing a ^{16}O atom could then be formed by the following reactions.

$$OH + O_2 \rightarrow HO_3 \rightarrow H + O_3$$

However, calculations [9] show that this reaction probably does not occur to any great extent. The HO_3 intermediate is only marginally below the OH + O_2 state on the ground state HO_3 potential energy surface. These workers have shown that the O + HO_2 and H + O_3 states are accessible in the gas-phase when the reacting O_2 and OH are in highly excited vibrational states. These excited states are likely to be very rapidly quenched in the cold ices in discussion in the present work.

Conclusions: Using a band strength of 1.4 x 10^{-17} cm $molecule^{-1}$ for the ν_3 band of O_3, and assuming that it is the same for all isotopologues, we have calculated that there is 0.14% O atoms by number relative to H_2O at the highest dose of 9.8 eV/16-amu molecule. In pure water ice, without the presence of $^{18}O_2$ to trap the ^{16}O atom as an ozone isotopologue, it could be argued that the highly reactive ^{16}O atom may react with water or another water radiation fragment (such as H or OH) before ever encountering a second radiolytically produced ^{16}O atom. If the ozone isotopologues produced in the present work were dissociated and the ^{16}O atoms were to reform exclusively as $^{16}O_2$, then there would be 0.07% O_2 by number, relative to H_2O. This small amount of O_2 is far beyond the detection limits of our spectrome-

ter in pure water, but using the O_3 tracer molecule, we can detect the O atom production which would otherwise form O_2.

It is common in radiation chemistry to present production rates as a yield, *G*, the number of molecules produced per 100 eV of energy absorbed. We have calculated an effective $G_{H+}(^{16}O)$ (calculated from the number of ^{16}O atoms measured in ozone isotopologues) to be 0.013. Again however, this value represents a lower limit due to the O atoms that cannot be directly measured in this experiment and it is only an effective G-value as we are actually not measuring ^{16}O atoms directly, but indirectly in the form of ozone isotopologues.

Estimates of the O_2 abundance on Ganymede range from 0.1 - 1.0% [10] to 1.4 - 4.2% [11]. While our percentage abundance is lower than these estimates, our value represents a lower limit estimate that is in good agreement with the observations.

References: [1] Orlando T. M. and Sieger M. T. (2003) *Surf. Sci. 528*, 1-7. [2] Petrik N. G. et al. (2006) *J. Phys. Chem. B 110*, 2723-2731. [3] Teolis B. D. et al. (2006) *Astrophys. J. 644*, L141-L144. [4] Spencer J. R. et al (1995) *JGR 100*, 19,049-19,056. [5] Spencer J. R. and Calvin W. M. (2002) *Astrophys J. 124*, 3400-3403. [6] Tokar R. L. et al. (2005) *GRL 32*, L14SO4; [7] Johnson R. E. et al. (2006) *Icarus 180*, 393-402. [8] Loeffler M. J. et al. (2006) *Astrophys J. 639* L103-L106. [9] Yu H. G. and Varandas A. J. C. (2001) *Chem. Phys. Lett. 334*, 173-178. [10] Calvin W. M. et al. (1996) *GRL 23*, 673-676. [11] Hand K. P. et al. (2006) *Astrobiology 6*, 463-482.

NEAR-INFRARED LABORATORY SPECTROSCOPY OF CH4/N2 ICE MIXTURES: IMPLICATIONS FOR ICY DWARF PLANETS

D. M. Cornelison[1], S. C. Tegler, W. Grundy, M. Abernathy
[1]Dept. of Physics and Astronomy, Northern Arizona University
(david.cornelison@nau.edu)

The near-infrared spectra of CH4/N2 ice mixtures grown at 21 K were measured for CH4 concentrations ranging from 100% down to 0.5%. As the CH4 concentration was reduced, the spectral features corresponding to the combination modes in the 4200−4300 cm^{-1} range showed a progressively greater shift to the blue. Surprisingly, even the 98% CH4 sample exhibited a small blueshift of approximately 0.4 cm^{-1}. The 6% sample exhibited a blueshift of approximately 2 cm^{-1}. Band pro-files of the 0.5% sample exhibited major differences compared to band profiles of samples richer in CH4. The blueshifts and band profile changes of the CH4 bands suggest they could serve as a proxy for CH4/N2 abundance on the surface of icy dwarf planets. To link the acquired lab data to possible astronomical spectra, a Hapke model was used to generate reflection spectra at resolutions comparable to spectrographs on a ground-based telescope and aboard the New Horizons spacecraft.

ELECTRICAL PROPERTIES OF AMORPHOUS AND CRYSTALLINE ICES. J.P. Cowin and M.J. Iedema, Pacific Northwest National Laboratories, M/S K8-88, Box 999, Richland WA 99352, jp.cowin@pnl.gov, 2Pacific Northwest National Laboratories, M/S K8-88, Box 999, Richland WA 99352, martin.iedema@pnl.gov.

Introduction: Water ices in space, whether vapor deposited on pre-planetary grains, or as part of moons and icy planets, can easily become highly electrically polarized. This is due to any one of: preferential molecular alignment during vapor-growth, charge accumulation from ambient charges or from photo-electron -ion ejection, or from ion rejection during freezing. These polarizations and voltages (1000's of volts), can cause enhanced sticking of icy grains, and help explain the rapid agglomeration of dust into planetesimals. It also can play a role in the chemical evolution of molecules imbedded in or upon ice. We explored several of these mechanisms, and also the highly inelastic nature of low-temperature vapor-grown amorphous ice. The stongly pryo-piezoelectric nature of water ice (demonstrated for the first time) helps assure that these electric fields are very difficult to mask.

Water ice deposited from the vapor phase occurs in the solar system over a wide range of temperatures. Below 120 K it deposits as amorphous ice, and above this, as crystalline. The asymmetry of the vacuum-ice interface causes the water molecules to deposit with a slight net O-end out [1] [2] (Figure 1), that leads to voltages across the water ice of 10's to 100 V per micron of water thickness. This is enough to create high electrtic fields that can drive transport of ions, and non-thermal chemistry.

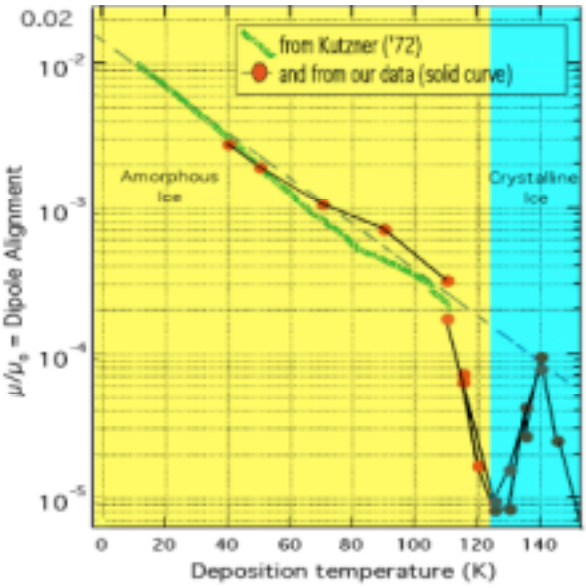

Figure 1: Spontaneous alignment of water dipoles in vapor grown ice. [1][2]

Such voltages derived from vapor deposition would in many cases be quickly masked, by ions/electrons, depositing and shielding the external fields. However, our recent work [3] shows that, contrary to what has been assumed, that water ice is strongly pyroelectric below 150 K. This means that as the temperature fluctuates in water ice from varying solar flux, or from collisions of icy grains, that large voltages can appear across ice that previously had no external fields.

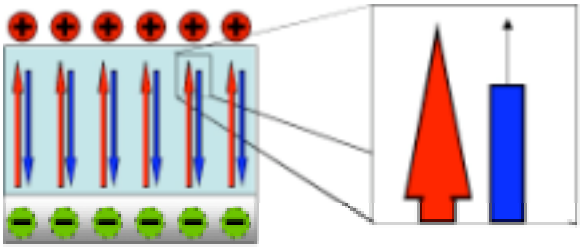

Figure 2. Pyroelectric water ice occurs from "poled" water ice. [3]

Figure 2 shows why. Above 150K, where the water dielectric constant is active,and large, the voltage that would be created by positive charges, only under the influence of electronic and vibrational/librational polarizability of the water, would give the voltage shown by the red arrow. Above 150 K, reorientation of water dipoles counters 95% of that voltage, with the blue voltage, to give the observed voltage (at right). Above 150 K, these stay in strict equilibrium. But below 150K, each arrow changes independently with T, though only a percent or two. That is enough to create large pyroelectricities, and can quckly generate 10 to 100's of volts across micron-thick ices. These effects were applied to help understand how icy grains might agglomerate fast enough to make planets [4], and may also help drive chemistry and transport in water ice.

References: [1] M.J. Iedema et al., (1998) JPC B, 102 (46), 9203 -9214. [2] K. Kutzner, (1972) *Thin Solid Films, 14*, 49-61. [3] H. Wang, et al., (2008) JPC (in press). [4] H. Wang, et al., (2005) *Astrophys. J., 620*, 1027–1032,

Cryogenic Infrared Reflectance Spectroscopy of Acetylene and Cyanoacetylene. John M. Curchin[1], Clark, R.N[1]., Shaffer, C.[2], Mc Mahon, R.J.[2], and Hoefen, T.M.[1], [1]U.S. Geological Survey, Mail Stop 964, Box 25046 Federal Center, Denver, CO, 80225, USA, jcurchin@usgs.gov, [2]Deptartment of Chemistry, University of Wisconsin, Madison, Wisconsin, 53706, USA

Introduction: As part of the USGS Spectroscopy Lab's continuing efforts to integrate organic compounds into its spectral database, the primary alkyne, acetylene (C_2H_2), and the first of the cyano-polyyne series ($HC_{2n+1}N$), cyanoacetylene, HC_3N have now been characterized in the visible and near to mid-infrared. Each compound was investigated in reflectance, over the wavelength range from 0.35 microns to 15.5 microns (Fig. 1). Measurements were taken at approximately 80 Kelvins for the pure substance, and in each case the sample was a white ice that was ground to a fine powder. Additionally, both compounds were mixed with a dark spectrally neutral compound and measured again in order to unsaturate the deep C-H stretch absorptions near 3 microns.

Results: In doing so, we explore the nature of the C-H stretch when associated with a carbon-carbon triple-bond skeleton, and find that the absorption moves from approximately 3.36+ microns in the singly carbon-bonded alkanes, to 3.24+ microns in the doubly-bonded alkenes, and to 3.05 microns in the alkynes [1], in response to the increasing strength of the multiply-bonded carbon backbone. As such, acetylene ice can be mistaken for water ice on a planetary surface when imaged by relatively low resolution spectrometers. We caution investigators not to mistake acetylene ice for water ice when interpreting spectra of icy satellite surfaces based on a 3 micron feature.

Numerous other fundamental, overtone and combination absorption bands are identified and compared, particularly absorptions due to the C≡C and C≡N bonds. This has allowed a current discrepancy in the organic spectroscopic literature regarding these triply-bonded band assignments to be resolved, as well as shed light on the nature of cyanide compounds in the mysterious 'dark component' of the icy surfaces of numerous Saturnian satellites. Finally, reflectance spectra of cyanoacetylene frost, a possible component in the haze aerosols and on the surface of Titan, will be presented publicly for the first time.

References:

[1] Clark, R.N., Curchin, J.M., Hoefen, T.M., and Swayze, G.A. (2008), Reflectance Spectroscopy of Organic Compounds I: Alkanes, J. Geophysical Research (in review).

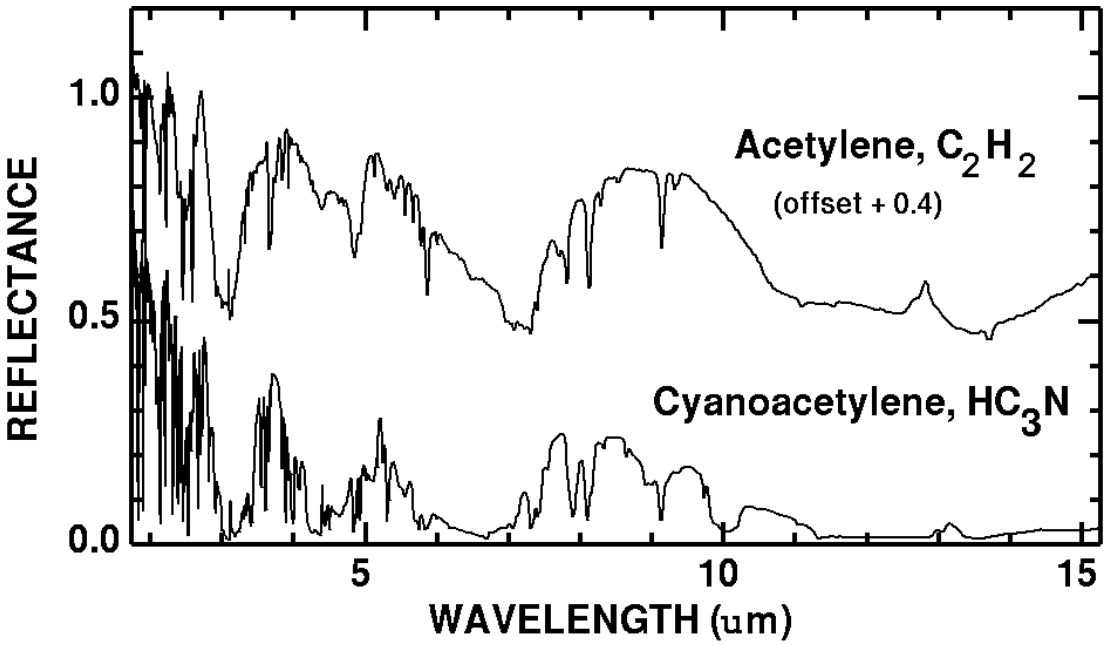

Figure 1. Reflectance spectra of pure acetylene and cyanoacetylene powders.

A SUMMARY OF MISSION-CRITICAL CRYOGENIC LABORATORY SPECTRAL MEASUREMENTS FOR DETERMINATION OF ICY SATELLITE SURFACE COMPOSITION FROM ORBITAL SPACECRAFT OBSERVATIONS. J. B. Dalton, III[1], [1]Planetary Ices Group, Jet Propulsion Laboratory, MS 183-301, 4800 Oak Grove Drive, Pasadena, CA 91109-8001.

Introduction: The bulk of our knowledge regarding icy satellite surface composition is derived from visible to near-infrared (VNIR) reflectance spectroscopy, much of it from spacecraft observations. Spectra of planetary surfaces can be modeled either as linear (areal) mixtures, or as nonlinear (intimate) mixtures, to yield estimates of relative abundance of surface compounds. Linear mixture analysis of planetary surface composition requires access to reflectance spectra of the candidate compounds. Nonlinear mixture analysis requires the real and imaginary indices of refraction (optical constants), which may be estimated from reflectance spectra, or derived from a combination of reflectance and transmittance measurements.

Characterization of Surface Compounds: To date, most candidate species proposed as icy satellite surface constituents have not yet been sufficiently characterized to enable such models. Most infrared spectra of candidate icy satellite surface materials published to date were measured in the mid-infrared (MIR) for purposes of understanding the interstellar medium. In order to constrain abundances of surface materials from spectral observations of icy bodies, cryogenic laboratory measurements for all candidate materials are needed with the following characteristics:

Required quantities. First, useful measurements must be of either reflectance or optical constants (real and imaginary indices of refraction). These are the quantities which enable quantitative abundance modeling. By themselves, transmittance, absorbance, absorption coefficient, line strength, optical depth, or other quantities which cannot be converted to reflectance (primarily due to poorly constrained scattering processes) are of limited usefulness.

Required wavelength range. Second, measurements are needed across the full spectral range of typical spacecraft instruments (298 to 5500 nm would cover the Galileo and Cassini cameras and spectrometers). While a compound may only have strong absorption features in part of the wavelength range, it still contributes to the continuum everywhere, including the vicinity of diagnostic features of other compounds. Deconvolving the observations requires laboratory measurements across the full range, for all proposed constituents, particularly where they may coexist.

Required sample thickness. Third, measurements must be conducted with samples sufficiently thick to yield useful absorption features, shapes and strengths. The overtones and combinations which make up most of the VNIR spectral signatures are far weaker than the MIR fundamentals. However, reflected sunlight from cold icy bodies in the outer solar system exhibits insufficient spectral contrast and inadequate signal to enable the identification of surface materials in the MIR so remote-sensing instrumentation for icy bodies concentrates upon the VNIR, where there is more available signal. Yet, a thin film (<~10 microns) in the laboratory does not engender sufficient path length for the weak VNIR absorptions to manifest. This is not a problem for a planetary regolith several meters to kilometers thick, but does present a challenge for laboratory work.

Required temperatures. Fourth, measurements must be temperature-appropriate to the bodies of interest. Most of the candidate compounds (especially ices) display marked spectral changes with temperature. Differences of as little as 5-10 K can be distinguished in laboratory spectra of many materials. In order to explain planetary observations, laboratory measurements in the 50-150 K range will be critical.

Important Candidate Materials: Names and/or chemical formulae (where applicable) for 122 materials proposed as surface materials for icy worlds of the outer Solar System are given in the table. Each of these has either been observed in comets, interstellar molecular clouds, or on icy bodies or asteroids, produced in the lab by chemical, photolytic, radiolytic, or other means, or predicted on the basis of numerical simulations. A search of the published literature reveals a dearth of temperature- and wavelength-appropriate spectral measurements of these materials which can be used for quantitative abundance modeling. This represents a major opportunity for laboratory spectroscopists to conduct measurements which will be of paramount importance in interpreting the available data from modern imaging spectrometers on recent (Galileo), current (Cassini, New Horizons) and planned spacecraft m issions.

Conclusion: Scientific return from spacecraft- and ground-based observations of planetary surfaces will be significantly enhanced by the proper application of cryogenic laboratory spectroscopy. With these measurements in hand, investigators may identify materials, derive their abundances, map their distributions, and infer their roles in the evolution of these enigmatic bodies.

Proposed Icy Satellite Surface Compounds			
Water	H_2O	Hydrogen Sulfide	H_2S
Deuterium Oxide	D_2O	Sulfur Dioxide	SO_2
Heavy Water	HDO	Sulfur Trioxide	SO_3
Hydrogen Peroxide	H_2O_2	Sulfuric Acid	H_2SO_4
Oxygen	O_2	H_2SO_4 Hydrates	H_2SO_4•$8H_2O$, H_2SO_4•$6.5H_2O$
Carbon Monoxide	CO	Sulfur	S_2
Carbon Dioxide	CO_2	Methyl Clathrate	CH_4•H_2O
Carbon Trioxide	CO_3	CO_2 Clathrate	CO_2•H_2O
Formyl ion	HCO	H_2O•graphite	…
Formaldehyde	H_2CO	Bisodium Sulfate	Na_2SO_4
Formic Acid	H_2CO_2	Bisodium Carbonate	Na_2CO_3
Carbonic Acid	H_2CO_3	Calcium Carbonate	$CaCO_3$
D-Carbonic Acid	D_2CO_3	Magnesium Sulfate	$MgSO_4$
Carbon Suboxide	C_3O_2	Dodecahydrate	$MgSO_4$•$12H_2O$
Methanol	CH_3OH	Epsomite	$MgSO_4$•$7H_2O$
Ethanol	CH_3CH_2OH	Hexahydrite	$MgSO_4$•$6H_2O$
Acetone	$(CH_3)_2CO$	Pentahydrite	$MgSO_4$•$5H_2O$
Methyl Formate	$HCOOCH_3$	Starkeyite	$MgSO_4$•$4H_2O$
Glycolaldehyde	CH_2OHCHO	Bassanite	$2CaSO_4$•H_2O
Ethyl Acetate	$CH_3CO_2CH_2CH_3$	Beryl	$Be_3Al(SiO_2)_6$
Dimethyl Carbonate	$(OCH_3)_2CO$	Bloedite	$Na_2Mg(SO_4)_2$•$4H_2O$
Ethylene Glycol	$(CH_2OH)_2$	Bronzite	$(Mg,Fe^{2+})_2(Si0_3)_2$
Methane	CH_4	Dolomite	$(Ca,Mg)(CO_3)_2$
Acetylene	C_2H_2	Burkeite	$Na_6CO_3(SO_4)_2$
Ethylene	C_2H_4	Calcite	$CaCO_3$
Ethane	C_2H_6	Cordierite	$Mg_2Al_4Si_5O_{18}$
Propane	C_3H_8	Eugsterite	$Na_4Ca(SO_4)_3$•$2H_2O$
Propdiene	C_3H_4	Gaylussite	$Na_2Ca(CO_3)_2$•$5H_2O$
1,3-Butadiyne	C_4H_2	Goethite	FeOOH
Carbon Trimer	C_3	Gypsum	$CaSO_4$•$2H_2O$
Cysteinesulfonic Acid	OCS	Hematite	Fe_2O_3
Nitrogen Oxide	NO	Jarosite	$KFe_3(SO_4)_2(OH)_6$
Nitrogen	N_2	Kaolinite	$Al_2Si_2O(OH)_4$
Ammonia	NH_3	Leonite	$K_2Mg(SO_4)_2$•$4H_2O$
Ammonia hydrate	NH_3•H_2O	Lepidocrocite	FeOOH
Hydrazine	N_2H_4	Magnetite	$Fe(II)Fe(III)_2O_4$
Hydrogen Isocyanide	HNC	Mirabilite	Na_2SO_4•$10H_2O$
Hydrogen Cyanide	HCN	Montmorillonite	$(Na,Ca)_{0.3}(Al,Mg)_2Si_4O_{10}(OH)_2$•$nH_2O$
Poly-HCN	poly HCN	Nahcolite	$NaHCO_3$
Acetonitrile	CH_3CN	Nontronite	$Na_{0.3}Fe^{3+}{}_2Si_3AlO_{10}(OH)_2$ • $4H_2O$
Ethylamine	CH_3CH_2CN	Natron	Na_2CO_3•$10H_2O$
Vinyl Cyanide	CH_2CHCN	Olivine	$(Mg,Fe)_2SiO_4$
Propinonitrile	C_2H_5CN	Palagonite	…
Methylcyanoacetylene	CH_3C_3N	Iron Sulfide	FeS
Cyanoacetylene	HC_3N	Pyroxene Bronzite	$Mg_{0.8}Fe_{0.2}SiO_3$
Cyanogen	C_2N_2	Iron Oxide	FeO
Dicyanoacetylene	C_4N_2	Plagioclase	$(Na,Ca)(Si,Al)_4O_8$
Ammonium Nitrate	NH_4NO_3	Picromerite	$K_2Mg(SO_4)_2$•$6H_2O$
Hydroxylamine	NH_2OH	Amorphic SiO_2 Quartz	SiO_2
Cyanate ion	OCN-	Pirssonite	$Na_2Ca(CO_3)_2$•$2H_2O$
…	XCN-	Amorphic Pyroxene	$(Mg,Fe)SiO_3$
Isocyanic Acid	HNCO	Polyhalite	$K_2Ca_2Mg(SO_4)_4$•$2H_2O$
Methyl isocyanate	CH_3NCO	Pyrophyllite	$Al_2Si_4O_{10}(OH)_2$
Formamide	$HCONH_2$	Ortho-Pyroxene	$XY(Si,Al)_2O_6$
…	HCO_2NH_2	Clino-Pyroxene	$XY(Si,Al)_2O_6$
Urea	H_2NCONH_2	Serpentine	…
Thiourea	H_2NCSNH_2	Syngenite	$K_2Ca(SO_4)_2$•H_2O
…	$HCOO^- + NH_4$	Tholin	*e.g.*, $C_3H_5N_2$
Ammonium Hydrosulfide	NH_4HS	Kerogen	$C_{200}H_{300}SN_5O_{11}$
Thiocyanic Acid	HNCS, HSNC	Trona	$Na_3CO_3HCO_3$•$2H_2O$

Table I. Candidate Icy Satellite Surface Compounds. These compounds have been predicted to occur on the the icy worlds of the outer solar system. Though hundreds of measurements have been performed, and the literature contains numerous examples of high-quality spectra at various temperatures, wavelength ranges, spectral resolutions, and sample thicknesses, to date only three compounds (H_2O, NH_3 , and CO_2) have been sufficiently characterized to permit quantitative abundance modeling of spacecraft observations across the full wavelength range of the visible to near infrared imaging and imaging spectrometer systems carried by spacecraft such as Galileo, Cassini, and New Horizons.

SIGNATURES OF ICES IN SPECTRA OF TNOs AND CENTAURS: PECULIARITIES AND PROBLEMS IN THEIR INTERPRETATION. C. de Bergh[1], M.A. Barucci[1], F. Merlin[1], and A. Guilbert[1, 1]LESIA-Observatoire de Paris (5 place Jules Janssen, 92195 Meudon, France, catherine.debergh@obspm.fr).

Visible and near-IR spectroscopy of the brightest (the only ones for which good enough data can be obtained) TNOs and Centaurs has shown that only few objects have signatures in their spectra. The signatures detected are essentially due to ices. Results of some of these observations are discussed by Guilbert et al. (this meeting).

We present here some peculiarities of the spectra and some limits in their interpretation:
1) the water ice seems to be always present in the crystalline state, even at the surface of small objects that are not prone to internal evolution. What does this mean ?
2) in some cases where water ice is detected, the band at 1.5 micron is absent (or much weaker than it should be compared to the band at 2 micron). What is it due to ?
3) absorptions of methane ice are detected in visible spectra of two TNOs (Eris and 2005 FY9) below 0.7 micron that have not been seen elsewhere (in particular, they do not appear in spectra of Pluto and Triton). These weak absorptions have not been studied in the laboratory.
4) wavelength shifts of some methane ice absorption bands are interpreted as being due to the presence of nitrogen ice, but is this the only possible interpretation ? And how much nitrogen would be required ?
5) in Charon (and maybe also Orcus) spectra, a weak band is detected around 2.2 microns that is currently assigned to some ammonia hydrate, but this interpretation relies on a single feature, and surface models cannot be run to secure it because of a lack of optical constants for such species.
6) the wavelength position of the 1.65 micron band of crystalline water ice has been used to get some information on the surface ice temperature, but this measurement is hampered by an insufficient knowledge of how irradiation affects the position of the band.

More generally, there is a lack of: optical constants, laboratory studies for temperatures appropriate for these objects (in the 20-60 K range), data on ice mixtures and mixtures of ices with other types of materials (minerals and/or carbonaceous materials), studies on the effects of irradiation on the spectra.

NUMERICAL SIMULATIONS OF THE DEFORMATION OF ICY-SATELLITE LITHOSPHERES. A. J. Dombard, Dept. of Earth and Environmental Sciences, Univ. of Illinois at Chicago, 845 W. Taylor St. (MC-186), Chicago, IL 60607 (adombard@uic.edu).

Introduction: The finite-element method is a powerful technique that can be used to simulate the deformation of icy-satellite lithospheres. Specifically, application of the method employing an elastoviscoplastic rheology allows a lithosphere to develop naturally depending on the thermal and stress state of the system, instead of having to a priori constrain the lithosphere. Also, this method permits multi-physics applications (e.g., thermomechanical simulations).

Tekton [1] is the standard bearer for the planetary geodynamical community. Originally designed for use in geodynamical problems, the main advantages of Tekton are the speed at which the code can be executed and the fact that the source code is freely available, allowing each user to adapt the code for specific problems. Tekton, however, only solves for mechanical deformation at present and is not the only option. I have traditionally used MSC.Marc [2-5], a commercial code with better pre- and post-processing capabilities and user subroutines that effectively permit adaption of the code. Marc also permits multi-physics simulations.

Here, I discuss the general set-up of my thermomechanical finite-element simulations, and review the state of knowledge of the experimentally determined parameters that go into these simulations. I concentrate on water ice, because it is the dominate component of icy satellite lithospheres. There are, of course, other components. CO_2 ice, hydrated salts, and inclusions of refractory particulates (i.e., dirty ice) may be important for the Galilean satellites (high-pressure phases of water ice are also present but at depths beneath the lithosphere). Other, more volatile species (ammonia, methane hydrates) may also be significant in the satellites of Saturn and beyond. Experimental work has shed some light on the parameters for some of these compositions, but none are as a well known or as complete as for water ice.

Thermomechanical Finite-Element Simulations: The basic procedure begins with construction of the finite-element mesh. A steady-state or evolving thermal simulation is first performed. The temperature of the nodes on the "surface" is constrained, a heat flow to the base of the mesh is set, and any thermal anomalies are applied. Material parameters, specifically the thermal conductivity and diffusivity, are then set.

Results from a thermal simulation are then piped into a mechanical simulation. Loads are generated by application of gravity. These simulations employ a rheology that possesses elastic, viscous (ductile), and plastic (to approximate faulting) components. The elastic properties are described by the Young's modulus and the Poisson's ratio. Ductile creep generally can be described by an empirical equation:

$$\dot{\varepsilon} = FAd^{-p}\sigma^{n}e^{-(E+PV)/RT} \quad (1)$$

where $\dot{\varepsilon}$ is the equivalent strain rate, F is a correction factor, d is grain size, σ is the equivalent deviatoric stress, P is pressure, R is the universal gas constant, and T is temperature. A, p, n, E, and V are determined via experiments [see 6]. The equivalent strain rate and deviatoric stress are scalar values that are proportional to the root of the second invariant of the respective tensors; the proportionality constants are different under different mathematical conventions and lead to the correction factor F. The same convention is used in Marc and the triaxial experiments under which the parameters are measured, so $F = 1$. Tekton uses a different convention, and $F = 3^{(n+1)/2}/2$ [6]. (Note that for yield strength envelopes, $F = (3^{1/2}/2)^{n+1}$.)

A common assumption in lithospheric modeling is that the material is pervasively fractured. Thus for sufficiently high stress, the material can be modeled to undergo plastic (time-independent, permanent) deformation. The yield criterion follows Byerlee's rule, an empirical relationship between the shear stress to cause slip and the normal force across the fracture [7].

Thermal Conductivity/Diffusivity: It is generally agreed that the thermal conductivity of ice is inversely proportional to temperature; the two most commonly used forms derive from Hobbs [8] and Klinger [9]. Over the range of likely temperatures, the two forms agree to within ~10%. I generally use the conductivity of Klinger [9] for its mathematical simplicity (= 567/T, in SI units).

Perhaps a more significant issue is the effect of porosity on the conductivity. This porosity can either be primary (a fluffily accreted satellite [10]) or secondary (an impact generated regolith). In either case, the effect is the same: by limiting pathways by which heat can be passed, the effective conductivity is lowered, perhaps by as much as an order of magnitude. On the other hand, thermal and pressure effects can anneal the ice, restoring the conductivity. Indeed, the insulating effect of a porous layer may be critical to explaining the evolution of Iapetus [10] or the lack of a latitudinal dependence of crater relaxation on Ganymede and Callisto [2,11], and thus, experiments exploring the evolution of porous ice are important [e.g., 12].

The thermal diffusivity of ice is also dependent on temperature [8], being of order 10^{-6} m^2 s^{-1} for ice at moderate temperatures and of order 10^{-5} m^2 s^{-1} for low-temperature ice (less than ~100 K). Of course, porosity will reduce the diffusivity.

Elasticity: The Young's modulus and Poisson's ratio of synthetic and natural ice samples has been measured in the laboratory to be ~9 GPa and ~1/3 [13,14]. There has been some question, however, on the applicability of the measured Young's modulus to larger scale natural systems. For instance, application of the measured modulus to elastic flexure models for ridges on Europa [15] results in implausibly thin effective elastic thicknesses. As reviewed by Nimmo [14], estimates of the Young's modulus from natural systems can be significantly lower than the laboratory measured value; however, this reduction is likely the product of non-recoverable deformation (i.e., brittle failure or ductile creep). Because this finite-element application incorporates these mechanisms, I use the laboratory measured elastic parameters.

Porosity will also reduce the effective Young's modulus of the material by 1-2 orders of magnitude. This reduction is potentially quite significant, adding an aspect soil mechanics to icy satellite studies. Again, understanding the evolution of porosity in ice and how it can "heal" into competent ice under conditions prevalent in icy satellites is critical. To date however, any porous layer has generally been smaller than the resolution of my finite-element meshes, and so I have ignored the mechanical consequences of porosity.

Ductile Creep: Several creep mechanisms operate at conditions present in icy satellite lithospheres, including dislocation creep, easy slip along the basal plane, sliding along grain boundaries, and diffusion creep [6,16,17]. (The parameters for diffusion creep have only been estimated, although diffusion creep is likely more important for low stress conditions associated with convection below the lithosphere.) Basal slip and grain-boundary sliding (GBS) are dependent mechanisms and rate-limit each other (strain rates add in parallel). In lithospheres, GBS is generally the slower, and so it dominates. These mechanisms are independent of dislocation and diffusion creep (strain rates add in series). There has been some disagreement over the measurement of the dislocation creep parameters, particularly in the identification of a "regime C" that may control dislocation creep at low temperatures and strain rates [17]. This regime, however, could be an artifact of the experimental procedures [6].

GBS (and diffusion creep) is sensitive to the grain size. Because grain size is unknown within the lithospheres of icy satellites, this sensitivity introduces a free parameter. Using glacial ice as an analogy, the grain size has been estimated to range from 0.1-10 mm [2]. Additionally, the grain size may also evolve as a function of temperature and stress.

Plasticity: The friction of ice has been measured [7], and like for rocks, it is insensitive to temperature and possesses shallow and deep branches. Curiously, the shallow branch appears to have a non-zero cohesion (i.e., the inherent stickiness of the fracture), although this could be an artifact of the experiment. Differences to a fit of the data constrained to possess no cohesion are small. The presence of a cohesion for the shallow branch is actually beneficial to finite-element simulations because zero cohesion implies strengthless material at the surface, which can crash the simulations because of unbounded deformation.

Discussion: The parameters needed to perform thermomechanical, finite-element simulations of a lithosphere composed of water ice are fairly well known; however, certain issues remain. For instance, further experiments can resolve the discrepancy concerning the nature of the dislocation creep mechanism(s) [6,16,17]. Such work will likely just refine the parameters and probably will not radically change any conclusions drawn from previous simulations.

The most outstanding issue is likely the thermal and mechanical properties of porous ice. Results from experiments have started to resolve these properties as a function of the porosity of ice, but what is needed is a model for the evolution of porosity as a function of pressure and temperature [e.g., 12]. With such a model, the effects of porosity can be more rigorously included in simulations of the lithosphere.

References: [1] Melosh, H.J. and A. Raefsky (1980) *Geophys. J. Roy. Ast. Soc., 60*, 333-354. [2] Dombard, A.J. and W.B. McKinnon (2006a), *JGR, 111*, E01001. [3] Dombard, A.J. and W.B. McKinnon (2006b) *J. Struct. Geol., 28*, 2259-2269. [4] Dombard, A.J. et al. (2007) *EOS Trans. AGU, 88*, P21B-0549. [5] Dombard, A.J. and A.F. Cheng (2008) *LPS XXXIX*, Abs. #2262. [6] Durham, W.B. and L.A. Stern (2001) *Ann. Rev. Earth Planet. Sci., 29*, 295-330. [7] Beeman, M. et al. (1988) *JGR, 93*, 7625-7633. [8] Hobbs, P.V. (1974) *Ice Physics*, Oxford U. Press. [9] Klinger, J. (1980) *Science, 209*, 271-272. [10] Castillo-Rogez, J.C. et al. (2007) *Icarus, 190*, 179-202. [11] Shoemaker, E.M. et al. (1982) in *Satellites of Jupiter*, U. Ariz. Press, 435-520. [12] Durham, W.B., et al. (2005) *GRL, 32*, L18202. [13] Gammon, P.H. et al. (1983) *J. Phys. Chem., 87*, 4025-4029. [14] Nimmo, F. (2004) *Europa's Icy Shell*, Abs. #7005. [15] Billings, S.E. and S.A. Kattenhorn (2005) *Icarus, 177*, 397-412. [16] Goldsby, D.L. and D.L. Kohlstedt (2001) *JGR, 106*, 11017-11030. [17] Durham, W.B. et al. (2001) *JGR, 106*, 11031-11042.

The viscous behavior of glacier ice; effect of impurities, grain size and liquid phase. P. Duval[1] and M. Montagnat[2], [1] LGGE/CNRS, B.P. 96, 38402 Saint Martin d'Hères Cedex, France; duval@lgge.obs.ujf-grenoble.fr, [2] LGGE/CNRS, B.P. 96, 38402 Saint Martin d'Hères Cedex, France; montagnat@lgge.obs.ujf-grenoble.fr.

Deformation of single-crystal: Single crystals undergo plastic deformation as soon as there is a component of shear stress on the basal plane. Basal slip takes place by the motion of basal dislocations. But, cross-slip of basal screw dislocations is invoked for the multiplication of dislocations. This non-basal slip does not significantly contribute to the deformation.

Due to the low lattice friction, dislocations glide cooperatively and long-range internal stresses develop with deformation. The plastic deformation takes place through isolated bursts or dislocation avalanches as long as diffusion processs are not significant. Then, the plastic deformation of the ice crystal is characterized by large spatio-temporal fluctuations with scale-invariant patterns [1].

Deformation of ice in polar ice sheets: For deviatoric stresses lower than 0.1 MPa, the stress exponent is lower than 2 [2], [3]. The deformation is essentially produced by basal slip. Basal slip is accommodated by grain boundary sliding, grain boundary migration or by intracrystalline deformation gradients. At the both scales of the ice crystal and the polycrystal, the deformation is highly heterogeneous [4]. This behavior is associated with the anisotropy of the ice crystal and the mismatch of slip at grain boundaries for the polycrystal. The viscoplastic deformation induces the development of lattice-preferred orientations (textures) giving a non-random orientation of the *c*-axes in the largest part of ice sheets and making ice strongly anisotropic. Recrystallization textures associated with dynamic *migration* recrystallization are generally found in temperate glaciers and near the bottom of polar ice sheets where temperature is the highest. It is worth noting that textures associated with *rotation* recrystallization are deformation textures.

Effect of grain size, impurities and liquid phase: Grain size in glaciers and ice sheets is typically in the range of 1 to 10 mm. In situ and laboratory measurements suggest that the secondary strain rate increases with decreasing grain size. An opposite effect is found for the primary creep. These grain size effects are in agreement with basal slip as the dominant deformation mode. There is no clear evidence of a grain size effect during the tertiary creep associated with migration recrystallization.

The effect of a high concentration of fine particles on the creep behavior is well documented. The creep rate generally decreases with increasing volume fraction of particles. Several mechanisms are put forward to explain these observations. A softening of ice by a high concentration of sediment particles was found in several glaciers. The presence of a liquid-like layer surrounding particles at temperatures as low as -15°C could explain this reduction of the ice viscosity.

The creep rate significantly increases with the presence of a small amount of water at grain boundaries. The effect of the liquid phase is viewed in considering this constituent as an element in the accommodation processes of basal slip [5]. The long-range internal stress field would be reduced by this liquid phase.

References: [1] Montagnat M. et al. (2006) *Philosophical Magazine*, 86, 4259-4270. [2] Mellor, M. and Testa, R. (1969) *J. of Glaciology*, 8, 147-152. [3] Montagnat M. and Duval P. (2004) *C.R. Physique*, 5, 699-708. [4] Lebensohn, R. A. et al. (2007) *Philosophical Magazine*, 87, 4287-4322. [5] De La Chapelle, S. et al. (1999) *Geophys. Res. Letters*, 26, 251-254.

REFLECTANCES OF ICY SOLAR SYSTEM BODIES AT λ > 2.5 μm. J.P. Emery[1], C.M. Dalle Ore[1], D.P. Cruikshank[2], Y.R. Fernandez[3], D.E. Trilling[4], J.A. Stansberry[4] [1]Carl Sagan Center, SETI Institute (jemery@carlsagancenter.org), [2]NASA Ames Research Center, [3]Dept. of Physics, Univ. Central Florida, [4]Steward Observatory, Univ. Arizona.

Introduction: Attendees of this workshop share a common understanding that ices and organics of various compositions are important in many planetary and astrophysical environments. In our collective efforts to characterize the compositions of these materials as fully as possible, observations spanning the electromagnetic spectrum are critical. Reflectance measurements at λ > 2.5 μm are particularly sensitive to the detection of most ices and simple and complex organics. The energies of fundamental vibrations of many relevant molecular bonds (O-H, C-H, N-H, C-O, etc.) fall in this wavelength range. The resulting absorption bands are much stronger than the overtone and combination bands detected at shorter wavelengths.

Unfortunately, ground-based observations at λ > 2.5 μm are very difficult (impossible at some wavelengths) due mainly to strong absorptions in Earth's atmosphere from gases such as H_2O, CO_2, and CH_4 and increasing levels and variability of thermal background flux. As a consequence, only the brightest asteroids, icy satellites, and KBO (Pluto) are observable from the ground in this wavelength range. Although the resulting data are not always of the highest quality, they have enabled the characterization of hydrated material on asteroids [e.g., 1], the H_2O and non-ice materials on satellites of Jupiter and Saturn [e.g., 2,3,4,5] and methane and non-volatile components on the surfaces of Triton and Pluto [6,7,8]. The mapping spectrometers NIMS and VIMS on the Galileo and Cassini spacecraft have brilliantly demonstrated the benefits of observing at λ > 2.5 μm from outside Earth's atmosphere, sensing a variety of materials on jovian and saturnian satellites, including CO_2 (perhaps bound), SO_2, several organics, amorphous H_2O, and H_2O_2 [e.g., 9,10,11,12,13,14].

This handful of observations has been critical for understanding these objects, but the sample represents only a miniscule fraction of bodies that are expected or known to contain volatiles. Moving forward with prospects for much larger sample sizes from SOFIA and James Webb, it is timely to re-evaluate the promise of reflectance observations at λ > 2.5 μm. As a start, we present an overview of photometric observations of KBOs, Centaurs, icy satellites, and Trojan asteroids using the Spitzer Space Telescope. These observations use the Infrared Array Camera (IRAC), an imager with filters centered at 3.6, 4.5, 5.8, and 8.0 μm.

KBOs and Centaurs: We have enacted two programs so far to observe KBOs and Centaurs with IRAC. The first, in cycle 2 (2005-2006) measured fluxes of 12 KBOs and 8 Centaurs. The second program, from cycle 4 (2007-2008), targets 20 additional KBOs and 5 Centaurs. Most of the targets from cycle 4 have not yet been observed. Reflected fluxes from KBOs in these programs are generally detectable at 3.6 and 4.5 μm with IRAC, but are too faint at 5.8 and 8.0 μm. From cycle 2, all 12 KBOs were detected at 3.6 μm and 11 of them were also detected at 4.5 μm. All but one (1996 TL66) exhibit significant absorption at λ > 2.5 μm (e.g., Fig. 1), even many with no discernable ice absorptions at shorter wavelengths. KBOs are all so cold that thermal flux is negligible in the IRAC bands.

H_2O ice has been detected on several KBOs and Centaurs through absorptions at 1.5 and 2.0 μm. Many others do not exhibit these bands, but much of the NIR data have low S/N. Because H_2O contains very strong absorptions at λ > 2.7 μm, the 3.6 μm IRAC channel provides a sensitive test for water ice. We have found that the IRAC data points are also sensitive to the presence of other ices, such as CH_4 and CH_3OH (see Fig. 1). Aside from a likely dynamical family associated with 2003 EL61, there is no apparent correlation between the presence of vis-NIR H_2O bands and any other dynamical or physical property [15,16]. The greater sensitivity provided by observations at λ > 2.5 μm will more robustly identify such correlations if they exist.

Pluto and other dwarf planets: Being much brighter than other KBOs, Pluto was easily detected in all four IRAC bands, significantly extending the wavelength coverage of reflectance measurements. Observations were made at eight distinct longitudes, providing rotational lightcurves in all four bands. The 3.6 μm band exhibits a strong absorption that is in agreement with ground-based spectra in this region and matches the expected behavior of the CH_4 apparent at shorter wavelengths. The other three bands show higher reflectivity, and the 4.5 μm lightcurve seems to be distinct from the lightcurve at any other wavelength.

Eris, 2003 EL61, and 2005 FY9 are included in the cycle 4 program, but have not yet been observed. Depending on the strengths of absorptions, these three bodies may also be detectable in all four IRAC bands.

Icy satellites: Several satellites of the outer planets have also been observed using IRAC. These are generally also bright enough to have been detected in all four bands. For many of them, however, scattered light from the planet is a bit of a problem, making the photometric extraction somewhat more complicated than for isolated targets.

Trojan asteroids: Though no ice has been detected on their surfaces, Trojan asteroids are often assumed to support interior ice, or to have at least originated in an ice-rich part of the solar nebula. The two KBO and Centaur programs mentioned above also include observations of 10 Trojan asteroids each. The Trojans are much warmer than KBOs and most Centaurs, and thermal flux dominates the 8-μm band and is a significant contributor to the flux at 5.8 μm. The 3.6 and 4.5 μm bands, however, do provide measurements of reflectance.

Along with searches for ices, characterization of the "dark material" that provides the low albedo and red slope is important for Trojan asteroids and many Centaurs with similar vis-NIR spectra. The neutral to moderately red spectra of these objects can be explained equally well with silicates or a variety of organics [e.g., 17,18]. Silicates and organics have very different spectral behavior at $\lambda > 2.5$ μm, and observations in this wavelength range will allow us to discriminate between these two possible surface compositions.

Thermal emissivity: With another instrument, the Infrared Spectrograph (IRS), Spitzer has also measured mid-IR (5.2 – 38 μm) emissivity spectra of a slew of asteroids, including Trojans, and several Centaurs and KBOs. These measurements are far more sensitive to the silicate component than the ice component of the surfaces, so are not directly relevant to the Science of Solar System Ices workshop. However, the emissivity signatures of the Trojan asteroids and some of the Centaurs, while showing clear signs of silicate mineralogy, are very different than we expect for a regolith based on current laboratory data and radiative transfer models [19]. It is unclear whether the differences are due to mineralogy, grain size, surface structure (e.g., porosity or inclusions), mixing, or some other effects. Additional laboratory studies of emissivity of materials and conditions appropriate for these outer Solar System surfaces are necessary to properly interpret the emissivity data.

References: [1] Rivkin, A.S. et al. (2003) *M&PS 38*, 1383-1398. [2] Calvin, W.M. et al. (1995) *JGR 100*, 19041-19048. [3] Owen, T.C. et al. (2001) *Icarus 149*, 160-172. [4] Cruikshank, D.P. et al. (2005) *Icarus 175*, 268-283. [5] Emery, J.P. et al.. (2005) *A&A 435*, 353-362. [6] Grundy, W.M. et al. (2002) *AJ 124*, 2273-2278. [7] Sasaki et al. (2005) *ApJ 618*, L57-L60. [8] Olkin, C.B. et al. (2007) *AJ 133*, 420-431. [9] McCord et al. (1998) *JGR 103*, 8603-8626. [10] Hibbitts, C.A. et al. (2000) *JGR 105*, 22541-22558. [11] Hansen, G.B. & McCord T.B. (2004) *JGR 109* E01012. [12] Clark, R.N. et al. (2005) *Nature 435*, 66-69, [13] Cruikshank, D.P. et al. (2008) *Icarus 193*, 334-343. [14] Hansen, G.B. & McCord T.B. (2008) *GRL 35*, L01202, [15] Barucci, M.A. et al. (2006) *A&A 455* 725-730, [16] Barkume, K.M. et al. (2008) *AJ 135*, 55-67, [17] Cruikshank, D.P. et al. (2001) *Icarus 153*, 348-360, [18] Emery, J.P. & Brown, R.H. (2004) *Icarus 170*, 131-142, [19] Emery, J.P. et al. (2006) *Icarus 182*, 496-512.

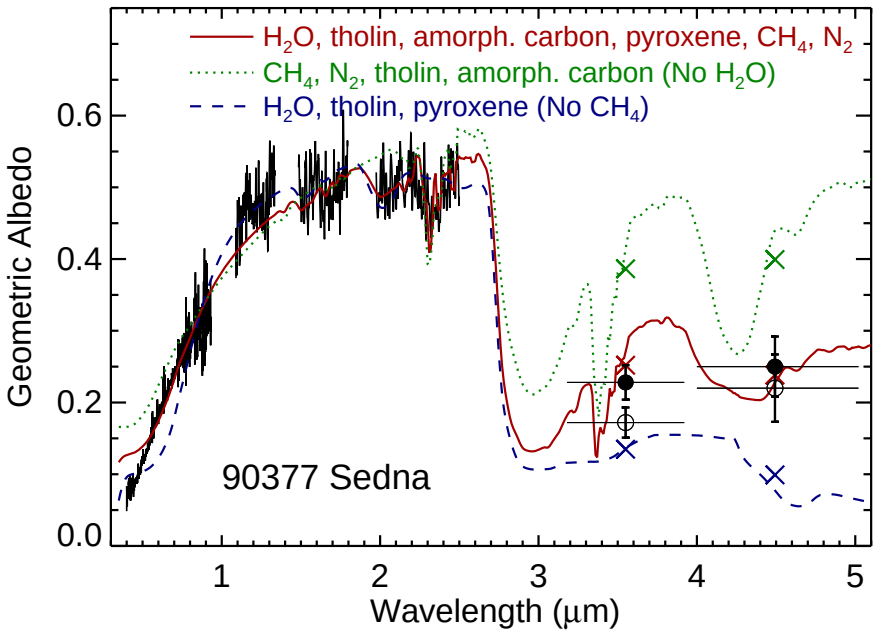

Figure 1. *IRAC data for the KBO Sedna (filled and open circles) along with the vis-NIR spectrum and three spectral models. The colored Xs are the values of the models convolved with the IRAC filter functions. The presence of CH_4 reported by Barucci et al. (2005) is confirmed. Furthermore, analysis of the full wavelength range suggests the presence of H_2O. Both ices are required to fit the IRAC reflectances.*

SPUTTERING OF ICE BY LOW ENERGY IONS: EFFECTS ON ICE GRAINS AND ICY SATELLITES IN SATURN'S INNER MAGNETOSPHERE. M. Famá[1], R. E. Johnson[1,2], J. Shi[1], R. A. Baragiola[1], M. Liu[1], E. C. Sittler Jr.[3], H. T. Smith[4], [1]University of Virginia, Charlottesville, VA 22904, [2]New York University, New York, NY 10003, [3]Goddard Space Flight Center, Greenbelt, MD 20771, [4]Johns Hopkins University, Laurel, MD 20723

Introduction: Icy grains and satellites orbiting in Saturn's magnetosphere are immersed in a plasma that sputters their surfaces. This limits the lifetime of the E-ring grains and ejects neutrals that orbit Saturn until they are ionized and populate its magnetosphere. Modeling the production of tenuous atmospheres or estimating the lifetime of icy grains requires reliable values for the plasma parameters and also accurate laboratory data for the sputtering yields at ion energies and ice temperatures relevant to those environments. Here we re-evaluate the sputtering rate of ice in Saturn's inner magnetosphere using the recent Cassini data on the plasma ion density, temperature and composition [1] and a recent measurements and analysis of relevant sputtering data for ice [2].

Sputtering of Ice: For atomic targets, the standard linear collision cascade theory (SCL) predicts that the elastic sputtering yield is proportional to the nuclear-stopping cross section S_n. The proportionality factor is inversely proportional to the elastic differential cross section in the binary collision approximation, and it is also inversely proportional to the surface-binding energy of the target atoms. Molecular targets, on the other hand, contain internal chemical structure which can absorb some of the elastic energy transferred to the molecule into internal inelastic energy, rather than being used for displacement of molecules. For this reason we tested the validity of the SCL theory for water ice in an extended range of energies using a modified elastic scattering differential cross section. Additionally, we include electronic sputtering that occurs due to long lived repulsive electronic excitations which lead to atomic or molecular motion. The extant literature is consistent with the total electronic sputtering yield Y being proportional to S_e^2, where S_e is the electronic stopping cross section. Including a term proportional to S_n and another term proportional to S_e^2, we could fit a complete analytical expression for the total sputtering yield of water ice valid for temperatures and projectile energies relevant to the astrophysical environments of interest. Figure 1 shows a comparison of our model with the available experimental data for the sputtering yield of ice.

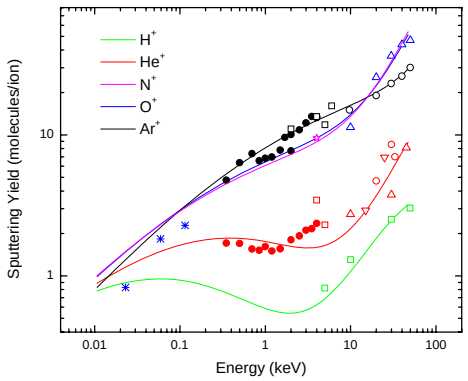

Figure 1 *Solid and open symbols: experimental data for the sputtering yield of ice for H, He, N, O and Ar ions from Ref. [2] and references therein. The solid lines represent our model for Y. Crosses: Molecular dynamics simulations.*

Saturnian Plasma: Since heavy ions with energies > 10 keV were found to be the dominant sputtering agent for icy materials in the Jovian magnetosphere [3], this was initially assumed to be the case also at Saturn [4,5]. Cassini data showed that the presence of a relatively dense and extended population of neutrals suppresses the very energetic ions in the region inside of 10 R_S. The energetic electron population, which at Europa contributes to forming the O_2 atmosphere, is also considerably reduced in Saturn's inner magnetosphere (<~ 15 R_S; [6]). Therefore, the erosion of E-ring grains and sputtering of satellite surfaces inside the orbit of Rhea is likely dominated by ions with energies <10 keV, opposite to what was assumed in earlier research. Figs. 2a and 2b give the ion densities and temperatures in Saturn's inner magnetosphere as measured by the CAPS instrument [1]. These are given in Saturn's equatorial plane as a function of radial distance from Saturn from 3.5 to 10 R_S ($R_S \approx$ 60,268 km), a region orbited by many of the icy satellites and the E-ring grains. The plasma is primarily produced from the water plumes on Enceladus and the densities are given for H^+ and for water-like species summed together as W^+ (O^+, OH^+, H_2O^+, and H_3O^+). The composition of this component varies with radial distance, with H_3O^+ being an important contribution near Enceladus (~4 R_S) and O^+ becoming dominant by

10 R_S near the orbit of Rhea [1]. Although Fig. 2 gives a single temperature at each value of R, the plasma ion velocity distributions are not isotropic. The velocity distribution is divided into components perpendicular to the local magnetic field, $T_\perp$, and parallel, $T_{//}$, with $T = (2T_\perp + T_{//})/3$. The relative contribution of these to the total flux differs between ions and varies slowly with R. Sittler et al. [1] suggests $T_{//}/T_\perp \sim 0.5$ for protons and $T_{//} / T_\perp \sim 0.2$ for W^+ at the magnetic equator. Such ratios indicate that the ion lifetimes are too short for the temperature to isotrophize.

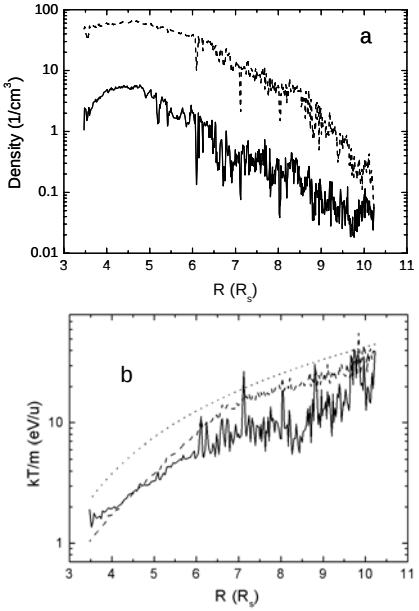

Figure 2 *(a) shows the ion densities in Saturn's inner magnetosphere as measured by the CAPS instrument. The densities are given for H^+ (solid line) and water-like species summed together as W^+ (O^+, OH^+, H_2O^+, and H_3O^+) (dashed line); (b) shows the ion temperatures for H^+ (solid) and W^+ (dashed) measured relative to the plasma flow speed. The dotted line in (b) corresponds to the energy associated with the flow past a grain or satellite orbiting in Saturn's magnetosphere.*

Since these temperatures are measured relative to the plasma flow speed, we also show in Fig. 2b the energy associated with the flow past a grain or satellite orbiting in Saturn's magnetosphere. That is, the ions obtain gyro-motion on pick-up given as $m_i\,(\boldsymbol{v}_{co}-\boldsymbol{v}_o)^2/2$, where $\boldsymbol{v}_{co}$ is the tangential velocity of rotation of the magnetic field which confines the plasma, and $\boldsymbol{v}_o$ is the orbital speed of the body. Since Saturn's field is closely aligned with its spin axis, for bodies in circular orbit these velocities have, roughly, the same direction; Using Saturn's rotational speed and gravity at its equator, the speeds are $v_{co} \approx 9.87R(R_S)$ km/s and $v_o \approx 25.1/[R(R_S)]^{1/2}$ km/s, where R is the radial distance in R_S. These ion speeds and densities are used to calculate sputtering rates.

Sputtering Flux: Using the ion density, n_i, and velocity distribution, $f(\boldsymbol{v})$, along with the sputtering yield above, the surface-averaged ion flux impacting the surface and the surface-averaged sputter flux can be written:

$$\Phi_i = \iint [-\mathbf{n}\cdot(\mathbf{u}+\mathbf{v})] n_i f(\mathbf{v}) d^3v \frac{d\Omega_s}{4\pi}$$

$$\Phi_{sputtering} = \iint Y(E_i)[-\mathbf{n}\cdot(\mathbf{u}+\mathbf{v})] n_i f(\mathbf{v}) d^3v \frac{d\Omega_s}{4\pi}$$

Here **u** is the average flow velocity of the ions relative to the body and **n** is the local surface normal. The flux is averaged over the body by integrating $d\Omega_s$ over the direction of the surface normal which varies with the position on the body.

The net sputter flux of icy surfaces in the Saturnian system is seen to be primarily due to the water ion group and is non-negligible even though the energetic ion component of the plasma in Saturn's inner magnetosphere differs from that in the Jovian magnetosphere, both in the absence of a significant 'hot' component (>10 keV) and in the absence of energetic sulfur ions which sputter very efficiently [3]. It is also seen that for the sputtering of the icy satellites in the Saturnian system, where the $(v_{co}-v_o)$ is much smaller than it is for the icy jovian satellites, the yield is sensitive, not surprisingly, to the ion temperature. Therefore, accurate ion temperatures, as well as ion composition are important in determining satellite and grain erosion rates. Here we have used recently available data, as described above, so that the lifetime of the E-ring grains and the sputter contribution to the neutral torus can now be estimated.

Acknowledgement: This research was supported by the Cassini mission through NASA/JPL under contract with SWRI.

References:

[1] Sittler Jr. E. C. et al. (2007) *Planet. Space. Sci., 56,* 3. [2] Famá M. et al. (2008) *Surf. Sci., 602,* 156. [3] Cooper J. F. et al. (2001) *Icarus, 149,* 133. [4] Shi M. et al. (1995) *J. Geophys. Res., 100,* 26,387. [5] Jurac S. et al. (2001) *Icarus, 149,* 384. [6] Rymer A. M. (2007) *JGR, 112,* A02201.

AB INITIO APPROACHES TO THE PHYSICAL PROPERTIES OF PLANETARY ICES. A. D. Fortes[1] J. P. Brodholt,[1] and L. Vočadlo[1], [1]Centre for Planetary Sciences, Department of Earth Sciences, University College London, Gower Street, London WC1E 6BT, United Kingdom (andrew.fortes@ucl.ac.uk).

Introduction: Planetary bodies are essentially crystalline aggregates. The structure and evolution of all such bodies are thus fundamentally due to the microscopic behaviour of the component crystals - equilibrium structures, elasticity, and transport properties for example. Determining the magnitudes of these properties for the different 'ices' and for the highly hydrated phases thought to exist in the interiors of outer solar-system moons requires a coordinated multidisciplinary approach involving a combination of experimental and computational techniques. All of the substances of interest exhibit complex polymorphism over the range of pressures and temperatures found in the largest icy moons; however, apart from the case of water ice, little is known about the existence, stability fields, and physical properties of these numerous polymorphs. The objective of this contribution is to describe the applicability of quantum mechanical first-principles techniques to addressing a range of problems, with a particular emphasis on diffusion creep.

Computational method: Material properties can be calculated with high precision from quantum mechanical first principles. These so-called '*ab initio*' methods use only the fundamental physical constants (e.g., the Planck Constant and the mass of the electron), the nuclear mass and the atomic coordinates as inputs. There are no empirical parameters in the ideal solution and so the problem of transferability does not arise, as it does with fitted potentials. The most efficient (i.e., least computationally expensive) technique is the electron density-based approach embodied in Kohn-Sham Density Functional Theory (DFT) [1]; the approximations necessary to solve the Schrödinger equation (in particular those relating to the electron exchange and correlation energy) have been shown to give good results with hydrogen-bonded crystals [e.g., 2]. Any property we wish to determine may be found from derivatives of the total energy of the crystal as it is perturbed from its equilibrium state. For example, the incompressibility is determined from the change in internal energy due to changes in the molar volume (at absolute zero temperature); elastic constants are found by calculating the change in internal energy when a crystal structure is strained; and vibrational frequencies are found from the change in internal energy as individual atoms are shifted fractionally from their equilibrium positions. We can sample the total energy hypersurface any way we desire. Although many planetary ices and hydrates have complex crystal structures (low symmetry and large unit-cells), *ab initio* calculations are tractable, as demonstrated in the contribution by Brand *et al*. (this volume).

Applicability to diffusion creep: At very low strain rates, such as obtain in planetary interiors, solid-state flow is most likely to be dominated by diffusion creep processes, controlled by molecular or atomic volume diffusion and grain-boundary diffusion. These diffusion coefficients have the general form of an Arrhenius law, $D = D_0\exp(-E/kT)$, where E is the activation energy, typically ~ 20 $kJmol^{-1}$. In water ice, laboratory creep rates are - necessarily - measured at much larger strain rates, where the deformation is controlled by other processes (such as grain boundary sliding). Due to grain growth, and the practical difficulties involved, it is thought unlikely that pure diffusion creep in water ice can be measured in the laboratory [3]. Note that much of the contemporary discussion pertains only to the low-pressure phase ice Ih; data on the diffusion creep of high-pressure ice phases is equally relevant (ice VI, for example may form layers up to 400 km thick in the largest icy moons), and considerably more difficult to measure. Creep measurements upon other planetary hydrates and ice-rock mixtures are fairly sparse (see contributions by Grindrod *et al.,* and Middleton *et al*., this issue).

Volume diffusion in ice might normally be expected to occur by atomic diffusion (H and O), but spectroscopic measurements indicate identical rates for both species, leading to the conclusion that the mechanism in ice Ih is *molecular* interstitial diffusion [4]. Given the relatively large voids in the structure of low-pressure ices, it is likely that molecular diffusion is also important in ices II and III. The increasing tendency towards interpenetrating hydrogen bonds in ices IV, V, and VI, means that pathways for molecular interstitial diffusion are blocked [e.g., 5]. Thus, in the high-pressure ices, atomic diffusion is likely to dominate. However, only in ice VII has the proton diffusion coefficient been measured [6]. In sulfate hydrates, volume diffusion of H_2O may be related to the availability of non cation-coordinated water molecules, of which there is one in epsomite ($MgSO_4{\cdot}7H_2O$), two in mirabilite ($Na_2SO_4{\cdot}10H_2O$), and five in meridianiite ($MgSO_4{\cdot}11H_2O$); the sparse data suggest a rheological trend from rock-like strength in epsomite through to ice-like strength in meridianiite. Sulfuric acid hydrates (6½ and $8H_2O$), which are plausibly of relevance in the icy crust of Europa, are molecular sandwiches containing layers with ice-like structure [7,8], and are therefore likely to be relatively weak.

Dealing with grain-boundary diffusion is potentially more difficult, although it has been suggested that a good proxy is the self-diffusion coefficient of supercooled water [9]. This has interesting implications for the rheological behaviour of high-pressure ices, since supercooled water actually becomes more fluid at high-pressure [10].

An early *ab initio* approach to calculating absolute diffusion coefficients employed static DFT to determine the activation-energy term (by exploring the energy surface surrounding an atomic defect), and then used a statistical theory to determine the rate at which defects attempt to 'jump' the activation-energy barrier. This methodology met with success for simple oxides, employing Vineyard theory [11] to determine the pre-exponential frequency factor [e.g., 12,13]. However, the static *ab initio* calculations do not account for important contributions from vibrational entropy or anharmonicity (which must be addressed by corrections to Vineyard theory). Furthermore, the technique requires some *a priori* knowledge of diffusion pathways through the structure, which is relatively straightforward in simple close-packed ionic crystals, but becomes increasingly intractable in complex molecular crystals.

A dynamic rather than a static computational technique is therefore more desirable, in which no *a priori* knowledge of diffusion paths or mechanism are necessary, and the system evolves over time (i.e., atoms and/or molecules diffuse) according to the classical- or quantum-chemical rules imposed upon it. This is the basis of molecular dynamics (MD) calculations, which are capable of yielding both the activation energy and the pre-exponential term. In MD, atoms are moved according to a force matrix obtained from either classical interatomic potentials, or quantum mechanical *ab initio* calculations [14] - so-called 'on-the-fly' DFT. MD is well suited to the study of diffusion in liquids, since the rates are rapid and the calculation timescales are short (order 10^{-11} s). In solids, we are faced with the twin problems of needing to simulate large supercells, possibly containing many hundreds of atoms, and extremely long - for MD - simulated timescales (order 10^{-7} s) for determination of slow diffusive processes. It is for this reason that computationally cheap classical MD studies of solid-state diffusion are primarily carried out. A number of researchers have employed classical MD to investigate self-diffusion in water-ice and clathrates and the diffusion of small molecules through the ice lattice [15-17]. However, interatomic potentials are notoriously difficult to transfer from one structure to another, and only *ab initio* MD offers the certainty of obtaining reliable diffusion coefficients, despite the very considerable computational expense, since the dynamics naturally incorporate vibrational entropy and anharmonic effects. The most popular implementation of *ab initio* MD is the Car-Parinello method [18], which nonetheless suffers from poor scaling (the size of the calculation scales as N^3, where N is the number of atoms in the system), although more efficient algorithms - which scale linearly in N - are becoming available [19]. To date, *ab initio* MD studies of diffusion have been limited to liquids [20].

Summary: The substantial experimental obstacles associated with the measurement of diffusion creep processes in water ice and related planetary hydrates, means that calculations are able to make a significant contribution to understanding the creep of solids under planetary conditions. Some of the techniques described here have already borne fruit in determining the rheology of terrestrial mantle minerals [e.g., 21], and we will make similar strides in advancing understanding of ice diffusion creep at a range of pressures and temperatures relevant to icy moon interiors. Advances in computer technology mean that the extension of *ab initio* MD to the study of diffusion in solids is becoming tractable, and offers the hope that diffusion creep in ice can be determined *in silico* if not in the laboratory.

References: [1] Kohn, W., & L. J. Sham (1965): *Phys. Rev.* **140**(4A), A1133. [2] Fortes, A. D. (2004): *PhD Thesis,* University of London. [3] Goldsby, D. L., & D. L. Kohlstedt (2001): *J. Geophys. Res*. **106**, 11017. [4] Onsanger, L., & L. K. Runnels (1963): *Proc. Natl. Acad. Sci. USA* **50**(2), 208. [5] Azaroff, L. V. (1961): *J. Appl. Phys*. **32**(9), 1658. [6] Aoki, K., *et al*. (2002): *High Press. Res*. **22**(1), 9. [7] Fortes *et al*., (2006): *J. Chem. Phys*. **125**(14), 144510. [8] Fortes *et al*., (2008): *J. Chem. Phys*. **128**(5), 054506. [9] Petrenko, V. F., & R. W. Whitworth (1999): *Physics of Ice*, Oxford University Press. [10] Prielmeier, F. X., *et al*. (1987): *Phys. Rev. Lett.* **59**(10), 1128. [11] Vineyard, G. H. (1957): *J . Phys. Chem. Solids* **3**, 121. [12] M. J. L. Sangster, & A. M. Stoneham (1984): *J . Phys. C* **17**, 6093. [13] Vočadlo, L., *et al.* (1995) *Phys. Earth Planet. Int.* **88**, 193. [14] Marx, D., & J. Hutter (2000) In, *Modern Methods and Algorithms of Quantum Chemistry* (J. Grotendorst, Ed), Neumann Institute for Computing series, vol. 1, 301-449. [15] Demurov, A., *et al*., (2002): *J. Chem. Phys.* **116**(2), 702. [16] Ikeda-Fukazawa, T., *et al*. (2002): *J. Chem. Phys*. **117**(8), 3886. [17] Ballenegger, V., *et al.* (2006): *Chem. Phys. Lett*. **432**, 78. [18] Car, R., & M. Parinello (1985): *Phys. Rev. Lett*. **55**, 2471. [19] Schlegel, H. B., *et al*. (2001): *J. Chem. Phys*. **114**, 9758. [20] Marx, D. (2006): *Chem. Phys. Chem*. **7**, 1848. [21] Brodholt, J. P., & L. Vočadlo (2006): *MRS Bull*. **31**(9), 675.

THE RHEOLOGICAL PROPERTIES OF ICE — WHERE WE ARE AND WHITHER WE ARE TENDING. D. L. Goldsby, Department of Geological Sciences, Brown University, 324 Brook Street, Providence, Rhode Island, 02912, David_Goldsby@brown.edu

Introduction: The dynamical properties of glaciers, ice sheets, polar ice caps, and icy planetary interiors are controlled in large part by the grain-scale deformation of ice. Here I review our current state of knowledge of the rheological properties of ice I, and identify crucial areas of current and future research that will provide fundamental constitutive laws and physical properties data required for modeling the dynamics of icy satellites and other cryospheric bodies.

Background: The rheological behavior of ice has classically been described by the Glen flow law, a power law relationship between strain rate and stress [1].

$$\dot{\varepsilon} = B\ \sigma^n \qquad (1)$$

Here $\dot{\varepsilon}$ is strain rate, B is a constant at a given temperature, σ is stress, and n is the stress exponent (=3). The Glen law is predicated upon a large number of creep experiments on relatively coarse-grained ice (grain size > 1 mm) at relatively high temperatures (>250 K). Glen law flow is attributed to dislocation creep and deemed to be independent of grain size [2].

The flow of materials is often described by a generalized constitutive law of the form

$$\dot{\varepsilon} = A\ \sigma^n\ \frac{1}{d^p}\exp\left(-\frac{Q_c}{RT}\right) \qquad (2)$$

where A is a materials parameter, d is grain size, p is the grain size exponent, Q_c is the activation energy for creep, R is the gas constant and T is temperature. Major advances in the laboratory within the past two decades [3-9] have demonstrated unequivocally that the rheological behavior of ice is much more complex than suggested by the simple Glen law. Ice flows via any of four creep mechanisms, each characterized by a flow law of the form of Eq. 2, and each of which limits the overall creep rate over different conditions of σ, T, and d. These studies have demonstrated, in fact, that the Glen law represents transitional behavior between dislocation creep (characterized by n=4) and grain boundary sliding-accommodated dislocation creep (characterized by n=1.8) [3], and thus cannot be meaningfully extrapolated to stresses outside the limited range explored in the laboratory experiments considered by Glen.

Dislocation creep - An exhaustive study of the flow of ice at elevated confining pressures, conducted primarily with planetary applications in mind, reveals that coarse-grained ice (d >250 μm) deforms via *dislocation creep*, characterized by $n \approx 4$, over a wide range of σ and T [7-9]. This $n \approx 4$ behavior is also observed in 1-atm experiments on fine-grained samples (d <100 μm) at stresses >1 MPa [3]. Fine grain sizes prevent microcracking at these stresses at ambient pressures. Excellent agreement between creep data from high-pressure experiments on coarse-grained samples and from ambient-pressure tests on fine-grained samples [3] demonstrates that dislocation creep of ice is independent of grain size (i.e., p=0). In accordance with the von Mises criterion for compatible deformation of polycrystalline solids, dislocation creep of ice cannot occur solely via dislocation slip on the easily activated basal slip system, and requires activation of more creep resistant, non-basal slip systems [10].

Grain size-sensitive (GSS) flow – The flow of materials at low stresses and high temperatures is controlled by GSS creep processes, wherein the creep rate increases with decreasing grain size [11]. Such GSS creep mechanisms control the creep rate in low differential stress natural environments, such as the interiors of the icy satellites. The grain size dependence embodied in Eq. 2 is a natural consequence of grain boundary sliding (GBS), whereby neighboring grains in a material are translated along their mutual grain boundaries. To provide compatible deformation of polycrystalline materials, GBS must be accommodated by dislocation motion or diffusional flow.

Mutually accommodating GBS and dislocation slip - Laboratory experiments on fine-grained ice samples (d = 3-200 μm) [3-5] reveal that over a broad range of conditions compatible flow of ice occurs via slip on the basal dislocation slip system acting in concert with GBS, with the overall creep rate limited by the slower of these two processes. For *GBS-accommodated basal slip creep*, characterized by n=1.8 and p=1.4, the creep rate is limited by GBS, whereas for *basal-slip accommodated GBS creep*, characterized by n=2.4 and p=0, the overall creep rate is limited by basal slip [3]. Extrapolations of the flow laws for each of these creep mechanisms to the larger grain sizes characteristic of natural ice bodies demonstrates that GBS-accommodated basal slip creep, hereafter termed GBS creep or GBS flow for brevity, rate limits the flow of ice over a broad range of conditions overlapping those in glaciers, ice sheets, and icy planetary interiors [3]. The GBS law has been employed in modeling a host of glaciological and icy planetary phenomena [12-16].

Outstanding Problems: In spite of the great advances in our understanding of the rheological properties of ice within the last two decades and the successful application of the GBS creep law in models of

various planetary phenomena, crucial gaps remain in our knowledge. Outstanding problems include 1) the nature and extent of the diffusion creep regime for ice, 2) the influence of impurities on ice flow, particularly for grain size-sensitive flow mechanisms, and 3) the relationship between ice flow and the development of lattice preferred orientation (LPO).

Diffusion creep - For a given grain size and temperature, diffusion creep should dominate the rheological behavior of ice at stresses lower than for GBS creep [17], and therefore should compete with that mechanism for dominance in low stress planetary environments. Recently, the role of diffusion creep as a rate-controlling creep mechanism in convective processes within icy satellites has been emphasized [e.g., 18]. In spite of its importance, however, the diffusion creep regime for ice has never been accessed in laboratory experiments [3]. Experimental validation of diffusion creep for ice and quantification of the diffusion creep rate would represent major advances in our understanding of planetary ice flow.

The diffusion creep rate is given by the classical diffusion creep equation [11]

$$\dot{\varepsilon} = \frac{C\,\Omega\,\sigma}{d^2 RT}\left[D_v + \frac{\delta D_b}{d}\right] \qquad (3)$$

where C is a constant which depends on grain geometry, Ω is molar volume, k is Boltzmann's constant, D_v is the volume diffusion coefficient, δ is the grain boundary width, and D_b is the grain boundary diffusion coefficient. The diffusion coefficients are of the form $D=D_o\,exp(-Q_d/RT)$, where D_o is a constant and Q_d is the activation energy for diffusion. Volume and grain boundary diffusion contribute independently to the creep rate, i.e., are parallel kinetic processes, yielding a $1/d^2$ dependence of the creep rate when volume diffusion dominates, and a $1/d^3$ dependence when boundary diffusion dominates. A hallmark of diffusion creep is the linear dependence of creep rate on stress.

Diffusion creep and GBS creep are parallel kinetic processes, such that the faster process dominates the creep rate. Comparison of diffusion creep rates calculated via Eq. 3, using known and estimated equation parameters, with GBS creep rates for all possible combinations of σ, T, and d indicate that in order for diffusion creep to be *faster* than GBS creep or basal-slip limited creep, samples with d <3 μm must be deformed at T >248 K, a practical impossibility due to rapid grain growth. The diffusion creep regime will therefore likely never be accessed in the laboratory for pure ice samples, underscoring the need for measurements of the grain boundary diffusion coefficient in ice, the sole unknown in the diffusion creep equation, as a means of constraining the diffusion creep rate.

Effects of impurities on ice flow – Despite the successful application of the GBS and dislocation creep laws in modeling icy planetary phenomena, important questions remain about the effects of particulates, likely common in icy satellites, on the rheological behavior of ice. The effects of particulates on dislocation creep of ice remain poorly constrained; the effects of intergranular and intragranular particulates on GBS flow of ice are unknown and are the subject of current research. Similarly, the effects of ionic impurities segregated to grain boundaries on ice flow have never been investigated for any ice creep mechanism. Grain growth kinetics for particulate-laden ices also require quantification, and are the subject of current research.

LPO development during GSS creep – Unlike the icy satellites, glaciers and ice sheets provide a natural laboratory where theories and predictions about ice flow in nature can be tested directly. Comparison of GBS flow laws with rheological data from glacier field experiments strongly suggests that under most conditions, the flow of these natural ice bodies occurs via GBS creep [3, 19]. Microstructures from samples deformed by GBS creep are also remarkably similar to those observed in glaciers and ice sheets [3, 19]. Despite the excellent agreement between mechanical and microstructural data for GBS creep from the laboratory and those from field studies, however, important questions remain regarding the development of LPO during GBS flow. Ice crystals in glaciers and ice sheets display strong LPO. Conventional wisdom holds that creep mechanisms involving GBS do not lead to LPO. However, when dislocation slip and GBS are mutually accommodating and significant strain occurs via dislocation slip, as in the GBS creep regime for ice, LPO development is expected theoretically, and observed for other materials [10]. LPO development during GBS creep of ice is a subject of active current research.

References: [1] Glen J.W. (1955) *J. Glaciol.*, 2, 111-114. [2] Paterson W.S.B. (1998) *The Physics of Glaciers*, 496 pp. [3] Goldsby D.L. and Kohlstedt D.L. (2001) *JGR, 106, 11017-11030.* [4] Goldsby D.L. and Kohlstedt D.L. (1997) *Scr. Mater., 37, 1399-1406.* [5] Goldsby D.L. (1997) *Ph.D. thesis, Univ. Minn., 155 pp.* [6] Durham W.B. et al. (2001) *JGR, 106, 11031-11042.* [7] Durham W.B. et al. (1988) *JGR*, 93, 10191-10208. [8] Durham W.B. et al. (1992) *JGR*, 97, 20883-20897. [9] Durham et al. (1997) *JGR*, 102, 16293-16302, [10] Goldsby D.L. and Kohlstedt D.L. (2002) *JGR*, 107, koi:10.1029/2002JB001842. [11] Frost H.J. and Ashby M.F. (1982) *Deformation Mechanism Maps, 166 pp.* [12] Peltier W.R. et al. (2000) *Ann. Glaciol.*, 30, 163-176. [13] Dombard A.J. and McKinnon W.B. (2001) *Icarus, 154, 321-336.* [14] Dombard A.J. and McKinnon W.B. (2000) *GRL, 27, 3663-3667.* [15] Nye J.F. (2000) *JGR, 46, 438-444.* [16] Pappalardo R.T. and Barr A.C. (2004) *GRL, 31, doi:10.1029/ 2003GL019202.* [17] Mukherjee A. K. (1971) *Mat. Sci. Eng., 8, 83-89.* [18] McKinnon W.B. (2006) *Icarus, 183, 435-450.* [19] Goldsby D.L. (2006) in *Glacier Science and Environmental Change*, ed. Peter Knight, 567 pp.

A THERMODYNAMIC MODEL FOR WATER AND HIGH-PRESSURE ICES: A WAY TO INVESTIGATE THE STABILITY OF WATER COMPOUNDS IN PLANETOLOGICAL CONDITIONS.

O. Grasset[1], M. Choukroun[2], G. Tobie[1], C. Sotin[2]. [1]UMR-CNRS 6112 Planétologie et Géodynamique, Université de Nantes, France., [2]NASA Jet Propulsion Laboratory, MS 79-24, 4800 Oak Grove Dr., Pasadena, CA 91106.

Introduction

The behavior and the melting of ice under pressure has been the subject of numerous studies since the very beginning of the 20th century [1-6]. Surprisingly, thermodynamic models of the ice behavior have not been thoroughly developed so far, except for the low pressure domain where ice Ih is stable. The IAPWS, among others, has proposed several accurate equations of state for liquid water [7], and a recent study developed such equations for ice Ih [8]. However, a good prediction of these phases' behavior outside their stability domains is a prerequisite to further understand the roles of dissolved compounds in water-rich chemical systems.

A new thermodynamic model of the properties of liquid water and ices I, III, V and VI that can be used in the ranges [0-2200 MPa] and [180-360 K] is proposed. These wide ranges exceed the stability domain of all phases, therefore developing empirical or semi-empirical expressions for the specific volumes of liquid water or ices has been necessary. This new model allows extrapolation of the thermodynamic properties in the low-temperature metastable domain, which is necessary for further investigating the effect of inhibitors. As an example, a strong inhibitor of ices such as ammonia allows the coexistence of ice Ih with its liquid down to 180 K, therefore requiring good prediction of the metastable phases' behavior. Further developments of the model for planetological purposes will be discussed.

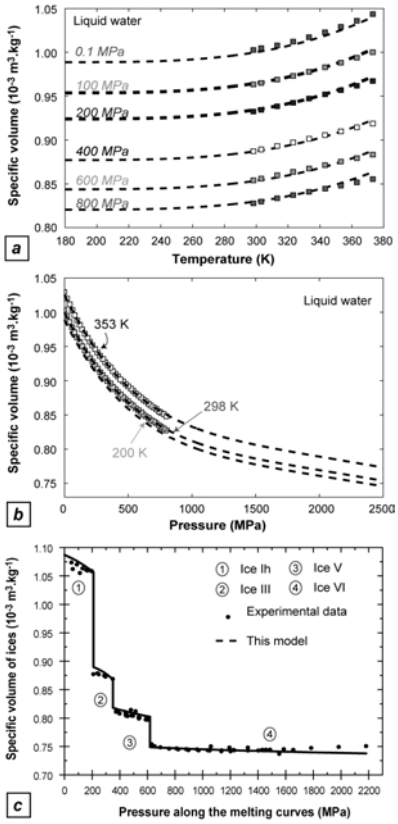

Figure 1: Variations in specific volume of liquid water with temperature (1-a), with pressure (1-b), and of water ices along the melting curves (1-c). Lines correspond to the model proposed in this work.

Thermodynamic modeling of water.

Thermodynamic modeling requires precise determination of the chemical potentials, the heat capacities and the specific volumes of all phases involved:

$$\mu_{H_2O}(P,T) = H^0(P_0,T_0) + \int_{T_0}^{T} C_p dT' - T\left(S^0(P_0,T_0) + \int_{T_0}^{T} C_p dT'/T' \right) + \int_{P_0}^{P} V.dP'$$

$$C_p(P,T) = C_{p0}(P_0,T) - T.\int_{P_0}^{P} V\left(\frac{\partial \alpha}{\partial T} + \alpha^2\right).dP'$$

$$V(P,T) = V_0(P_{ref},T_{ref}) * \xi_T(P_{ref},T) * \xi_P(P,T_{ref})$$

where $H^0(P_0,T_0)$ and $S^0(P_0,T_0)$ are respectively enthalpy and entropy of a given phase at reference (P_0,T_0) conditions, C_p is the heat capacity of that phase, and V corresponds to its specific volume.

Parameter α is the thermal expansion coefficient of the considered phase and depends on temperature and pressure. $V_0(P_{ref},T_{ref})$ is a reference value at (P_{ref},T_{ref}) conditions, $\xi_T(P_{ref},T)$ and $\xi_P(P,T_{ref})$ two functions describing the temperature and the pressure dependence of the specific volume, respectively:

$$\xi_T(P_{ref},T) = a_{T1} + a_{T2}.(T - T_{ref}) + a_{T3}.(T - T_{ref})^{a_{T4}}$$

$$\xi_P(P,T_{ref}) = a_{P1} + a_{P2}(P - P_0) + a_{P3}.(P - P_0)^{a_{P4}}$$

Exact values of the parameters, in addition with the different strategies that have been used for finding the best values with respect to the available experimental data [10] can be found in [9]. In figure 1 the modeled specific volumes are compared with available experimental dataset. Our model reproduces the experimental data with a precision better than 1%, and it provides means for extrapolating the specific volume of liquid

water in the low-temperature metastable domain and at high pressure up to 2.5 GPa.

In order to check the validity of the thermodynamic approach, the melting curves of pure water have been estimated. On the overall, all melting curves are reproduced with a fair accuracy (Figure 2). The melting curve of ice Ih is best fitted among all, with the thermodynamic model remaining within experimental uncertainties. For ices III and V (not shown in the figure), the model provides melting curves with a very satisfying accuracy, even for the low-temperature metastable data. Finally, the melting curve of ice VI is reproduced fairly well, with larger deviation on the experimental data at pressure above 1.5 GPa.

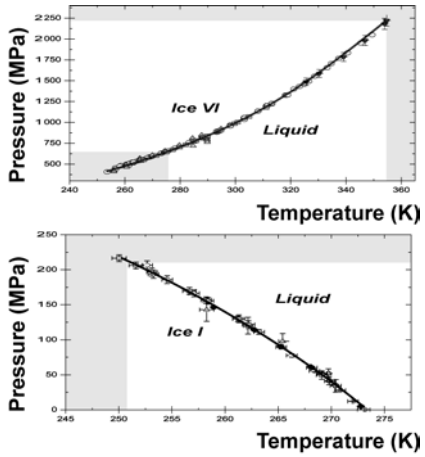

Figure 2: Diagrams showing the melting curves of ices. Symbols are the experimental data points. Error bars correspond to the experimental uncertainties. Gray zones in the diagrams show the metastable domains, above the upper triple point or below the lower one. Black solid lines correspond to the thermodynamic model calculation.

Planetological implications.

In planetary ices, several compounds are suspected to be mixed with water: salts, ammonia, methane, ... Unfortunately, the amount of experimental data is very limited, and the P-T stability of pure ices or hydrates in complex water-rich mixtures is still debated in many cases. Being one of the key parameters for describing internal structures and dynamics within icy moons and water-rich exoplanets, a general thermodynamic tool might be very useful because it allows to investigate a large amount of complex mixtures within P-T space even with a limited number of experimental data. In order to illustrate this point, a first attempt to describe the NH_3-H_2O mixture at low pressure is presented below. This example is chosen because it is well constrained by experiments and it illustrates well the accuracy of the thermodynamic approach in both stable and metastable domain of ices. In addition, it is of particular interest for Titan. Application of the thermodynamic approach to the high-pressure domain is currently in progress. Details of the thermodynamic approach in the binary mixture can be found in [9].

In the NH_3-H_2O system, thermodynamic equilibrium is achieved when solid and liquid chemical potentials are equals. The effect of ammonia is expressed via a mixing rule in the term of liquid water activity, which is the only term requiring further modeling. It can be estimated as the product of an activity coefficient and the molar fraction of H_2O [9]. The main diagram of Figure 3 shows the relative deviations of the calculated temperature (T_{calc}) and the "experimental" temperature [11-13] (T_{th} plotted in the upper left part of the figure).

The use of such a thermodynamic approach in thermal evolution models will permit a better description of crystallization rate of internal liquid layers within Titan and other moons. It will also be useful for exploring the hydrates structures which can be in equilibrium with the remaining liquids in the icy mantles.

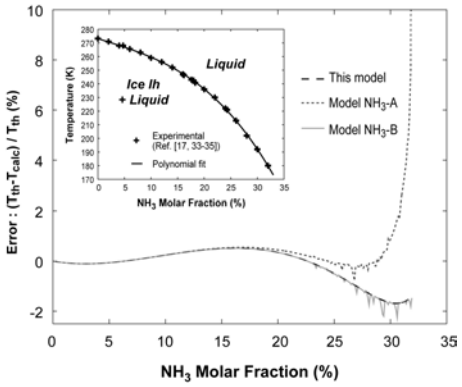

Figure 3: Diagram showing the deviation of the calculated temperature (T_{calc}) from the experimental melting temperature (T_{th}). Experimental data and polynomial fit are shown in the enclosed pressure – temperature diagram. Models A and B are issued from previous studies. Our approach is the only one which allows to investigate the metastable domain.

References: [1] Bridgman P.W. (1912) *Proc. Am. Acad. Arts Sci*. [2] Bridgman P.W. (1937*), J. Chem. Phys*. [3] Henderson S.J. and Speedy R.J. (1987) *J. Chem. Phys*. 91. [4] Pistorius C. (1963) J.W.F.T., *J. Chem. Phys*. 38 (3). [5] Mishima O. and Endo S. (1978) *J. Chem. Phys*. 68 (10). [6] Grasset et al. (2005) *High Press. Res*. 25 (4). [7] Wagner W. and Pruß A. (1994) *J. Phys. Chem. Ref. Data* 31 (2). [8] Feistel R. and Wagner W. (2006) *J. Phys. Chem. Ref. Data* 35 (2). [9] Choukroun M., Grasset O., (2007) *J. Chem. Phys*, 127. [10] Grindley T. and Lind J.E. (1971) *J. Chem. Phys*. 54 (9). [11] Rollet A.P., Vuillard G. (1956) *Compt. Rend. Acad. Sci.* 243. [12] Rupert F.F. (1909) *J. Am. Chem. Soc*. 32. [13] Postma S. (1920) *Rec. Trav. Chim*. 39.

ELECTRICAL PROPERTIES OF SALINE ICES, SALT HYDRATES, AND ICE-SILICATE MIXTURES: APPLICATIONS TO SOLAR-SYSTEM EXPLORATION. R. E. Grimm[1] and D.E. Stillman[1], [1]Dept. of Space Studies, Southwest Research Institute, 1050 Walnut St. #300, Boulder, CO 80302 (grimm@boulder.swri.edu; dstillman@boulder.swri.edu).

Introduction. The electrical properties of ices and associated mixtures influence the ability of both radar and low-frequency electromagnetic (EM) soundings to penetrate and recover information on the icy satellites and polar regions of Mars and the Moon. They also have fundamental implications for mechanical properties and habitability.

Measurements. Four approaches are used to understanding the electrical properties of ices: *1. Single-crystal laboratory measurements*. These classic studies focused on basic physical chemistry and used low impurity levels (doping) to develop understanding of fundamental solid-state electrical-conduction mechanisms. *2. Polycrystalline laboratory measurements*. This is our approach for planetary studies, in order to elucidate multiphase relationships (ice, brines, hydrates, silicates). *3. Ice cores*. Large quantities of natural polycrystalline ices provide rich empirical correlations on the variations of electrical properties with various impurities and environments, but are uncontrolled. *4. Geoelectrical/EM sounding*. Field studies that recover electrical properties at depths of kilometers or more can be compared to lab and core work.

Electrical Properties, Dispersion, and DC Conductivity. The complex dielectric constant $\varepsilon'-i\varepsilon''$ describes the storage of electrical energy (capacitance) in ε' and dissipation (resistance) in ε''. Below the infrared, frequency dependence or dispersion is caused by dielectric relaxations, where bound charge carriers fail to keep in phase with an applied EM field over some critical frequency range and so convert that energy to heat. This results in a peak in absorption in that region and an increase in real dielectric constant with decreasing frequency. It is important to recognize that causality constraints (Kramers-Kronig relations) require that the real dielectric constant increases monotonically with decreasing frequency. The DC conductivity by definition is added to all frequencies and represents the motion of free charges.

Water Ice. Electrical conduction is by point defects, analogous to semiconductors [1]. There are two kinds of protonic point defects in the tetrahedral lattice, each with two states, that allow charge movement. Rotation of a water molecule produces one hydrogen-bond site with no protons (Bjerrum L-defect) and another with two (Bjerrum D-defect). Bjerrum defects are caused by molecular or anionic substitution for H_2O; NH_4^+ and compounds containing F^- and Cl^- can substitute due to their small size. Translation of protons between molecules transfers ionization state by a charge surplus (H_3O^+ ionic defect) or deficit (OH^- ionic defect). Acids and bases easily contribute such ionic defects. Intrinsic Bjerrum defects greatly outnumber intrinsic ionic defects in "pure" ice.

A fundamental feature of ice is its dielectric relaxation, ~1 kHz for pure ice at 252 K and decreasing in frequency with decreasing temperature and increasing impurity content. The "high-frequency" (above the relaxation) conductivity is dominated by most efficient mechanism, i.e., Bjerrum defects. The "low-frequency" (below the relaxation) conductivity requires both mechanisms, and so is controlled by the much-less-abundant ionic defects.

Conductivity Crossover. Single-crystal ice grown from solutions with just tens of umol/l impurities have comparable numbers of both ionic and Bjerrum defects; the former eventually dominate due to their higher mobility and effective charge. This results in a crossover of conduction mechanisms where now the ionic defects control the high-frequency conductivity and the Bjerrum defects are dominant at low frequency. However, it has not heretofore been recognized that the modest impurity levels in polar ices (typically 10s-100s of umol/l) should be above this crossover limit, but no crossover is observed: acid alone still controls the low frequency response and the total active impurities—basically hydrogen, chloride, and ammonium—determine the high-frequency limit [2]. The crossover or its absence has profound, still unresolved effects on low-frequency exploration because it is unknown whether measured ice conductivity will be sensitive to acid/base or salt/ammonia. Radar sounding, well beyond ice high-frequency limit, will be affected by sum of both acid/base and salt/ammonia.

Cation Incorporation. Salts have been supposed to act exactly as acids with respect to lattice substitution [3], e.g., NaCl dissociates in water and enters the lattice as H_3O^+ and Cl^-, leaving Na^+ and OH^- in solution. Our experiments instead indicate that Na^+ accompanies Cl^- into the ice, and must be accommodated interstitially instead of as a lattice defect. This follows from calculation of the defect rate as follows: the lattice appears to saturate for initial NaCl solutions >1-10 mmol/l; using our measured relaxation time constant and known Bjerrum L-defect mobility at –20ºC [1], $\sim 4\times10^{-6}$ defects/H_2O molecule can be derived, or an equivalent concentration ~0.2 umol/l. The corresponding water-ice partition coefficient for Cl^- is then $\sim10^{-4}$.

In order to supply enough H_3O^+ for charge balance using the same partition coefficient, the pH must be <2.7. Our NaCl solutions were pH ~5.7, consistent with carbonic acid in equilibrium with the atmosphere. The small H_3O^+ supply leds to the conclusion that charge balance is achieved by interstial cations. We have confirmed this by observing that relaxation times do not depend on pH. Longer time constants for $CaCl_2$ ices are consistent with a smaller defect rate due to increasing difficulty of substitution.

Salt Hydrates. Even HCl has a saturation limit ~10 uM in the ice lattice [4]. Excess impurities are rejected during freezing and for a single impurity at concentrations of interest, the amount and composition of liquid follow classic binary eutectic phase relations. The last fluid at maximum freezing-point depression is the eutectic composition and subsequently crystallizes to a mixture of ice and hydrate. For starting concentrations of NaCl less than the eutectic composition of 23 wt%, we found that the electrical-mixing fit describing $NaCl•2H_2O$ (hydrohalite) and ice implies that the eutectic mixture (22 vol% hydrohalite) is the conductive phase and is distributed as interconnected shells enclosing the "pure" ice, consistent with the expected binary phase relations. For initial NaCl above the eutectic composition, pure hydrohalite is the conductive phase relative to the excluded eutectic mixture, but the latter now appears electrically as the inclusion phase, i.e., as disconnected shells around the former.

Antarcticite ($CaCl_2•6H_2O$) is a factor of ~100 more conductive than hydrohalite as revealed through measurements at supereutectic composition. Moreover, its eutectic mixture (31% antarcticite) is ~1000x more conductive than its NaCl counterpart for >10 mM initial solution. At lower concentrations, the rapid increase in conductivity with concentration evokes a differential mixing rule [5] or percolation threshold, perhaps indicating that antarcticite is progressively becoming better connected within the eutectic mixture as concentration increases.

The conductivity of meridianiite ($MgSO_4•11H_2O$) has been indeterminate to date because the values measured (at relatively low, subeutectic compositions) closely followed those for antarcticite for solutions with the same chloride content. Our reagent-grade salts contained up to 1% impurities including Ca and Cl; evidently even minor quantities of antarcticite are sufficient to overwhelm any signature of meridianiite. The relevant volumetric ratios indicate that the conductivity of meridianiite must be comparable to or less than that of hydrohalite. This contamination also serendipitously demonstrates that the conductivity of antarcticite exceeds any contribution from Cl doping of meridianiite and therefore suggests that hydrate conductivity is dominantly through intrinsic defects.

Brine Channels. A well-connected fluid phase is evident in some measurements as a distinct segment of DC conductivity above the eutectic temperature (–23ºC for NaCl and –51ºC for $CaCl_2$). Conductivity decreases regularly with decreasing temperature in good agreement with fluid abundance and composition predicted from equilibrium theory, but with an overall signature determined by Archie's Law, the classic formula for the electrical conductivity of brine-saturated clastic rocks. The exponent ~2 indicates welded grain contacts.

Brine channels only appear for initial fluid concentrations > 3 mmol/l. This threshold for brine-channel formation is consistent with the minimum salt concentrations in electrically conductive sea ice [6]. It has the important implication that brine drainage will not occur in icy satellites [7,8] for low bulk impurity levels and it will furthermore cause a discontinuity in bulk viscosity.

Ice/Hydrate/Silicate Mixtures. These experiments are aimed primarily at understanding EM exploration and habitability in icy regoliths. We have measured ice/hydrates mixed with silica beads, sands, clays, and JSC-Mars-1. Preliminary results suggest that the dielectric dispersion and DC conductivity are dominated by the H_2O phases. A mixing model indicates that the ice fraction can be recovered from the low-frequency dielectric constant; this is the fundamental principle behind measuring subsurface ice content on Mars and the Moon from surface measurements [9,10]. Interfacial water due to capillary/adsorption forces at subeutectic temperatures has been confirmed by us using NMR, but its DC conductivity is indistinguishable from that of the ice/hydrate. Without useful ionic transport, interfacial water is unlikely to be a viable microbial habitat on Mars unless temperatures are within a few tens of degrees of melting [11,12]. We have observed an additional dielectric relaxation near 1 MHz in JSC-Mars-1 that is likely associated with the material itself [13]. Future work will seek to determine if the interfacial water has a rotational dielectric relaxation at higher frequency, which could then contribute significantly to strong radar attenuation observed for most of the silicate surface of Mars [14].

References. [1] Petrenko V.F. and R.W. Whitworth, *Ice Physics*, Oxford, 1999. [2] Wolff E.W. et al., *J. Phys. Chem. B, 101*, 6090, 1997. [3] Gross G.W. et al., *J. Chem. Phys., 67*, 5264, 1977. [4] Dominé F. et al., *GRL, 21*, 601, 1994. [5] Sen P.N. et al., *Geophysics, 46*, 781, 1981. [6] Moore J.C. et al., *JGR, 99*, 5171, 1994. [7] Gaidos E.J. and F. Nimmo, *Nature, 405*, 637, 2000. [8] Pappalardo R.T. and A.C. Barr, *GRL, 31*, 10.1029/2003GL019202, 2004. [9] Stillman D.E. and R.E. Grimm, 7th Intl. Conf. Mars, #3311, 2007. [10] Stillman D.E. and R.E. Grimm, LEAG Workshop, #3014, 2007. [11] Jakosky, B.M. et al. (2003) *Astrobiology, 3*, 343. [12] Jepsen, S.M. et al., *Astrobiology*, 7, 342, 2007. [13] Stillman D.E. (2005) Ph.D. Dissertation, Colo. Sch. Mines.[14] Grimm R.E. and D.E. Stillman, LPSC XXXIX, #2251, 2008.

EXPERIMENTAL RHEOLOGY OF PLANETARY ICES: TRIAXIAL DEFORMATION TESTS ON $MgSO_4 \cdot 11H_2O$ (MERIDIANIITE). P. M. Grindrod,[1] A. D. Fortes,[1] I. G. Wood,[1] P. R. Sammonds,[1] D. P. Dobson,[1] C. A. Middleton,[1] and L. Vočadlo,[1] [1]Centre for Planetary Sciences, Department of Earth Sciences, University College London, Gower Street, London WC1E 6BT, United Kingdom (p.grindrod@ucl.ac.uk).

Introduction: The hydrated sulfate salt meridianiite ($MgSO_4 \cdot 11H_2O$) may be the most likely source of liquid on Mars, especially in low latitudes where ice is less common or even absent in the regolith [1]. Stability studies in the $MgSO_4$-H_2O system show that there could be cycling between different phases during the course of a martian day (Figure 1), although sluggish hydration reactions and metastability in this system mean that, at present, it is difficult to predict accurately the phase transitions under martian conditions [2]. On the basis of their presence in chondritic meteorites, hydrated sulfate salts, including meridianiite, have been suggested to be major rock-forming minerals in the mantles of large icy moons [3].

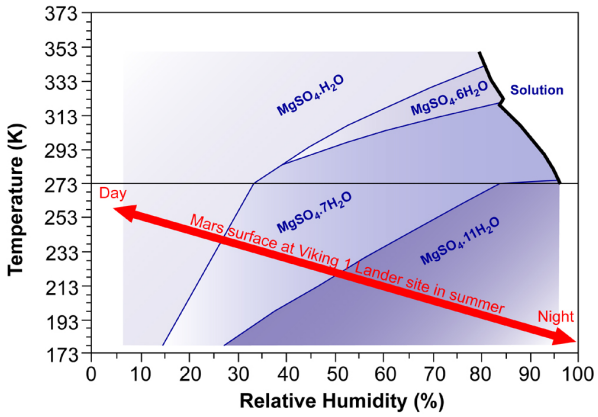

Figure 1. Phase relations for the $MgSO_4$-H_2O system at 0.1 MPa (after [1]). The red line indicates the conditions at the Viking Lander 1 site in summer.

Mono- and poly-hydrated sulfates have been identified from orbit in several different places on Mars, in outcrops several kilometers thick in the walls of Valles Marineris for example [e.g., 4], and inferred *in situ* at the Opportunity landing site in Meridiani [e.g. 5,6]. The Near Infrared Mapping Spectrometer (NIMS) instrument aboard the Galileo space-craft has also found evidence for hydrated salts on the jovian satellites [7,8].

This work forms part of our ongoing cross-disciplinary research program into planetary ices and hydrates (see contributions by Fortes *et al.*, Brand *et al.*, and Middleton *et al.*, this volume). Here we address the importance of rheology of hydrated phases in understanding the water budget of Mars and convection in icy satellites, focusing on meridianiite deformation.

Sample Preparation: Meridianiite poses experimental challenges for deformation tests [e.g., 9]. For this study, we prepare stoichiometric solutions (37.78 wt. % $MgSO_4$) at ~100°C, which are placed in Perspex sample tubes of 25 mm diameter. These tubes are dipped in liquid nitrogen, thus flash-freezing the solutions. This method successfully avoids the formation of metastable epsomite near the eutectic composition [e.g. 10]. No attempt has been made to control the grain size of the samples in this study. However, preliminary SEM analysis of the surface of a used indium jacket suggests that the mean grain size obtained by rapid quenching is very fine, typically <5 μm (Fig. 2).

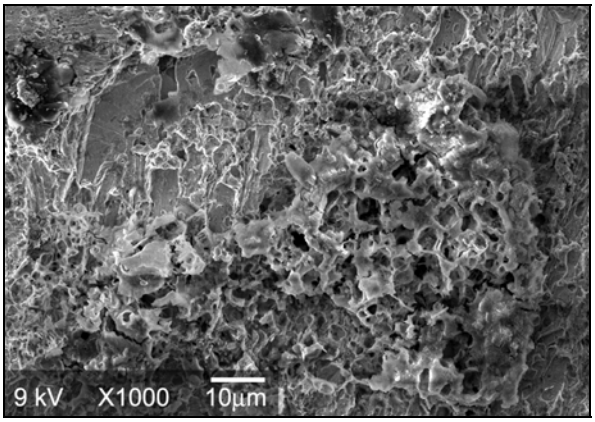

Figure 2. SEM image of the inside of an indium jacket used in one of the deformation tests. Raised material near centre-right is dehydrated meridianiite (probably epsomite), showing crystal molds of the original material.

Experimental Methods and results: We use a typical triaxial deformation cell in our experiments, described in more detail in [11], the only significant difference being the use of a balanced ram. Here we report the results of our tests carried out on 25 mm diameter samples under confining pressure of 50 MPa, and at a temperature of 263 K (Figure 3). Our preliminary results show that meridianiite is considerably weaker than other sulfate hydrates (e.g., epsomite and mirabilite), with a rheology at 263 K similar to low-pressure water ice. Further deformation experiments on meridianiite, and other sulfate hydrates, are re-

quired under different conditions to corroborate our findings, although they appear to match well with other preliminary results [e.g., 12,13]. If meridianiite has a similar rheology to water ice, the behaviour of which is quite well-known under planetary conditions, then it may have important implications for studies of martian permafrost, and icy satellite interiors, which we discuss below.

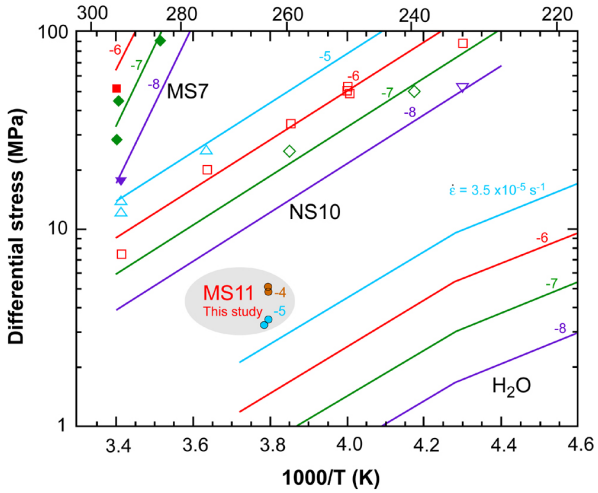

Figure 3. Arrhenius plot showing the strength of meridianiite (MS11) from this study, compared with epsomite (MS7), mirabilite (NS10) and water ice (after [9]). Note the relative weakness of MS11, whose behaviour at the stoichiometric composition is closer to water ice than epsomite (MS7), or even mirabilite (NS10).

Discussion: The rheological properties of meridianiite have an impact on models of the mechanical stability of 'permafrost' in the martian regolith - with consequences for putative martian glaciers and the origin of gullies - as well as the stability to convection of ice/hydrate shells in the outer solar system. Our preliminary results indicate that meridianiite behaves much more like water-ice than other sulfate hydrates, which may be consistent with the molecular architecture (more non cation-coordinated water molecules than epsomite and mirabilite), but further work is necessary to quantify the effects of temperature and grain size on the creep behaviour.

References: [1] Chou I.-M. and Seal R.S. (2007): *JGR*, **112**, E11004. [2] Vaniman D.T. and Chipera S.J. (2006): *Am. Mineral*, **91**, 1628-1642. [3] Kargel, J. S. (1991): *Icarus* **94**, 368-390. [4] Bibring J.-P. *et al* (2007): *Science*, **317**, 1206-1210. [5] Squyres S.W. *et al* (2007): *Science*, **306**, 1731-1733. [6] Peterson R.C. and Wang R. (2006): *Geology*, **34**, 967-960. [7] Dalton *et al.* (2005): *Icarus* **177**, 472-490. [8] Orlando *et al.* (2005): *Icarus* **177**, 528-533. [9] Durham W. B. *et al*. (2005): *JGR*, **110**, E12010. [10] Hogenboom D. L. *et al.* (1995): *Icarus*, **115**, 258-277. [11] Grindrod P. M. *et al*. (2008): *LPSC* **39**, #1199. [12] McCarthy C. *et al.* (2006): *LPSC*, **37**, #2467. [13] McCarthy C. *et al.* (2007): *LPSC*, **38**, #2429.

AMORPHOUS VERSUS CRYSTALLINE WATER ICE. W. M. Grundy, Lowell Observatory, 1400 W. Mars Hill Rd., Flagstaff AZ 86001.

H_2O Ice Crystallinity: When liquid water freezes at low pressure, it forms a solid with a hexagonal crystal structure, ice I_h. However, many other ice phases exist. Of particular interest to planetary scientists are various forms of amorphous ice I_a. Amorphous ice occurs when H_2O vapor condenses on a surface so cold that, upon sticking, molecules are unable to move to the minimum energy sites corresponding to an orderly crystal structure [1]. Ice I_a can have abundant micropores, leading to low bulk density [2] and a tendency to trap volatile gases such as CO, N_2, CH_4, or Ar [3]. On warming, H_2O molecules in ice I_a mobilize, and over time are able to reorganize themselves into the more energetically favorable cubic ice I_c (expelling trapped volatiles in the process). On laboratory time scales, irreversible crystallization from ice I_a to ice I_c is observed to occur above ~135 K and from ice I_c to ice I_h above ~170 K. By assuming that thermally induced crystallization obeys an Arrhenius relation (rate proportional to $e^{-E_a/kT}$), one can extrapolate many orders of magnitude from laboratory to geological time scales and arrive at the conclusion that below ~85 K, amorphous ice should be stable for millions of years [1].

Processes which disrupt the crystal structure of ice can also produce ice I_a. For example, exposure of cold ice to energetic photons [4,5] or charged particles [6,7] produces amorphous ice. In the laboratory, photolytic and radiolytic amorphization are only observed at temperatures below ~100 K [7], suggesting that at higher temperatures, H_2O molecules and their fragments dislodged by energetic radiation have, at least briefly, sufficient mobility to be able to reoccupy their sites in the crystal structure. Icy Solar System objects with surface temperatures permanently below 100 K include satellites of Uranus, Neptune, and Pluto, as well as transneptunian objects (TNOs). Radiation environments vary considerably with heliocentric distance and within giant planet magnetospheres, but in general, these bodies are all exposed to sufficiently high radiation doses that their uppermost surfaces should become amorphized on geologically short time scales [7,8].

Observational Evidence: Near-IR spectral features can be used to distinguish amorphous ice I_a from crystalline ice I_c or I_h (ices I_c and I_h share similar spectral features and thus are not distinguishable from one another [9]). In the laboratory, these features are studied in transmission geometry and reported as optical constants [7,8,10], but for remote-sensing, light needs to be multiply scattered from grain boundaries, voids, inclusions, or defects in the ice in order to escape from the surface and be detected by an observer [11]. Remote sensing purposes are best served by intermediate-strength absorption bands, deep enough to be detectable but not be completely saturated. Thus the best known spectral feature for probing crystallinity of ice is an intermediate strength band at 1.65 μm, part of an absorption complex from 1.45-1.7 μm. This band is prominent in reflectance spectra of cold, crystalline ice [10], but muted or non-existent in amorphous ice [7,8]. In reflectance, typical depths within an icy surface probed by this band are of the order of **millimeters**. The much stronger fundamental O-H stretching band at 3.1 μm is usually saturated in reflectance spectra, but at its core, a metal-like reflectance peak sometimes appears. The shape of this peak is diagnostic of ice phase within the uppermost **microns** of an icy surface. At the opposite extreme, a weak band complex at 1.2-1.3 μm has components at 1.27 and 1.31 μm which appear only in cold crystalline ice [8,10]. These bands are so weak that they require long optical path-lengths in ice to produce appreciable absorption and are therefore typically formed at greater depths, of the order of **centimeters**, a depth to which reflected light probes only in surfaces having relatively large ice particle sizes and low absorption by other contaminants.

Spectral observations of icy satellites of all four giant planets show 1.65 μm bands characteristic of crystalline ice [12-14]. Although they are much fainter and thus more difficult to observe, that band is also apparent in spectra of some larger TNOs, including (136108) 2005 EL_{61} [15], Orcus [16], and Quaoar [17]. Pluto's largest moon Charon also shows it [18]. These observations tell us that crystalline ice exists at millimeter depths on these bodies, despite the expectation of radiolytic or photolytic amorphization on geologically short time scales.

Although the 1.65 μm band implies crystalline ice is ubiquitous, amorphous ice is also seen in the outer Solar System. A study of the 3.1 μm reflectance peak (probing orders of magnitude less deep than the 1.65 μm band) found increasing abundance of ice I_a with proximity to Jupiter from Callisto through Europa, consistent with radiolytic production driven by the jovian magnetosphere [19].

Additional lines of evidence for amorphous ice in the interiors of small TNOs comes from their remarkably low bulk densities determined from mutual orbits of binaries in conjunction with thermal infrared Spitzer

observations [20] and also from studies of photometric lightcurves, assuming fluid interiors [21]. Both methods find bulk densities of the order of 0.5 g cm^{-3}, requiring considerable internal void space, consistent with never-compacted, primordial, amorphous ice compositions. Such compositions also fit with the model of distant activity on Comets and Centaurs driven by crystallization of amorphous ice and expulsion of trapped gases [22].

Apparent Paradox: Why is crystalline ice so prevalent on outer Solar System surfaces where it should be amorphized by energetic radiation more rapidly than it can thermally recrystallize?

A tantalizing interpretation involves ongoing geological activity, with eruptions of warm H_2O onto the surfaces of distant objects [23]. Interiors of large icy objects could have been quite warm soon after they formed [24], and some icy bodies evidently remain active, like Enceladus with its warm, geysering "tiger stripes" (which show more crystalline ice [25]), and Triton with its odd geomorphology and scarce craters [26]. But many more icy satellites couple crystalline ice with ancient-looking, cratered surfaces. It strains Occam's razor to imagine these bodies are still active.

Another possibility is that heating by micro-meteoroid impacts enables local recrystallization. Impact rates are very uncertain, but it may be possible to use albedos to place limits on accumulated dust over the age of the Solar System. Dust impacts also remove ice via sputtering, as does energetic radiation. Could sputtering rates balance amorphization rates such that only a thin coating of ice I_a can ever accumulate?

Other energy inputs could also be important. Laboratory studies of ion bombardment of ices involve micron thin ice films. Most of the energy of incident ions passes right through the ice into the substrate. That energy would be deposited in bulk ice through a cascade of daughter particles, with lower energies and greater numbers at each successive generation until the energy is ultimately thermalized [27]. Many more ice molecules at depth should experience the effects of low-energy daughter products than experience the more disruptive effects of incident particles near the surface.

These questions can be addressed experimentally with additional laboratory and observational studies.

Laboratory Work Needed: Studies of what happens to *bulk* ice as its *surface* is amorphized by energetic particle bombardment would be valuable to get a better idea of the net effect of the cascade of energy unleashed by incident particles. This should be done as functions of temperature and depth, as well as particle energy and type. It would also be valuable to learn more about crystallization on geological time scales. Are modifications to the Arrhenius equation needed to extrapolate that far? Do ions or other impurities in ice affect recrystallization? Finally, the effects of overburden pressure on ice I_a should be studied to see how it would behave in the interiors of 100 km objects.

Observations Needed: If large TNOs with crystalline ice really are geologically active, smaller TNOs should be less active, and below some threshold size, should be geologically inert. Spectral observations of smaller TNOs are needed to see if there is a size below which their surfaces become dominated by amorphous ice. New Horizons studies of Pluto satellites Charon, Nix, and Hydra in 2015 will also test whether crystalline ice implies ongoing geological activity.

Acknowledgments: The author gratefully acknowledges support from NASA Planetary Geology & Geophysics grant NNG04G172G and also thanks the free and open source software communities for providing key software tools used in this project, notably Linux, the GNU tools, OpenOffice.org, GDL, MySQL, Tcl/Tk, Evolution, the Gimp, and Mozilla.

References: [1] Jenniskens et al. (1998) In *Solar System Ices*, pp. 139-155. [2] Bar-Nun et al. (2007) *Icarus 191,* 562-566. [3] Bar-Nun et al. (1985) *Icarus 63,* 317-332. [4] Kouchi and Kuroda (1990) *Nature 344,* 134-135. [5] Leto and Baratta (2003) *Astron. & Astrophys. 397,* 7-13. [6] Moore and Hudson (1992) Astrophys. J. 401, 353-360. [7] Mastrapa and Brown (2006) *Icarus 183,* 207-214. [8] Mastrapa et al. (2008) *Icarus* (submitted, and abstracted in this volume). [9] Devlin (2001) *J. Geophys. Res. 106,* 33333-33349. [10] Grundy and Schmitt (1998) *J. Geophys. Res. 103,* 25809-25822. [11] Hapke (1993) *Combined theory of reflectance and emittance spectroscopy*. [12] Grundy et al. (1999) *Icarus 142,* 536-549. [13] Bauer et al. (2002) *Icarus 158,* 178-190. [14] Grundy and Young (2004) *Icarus 172,* 455-465. [15] Barkume et al. (2006) *Astrophys. J. 640,* L87-L89. [16] Barucci et al. (2008) *Astron. & Astrophys.,* 479, L13-L16. [17] Jewitt and Luu (2004) *Nature 432,* 731-733. [18] Buie and Grundy (2000) *Icarus 148,* 324-339. [19] Hansen and McCord (2004) *J. Geophys. Res. 109,* E01012.1-19. [20] Stansberry et al. (2008) In *The Solar System Beyond Neptune,* pp. 161-179. [21] Sheppard and Jewitt (2002) *Astron. J. 124,* 1757-1775. [22] Meech and Svoreň (2004) In *Comets II*, pp. 317-335. [23] Cook et al. (2007) *Astrophys. J. 663,* 1406-1419. [24] Merk and Prialnik (2006) *Icarus 183,* 283-295. [25] Newman et al. (2008) *Icarus 193,* 397-406. [26] Schenk and Zahnle (2007) *Icarus 192,* 135-149. [27] Johnson (1990) *Energetic charged-particle interactions with atmospheres and surfaces*.

UNDERSTANDING THE RADIATION CHEMISTRY OF PURE AND IMPURE SOLAR SYSTEM WATER ICES – THE ROLE OF LABORATORY STUDIES. Murthy S. Gudipati (Gudipati@jpl.nasa.gov), Jet Propulsion Laboratory, California Institute of Technology, Mail Stop 183-301, 4800 Oak Grove Drive, Pasadena, California 91109, USA

Introduction: One of the goals of remote sensing is to identify external signatures of internal processes. This method is particularly relevant to the study of Solar System icy bodies under radiation environment such as Mars, Europa, Enceladus, Ganymede, and Saturn's rings. In order to interpret, understand, and quantify the observed spectroscopic data and create geophysical models, it is necessary to have: (a) laboratory spectroscopic data that are derived from studies on analog materials, and (b) a fundamental understanding of the physicochemical processes that result in the spectroscopic data obtained in the laboratory.

Our research goal is to start with (b) above. Our approach is to understand the fundamental physicochemical processes that occur in ices through laboratory research, then derive the appropriate spectroscopic data (a). This will allow us to guide and support analysis of the observational data, which will lead to improved geophysical models. Our laboratory research forms one of the four vertices of the Space Science Endeavor represented by the Platonic structure "Tetrahedron", interacting with the other three vertices as shown in Figure 1.

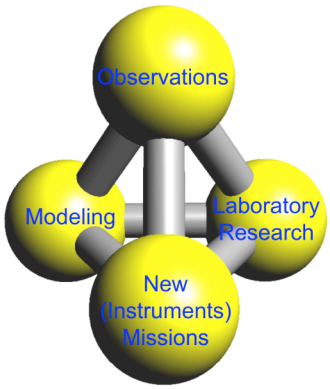

Figure 1: Four branches of the Space Science Endeavor – Missions, Observations, Laboratory, Modeling, represented by the Platonic solid Tetrahedron, cross-connecting each branch to the rest.

Back to Basics (Radiation and Molecules): Though yet to be fully explored, most laboratory studies show that radiation is absorbed/scattered in several different quanta. This results in different excitations within the atoms and molecules – nuclear, electronic, vibrational, and rotational. These excitations can lead to chemical reactions, molecular dissociations, and ionization (removal of an electron from an atom or molecule), as shown in Figure 2. Physicochemical consequences of ionization differ from dissociation in three ways. First, ionization results in creation of charge centers through electron and hole (ion) separation. Second, ionized atoms and molecules are generally more reactive than the radicals. Last, the interactions between ionized molecules and their surroundings is much stronger due to Coloumbic forces.

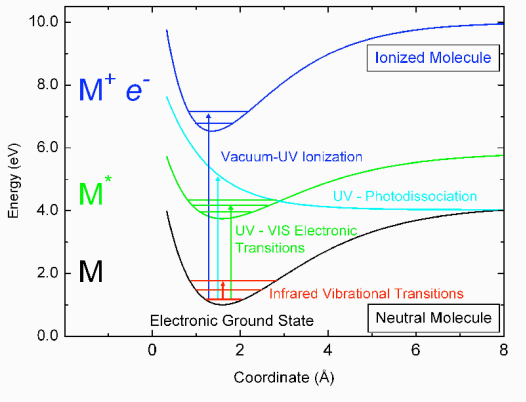

Figure 2: Simplified view of radiation induced molecular excitations that lead to dissociation and ionization processes.

The ice penetration depths of solar wind, γ-rays, and magnetospheric electrons and protons of the giant planets Saturn and Jupiter can be on the order of a meter [3; 4]. Photon penetration is limited by the optical quality of the ice and the particle sizes of the ice grains [5]. The extent of the radiation-induced chemistry is determined by the dosage of a given quanta of energy reaching the molecules embedded in ices and the water molecules of ice themselves.

Laboratory Research (Ionization in Ices): Laboratory studies and observations of Europa and Saturn have shown that radiation processing results in the dissociation of H_2O molecules to O, OH, and H radicals, which recombine to form O_2 [6], H_2O_2 [7; 8], etc. Sputtering of protons (H^+) from ice surfaces [9], chemistry resulting from implantation of keV heavy ions (C^+, N^+) into ice [10], have also been documented in the laboratory.

We found [1; 2; 11; 12] direct evidence for radiation-induced ionization in ice using polycyclic aromatic hydrocarbons (PAHs) as probe molecules (Figure 3). Further highlights of our recent research include: (a) stability of large ionized PAH molecules up to 120 K, while smaller molecules react with the ice matrix even at 50 K; (b) reactions between ionized molecules and the irradiated ice matrix resulting in oxidized molecules (incorporation of oxygen and hy-

drogen into the organic molecules); and (c) sequential multiple ionizations occuring within the ices, leading to higher density of charge and electrons.

These discoveries raise further key questions, being addressed in the laboratory. For example:

(1) what is the fate of the electrons generated in the ices through radiation-induced ionization or electron/ion bombardment?

(2) what is the conductivity (electron mobility) of irradiated ice surfaces containing impurities?

(3) what are the optical properties and spectroscopy of ices in radiation and sputtering environments?

Applications to Solar System Ices: The breadth of astrophysical applications of this work has not yet been fully explored, but some of the applications to Solar System icy bodies include the following.

(a) Coloration of Saturn's rings could be due to ionized large PAH-like molecules imbedded in ices. Generally, ionized atoms and molecules are more strongly colored than the corresponding neutrals, as shown in Figure 3. At temperatures around 100 K, ices can efficiently store these ions indefinitely.

(b) Charged ice grains can enhance adhesion process through strong Coloumbic forces.

(c) The surface ice conductivity of Europa and Enceladus, which are both under strong magnetospheric radiation environments, is yet to be probed. Due to the hemispherical dichotomy of Europa's radiation environment [13], a significant diffrence in surface conductivity between the leading and trailing hemispheres is expected.

(d) Molecular mobility and convection within the ice layers of Europa, Enceladus, and Ganymede could be significantly enhanced. Due to the long-range and stronger nature of Coloumbic forces, charged molecules move faster under a charge gradient than the neutral molecules.

(e) Energy deposited into the ice surface through ionization can be transported into the interior through the above mentioned convection process.

(f) Opening of unique ionization-driven new chemical reaction pathways in ices.

Acknowledgments: The author's research activity presented here is funded by the following NASA programs: Planetary Geology and Geophysics (Grant No. NNG05GI01G), Planetary Atmospheres (Grant No. NNX07AF31G), Discovery Data Analysis Program (Grant No. NNX07AG05G). The author also thanks his collaborators: Drs. Lou Allamandola, Ted Roush, Dale Cruikshank, John Cooper, and Bob Johnson.

References:

1. Gudipati, M. S., Allamandola, L. J., 2003. Facile generation and storage of polycyclic aromatic hydrocarbon ions in astrophysical ices. Astrophysical Journal Letters. 596**,** L195-L198.

2. Gudipati, M. S., 2004. Matrix-Isolation in Cryogenic Water Ices: Facile Generation, Storage and Optical Spectroscopy of Aromatic Radical Cations. Journal of Physical Chemistry A. 108**,** 4412.

3. Cooper, J. F., et al., 2001. Energetic ion and electron irradiation of the icy Galilean satellites. Icarus. 149**,** 133-159.

4. Gerakines, P. A., et al., 2001. Energetic processing of laboratory ice analogs: UV photolysis versus ion bombardment. Journal of Geophysical Research - Planets. 106**,** 33381-33385.

5. Neshyba, S. P., et al., 2003. Representation of a nonspherical ice particle by a collection of independent spheres for scattering and absorption of radiation: 2. Hexagonal columns and plates. Journal of Geophysical Research-Atmospheres. 108**,** 18.

6. Johnson, R. E., et al., 2006. Production, ionization and redistribution of O-2 in Saturn's ring atmosphere. Icarus. 180**,** 393-402.

7. Loeffler, M. J., et al., 2006. Synthesis of hydrogen peroxide in water ice by ion irradiation. Icarus. 180**,** 265-273.

8. Carlson, R. W., et al., 1999. Hydrogen peroxide on the surface of Europa. Science. 283**,** 2062-2064.

9. Herring-Captain, J., et al., 2005. Low-energy (5–250 eV) electron-stimulated desorption of H+, H2+, and H+(H2O)nfrom low-temperature water ice surfaces. Physical Review B. 72**,** 035431-10.

10. Strazzulla, G., et al., 2003. Implantation of carbon and nitrogen ions in water ices. Icarus. 164**,** 163-169.

11. Gudipati, M. S., Allamandola, L. J., 2006. Unusual stability of polycyclic aromatic hydrocarbon radical cations in amorphous water ices up to 120 K: Astronomical implications. Astrophysical Journal. 638**,** 286-292.

12. Gudipati, M. S., Allamandola, L. J., 2006. Double ionization of quaterrylene (C40H20) in water-ice at 20 K with Ly(alpha) (121.6 nm) radiation. Journal of Physical Chemistry A. 110**,** 9020-9024.

13. Cassidy, T. A., et al., 2007. The spatial morphology of Europa's near-surface O-2 atmosphere. Icarus. 191**,** 755-764.

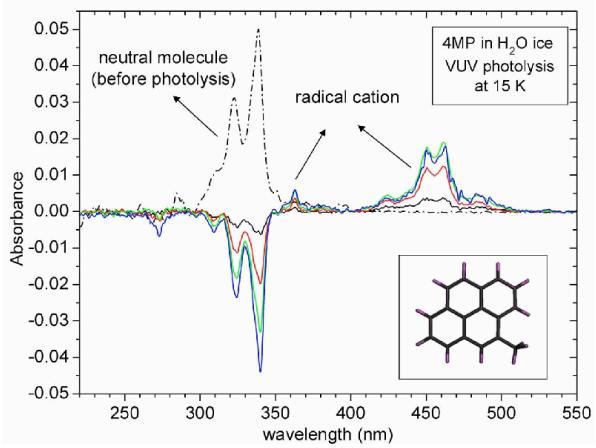

Figure 3: Radiation induced ionization of a PAH 4-methylpyrene imbedded in H_2O ice [1; 2]. From each molecule ionized, an electron is injected into the ice.

NEAR-INFRARED SPECTRA OF TNOs: FIRST RESULTS OF THE NEW ESO-LARGE PROGRAM AND IMPLICATIONS. A. Guilbert[1], M.A. Barucci[1], A. Alvarez-Candal[1], F. Merlin[1], A. Coradini[2], C. DeBergh[1], C. Dumas[3], O.R. Hainaut[3]. [1]LESIA, Observatoire de Paris-Meudon, 5 place Jules Janssen, 92195 Meudon Principal Cedex, France, e-mail: aurelie.guilbert@obspm.fr. [2]INAF-IFSI, Via del Fosso del Cavaliere, 00133 Roma, Italy. [3]ESO, Alonso de Cordova 3107, Vitacura, casilla 19001, Santiago 19, Chile.

Introduction: Trans-Neptunian Objects (TNOs) are believed to be the most pristine remnants of solar system formation. Because of their large heliocentric distance and their resulting faintness of these bodies, their composition is still difficult to assess, and only few spectra are available. Centaurs may be a transition population between TNOs and Jupiter family comets [1]: they are much easier to study than TNOs because they are closer to the Sun.

Some ices' signatures have been detected: methane ice [2-3], crystalline and amorphous water ice [4-5] or methanol [6]. Ammonia even may have been detected [7-8-9], which raises questions on possible internal activity of such objects. Indeed, the presence of either crystalline water ice or ammonia on the surface suggests recent surface renewal mechanisms, since they should have been depleted from the surface within 10^{7-8} years [10]. Therefore, our current knowledge of TNOs seems to indicate a very complicated picture that needs to be further studied.

An ESO-Large Program (PI: M.A. Barucci) has consequently been undertaken with the aim of collecting both photometric and spectroscopic information on about 40 objects.

Discussion: We will consider the results of one year of observations (from October 2006 to September 2007) carried out with the ESO-instrument SINFONI. SINFONI is an integral field spectrometer [11-12] that, while choosing the H+K grating, allows the observations of both H and K bands simultaneously, with a spectral resolution of about 1500. We chose to use the 8" field of view, and did not use any correction by adaptive optics during the observational runs. The data were reduced using the SINFONI pipeline provided by ESO. The signal to noise ratio of each spectrum has been improved by rebinning it, thus achieving a lower spectral resolution. 21 objects were observed: the spectra will be presented, along with relevant physical properties of the ices identified.

Methane is detected on the surface of Eris [13]. The spectra of objects such as Typhon, Thereus, Bienor or 2003 AZ84 show the presence of water ice (absorption band at 2.0 microns). Some other objects seem to have a featureless spectrum (Ixion, 1999 TC36, 2002 KX14, 2004GV9 or 2005 RN43). A radiative transfer model has been run to provide an upper limit on the amount of water ice that can be present on the surface. The case of Chariklo will also be discussed, since the spectrum we obtained is unambiguously featureless: this is in contradiction with previous results [14-15] where water ice was detected.

Crystalline water ice is unambiguously detected -due to the 1.65 microns absorption band- on the spectra of Orcus and Quaoar. Some other small absorption bands are detected on those two spectra: a 2.2 microns band is detected in both, while a 1.73 microns band is detected (within the noise) in the spectrum of Quaoar only. In the case of Quaoar, we can attribute those features to the presence of methane and ethane ices on the surface, as suggested by [16]. The case of Orcus will be discussed extensively. Indeed, the 2.2 microns absorption band can be attributed to either ammonia or methane [9]. If such volatile ices are indeed present, this most likely implies resurfacing mechanisms induced by internal activity, since Schaller & Brown [17] predicted that no volatile ice would survive on the surface of Orcus.

Thermal evolution models have shown that some TNOs can remain partly or entirely pristine, while some others can be completely depleted of volatile ices [18-19-20]. A fully 3D thermal model is under development in our group, and its application would help to better understand the formation and evolution of such curious bodies.

References: [1] Levison H.F. & Duncan M.J. (1997) *Icarus, 127, 13*. [2] Brown M.E. et al. (2005) *ApJ, 635, 97*. [3] Dumas C. et al. (2007) *A&A, 471, 331*. [4] Trujillo C. et al. (2007) *ApJ, 655, 1172*. [5] Merlin F. et al. (2007) *A&A, 466, 1185*. [6] Barucci, M.A. et al. (2006) *A&A, 455, 725*. [7] Dumas C. et al. (2001] *AJ, 121, 1163*. [8] Cook J. et al. (2007) *ApJ, 663, 1406*. [9] Barucci M.A. et al. (2008) *A&A, 479, 13*. [10] Cooper J.F. et al. (2003) *EM&P, 92, 261*. [11] Eisenhauer F. et al. (2003) *SPIE, 4841, 1548*. [12] Bonnet H. et al. (2004) *The ESO Messenger, 117, 17*. [13] Merlin F. et al. i*n preparation*. [14] Brown R.H. et al. (1998) *Science, 280, 1430*. [15] Dotto E. et al. (2003) *Icarus, 164, 122*. [16] Schaller E. & Brown M.E. (2007) *ApJ, 659, 61*. [17] Schaller E. & Brown M.E. (2007) *ApJ, 670, 49*. [18] DeSanstis M.C. (2001) *AJ, 120, 1571*. [19] McKinnon W.B. (2002) *ACM 2002, 29*. [20] Merk R. & Prialnik D. (2006) *Icarus, 183, 283*.

LABORATORY EXPERIMENTS TOWARD DISTINGUISHING ABIOTIC RADIOLYTIC CHEMISTRY FROM RADIOLYTICALLY MODIFIED BIOLOGICAL MATERIAL ON ICY WORLDS. K. P. Hand[1] and R. W. Carlson[1], [1]Jet Propulsion Laboratory California Institute of Technology, Pasadena, CA 91109 (khand@jpl.nasa.gov).

Introduction: We have constructed a vacuum chamber assembly capable of replicating the temperature, pressure, and electron irradiation environment of icy worlds such as Europa, Ganymede, Callisto, and Enceladus. Thin ice films (~3μm) containing water, short-chain hydrocarbons (e.g. propane, propene, butane), and ammonia were irradiated at 70-100K with high-energy electrons and resulting products were monitored in-situ using mid-infrared spectroscopy (FTIR) and residual gas analysis (RGA) up to 300 a.m.u. Similarly, we generated thin films containing spores of *Bacillus pumilus* and subjected the sample to electron bombardment for ~24 hours with 20 keV electrons at 500 nA. Again, the sample was monitored in-situ during irradiation with the FTIR and RGA. All experiments were also monitored during warming from initial temperature to room temperature. Results from these experiments provide information that may be of utility when trying to distinguish abiotic radiotlytic chemistry from possible biosignatures on icy worlds.

Results: The lowermost spectrum in Figure 1 is of the bacterial spores before irradiation, the middle spectrum (red) is after irradiation, and the uppermost spectrum is of abiotic organic chemistry resulting from electron radiolysis of water, ammonia, and propene.

We find that the ~3.44 μm (2870-2970 cm^{-1}) hydrocarbon bands in the biological material are largely indistinguishable from the abiotic spectrum. The asymmetric stretch of $–CH_3$ at 2966 cm^{-1}, the symmetric stretch of $–CH_3$ at 2874 cm^{-1}, and the asymmetric stretch of $–CH_2$- at 2936 cm^{-1} show no variation from one spectrum to the next.

The irradiated spore sample shows production of CO_2 (2340 cm^{-1}), CO (2130 cm^{-1}) and a nitrile band (C≡N) at 2164 cm^{-1}. This nitrile band is typically assigned to the cyanate ion, OCN^- [1]. The abiotic film shows similar features emerging during irradiation. Relative bands strengths are also comparable across the sample spectra, indicating that while the initial chemical compositions may be quite different (cells vs. simple compounds), the suite of new products is quite similar. Taken together with the C-H results, the region from 3-5 μm is devoid of compelling spectroscopic biosignatures.

At wavelengths longer than 5.88 μm (<1700 cm^{-1}), however, differences are seen between the abiotic and biotic samples. In the *B. pumilus* spectrum taken prior to irradiation we observed strong peaks in the region from 1700 cm^{-1} to 1500 cm^{-1}. Several of these peaks correspond to the amide I and amide II bands of proteins. The amide bond, and the associated vibrational excitations, specifically refers to the C-N linkage between amino acids and the interaction with the C=O and N-H on either side of that bond. The bands at 1660 cm^{-1} and 1645 cm^{-1}, as seen in our spectra, are consistent with the N-H and carbonyl vibrational modes in the amide I of the right-handed spiral in α-helical structures of proteins [3]. Also contributing to this region is the amide I band of the β-pleated sheet structures in proteins. This band, at 1637 cm^{-1} [2], is due to the carbonyl stretch interacting with the amide N-H, but in this case the strands of linked amino acids form a sheet by hydrogen bonding with neighboring strands. These protein bands overlap considerably with bands in the same region attributed to the ν_4, 1645 cm^{-1} band of NH_3 [4]. The ammonia bands were seen in our abiotic experiments. The band seen at 1514 cm^{-1}, persists through irradiation and is seen only in the biological sample. This band is sometimes referred to as the tyrosine band [2,3], as it is indicative of proteins containing that amino acid. Similarly, the amide II band at 1549 cm^{-1} persists and is characteristic of the C-N stretch and C-N-H bend in the peptide structures of proteins.

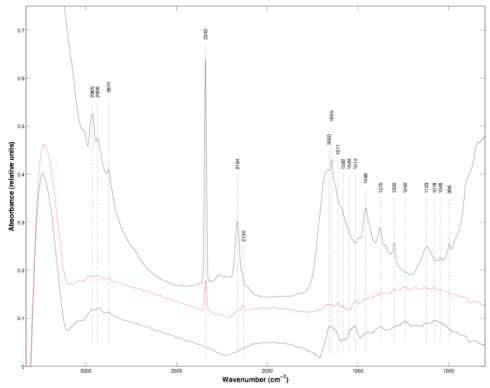

Figure 1: Spectra of irradiated spores vs. electron irradiated H_2O+C_3H_6+NH_3 ice.

The observed decrease in band strength in our experiments indicates destruction and loss of proteins, but importantly, these bands persist and are readily observed in the irradiated sample. These bands are not seen in the abiotic sample. Though HPLC work on our samples indicates production of amino acids, these amino acids are not arranged and polymerized as in the

protein fragments remaining in the spore sample. The survival of biopolymer fragments yields the spectroscopic difference between the biotic and abiotc samples, thus providing a possible spectroscopic biosignature. Matrix-assisted laser desorption and ionization was used to investigate the size of the biopolymer fragments. We found evidence for compounds as large as m/z ~2500.

At longer wavelengths hydrocarbons bands are seen in all samples at 1458 cm^{-1}, 1375 cm^{-1}, and the methane band at 1300 cm^{-1}. A pair of strong broad bands were seen in the irradiated spore sample at 1240 cm^{-1} and at 1078 cm^{-1}. These bands have no direct pairing with the bands in the abiotic NH_3 sample. The former band corresponds to the asymmetric stretch of P=O in phosphodiester bonds ($>PO_2^-$) [3]. The phosphodiester bond connects the nucleotides of RNA and DNA. The diesters of ATP occur at slightly shorter wavelengths, ~1260 cm^{-1}, compared to what we observed [5]. The second broad band, centered at 1078 cm^{-1}, also corresponds to the phosphodiester bond, but in this case the band results from the symmetric stretch of P=O [3, 6]. Our abiotic experiments did not contain phosphorous. Thus direct comparisons with these bands are incomplete and require adding phosphorous (and sulfur), for more comprehensive understanding of abiotic vs. biotic differences in this region.

During radiolysis, results from the RGA show no measurable peaks beyond m/z = 44, consistent with CO_2 or short-chain hydrocarbon loss. Under steady-state radiolysis at ~100 K, these results indicate that no mass spectral biosignature would be detectable from orbit with just electron radiolysis (see Carlson and Hand, this volume, for sputtering effects). (Note, we have not yet analysed differences in isotopic composition.) During warming, larger mass fractions were observed with the RGA. Figure 2 shows the integrated spectrum of mass fractions observed during warming from 100 K to 298 K. Most of the species are also seen in the abiotic sample, but the two peaks at m/z = 55 and m/z = 69 were strong and distinct in only the biological sample. We have not yet uniquely identified these fragments, but working with a new mass spectrometer on our system we hope to identify these species. No fragments were observed with appreciable signal strength beyond m/z = 69.

Conclusion: Spectroscopic biosignatures associated with the biopolymers of terrestrial life may persist under the temperature, pressure, and electron radiolysis conditions found on worlds like Europa, Ganymede, Callisto and Enceladus. The critical spectroscopic region to explore is that of the amide band region, ~5-7 µm. Future missions must seriously consider included spectroscopic capabilities in this region if astrobiology is seen as an important mission objective.

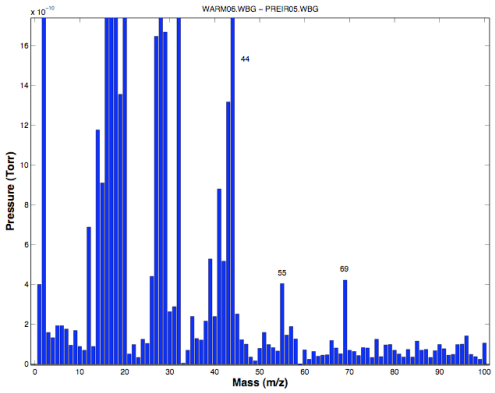

Figure 2: RGA spectrum of irradiated spores collected during warming from 100 K to 298 K.

References:

[1] Hudson et al., 2001, The Astrophysical Journal 550 (2), 1140–1150. [2] Naumann et al., 1996. In: Mantsch, H., Chapman, D. (Eds.), Infrared Spectroscopy of Biomolecules. pp. 279–310. [3] Maquelin et al., 2002, Journal of Microbiological Methods 51 (3), 255–271. [4] Moore et al., 2007, Icarus 190 (1), 260–273. [5] Liu et al., 2005, Biophysical Journal 89 (6), 4352–4363. [6] Choo-Smith et al., 2001, Applied and Environmental Microbiology 67 (4), 1461–1469.

FLAVORS OF AMORPHOUS SURFACE ICE ON EUROPA: A BROADER PEAK ON THE TRAILING SIDE. G. B. Hansen, Department of Earth and Space Sciences, University of Washington, Box 351310, Seattle, WA 98195-1310 (ghansen@ess.washington.edu).

Introduction: The grain surfaces of the ice on Europa, illustrated by the Fresnel peak near 3.1 µm, have an amorphous crystal structure [1]. Hansen and McCord [1] used several example average spectra of Europa from the Galileo Near Infrared Mapping Spectrometer (NIMS) to show the broad, featureless peak near 3.1 µm characteristic of amorphous ice. If one looks in detail at these spectra, some of the Europa spectra have a triangular peak like the amorphous ice model, while many others have a broader flat-topped peak extending to longer wavelengths. Now that we have a calibrated and despiked Europa cube (covering 140 to 270 degrees longitude at mid latitudes [2]) from which five of the nine spectra shown in [1] come from, we decided to look at the occurrence and distribution of different Fresnel peak shapes from the ice.

Data: The NIMS instrument measures reflected sunlight between 0.7 and 5.3 µm with up to 408 channels and a resolution of 28 nm. The spectra are built up from grating motion and 17 discrete detectors, so that each spectrum has 17 segments. The motion of a mirror and the spacecraft scan platform allows for the construction of three-dimensional spectral image cubes [3]. The observation used here is from the sixth orbit, by which time one of the detectors had failed (2.40-2.67 µm). An image from 0.7 µm from the observation TERINC is shown in Figure 1.

Two average spectra are extracted from this observation, one from the right edge (leading hemisphere) and one from the middle (trailing hemisphere). The locations are indicated in Figure 1 by X's. The spectra are plotted in Figure 2, with the leading side spectrum in black and the trailing side spectrum in red. The near-infrared water ice bands are shown in the upper panel (to 2.5 µm) and the dark part of the spectrum beyond 2.5 µm is shown in the lower panel. The 3.1-µm peaks are indicated with arrows in the lower panel. Parts of the leading side spectrum between 1.2 and 1.5 µm are saturated and not shown in the upper panel.

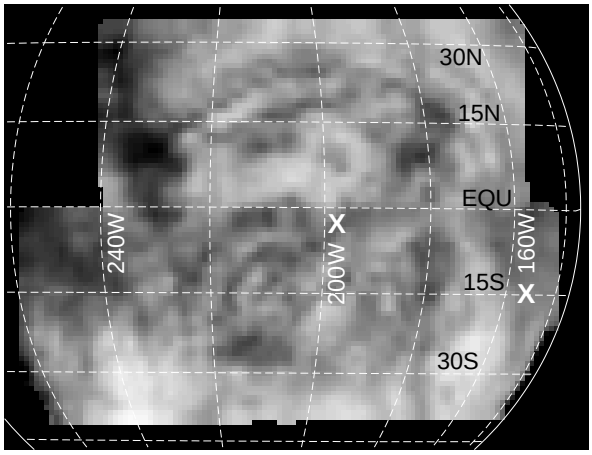

Figure 1. Albedo image from 0.7 µm of the e6 TERINC NIMS observation of Europa. The two white X's indicate where average spectra have been taken from.

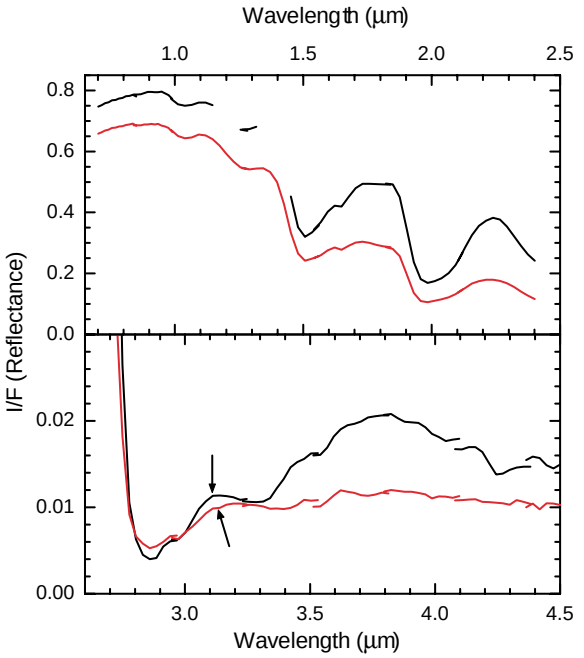

Figure 2. Average spectra from the two locations on Figure 1, the black spectrum from the right edge and the red spectrum from the middle.

The upper panel shows water ice bands mixed with some hydrates. The deeper bands in the black spectrum and the peak at 3.6 µm are indicative of finer grained (<50 µm radius) snow, while the red spectrum is consistent with coarser-grained ice. The 3.1-µm peak is broader and flatter in the red spectrum compared to the triangular band in the black spectrum.This is illustrated better by removing a continuum from below the peaks and scaling the slightly weaker red peak to the same height as the black one, as seen in Figure 3. Here the flat top of the red peak is evident as is the increased width (by about 0.08 µm)

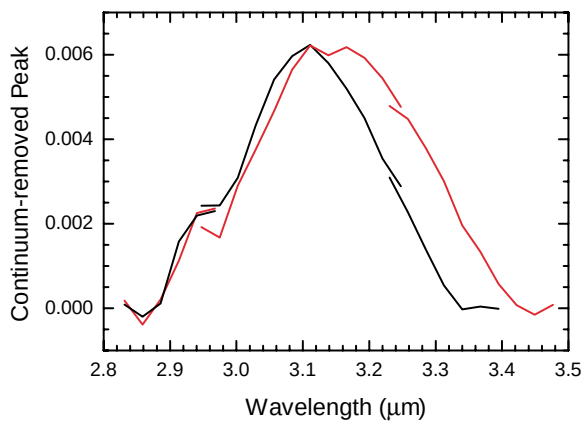

Figure 3. Continuum-removed Fresnel peaks for the two example spectra (the red one has been scaled by 1.5 to match the height of the black). The read peak is about 0.08 μm wider than the black peak and has a flat top, as seen in other Europa icy average spectra.

Discussion: According to Hagen *et al.* [4], the longer position of the red peak is not consistent with any amorphous form. In fact a center at 3.14 μm (3185 cm^{-1}) is outside the range of any ice they measured and beyond the range for crystalline ice (3207–3220 cm^{-1}). The increased width (250 to 330 cm^{-1}) is only slightly larger than the most unannealed forms of amorphous ice, though.

In this observation, triangular bands like the black spectrum are limited to the right edge and part of the top edge. Mixed broader bands are found through the rest of the observation. The flat-topped broader bands shown in [1] are apparently common on the trailing hemisphere, but are also found at higher latitudes on the leading hemisphere, while the triangular bands are found throughout most the fine-grained leading.hemisphere terrains. This pattern implies that perhaps radiation levels, which are enhanced on the trailing side [5], could be the cause of the broader peaks.

Conclusions: The signature of amorphous ice on the surface of Europa, the Fresnel peak near 3.1μm, varies across the surface from a form consistent with laboratory measurements of center and width to a much broader peak that is not consistent with current laboratory measurements. The locations of the broader peaks is coincident with larger radiation levels [5], and is perhaps an indication of the effect of very high radiation levels on the spectrum of water ice.

References: [1] Hansen, G. B., and T. B. McCord (2004), *JGR, 104*, 16471–16486. [2] Hansen, G. B., and T. B. McCord (2008), *GRL, 35*, L01202. [3] Carlson *et al.* (1992), *Space Sci. Rev., 60*, 457–502. [4] Hagen, W., A. G. G. M. Tielens, and J. M. Greenberg (1981), *Chem. Phys., 56*, 367–379. [5] Paranicas, C., R. W. Carlson and R. E. Johnson (2001), *GRL, 28*, 673–676.

TITAN'S SURFACE COMPOSITION: CONSTRAINTS FROM LABORATORY EXPERIMENTS AND CASSINI/VIMS OBSERVATIONS. P. Hayne[1,2], T. B. McCord[2], C. Sotin[3], M. Barmatz[3], R. Mielke[3], J-Ph. Combe[2], G. B. Hansen[2,4]. [1]University of California, Los Angeles (595 Charles Young Blvd E, Los Angeles, CA 90095; phayne@ucla.edu), [2]The Bear Fight Center (PO Box 667, Winthrop, WA 98862), [3]Jet Propulsion Laboratory-California Institute of Technology (Pasadena, CA), [4]University of Washington (Seattle, WA).

Introduction: Observations of Titan's surface are severely hindered by the presence of an optically thick, scattering and absorbing atmosphere. For this reason, very little was known of Titan's surface composition prior to Cassini. Observations from this mission have revealed a surface rich in geologic diversity, but its composition remains elusive [1, 2]. Surface composition has important consequences for models of Titan's interior, surface, and atmosphere, especially in the search for an endogenic methane source. Recent analysis of data from the Cassini Visual and Infrared Mapping Spectrometer (VIMS) [1, 3] confirms the presence of "dirty" water ice deduced from earlier ground-based studies [4, 5]. However, many regions of Titan are not spectrally consistent with water ice as the dominant component, and the identity of the other constituents remains ambiguous.

Evidence from VIMS spectra suggests CO_2 frost is

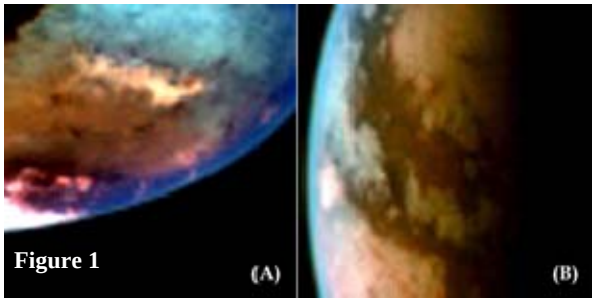

Figure 1

consistent with the bright terrain [1], especially concentrated on two features suggested to be cryovolcanoes (Fig. 1) [6, 7]. CO_2 is not a likely cryomagma component [8], but instead is probably condensed from the atmosphere, as predicted by photochemical models [9]. On the other hand, some ice mixtures predicted by atmosphere and interior models to be on Titan's surface have unknown reflectance properties in the near-IR. Here we describe a series of infrared reflectance experiments on Titan-analogue ices, which are being planned at the Jet Propulsion Laboratory. An ongoing complementary effort to classify and map Titan's compositional units with the VIMS data will be constrained by the laboratory results.

Spectral Information from VIMS: We use two methods to infer surface composition from VIMS reflectance data.

(1) *Spectral Mixture Analysis (SMA)*: Titan spectra are modeled as a linear combination of endmember spectra, using only reflectance values within the methane "windows" [1]. Dark material can be modeled well by H_2O ice and a spectrally neutral contaminant, plus CO_2. Bright terrain, particularly Tui Regio (Fig. 1A) and Hotei Regio (Fig. 1B), are modeled well by CO_2 ice and an unknown component, which is bright at 2.0 μm.

(2) *Absorption band search*: A custom band-fitting algorithm was developed to search for molecular absorptions within Titan's methane windows [1]. Only one absorption has been detected so far, near 4.92 μm and perhaps corresponding to the 4.90 (2042 cm^{-1}) triphonon band of CO_2 [11]. This absorption feature is again concentrated at Tui Regio and Hotei Regio. If CO_2 were present, we would expect the spectral contrast 2.8-2.7 μm to be positive and correlated with the strength of the 4.9-μm feature. This is indeed observed. The three correlated spectral traits are shown in Figure 2 for Tui Regio (the bright elongated feature): (a) 4.9-μm band depth, (b) 2.8/2.7-μm ratio, and (c) SMA CO_2 endmember. Whether or not the material is CO_2, we infer that all three spectral traits are due to the same compound or mixture.

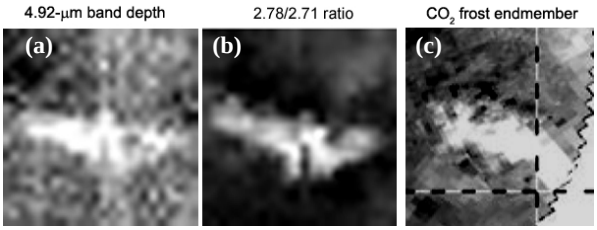

Figure 2

Laboratory Experiments: Discriminating among possible surface constituents with VIMS is only possible with the benefit of laboratory reflectance data for each candidate material. While spectra of pure compounds such as CO_2, CH_4 (liquid), NH_3, CH_3OH, hydrocarbons, and nitriles are generally well characterized in the region 1–5 μm, the reflectance properties of mixtures are poorly constrained. For instance, the 4.9-μm band of CO_2 may be shifted by bonding with H_2O ice, which could account for the ~20 nm shift observed in the VIMS spectra. Frequency shifts this large (and in the same direction) have been observed in the laboratory for $H_2O{\cdot}CO_2$ mixtures, but this particular band

was not examined [12]. The spectral properties of liquid methane pooled on an H_2O-ice substrate are also unknown, and will be a starting point for a series of reflectance measurements to be carried out at the Jet Propulsion Laboratory (JPL). Such measurements will inform VIMS observations of Titan's North Polar lakes, which are gradually becoming illuminated by the rising springtime sun. Other compounds and mixtures, especially CO_2 and CH_4 clathrate hydrates, will be considered for study at high spectral resolution under Titan conditions. Components important for models of cryovolcanism on Titan also may be considered, including NH_3 hydrate and possibly ammonium sulfate [13].

Our experimental setup, which is presently in the construction phase, includes a monochromator capable of ~1 nm spectral resolution, and an imaging mid-wavelength infrared camera with nominal spectral range ~1–14 μm. Gas- or liquid-phase samples will be introduced and allowed to condense in the optical dewar, which will contain a water-ice substrate at ~90 K and 1.5 bar N_2. Reflectance spectra will be measured for all regions of the sample, including both transition regions and pure phases. Preliminary tests resulted in the successful delivery of liquid CH_4 to the substrate (Fig. 3).


Figure 3

Discussion and Future Work: Initial results from VIMS indicate Titan's surface is dominated by H_2O-ice mixtures, but the remaining components are poorly constrained. The surface is diverse in morphology and spectral shape, indicating a commensurate level of diversity in composition. Some interpretations suggest the IR-dark dune material is depleted in water ice, and possibly enriched in hydrocarbon and nitrile grains, while the bright terrain is covered by a patina of tholin-like haze particles [14]. However, the presence of CO_2 is perhaps quantitatively a better fit, especially for the bright terrain [1]. Our goal is to use new laboratory data to discriminate between proposed materials and map their distribution on Titan's surface. Of particular interest is the suggested CO_2 absorption feature, but we will also attempt to provide constraints on CH_4 liquid and clathrate hydrate, and possibly NH_3 hydrate and methanol – all of which are important cryomagma candidates [8].

Application of a full radiative transfer model to the VIMS data will allow modeling of atmospheric scattering and absorption, improving estimates of *I*/*F* for the surface. With improved reflectance spectra, results from the SMA will more realistically represent materials studied in the laboratory. An improved version of the band-fitting algorithm will be used to search for additional molecular absorptions due to surface materials.

References: [1] McCord, T. B. *et al.* (2008) *Icarus* 194, 212-242. [2] Stofan, E. R. *et al.* (2007) Nature, vol. 445, p. 61-64. [3] McCord, T. B. *et al.* (2006) Planetary and Space Science, v. 54, iss. 15, p. 1524-1539. [4] Coustenis, A. *et al* (1995) Icarus 118, 87. [5] Griffith *et al* (2003) Science 300, 628-630. [6] Barnes, J. W. *et al.* (2006) *GRL, 33,* L16204. [7] Hayne, P. *et al.* (2006) *AGU Fall Meeting*, #P13A-0166. [8] Kargel, J. S. (1992) *Icarus 100*, 556-574. [9] Planetary and Space Science 51, 1017-1033. [10] Combe, J-Ph. *et al.* (2008), Planetary and Space Science, *in press*. [11] Bini *et al.* (1991) *Phys. Lett. A*, 157, p. 273. [12] Sandfordm, S. A. and Allamandola, L. J. (1990) Astrophysical Journal 355, 357-372. [13] Fortes, A. D. et al. (2007) *Icarus 188*, 139-153. [14] Soderblom, L. A. et al. (2007) Planetary and Space Science *55*, 2025-2036.

Acknowledgement: A portion of this work was supported by the NASA/ESA Cassini Project. A portion of this work was performed at the Jet Propulsion Laboratory - California Institute of Technology under contract to NASA.

UV SPECTRA OF THE ICY MOONS OF JUPITER AND SATURN. A. R. Hendrix[1], [1]Jet Propulsion Laboratory/California Institute of Technology, Mail Stop 230-250, Pasadena, CA 91109; arh@jpl.nasa.gov.

Introduction: Ultraviolet spectroscopy is a useful tool for surface composition studies: the short penetration depth means that weathering products are readily detected;. ultraviolet wavelengths sense the topmost layers of the surface, and are therefore very sensitive to exogenic effects. A thorough analysis of UV data can lead to a determination of the abundances and distribution of radiation products such as H_2O_2, O_3 and SO_2. Furthermore water ice has a distinctive absorption edge in the far-UV However, in order to more fully utilize the existing UV datasets of icy surfaces in the solar system, and to better prepare for future observations, ultraviolet laboratory measurements of a range of candidate materials are needed. Here we briefly review what has been learned from UV measurements of the surfaces of the icy moons of Jupiter and Saturn, within the context of needed laboratory measurements.

The Icy Galilean Satellites: The first in-depth ultraviolet studies of the icy Galilean satellites (Europa, Ganymede and Callisto) were accomplished with the use of the International Ultraviolet Explorer (IUE) satellite [1]. Subsequent disk-integrated observations with Hubble Space Telescope (HST) supported the initial findings of IUE, in addition to adding to our knowledge of the composition of the surfaces of these satellites. Galileo UVS observations contributed to disk-resolved studies of these bodies.

The ratio of IUE spectra of Europa's trailing hemisphere to its leading hemisphere led to the discovery of an absorption feature present primarily on the trailing hemisphere centered near 280 nm. The absorption feature, was attributed to an S-O bond and was suggested to be due to implantation of sulfur ions into the ice lattice on the trailing hemisphere [2]. HST measurements confirmed the absorption feature and it was suggested that the feature was similar to laboratory spectra of SO_2 frost on water ice [3]. Subsequent disk-resolved Galileo UVS measurements showed that the 280 nm absorption feature is strongest in regions associated with visibly-dark terrain [4]. These locations have also been found to have relatively high concentrations of non-ice material, interpreted to be hydrated sulfuric acid or hydrated salt minerals. An additional Galileo discovery was the presence of hydrogen peroxide (H_2O_2) on Europa, primarily in regions of lower non-ice concentrations, such as on the leading hemisphere [5].

IUE spectra of Ganymede's trailing hemisphere ratioed to the leading hemisphere revealed the presence of a possible absorption feature centered close to 260 nm [1], though the signal was approaching the IUE detection limits. It was suggested that ozone (O_3) in the ice could explain the apparent absorption feature. Subsequent HST measurements confirmed the presence of the O_3 absorption feature in the ice lattice on the trailing hemisphere [6]. Disk-resolved observations of Ganymede from Galileo showed that the O_3 feature was strongest in the polar regions, and at large solar zenith angles, suggesting a connection with the magnetic field lines, or with photolysis or ice temperatures [7].

New results from Callisto [8] show that at high southern latitudes, the NUV spectra tend to be spectrally blue (or "roll over") >280 nm – suggesting the shoulder of an absorption feature with a band center ~350 nm. The lower latitudes are generally darker and largely spectrally redder than the high southern latitude region. This suggests that an absorber is present at high latitudes, which is weathered away by charged particle or UV bombardment at low latitudes. We suggest that the high latitude absorption feature could be due to an organic species. A carbon cycle may be occurring on Callisto, with CO_2, carbonates and carbon sub-oxides are principal end-products. The overall dark grey visible appearance of Callisto is consistent with laboratory measurements of carbonization of organics through radiation.

The Icy Saturnian Moons: HST observations of Dione and Rhea [9] detected an absorption similar to the 260 nm absorption feature detected by HST on Ganymede and has been attributed to the presence of ozone on both satellites. Like Ganymede, Dione and Rhea orbit within the magnetosphere of their planet. Ozone on these satellites may be a product of radiolysis, though radiolysis is likely a much less important process in the Saturnian system than in the Jovian system.

More recently, with the arrival of the Cassini spacecraft at the Saturn system, far-UV measurements of the icy satellites have been made with the Ultraviolet Imaging Spectrograph (UVIS). The far-UV spectra of the icy satellites are dominated by the strong water absorption feature at ~165 nm (Fig. 1). At wavelengths shortward of ~165 nm, the icy satellites are extremely dark due to the presence of water ice. However, the spectra of the icy moons of Saturn do not exactly match the H_2O ice models, either in shape or in magnitude – and thus lab data of candidate non-water ice species are very much needed to address these data. We take for example Enceladus (Fig. 2). Notice that the albedo of Enceladus is ~0.3 at 180 nm, compared with ~0.65 at the same phase angle at 439 nm [11] – *so some species is present in the surface of Enceladus*

that is spectrally active in the 180-440 nm region, causing the reflectance to drop by a factor of ~2 [12].

The absorbing species on Enceladus must be spectrally active primarily in the NUV, since Enceladus is very bright (non-absorbing) in the visible and NIR. Candidate species are shown in Figs. 3 and 4. A tholin mixed with water ice may be the most appropriate choice to match the Enceladus spectrum, as the VNIR spectra of tholins are relatively bright and spectrally bland, with a strong drop-off in brightness in the NUV; mixture models are in progress. More laboratory data are needed to better understand Enceladus and the other icy Saturnian moons.

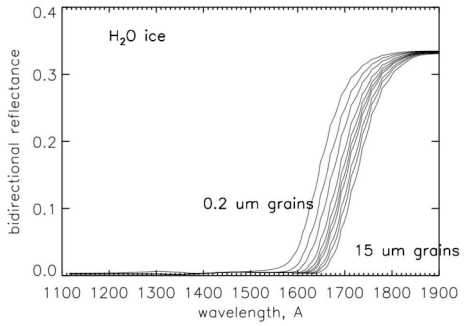

Fig. 1. Models of water ice reflectance spectra for several grain sizes, using optical constants [10].

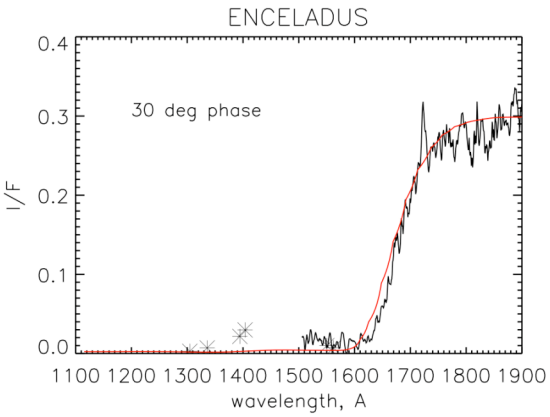

Fig. 2. Cassini UVIS spectrum of Enceladus with sample water ice model overplotted. The measured albedo, compared with the visible albedo at the same phase angle, suggests a strong absorption in the FUV-NUV-VIS region.

Laboratory Data Needs: Measurements of the optical constants of candidate ices and ice mixtures are needed in the ultraviolet (100-400 nm) to compare with spacecraft data of the icy moons of Jupiter and Saturn. The optical constants of non-ice species such as organics and different tholins are needed. In particular for the case of the Galilean satellites, laboratory studies of irradiated samples are needed.

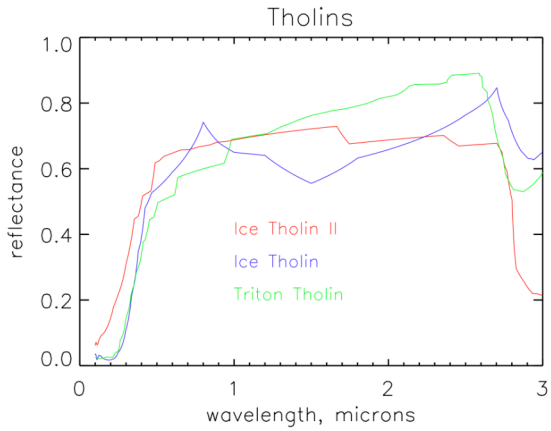

Fig. 3. Model reflectance spectra of tholins (after [13]). (The spectrum of ice tholin II is an extrapolation into the FUV.)

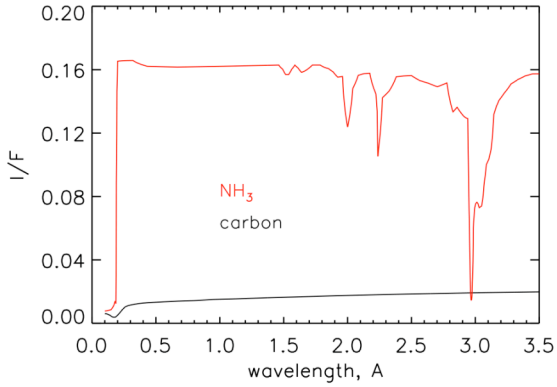

Fig 4. Model reflectance spectra of ammonia and carbon.

References: [1] Nelson R. M. et al. (1987) *Icarus, 72,* 358-380. [2] Lane A. L. et al. (1981) *Nature, 292,* 38-29. [3] Noll K. S. et al. (1995) *JGR, 100,* 19057-19059. [4] Hendrix A. R. et al. (1998) *Icarus, 135*, 79-94. [5] Carlson, R. W. et al. (1999) *Science, 283,* 2062-2064. [6] Noll, K. S. et al. (1996) *Science, 273,* 341-343. [7] Hendrix, A. R. et al. (1999) *JGR, 104,* 14169-14178. [8] Hendrix, A. R. and Johnson, R. E., *LPSC 2007.* [9] Noll, K. S. et al. (1997) *Nature, 388,* 45-48. [10] Warren, S. G. (1984) *Appl. Optics, 23,* 1206-1225. [11] Verbiscer, A. J. et al. (2005) *Icarus, 173,* 66-83. [12] Hendrix, A. R. and Hansen, C. J. (2007) *Fire & Ice Workshop abstract.* [13] Cruikshank, D. P. et al. (2005) *Icarus, 175,* 268-283.

VOLATILES BUT NOT ICES, FROM ICY SATELITES TO OUR MOON. C. A. Hibbitts[1], [1]A Johns Hopkins University Applied Physics Laboratory, 11100 Johns Hopkins Rd., Laurel, Md. 20723. karl.hibbitts@jhuapl.edu

Introduction: One of the most abundant volatiles in the outer solar system is CO_2. On Ariel, CO_2 is ice [1], however, on warmer surfaces closer to the Sun, such the surfaces of the Saturnian and Galilean satellites, this CO_2 is complexed with another material [2,3]. This interaction with the second, presumably less volatile, material has been invoked to account for the presence of CO_2 in these surfaces at temperatures which CO_2 is thermally unstable and should not reside [4,5,6,7,8]. The physical state, how the CO_2 is 'trapped' in the surface, and the nature of its host material remains debated [8,9] with inferences being drawn in part from the position of its ν_3 absorption band (Figure 1).

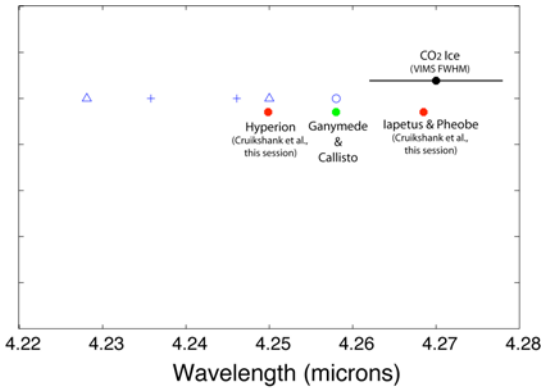

Figure 1. Wavelength at which CO_2 absorbs when phyisorbed onto clays (blue symbols) under vacuum cryogenic conditions, compared to observed wavelengths of CO_2 on icy satellites.

Keeping volatiles on icy satellites: Whereas this host material may be either water ice or nonice materials (or both) on the Saturnian satellites, on the Galilean satellites, spectral modeling [4,5] and thermal modeling [10] of the stability of waterice support the argument that the host material of CO_2 there is the nonice material. Hibbitts and Szanyi, (2007) propose a weak phyical interaction akin to van der Waals bonding that, when operating at the cold temperatures of these satellites surface, can overcome the kinetic energy of the CO_2 molecules, effectively resulting in the physisorptoin of this gas even under no overburden pressure. Their results suggest that this adsorption is site speicific with the local electric environment playing an important role by inducing a dipole in the CO_2, casuing a dipole – induced dipole attraction (akin London forces). Not explored by them is the alternative that permananent electronic quadropole moment of the CO_2 molecule and the local electrostatic field of cations, dangling bonds, etc. could be the origin of this force.

Water on the Moon: It is worth considering the possibility that this type of electrostatic interaction between normally unstable volatiles and a more stable host material could be a pervasive mechanism operating throughout the solar system. If pervasive, then our understanding of how volatiles are distributed within the solar system may be altered. For instance, CO may be trapped onto stabilizing host materials on satellites of Uranus. Alternatively, water, which is thermally stable on the surfaces of some outer satellites, but is ephemeral closer to the Sun, may be similar held onto surfaces (distinct from hydrogen bonding). Waterice on the surface in permanently shadowed craters on the moon would be stable [e.g. 11] and has been postulated to exist [e.g. 12,13]. However, any water at the lunar poles may instead exist as adsorbed molecules. Water originating from cometary residue would accumultate slowly, statistically more likely to first encounter a lunar regolith particle than another water molecule given the 1000ppm upper estimate of abundance for water at the poles [14]. Some preliminary measure-

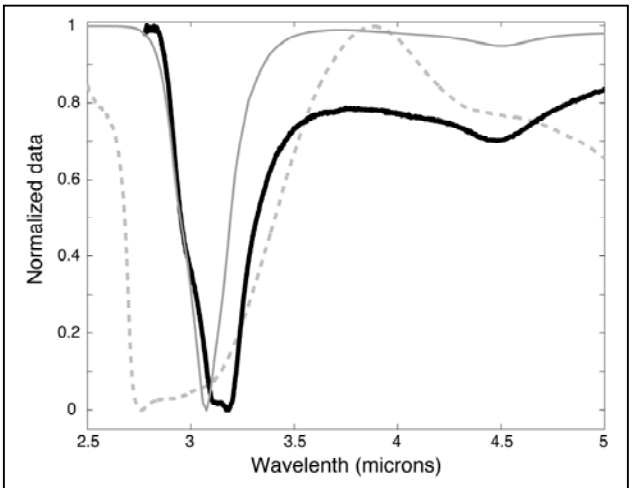

Figure 2. The 3-μm fundamental absorption band in water adsorbed onto montmorillonite at ~ 150K (thick blackline) is shifted ~ 80-100 nm to long wavelengths compared to the same band in crystalline water ice (thin grey line). The adsorbed water is also spectrally distinct from chemisorbed water in room-temperature montmorillonite (dashed line) - the small depression in the bottom of the broad feature (Salisbury, 1991). Note: there is no temperature dependency in this band for water ice or hydrated minerals at this spectral resolution.

ments exploring the physisorption of water onto lunar analogs (powdered anorthositic rocks) provide some evidence for this process occurring (Figure 2). Previous experiments by others [e.g. 12]conducted on lunar samples demonstrate that although the lunar regolith will quickly chemisorb water at room temperature, there is little data on the interaction of pristine regolith and water vapor under vacuum cyrogenic conditions. The possibility that water may be adsorbed (not chemically bound) to the lunar regolith may warrant consideration. This mechanism may also enable water to exist at temerpatures where ice would otherwise be thermally unstable. Also, water in this physical state may not be detectable by the effect of its electric permittivity at radar wavelengths although it would still be detected by neutron spectroscopy.

References::

[1] Grundy, W., L Young, E. Young (2003) Icarua, 162, 222-229. [2] McCord et al., 1998, [3] Brown et al., 2006/ [4] Hibbitts et al., 2000, [5] Hibbitts et al., 2001, [6] Buratti et al., 2005; [7] Clark et al., 2005; [8]Cruikshank et al., 2008. [9] Hibbitts and Szanyi, 2007. [10] Spencer, 1984. [11] Vasavada et al., Icarus, 141, 179-193, 1999. [12] Epstein and Taylor, , Proc. Lunar Sci. Conf. 4th, 1559-1575, 1973. [13] Hodges et al., J. Geophys. Res., 107, 10.1029/2000JE001491, 2002... [14] Feldman et al., Science, 281, 1496-1500,1998.

SUBLIMATION, DEPOSITION AND UV PHOTOCHEMISTRY OF ENCELADUS PLUME MIXTURES.
R. Hodyss[1], P. V. Johnson[1], J. D. Goguen[1], J. V. Stern[1], C. F. Campbell[2] and I. Kanik[1], [1]Jet Propulsion Laboratory, California Institute of Technology, 4800 Oak Grove Drive, Pasadena, CA 91109 (Robert.Hodyss@jpl.nasa.gov), [2]California State University, Fullerton, CA 92831.

Introduction: The south polar region of Enceladus is the source for a plume of gas and water ice particles that are a source for Saturn's E ring [1]. The plume emanates from multiple locations on the surface that correspond to the fractures referred to as the "tiger stripes" [2]. INMS data show the plume is composed of 91 ± 3% H_2O, 3.2 ± 0.6% CO_2, 4 ± 1% N_2 or CO, and 1.6 ± 0.4% CH_4 [3]. Temperatures on Enceladus range from ~37 K in the north polar night to a diurnal range of 50-75 K at low latitudes to perhaps 145 K or more in the warmest surface area of the tiger stripes [4]. Within this large temperature range, water ice undergoes significant structural reorganizations which influence the inclusion, mobility, and escape of trapped gases [5; 6].

We have conducted preliminary experiments with ices similar in composition to the plume gases in order to assess the contribution of phase change and sublimation related gas release in the formation of Enceladus' plume. While this behavior may not completely explain the presence of the plume, it undoubtedly contributes to its formation.

Regardless, some portion of the plume will be deposited on the surface of Encladus. Remote sensing of surface composion will, at least in part, reflect the temperature dependent depostion efficiency of the plume constituent species in combination with subsequent chemistry driven by ultraviolet (UV) solar photons. We have therefore begun an investigation into the depostion efficiency of the plume materials as a function of temperature, as well as the UV photochemistry of the subsequent ices.

Experimental: We performed temperature programmed desorption experiments on ice films deposited from a gas sample of composition 1.6% CH_4, 3.1% CO_2, 3.8% N_2, and 91.5% H_2O. The thickness of the ice film was approximately 0.15 μm, deposited at a rate of approximately 0.5 μm/hr. Samples were deposited at 20 K and 70 K and were warmed at a rate of 1 K/min. These deposition temperatures were selected to bracket the range of insolation driven temperatures on Enceladus.

An Ar-mini arc discharge lamp was used to provide a broadband UV spectrum, roughly analogous to the solar spectrum. Photochemical products were monitored via Fourier transform infrared (FTIR) spectroscopy.

Results: Figure 1 shows the results of our TPD studies. A number of desorption features are common

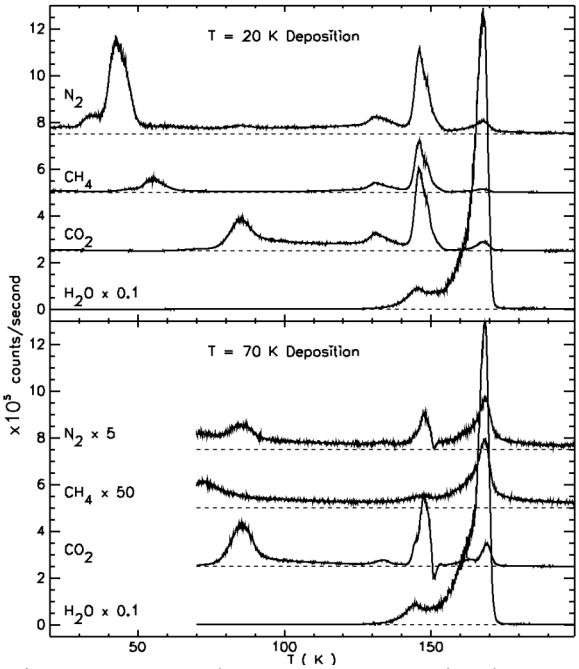

Figure 1. Measured mass spectrometer signal *S* vs. temperature for each of the 4 ice component molecules for ices deposited at T=20 K (top) and T=70 K (bottom). Traces are offset vertically for clarity.

to both the 20K and 70 K depositions. Desorption of N_2, CH_4 and CO_2 is seen at 42 K, 55 K, and 85 K, respectively. These desorptions correspond to the sublimation of these species from the surface of the highly porous, amorphous water ice film [7; 8].

Significant N_2, CH_4 and CO_2 desorption features are also seen at 131 K and ~145 K. These are probably caused by phase changes within the water ice matrix from an amorphous solid to a third amorphous phase or a 'strong viscous liquid.' [9] and during crystallization to the hexagonal form, respectively. Water also begins to desorb significantly in the latter temperature range. Some of the more volatile gases are also released along with water as the rate of water sublimation reaches its peak.

Consider the temperature range 135 to 155 K in the "instantaneous outgassing" plot Fig. 2. This is where the H_2O is just beginning to desorb while the other gases are still trapped in significant amounts. This initial burst of outgassing results in a high fraction of H_2O plus significant quantities of CO_2, N_2 and CH_4. The T=20 K deposited ice could easily produce a plume-like mixture of gases if it were warmed to 135

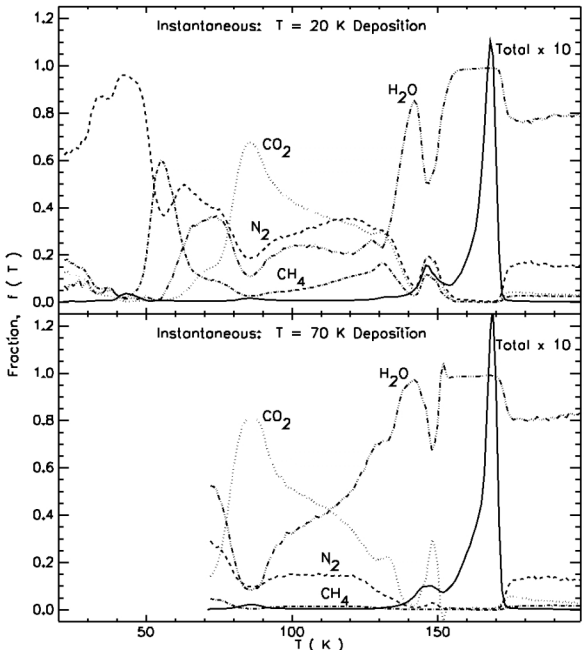

Figure 2. The "instantaneous outgassing" for ices deposited at T=20 K (top) and T=70 K (bottom). The ordinate value where a vertical line drawn at any T intercepts the $f_i(T)$ curves gives the instantaneous fraction of each component gas escaping during a $\Delta T = 1$ K interval. The solid lines labeled "Total" denote the fraction of all gas release that occurs within the $\Delta T =$ 1 K interval.

to 155 K. The T=70 K deposited ice would be depleted in CH_4 and CO_2 would be enriched over N_2. Fig. 2 also shows that if ice deposited at either T=20 K or 70 K were warmed to T>155 K, then the escaping gas will be essentially pure H_2O because nearly all of the other trapped gases escape in the range from 135 to 155 K.

This 135 to 155 K temperature range is also precisely the temperature range that includes the CIRS measured temperatures of Enceladus South pole and Tiger stripes [4], which strongly suggests that the gas escape phenomena that we measure in our experiments are an important process for similar composition and temperature ices on Enceladus. Our results show that plume-like composition ices heated to the 135 to 155 K temperatures measured by CIRS will result in gases escaping with composition similar to the INMS plume composition. In contrast, similar ices heated to higher or lower T will not reproduce the measured plume composition.

Photolysis of ices depostited from the plume-like gas mixtures are difficult to analyze given the low concentrations of the non-water species, and subsequent

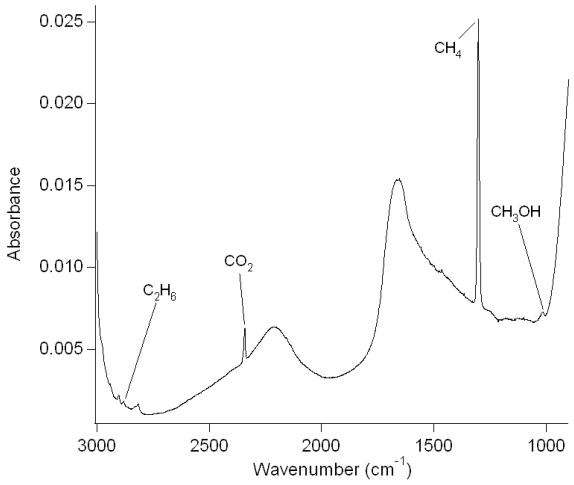

Figure 3. FTIR spectrum of 10% CH_4 in H_2O at 20K photolyzed for 30 minutes.

photolytic products. Therefore we are examining a series of binary and tertiary mixtures at proportions that enable product detection in our FTIR spectra. Figure 3 shows a preliminary FTIR spectrum of a UV photolyzed, 10% mixture of CH_4 in water. In this case, the deposition was performed at 20K to ensure the ratio of CH_3 in the gas mix was representative of the depositied ice. Clear evidence for the production of CO_2, CH_3OH, and C_2H_6 is seen in the figure. Other species such as CO are produced, but are not visible at the scale displayed. The photolytic chemistry seems to be dominated by the reaction of OH radicals with CH_4 and its subsequent products. This is similar to the result of proton irradiation of similar ice mixtures

Acknowledgements: This work was performed at the Jet Propulsion Laboratory (JPL), California Institute of Technology, under a contract with the National Aeronautics and Space Administration (NASA). Financial support through JPL's Research and Technology Development program is gratefully acknowledged.

References:. [1] Spahn, F., et al. (2006). *Science* **311**: 1416-1418.
[2] Spitale, J. N. and C. C. Porco (2007). *Nature* **449**: 695-697.
[3] Waite, J. H., et al. (2006). *Science* **311**: 1419-1422.
[4] Spencer, J. R., et al. (2006). *Science* **311**: 1401-1405.
[5] Sandford, S. A. and L. J. Allamandola (1990). *Astrophysical Journal* **355**: 357-372.
[6] Hodyss, R., et al. (2007). *Icarus*: doi:10.1016/j.icarus.2007.10.005.
[7] Ayotte, P., et al. (2001). *Journal of Geophysical Research-Planets* **106**: 33387-33392.
[8] Collings, M. P., et al. (2004). *Monthly Notices of the Royal Astronomical Society* **354**: 1133-1140.
[9] Jenniskens, P. and D. F. Blake (1994). *Science* **265**: 753-756.
[10] Moore and Hudson (1998). *Icarus* **135**:518-527.

Thermal and Surface Implications of Ices in the Outer Solar System.

David Jewitt[1], Institute for Astronomy, University of Hawaii, 2680 Woodlawn Drive, Honolulu, HI 96822 (jewitt@ifa.hawaii.edu).

Recent models of energy balance in the evolving protoplanetary disk of the Sun suggest that the snow-line (the surface outside which water was stable in the solid phase) danced around with time, in the (roughly) 1 AU to 3 AU heliocentric distance range. This means that, depending on their time of formation, ice-bearing solid objects could have formed anywhere in the protoplanetary disk from the middle of the Terrestrial planet region out to the extremities of the Kuiper belt. Observational evidence indeed shows that ice-rich bodies ("comets") are divided into at least three distinct groups spread over the above-mentioned range. The Oort cloud comets (OCCs) probably formed in the middle Solar system, in the vicinity of the gas and ice giant planets and were later scattered out to their current orbits much larger than the planetary region. The Kuiper belt comets (KBCs) may have formed, in part, in the outer Solar system where they now reside, beyond the outermost giant. The Main-belt comets (MBCs) orbit within the asteroid belt at about 3 AU. Their formation location is unknown. They might be products of in-situ accretion or they could have been captured in the early Solar system from more distant locations.

The survival of ice formed over a wide range of distances and temperatures opens the possibility for a kind of "ice archaeology" of the Solar system. Several important properties of the ice are likely to depend upon the formation temperature and therefore to vary as we move outwards from the MBCs to the KBCs. The most fundamental of these temperature-dependent effects is the physical state of the ice, whether it be crystalline or amorphous. Ice in the outer Solar system (KBCs and OCCs) formed cold enough to be amorphous whereas ice accreted in the asteroid belt would almost certainly have been crystalline from the beginning. The difference is extremely important for understanding a range of observations of small bodies in the Solar system. In particular, the trapping of other molecules is much higher in amorphous ice and the efficiency is a strong function of the temperature, as experimentally documented by Bar-Nun and others over the years. Complicated thermal models of amorphous cometary nuclei are able to fit a range of observations (for example, of outgassing activity exhibited beyond the orbit or Jupiter, where crystalline water ice should be involatile). The question is whether the amorphous ice is really there. Spectral evidence from the outer Solar system, for example, typically shows that the ice is crystalline (as evidenced by the 1.65 micron absorption band).

In this presentation I will discuss telescopic observations relating to the crystalline state of the ice and recent laboratory work conducted to understand the stability of crystalline ice when exposed to energetic particles. In addition, I will discuss the long-term survival of the ice in the context of thermal evolution models, and highlight parameters that could be usefully measured both using large telescopes and in the laboratory.

RADIATION EFFECTS ON THE ICY SATELLITES AND RING PARTICLES R. E. Johnson[1] , A. R. Hendrix[2], T. A. Cassidy[1], [1] Wilsdorf Hall, University of Virginia, Charlottesville, VA 22902 (rej@virginia.edu), [2] JPL, , 4800 Oak Grove Dr., MS 230-250, Pasadena, CA, 91109 (arh@jpl.nasa.gov)

Introduction: Icy materials in the outer solar system are exposed to both the solar UV and plasma radiation. The incident radiation produces defects, sputtering and radiation-induced chemistry [6, 8, 11]. Such effects can be seen in the composition of the ambient neutrals and plasma as well as in the reflectance spectra.

One of the more important effects is the decomposition of ice by the incident radiation: $2H_2O$ + radiation→ $2H_2 + O_2$ [5,12] and the production of peroxide [2, 8]. The very volatile molecules, H_2 and O_2, can escape into the gas phase. The efficiency of escape depends on the defect density, the surface temperature and on how deep into the surface they are produced. Volatile formation and loss to space has been shown to compete with surface sputtering for production of ambient neutrals about the icy satellites and rings [11, 13, 14, 15, 17].

Since the more volatile species, H_2, is lost preferentially, the trace surface species in an ice matrix tend to be oxidized [10,11]. In addition, depending on the temperature oxygen molecules can be trapped as micro-bubbles [1,7] in which O_3 can then be produced, as seen in the surfaces of a number of icy satellites [16].

Although the decomposition and sputtering of ice have dominated the discussion of radiation effects for some time, the incident radiation can drive other interesting chemistry. For instance, radiation can also drive-off hydrogen from ammonia, methane, and hydrogen sulfide trapped in a surface [9], hydrocarbons and organics are degraded [10], and carbonates and sulfates can be formed and destroyed in a quasi-steady state [11].

Discussion: The abvoe effects will be reviewed for the icy bodies in the outer solar system. Particular emphasis will be on recent analysis of Cassini data for the rings and the icy satellites and on evidence for such processing from a recent analysis of the Galileo UVS data will be described [4].

References: [1] Calvin, W., J et al. Geophys. Res. Lett 23, 673-676 (1996) [2] Carlson, R.W., et al. Science 283, 2062-2064 (1999) [3] Carlson, R.W, et al., Icarus 77, 461-471 (2005), [4] Hendrix, A. and R.E. Johnson to be submitted (2008)[5] Johnson, R. E., et al., W. L., Nucl. Instrum. Methods 198, 147 (1982) [6] Johnson, R.E. Energetic Ion Interactions with Atmospheres and Surfaces, Springer-Verlag, Berlin, (1990) [7] Johnson, R.E. and W.A. Jesser, Astrophys. J. Letts. 480, L79-L82 (1997) [8] Johnson, R.E. and T.I. Quickenden, J. Geophys. Res.102, 10985-10996 (1997) [9] Johnson, R.E., in Solar System Ices, ed, B. Schmitt and C. beBergh, Kluwer Acad. Pub., Netherlands, p. 303-334 (1998). [10] Johnson R.E. in, AdvSerPhysChem 11, eds R. Desseler (World Scientific, Singapore) Chap 8. pps 390-495 (2000) [11] Johnson, R.E., et al. in Jupiter-The Planet, Satellites and Magnetosphere, ed. F. Bagenal, et al. , Cambridge Univ. Press, Cambridge, Chapter 20, p. 485-512(2004). [12] Johnson, R.E., et al. J. Chem. Phys. 123, 184715-1-8 (2005) [13] Johnson, R.E., et al. Icarus180, 393-402 (2006). [14] Johnson, R.E., et al, Planet. & Space Sci. submitted (2008). [15] McGrath, et al. in Jupiter-The Planet, Satellites & Magnetosphere, eds. F. Bagenal, T. Dowling, W.B. McKinnon, Cambridge Univ. Press, Cambridge. Chap.19, p.457-483 (2004) [16]Noll, K.S., et al. Science 273, 607-670 (1996) [17] Shematovich, et la. Icarus 173, 480-498 (2005)

Thermal Conductivity and Melting Properties of Materials Forming Icy Satellite Crusts. J.S. Kargel, University of Arizona, Tucson, AZ85721 (kargel@hwr.arizona.edu).

Introduction: Temperature is a key state parameter that, along with stress, controls much geologic activity known or suspected on icy satellites, for instance, melting, cryovolcanism, geyser processes, and the occurrence and activity of subsurface oceans; folding, faulting, and plate flexure; diapirism and solid-state convection; thermal convection of fluids in porous media; decollement; viscous dissipative heating; and glacial flow. Temperature and stress conditions control much geology, but temperature also partially controls visco-elastic responses and stress conditions. Four major things control crustal temperatures: surface temperature (affected by albedo, hence, composition), interior heat generation and heat flow (affected in some cases by viscoelastic dissipation, hence rheology and composition), thermal conductivity (strong control by composition), and nonconductive heat transport (dependent on phase state and rheology, hence composition). Crustal volatile composition—especially its influence on thermal conductivity and crustal temperatures—is a key variable property of icy satellites that underlies much of the geologic behavior of icy satellites, yet the links between composition, crustal temperatures, and geologic behavior are barely explored. Nearly all thermal models assume thermal conductivity relevant to a water-ice crust for icy satellites and a rock material for asteroids. As reviewed below, thermal conductivity data available in the literature suggests that this common assumption can lead to large errors that would seem to preclude geologic activity in objects where it is rampant. Melting properties of materials and their mixtures are also key aspects controlling the geologic responses of icy satellites to heat inputs. Together, composition-dependent thermal conductivity (which controls the retention of heat), and composition-dependent melting behaviors (which control the stability of solids) underlies much of the phenomenological complexity of icy satellites.

Thermal conductivity of materials.

Water ice, in fact, is by far the most thermally conductive phase making up the preponderance of icy satellites' crusts. Other known or suspected major constituents, such as most salt hydrates, clathrate hydrates, other molecular ices, frozen hydrocarbons, elemental sulfur, and other common materials, have thermal conductivities factors of 2 to 10 less than water ice Ih. Most other water ice phases also have thermal conductivities much lower than water ice Ih. Considering also the crucial influence of porosity in controlling thermal conductivity of materials, the use of thermal conductivity values approporiate for fully dense ice Ih to represent the thermal conductivity of icy satellite crusts can be like using the thermal conductivity of nails to represent that of a house's wall. Icy satellites may be much more retentive of heat than usually modeled, and this can help explain the startling geologic activity of many icy satellites.

Figure 1 summarizes some thermal conductivity data for fully dense (nonporous), well-crystalized ices, hydrocarbons, salt hydrates, and other volatile materials. Also important is the porosity of materials and the effects of mixtures (including the important effects of texture-- the spatial organization of materials that are mixed).

A new conceptual regimen will be described that explains how icy satellite geology and geophysics is related closely to heat budget and composition. That this is so has been long recognized, but the new scheme explains additionally why there is geologic activity even on very small icy objects and why some familiar geologic behaviors are repeated across the Solar system even when material and conditions vary drastically. The scheme relies partly on the diverse thermal conductivity and melting behaviors of materials occurring naturally in the Solar System.

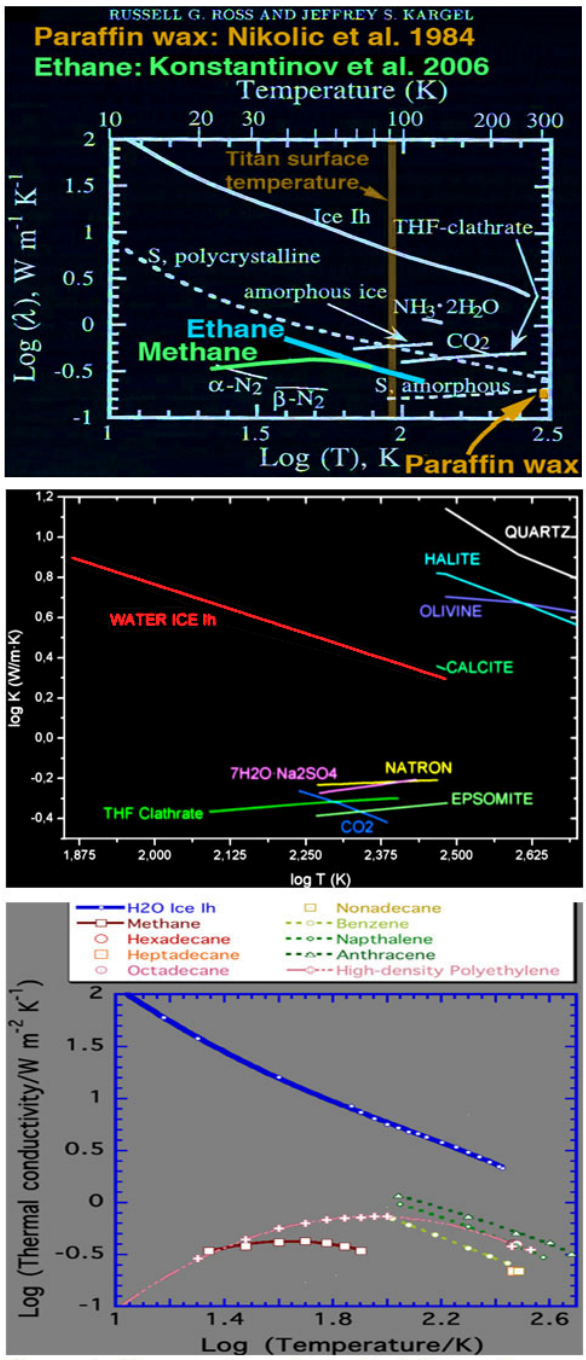

Figure 1. Temperature-dependent thermal conductivities of various materials plotted with data for water ice 1h. Top panel: ices (after Ross & Kargel 1998). Middle panel: salt hydrates (from Prieto-Ballesteros and Kargel 2005). Bottom panel: hydrocarbons (from literature sources).

INVESTIGATING GAS CLATHRATE HYDRATE STRUCTURE, FORMATION AND DECOMPOSITION. C.A. Koh, K.C. Hester, J. Lachance, H. Ohno, L.J. Rovetto, T.A. Strobel, S.F. Dec, E.D. Sloan, Colorado School of Mines, Center for Hydrate Research, Chemical Engineering Department, Golden, CO 80401 (Email: ckoh@mines.edu).

Introduction: Gas clathrate hydrates are crystalline inclusion compounds composed of a lattice of hydrogen-bonded water cages which can encage small guest molecules, such as methane, carbon dioxide, and hydrogen [1]. Applications of hydrate technologies include the assessment of hydrates as a potential future energy source, in energy storage, and industrial flow assurance. New insight into controlling hydrate formation and decomposition in these technological applications requires fundamental understanding of clathrate hydrate structural and physical properties, and crystal growth and decomposition processes.

Clathrate Hydrates in Solar System Ices: Gas clathrate hydrates have been also suggested to exist in association with the icy environments of outer planetary bodies in the solar system, including Enceladus, Titan, Saturn's icy moons, and even in comets [2-4]. Discussion will be given to how the knowledge-base and methods applied to the technological applications of clathrate hydrates could impact studies of extra-terrestrial clathrate hydrates.

Structural Studies of Natural Hydrated Deposits versus Synthetic Hydrates: The structural properties of natural hydrated deposits and synthetic hydrates have been measured and compared using Raman and NMR spectroscopy and X-ray and neutron diffraction. The natural samples were recovered from Barkley Canyon, off Vancouver Island (sea-floor hydrates), the KG Basin, India (oceanic hydrates), and the Northern Cascadia Margin (IODP 311; oceanic hydrates). Discussion will be given to how structural and physical property measurements of hydrates can contribute to the paradigm shift from hydrate exploration to hydrate production.

Clathrate Hydrate Formation and Decomposition Studies: The kinetics of gas hydrate formation and decomposition have been investigated using a combination of microscopic and macroscopic techniques. Molecular-scale studies on the formation and decomposition of single and binary gas hydrates have been performed using Raman and NMR spectroscopy. These studies have revealed the presence of long-lived metastable hydrate phases. The transformation of these metastable phases is dependent on gas composition, and can be significantly affected by the addition of polymer molecules (kinetic hydrate inhibitors). A new high pressure differential scanning calorimetric method has been developed to assess the effects of kinetic hydrate inhibitors on the nucleation and growth processes of gas hydrates.

Hydrogen Clathrates: Synthesis and Characterization studies have been performed on clathrate structures encapsulating molecular hydrogen (Figure 1). Storage of molecular hydrogen in clathrate hydrates has been achieved, with reversible release of hydrogen at ambient conditions. Hydrogen enclathration in different clathrate molecular compounds has been measured using Raman spectroscopy coupled with neutron diffraction.

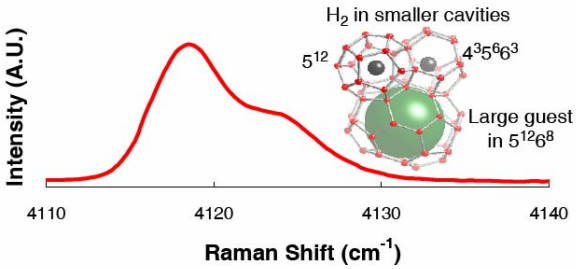

Figure 1: Molecular hydrogen encapsulated in the small cavities of sH clathrate hydrate, large guest molecules occupy the large eicosahedral cavities of sH [5]. The vibron region in the Raman spectrum reveals the environment of the hydrogen molecules.

References:

[1] Sloan, E.D. and Koh, C.A. (2008) *Clathrate Hydrates of Natural Gases*, 3rd Edition, CRC Press, Boca Raton, Fl. [2] Mao, W., Koh, C.A., Sloan, E.D. (2007) *Physics Today*, October issue, 42. [3] Kieffer, S.W. et al. (2006) *Science*, 314, 1764, [4] Clark, R.N. et al. (2007) unpublished work. [5] Strobel, T.A., Koh, C.A., Sloan, E.D. (2008) *J. Phys. Chem. B*, 112, 1885.

H_2O ICE FORMATION FROM THE REACTION OF COLD H ATOMS WITH SOLID O_2 AT 10 K.

A. Kouchi[1], N. Miyauchi[1], H. Hidaka[1], T. Chigai[1], A. Nagaoka[1] and N. Watanabe[1], [1]Institute of Low Temperature Science, Hokkaido University, Sapporo 060-0819, Japan (kouchi@lowtem.hokudai.ac.jp)

Introduction: Water is the most abundant solid molecule in space, and has been observed in various astrophysical environments. However, the formation mechanism of water molecules in molecular clouds has not been determined to date. It has been suggested that water molecules are synthesized by atomic reactions involving H and O on grains at around 10 K [1, 2]:

a) O+H→OH, (1) OH+H→H_2O (2)

b) OH+H_2→H_2O+H (3)

c) O_2+H→HO_2, (4) HO_2+H→H_2O_2, (5) H_2O_2+H →H_2O+OH. (6)

Hiraoka et al. [3] investigated reactions (1) and (2) by spraying D atoms onto O atoms trapped in an N_2O matrix at 12 K. Although they observed D_2O by temperature-programmed desorption spectroscopy, it remains unclear whether D_2O is formed at 12 K or during heating. For reactions (4) to (6), Klein and Scheer [4] performed pioneering experiments on the reaction of H atoms with solid O_2 at 20 K. However, they made no analysis of the products. To investigate the formation mechanism of water molecules in molecular clouds, we focus on reactions (4) to (6), and performed H/D addition experiments to solid O_2 at 10 K.

Experimental: Experiments were performed using the ASURA system[5,6]. Solid O_2 was deposited on an aluminum substrate at 10 K in an ultrahigh vacuum chamber. Cold atomic H (D) with a flux of 2×10^{14} cm^{-2} s^{-1} was irradiated onto solid O_2. Infrared absorption spectra of the sample solid during irradiation by atoms were measured by FTIR.

Results and discussion: We observed the formation of H_2O_2 and H_2O. No intermediate radicals were observed, suggesting that the reaction rate of (4) is much slower than that of (5). Figure 1 clearly shows that the formation of H_2O_2 (D_2O_2) and H_2O (D_2O) is very rapid and efficient; H_2O_2 and H_2O are observed even after exposure for 5 s. When H atoms are irradiated onto solid CO at 10 K [5], the production of H_2CO and CH_3OH are observed after 30 s and 1 min, respectively. The present experimental results confirm that reactions (4) to (6), which were initially proposed based on theoretical considerations [1,2], proceed at 10 K. Since reaction (4) essentially has no barrier [7], it is natural that this reaction proceeds very rapidly. While reaction (6) has an activation energy of 1800-2160 K [8], it has been suggested that this reaction does not proceed by an Arrhenius-type reaction at 10 K, but proceeds by a tunneling reaction even at 10 K.

Astrophysical implications: Our results have several implications for ices in molecular clouds. The H fluences in a 10-K molecular cloud over 10^4 and 10^5 years correspond to exposure times of 1 and 10 minutes in the present experiments, respectively. It is reasonable to say that water formation by reactions (4)-(6) occurs very quickly in molecular clouds.

Although solid O_2 is expected to occur on the grain surface, no positive detection has been reported so far [9]. Present experiments clearly explain why no O_2 has been observed: if an O_2 molecule is formed on grain surface it will react very quickly with H to form H_2O_2 and H_2O within $10^{4\text{-}5}$ years.

Considering the ratios of $k_{H(4)}/k_{D(4)}$=1 and $k_{H(6)}/k_{D(6)}$ =8 obtained in the present experiments, where $k_{H,D(n)}$ is a reaction rate constant of n^{th} reaction, and the D/H atom ratio of 0.1 or less expected in molecular clouds, deuterium addition to O_2 is favorable for producing the observed amount of HDO; the observed HDO/H_2O ratio of 0.03 can be achieved in a time scale between 10^4 and 10^5 years.

References: [1] Tielens A.G.G.M. and Hagen W. (1982) *A&A*, 114, 245-260. [2] Cuppen H.M. and Herbst E. (2007) *ApJ*, 668, 294-309. [3] Hiraoka K. *et al*. (1998) *ApJ*, 498, 710-715. [4] Klein R. and Scheer M.D. (1959) *J. Chem. Phys.*, 31, 278-279. [5] Watanabe N. *et al*. (2004) *ApJ*, 616, 638-642. [6] Watanabe N. *et al*. (2006) *Planet. Space Sci*., 54, 1107-1104. [7] Walch S.P. (1988) *J. Chem. Phys.*, 88, 6273-6281. [8] Koussa H. J. *et al*. (2006) *Mol. Struc- Theochem.*, 770, 149-156. [9] Vandenbussche B. *et al*. (1999) *A&A*, 346, L57-L60.

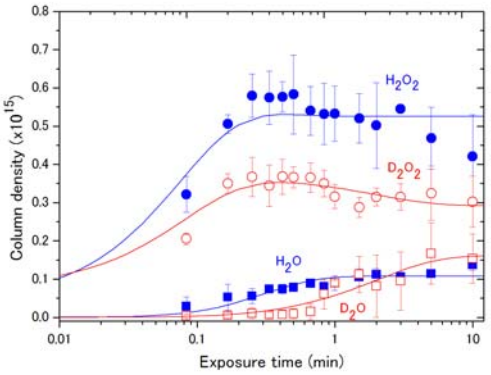

Figure 1. Variation of products for H_2O_2 (D_2O_2) and H_2O (D_2O) with H (D) exposure.

THERMO-PHYSICAL MODELING OF COMETARY NUCLEI WITH MOVING ICE BOUNDARIES. E. Kuehrt[1], N. Gortsas[2], and U. Motschmann[3],

[1]DLR, Rutherfordstr. 2, 12489 Berlin, Germany, ekkehard.kuehrt@dlr.de
[2]DLR, Rutherfordstr. 2, 12489 Berlin, Germany, nikolaos.gortsas@dlr.de
[3]TU Braunschweig, Mendelssohnstr.2, 38106 Braunschweig, Germany, u.motschmann@tu-bs.de

Introduction: Thermal-physical modeling of cometary nuclei is a basic tool to simulate cometary activity. Numerous approaches have been published (for a review, see [1]) but the feedback of the surface erosion caused by ice sublimation to the thermal state is commonly neglected. However, near perihelion the characteristic velocity of erosion can be considerably higher than that of heat diffusion.

Therefore, a novel thermal conduction code has been developed to study the effect of moving boundaries on the thermal state of icy bodies. The code that solves the so called Stefan problem has been applied to cometary nuclei. It takes the strong surface erosion caused by ice sublimation near perihelion into account. A substantial constraint is the conservation of energy at each time step.

To figure out the consequences of erosion at the surface for the thermal behavior of comets we start with the investigation of a spherical nucleus consisting of pure water ice. In a second step a mixture of water ice, dust and CO-ice has been simulated. Rotation, orbital motion, and porosity of the nucleus have been taken into account.

Figure 1 shows the temperature profile near the surface of a nucleus composed of water ice at perihelion for an orbit of a Jupiter family comet. Considering erosion a substantially less amount of heat penetrates into the nucleus compared to the case where the surface erosion has been neglected.

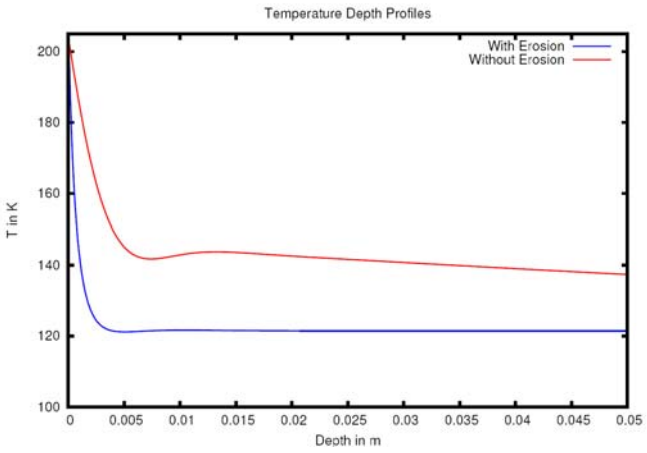

Figure 1: Temperature profiles at perihelion of a Jupiter family comet for a nucleus of pure crystalline water ice assuming a Hertz factor of 0.01. Surface erosion leads to a substantial reduction of heat that penetrates into the nucleus.

In the more complex multi-component system the subliming CO-ice front below the surface is also going down due to sublimation losses. Its depth shows an oscillating behavior with time. The effect of basic parameters as thermal conductivity and porosity on the results has been investigated.

Consequences of the reduced penetration of heat derived from this model approach, e.g. for the near surface structure of comets and for sample return missions, are discussed.

[1] Prialnik D., Benkhoff J., and Podolak (2003) In: Comets II (Ed. by M. Festou, H.U. Keller, and H.A. Weaver) 359–387.

INTERPRETING THE BASAL AND PRISM NATIVE SURFACE OF ICE I_h WITH SUM FREQUENCY GENERATION SPECTROSCOPY. I. Li[1], H. Groenzin[1] and M. J. Shultz[1], Tufts University, Department of Chemistry 62 Talbot Avenue Medford, MA 02155, irene.li@tufts.edu.

Introduction: The surface of ice is known to be a site whereby a number of important catalytic processes occur in the environment. It is of little surprise given the shear volume of ice on Earth and its presence in the solar system, that there is much interest to understand the behavior of ice surfaces [1-5]. The surface reactivity is likely influenced by the orientation of the H and O atoms, which is affected by the particular face (basal or prism) exposed. Surface-sensitive spectroscopic (sum frequency generation, SFG) experiments were carried out on basal and prism faces of single crystal I_h ice.

SFG Spectroscopy: SFG is a nonlinear technique that probes the interface or surface of a material using two beams (visible and tunable IR) to generate a signal at a frequency consisting of the sum of the two incident beams. The polarization of each beam is designated either *s* or *p* in reference to the plane of incidence, Figure 1. The *s* and *p* also denote the optical axis of the ice oriented perpendicular and parallel to the plane of incidence as defined by the incident angle and the surface normal. An SFG polarization combination of *ppp* refers to the polarization of the output beam, visible, and IR beam respectively.

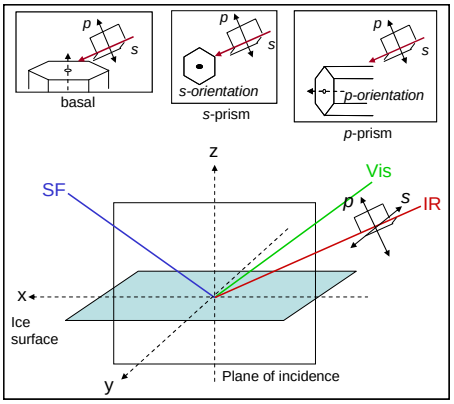

Figure 1. (Upper) Ice crystal orientation with respect to the input plane. (Lower) Schematic of *s* and *p* polarization.

Of the two SFG polarization combinations, *ssp* and *ppp*, only the *ppp* spectra are shown since it is more responsive to surface changes, specifically in the hydrogen-bonded region (3000-3600 cm^{-1}). The resolution and reproducibility of the structural features require a high quality ice surface. A clear spectroscopic distinction between the basal and prism faces is reproducibly seen, Figure 2. Five oscillators were identified. On the basal face the modes are 3098, 3132, 3211, 3281, 3393 cm^{-1}; and on the prism face the modes are 3096, 3146, 3205, 3253, 3386 cm^{-1}.

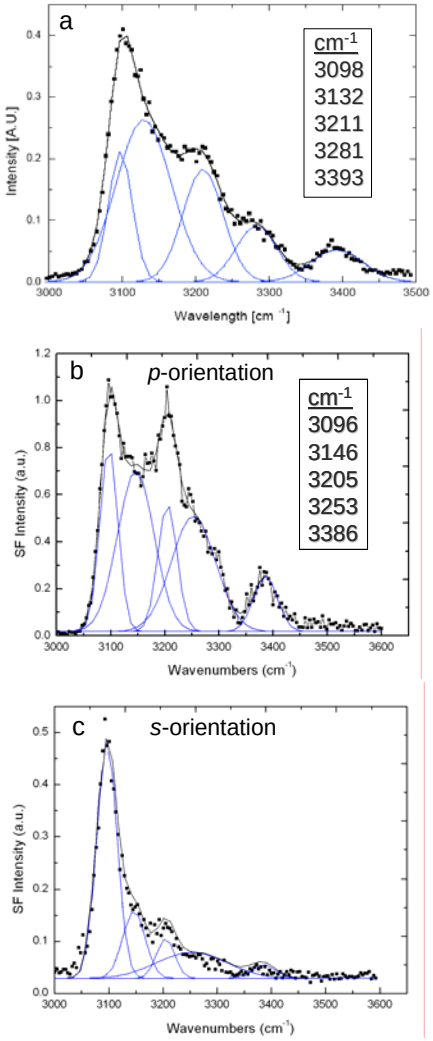

Figure 2. SFG spectra of ice on the basal (a) and prism (b and c) faces. The polarization is *ppp*. The surface temperature of the ice is 113K.

As the prism surface is rotationally anisotropic, two orientations were investigated: *s*- and *p*-orientation, see Figure 1 (upper). The most striking difference between these two orientations is the absence of the 3386 cm^{-1} oscillator in the *s*-orientation.

Polarization Angle Null Analysis: A polarization angle null (PAN) analysis was performed to extract the null angles of the individual peaks and their hyperpolarizability components χ_{xxz}, χ_{yyz}, χ_{zzz}. Typically the orientation of molecules is deduced by comparing the *ssp* and *ppp* intensities to get the ratio of χ_{xxz}/χ_{zzz} or χ_{yyz}/χ_{zzz}. However, measuring the null angles is a more accurate means of determining surface molecular orientation [6]. PAN is generated by setting the visible polarization to 45° (approximately equal parts *s* and *p* polarization) and the IR polarization set to *p*; the SF analyzer is tuned through the null for each individual oscillator.

Analysis of the basal face showed the robust 3098 cm^{-1} mode to be a transverse collective mode. In other words, χ_{xxz}/χ_{zzz} is large indicating the polarizability is mainly in the plane of the surface. The χ_{xxz}/χ_{zzz} ratios of the other oscillators are significantly smaller, implying their polarizability change is more longitudinal or normal to the surface plane. This is represented pictorially in Figure 3 [7].

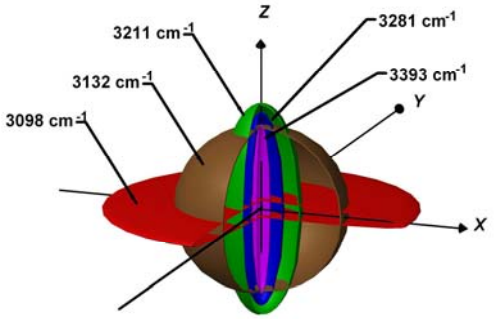

Figure 3. Polariability ellipsoids of the basal face oscillators.

The basal face is rotationally isotropic so there is no distinction between χ_{xxz} and χ_{yyz}. This is not the case on the prism face. PAN analysis on this face provides additional insight into how the ice responds to perturbation. For the 3096 cm^{-1} mode both χ_{xxz} and χ_{yyz} are again large relative to χ_{zzz}, meaning the mode associates with the surface plane. The mode has approximately 30% longitudinal and 70% transverse character on the prism face. The underlying bulk structure may be a main contributor to the peak's robustness which supports the treatment of the surface as collective modes rather than individual molecules [4, 7-10].

The 3146 cm^{-1} mode has almost equivalent ratios of χ_{xxz} and χ_{yyz} to χ_{zzz}, as depicted by its shape in Figure 4; it is neither strongly transverse nor strongly longitudinal but more an intermediate oscillator. The remaining bluer oscillators are more longitudinal in character with their polarizability along the surface normal.

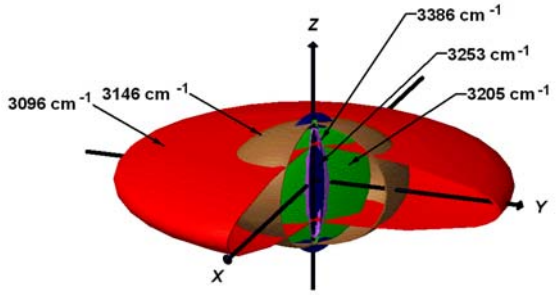

Figure 4. Polarizability ellipsoids of the prism face oscillators.

Summary: From the basal to the prism face, some conclusions may be drawn despite the oscillators being different; the first and third modes are essentially the same on the two faces. The second oscillator is always intermediate between longitudinal and transverse in character. The last three modes mostly follow the surface normal (i.e., longitudinal) and are the most fragile to any surface perturbations. Due to their fragility it is believed that these modes represent more surface oscillators.

There is no clear-cut interpretation and assignment of the bonded OH region of ice in literature. Thus, we purposely focused on the native ice to develop a physical interpretation of what is occurring at the surface. Although this physical interpretation is still evolving, the findings indicate that the vibrations in the bonded OH region must be taken as a collective; it is insufficient to simply treat the system as a sum of contributions of individual water molecules.

References: [1] Wei X. et al. (2002) *Phys Rev B*, 66, 085401-1 to13. [2] Wei X. and Shen Y. R. (2002) *Appl Phys B*, 74, 617-620. [3] Barone S. B. et al. (1999) *J Phys Chem A*, 103, 9717-9730. [4] Buch V. and Devlin J. P. (1999) *J Chem Phys*, 110(7), 3437-3443. [5] Dosch H. et al. (1995) *Surf Sci*, 327, 145-164. [6] Gan W. et al. (2005) *Chem Phys Lett*, 406, 467-473. [7] Groenzin H. et al. (2008) *submitted to J Chem Phys*. [8] Groenzin H. et al. (2007) *J Chem Phys*, 127, 214502-1 – 214502-8. [9] Buch V. et al. (2008) accepted Proc Natl Acad Sci U.S.A. [10] Buch V. et al. (2007) *J Chem Phys*, 127, 204710-1 – 204710-15.

Spectral Measurements for Improved Studies of the Role of Water Ice in Solar System Formation and Evolution. C.M. Lisse[1], C.A. Hibbitts[1], and R.E. Peale[2], [1] JHU-APL, 11100 Johns Hopkins Road, Laurel, MD 20723 carey.lisse@jhuapl.edu. [2]University of Central Florida, Department of Physics, 12201 Research Parkway, Orlando, FL 32826-3246 rep@physics.ucf.edu

Introduction: Water ice is an extremely abundant material in the make-up of solar systems. Found throughout the solar system beyond 1 AU, the extremely stable H-O bond is also found increasingly in primitive solar system bodies - a not surprising fact, as the early solar system was a highly reducing environment, with ~1000 H atoms for every oxygen. In select situations in our solar system and by proxy in the circumstellar material found around other stars, we can learn a great deal about the nature of the water ice input to the solar system. Observations of cometary coma, of material captured from the proto-planetary disk, presumably measure the compositional abundance of the nucleus, and deduce a mix of materials approximately half of water ice by mass [1; Fig 1]. In 2005, the more direct measurement of material excavated from comet 9P/Tempel 1 by the Deep Impact experiment [2-5] verified this assessment. Around other stars, evidence for cold Kuiper Belt dust is commonly found in Spitzer Space Telescope measurements of the mid-IR radiation emission from around other stars [6]. E.g., two belts of icy dust, one at 4-9 AU, and another at 40-80 AU, were deduced to be present in the 10-16 Myr system HD113766 undergoing terrestrial planet formation [7; Fig 2]. In the rockier primitive bodies, there is now evidence that water is captured in the form of ice in the Main Belt objects 133P/Elst-Pizzarro, P/2005 U1 Read, and asteroid 118401 (1999 Re70) [8]. The presence of water ice in asteroids is echoed by the finding of fine, 150-200K particulate water orbiting around the nearby K0V star HD69830 (12 pc distant, 2-10 Gyr old) created by collisional disruption of that system's analogue of an ~30 km P/D asteroid [9].

In all of these systems where water ice has been detected, the detailed nature and formation history of the ice is lacking. E.g., in the case of comets, it is now becoming clear that the refractory component of the nucleus has been reworked to temperatures upwards of 1000K [5,10], even though comet reservoirs are found outside the ice line. How then did the volatile ices become included in the cometary mass? If the material was accreted by condensation onto re-worked refractory material as it flowed into the out solar system, why then does it appear as extremely fine particulate matter in the Deep Impact excavation event [11]? What happens to the water ice as it sublimes as a comet approaches the Sun? Refreezing of water ice has been detected on the surface of 9P/Tempel 1 [12], indicating the presence of altered water ice phases, and indications for products of aqueous alteration have been reported in the same comet [5].

Water ice condenses in several forms at low pressures, including as many as three distinct types of amorphous ice [13], a metastable cubic crystalline ice as well as the hexagonal crystalline form which is characteristic of high-temperature ice. The exact morphology or mixture of morphologies of a deposit is not only a function of temperature, but of temperature history. In addition, ice can be amorphized by the interaction with particle radiation [14]. The hexagonal crystalline form is the most stable, and once ice achieves this form, it is retained at any temperature. Ice formed from vapor above about 160 K will be hexagonal, and ice formed at colder temperatures, when heated to 150–160 K or more, will transform to hexagonal crystals on time scales that are shorter at higher temperatures, being nearly instantaneous above 200 K. (Water ice much above 200K, however, is unstable versus sublimation into vacuum, and is thus is not found in interplanetary space. The presence of such 'warm' water ice is highly controversial, but also potentially highly diagnostic of recent events, depending on the lifetime vs. sublimation of the material - according to theory, this can vary by orders of magnitude depending on particle size and impurity level [15]. Around 130–140 K, on vapor deposition or heating, a mixture of cubic and amorphous ice occurs which seems stable (over laboratory time scales) until T > 150K. Below 130 K, amorphous ice is stable [16,17,13]; we can thus expect many solar system ice reservoirs to be mixtures of amorphous and crystalline material.

Spectral Signatures of Water Ice: The search for signatures due to water ice in fine dusty material are easiest done in the emission regime, where the flux due to the water ice can dominate the total emission from the system. Groundbreaking work on the spectral signatures of water ice in exosystems at 2 - 200 um was performed by the Infrared Space Observatory (ISO) in 1996. The advent of the extremely sensitive Spitzer Space Telescope has allowed detailed spectral studies of the warm water ice in multiple systems at 5-35 um, and the photometric search for cold water ice at 70 um. Deep Impact and STARDUST have greatly narrowed the number of possible refractory species mixed with the ice. The imminent launch of the Herschel will allow much more detailed spectral studies of cold water ice in the 60 - 700 um spectral range in the near future.

Typical work in the mid- and far-IR using the spectral signatures of water ice emission is based on the laboratory measurements of water ice presented in the review by Warren [18; Fig 3]. This study concentrated on measurements made within 30–40 degrees of the freezing point at 1 atm and 273K. It was noted by Warren that the optical properties were quite different at lower temperatures even at wavelengths outside the very sensitive 45-mm lattice absorption. Problems also arise with these values in that a major adjustment to the 45-mm band due to the lack of any measurements of this region at warmer temperatures. For ice at the temperatures of outer-planet satellites, one must consult other literature.

Improved Laboratory Measurements: What is required, then, for adequately refining mid- and far-IR measurements of fine water ice in primitive solar system bodies is the detailed laboratory study of the following :

- **Measurements of ices properties from 30 - 200K in 10K steps.**
- **Measurements of ice particle size, surface film, and fractal agglomeration effects.**
- **Measurements of water ice + refractory (silicates, metal sulfides, amorphous carbon, PAHs, carbonates) materials.**
- **Measurements of spectral changes due to radiation damage (e.g., proton/alpha particle dosing).**
- **Evaporation times and sublimation rates vs. particle size and refractory mix.**

A new laboratory program initiated in support of the Herschel Observatory mission by our team will make some of these measurements, but it would be highly desirable to include studies by multiple groups examining the issues from diverse directions. We call on the SSCI community to work with our team to make these measurements, and offer the results of our work in return.

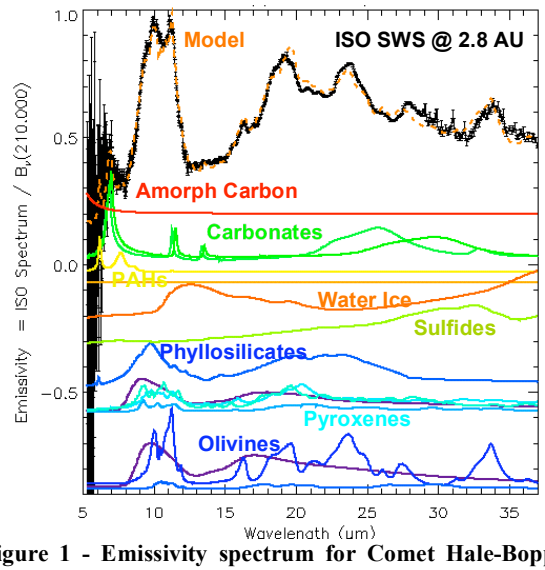

Figure 1 - Emissivity spectrum for Comet Hale-Bopp's coma, as measured at 2.8 AU from the Earth and ISO in Oct 1996. Error bars are ±2σ. Black: ISO coma spectrum, divided by a 210 K blackbody.

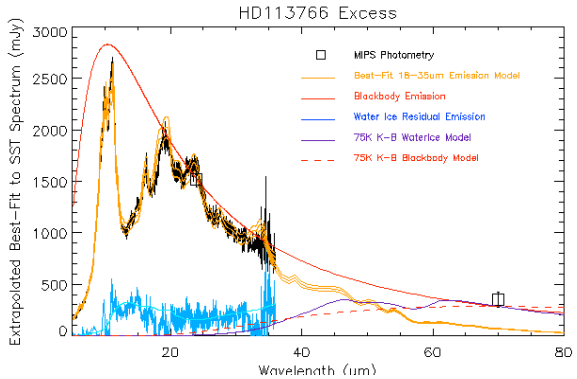

Figure 2 — Evidence for water ice in a young solar system. *Spitzer* MIPS 70 um photometry, 5–35 um IRS, and best-fit current model to dust thermal emission from HD 113766, after [7]. **Black** - IRS data. Orange—IRS emission model. The predicted flux of 67 ± 3 mJy from the best-fit model is less than 20% of the measured MIPS 70 µm flux of 350 ± 70 mJy. Red solid line—poor warm blackbody model normalized to the 24 and 70 um MIPS fluxes.. Dark Blue—residual emission due to warm water ice, produced by subtracting all other model fluxes from the IRS data. Light blue line—Warm ice emission model flux. Dark purple - predicted flux from a reservoir of 75 K water ice particles with PSD dn/da ~ $a^{-3.5}$, required in addition to the warm dust dominating the 5–35 µm spectrum to produce the observed 70 µm MIPS flux. Dashed red curve - predicted flux from a collection of blackbody emitters at T = 75 K. With current spectral knowledge of water ice em9ision, it is very hard to distinguish between these two models. All error bars are 2σ.

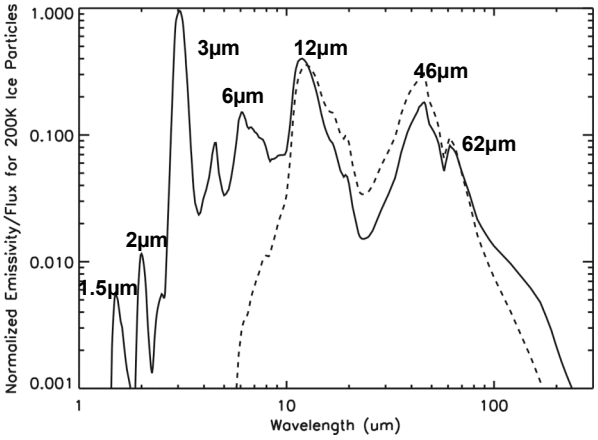

Figure 3 — Emission vs. wavelength for pure 1 um water ice particles, as calculated from the optical constants of Warren (1984), with important features labeled. Solid- Q_{abs}. Dashed line - Q_{abs} * B_ν(200K)., predicted flux for 'warm' ice.

References:

[1] Dello Russo, N., et al. (2007) *Nature 448,* 172-175, and references therein.
[2] A'Hearn, M.F. et al. (2005) *Science 310*, 258 - 264
[3] A'Hearn, M.F. et al. (2008) *Earth Plan. Space 60*, 61-66.
[4] Kueppers et al. (2005) Nature 437, 987-990
[5] Lisse, C.M.. et al. (2006) *Science 313,* 635 - 640.
[6] Bryden G et al. 2006, *Ap J 636,* 1098-1113.
[7] Lisse, C.M., et al..(2008) *ApJ 673,* 1106 - 1122
[8] Hsieh, H.H. and Jewitt, D. (2006) *Science 312,* 561-563.
[9] Lisse, C.M. et al. (2007) *Ap J 658,* 584-592.
[10] Ishi, H. et al. (2008) *Science 319,* 447 - 450.
[11] Sunshine, J., et al. (2007) *Icarus 191*, 73-83.
[12] Sunshine, J., et al. (2006) *Science, 311*,1453-1455.
[13] Jenniskens, P., & D. F. Blake (1994) *Science 265*, 753–756.
[14] Baratta, G. A. et al., (1994) *PSS. 42*, 759–766.
[15] Lien, D.J., *ApJ 355,* 680-692
[16] Hobbs, P. V. (1974) *Ice Physics*, Univ. Press, Oxford.
[17] Bar-Nun, A. et al.(1987) *Phys. Rev. B, 35*, 2427–2435.
[18] Warren, S. G., *Appl. Optics, 23*, 1206–1225, 1984.

Irradiation of Ammonia-Water Mixtures at 20 K and 120 K: A Complement to Previous Laboratory Studies.

M.J. Loeffler[1], U. Raut[1] and R.A. Baragiola[1]. [1] Laboratory of Atomic and Surface Physics, University of Virginia, Charlottesville, VA 22904.

Introduction: Enceladus, a small satellite of Saturn, has received a great deal of attention since the Cassini spacecraft detected a spectacular fountain of water ice particles and vapor emanating from its south-polar region [1-4]. Ever since this discovery, many theories have been proposed to explain how such a unique phenomena could exist on this icy body [5-12].

Here, we present additional laboratory results on the effects of ion irradiation on ammonia water mixtures at different temperatures – 20 K and 120 K. The results complement our previous work on the irradiation of ammonia-water mixtures at 70 K [5].

Experimental Details: The experiments were performed in vacuum at 2 x 10^{-10} Torr using a mass-analyzed beam of 100 keV protons. Solid ammonia-water films were grown at 80 K on the gold mirror surface of a quartz-crystal microbalance (QCM) to a thickness of ~2 μm (148 μg/cm^2), slightly larger than the depth of penetration of the ions. The mixtures were grown using two separate gas dosers with the 1:2 NH_3:H_2O ratio of the dihydrate, as this is one of the equilibrium phases for ice mixtures with < 65.4 wt% ammonia [13]. The samples were then annealed to 120 K to achieve uniform mixing. Irradiations were done at 20 K and 120 K while monitoring the samples with infrared reflectance (IR) (1.5-15 μm), a mass spectrometer (MS) aimed at the surface, and gravimetry using the microbalance.

Irradiation results at 20 K: Figure 1 shows the fluence dependence of the infrared absorption band area of NH_3, N_2, H_2, and NO. We note that the band area of the hydrogen absorption peaks at a value that is four times larger than in the experiments at 70 K.. This is probably due to both an increase in the retention of hydrogen at low temperatures, , and to a large temperature dependence in absorption coefficient, which we have seen in these diatomic molecules [14]. Also we detect NO (1871 cm^{-1}), which is not observed 70 K.

Figure 2 shows the formation of OH dangling bonds as a function of ion fluence; this feature was not observed at 70 K ,but has been observed in ion irradiation of hydrogen peroxide [14]. The band position of the dangling bond (here: 3671 cm^{-1}; pure water: 3696 cm^{-1}) observed here suggests that gas is attached to it, which is likely H_2 and/or N_2. We note that in previous experiments the position of the dangling bond shifted from 3692 to ~3676 cm^{-1} when N_2 was codeposited with water ice [15].

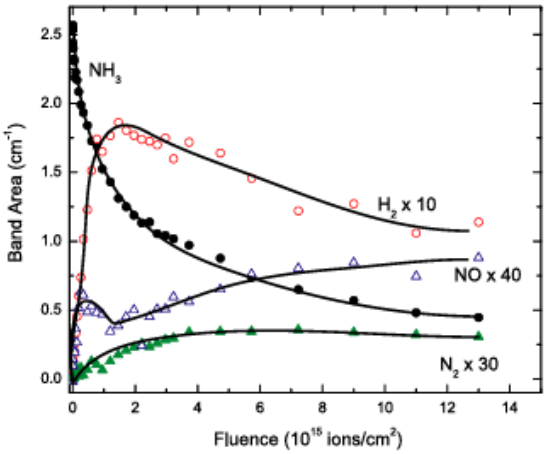

Figure 1. Fluence dependence of the infrared band area of NH_3, H_2, N_2, and NO absorptions in a 1:2 ammonia-water mixture (thickness ~ 2 μm) during irradiation with 100 keV protons at 20 K. The lines are to guide the eye.

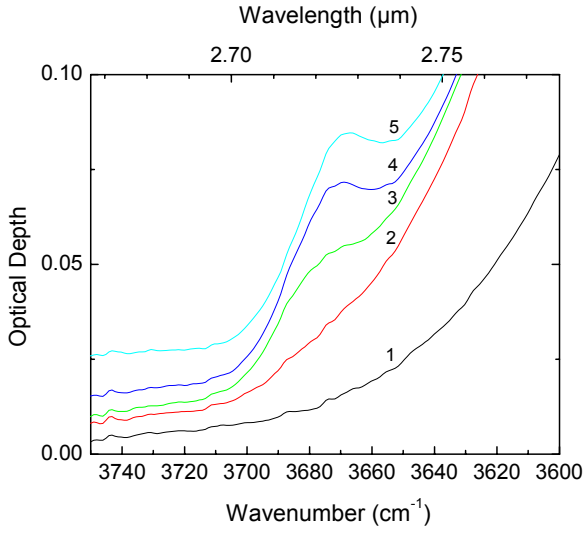

Figure 2. Production of OH dangling bonds as a function of fluence for a 1:2 ammonia-water mixture (thickness ~2 μm) irradiated at 20 K with 100 keV protons to a fluence of (1) 0, (2) 9.5, (3) 22, (4) 57, and (5) 13 x 10^{15} ions/cm^2.

Irradiation results at 120 K: Under otherwise the same experimental conditions as at 20 K, we irradiated samples at 120 K to study effects that temperature has on the irradiation chemistry. Figure 3 shows the destruction of ammonia versus irradiation fluence. We note that other new bands were observed at 2225 (N_2O), 1300, 1263 cm^{-1} and no bands were

observed for N_2 and H_2. At high fluences, the concentration of NH_3 remaining in the ice is about a factor of 5 less than it is at 70 K.

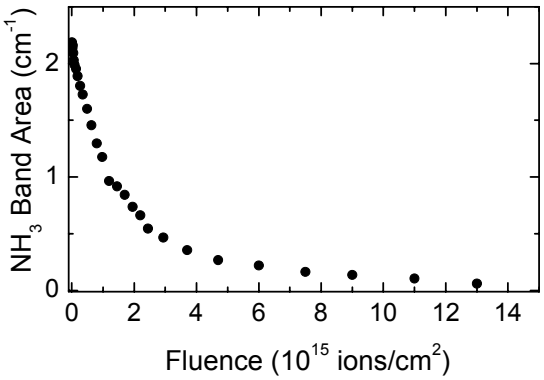

Figure 3. Fluence dependence of the infrared band area of NH_3 (4523 cm^{-1}) in a 1:2 ammonia-water mixture (thickness ~ 2 μm) during irradiation with 100 keV protons at 120 K.

Heating of irradiated films at 20 and 120 K: After irradiation, we warmed the films at 0.2 K/min and monitored changes with the MS, QCM, and IR. For the sample irradiated at 20 K, we observe some mass loss in the QCM, which probably is desorption of N_2 and H_2 from the surface that has not been caught in a trapping site. The remainder of the trapped gas stays in the ice until the high frequency spikes in the chamber pressure begin to occur as they did for irradiation at 70 K (Fig. 4). Here they appear to be stronger and they peak at a higher temperature (~135 K rather than 127 K). As for irradiation at 70 K, these bursts correlate with drops in the infrared reflectance.

Heating of the sample irradiated at 120 K yielded no outbursts like it did for irradiation at 20 and 70 K and no hydrogen desorbed below 150 K either. More details on all these results will be given at the conference.

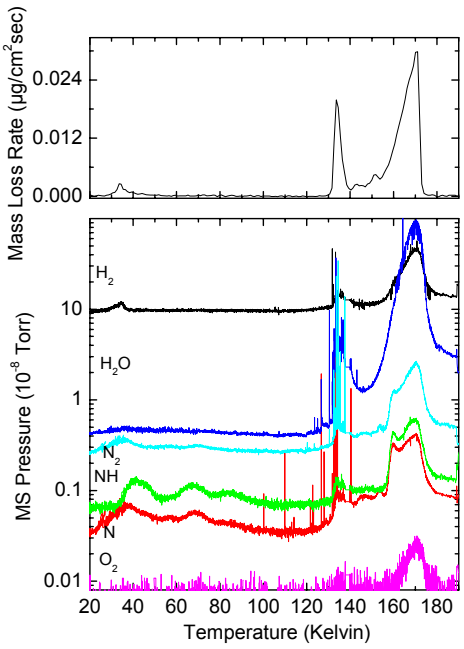

Figure 4. Mass loss rate (top) and mass spectrometer signal uncorrected for relative efficiencies (bottom) during post irradiation heating of a 1:2 ammonia-water mixture (148 μg cm^{-2}; thickness ~ 2 μm) irradiated with 1.3 x 10^{16} 100 keV H^+/cm^2 at 20 K.

References: [1] Hansen, C. J., et al. 2006, Science, 311, 1422. [2] Porco, C. C., et al. 2006, Science, 311, 1393. [3] Spahn, F., et al. 2006, Science, 311, 1416. [4] Waite, J. H., et al. 2006, Science, 311, 1419. [5]Loeffler, M.J. et al. 2006, ApJ, 649, L133. [6] Hurford, T.A. et al. (2007) *Nature*, 447, 292-294. [7] Nimmo, F. et al. (2007) *Natureture*, 447, 289-291. [8] Matson, D.L. et al. 2007, *Icarus*, 187, 569-573. [9] Kieffer, S.W. et al. 2006, Science, 314, 1764. [10] Fortes, A.D. (2007) Icarus, 191, 743-748. [11] Dombard, A.J., 2007, Nature, 447, 276. [12] Cooper, J.F. 2007, JGR submitted. [13] Hogenboom, D. L. et al. (1997), Icarus, 128, 171. [14] Loeffler, M. J. et al. 2006, J. 2006, ApJ, 639, L103. [15] Buch, V., & Devlin, J. P. 1991, J. Chem. Phys., 94, 4091

INFLUENCE OF NaCl ON ICE VI AND ICE VII PHASE RELATIONS AND PROPERTIES: IMPLICATIONS FOR SOLAR SYSTEM ICES. C. E. Manning[1] and I. Daniel[2], [1]Department of Earth and Space Sciences, University of California, Los Angeles, CA 90095-1567, USA, manning@ess.ucla.edu, [2]Laboratoire de Sciences de la Terre, Université Claude Bernard Lyon-1, 69622 Villeurbanne cedex, France, isabelle.daniel@univ-lyon1.fr.

Introduction: Ice VI and ice VII may be important in the interiors of Europa, Ganymede, Callisto and Titan. Oceans and interior pore waters in these bodies likely contain dissolved salts [1-4]; however, the influence of salts on the stability, composition and physical properties of ice VI and ice VII is poorly known. To address this, we investigated phase equilibria in the system H_2O-NaCl at 1 molal (5.5 wt%) NaCl in a diamond-anvil cell (DAC) to 150°C and 5 GPa.

Previous Work: Previous experimental studies of salt-H_2O systems at high pressure have focused chiefly on lower density H_2O ices (ice Ih to ice V) in the presence of $MgSO_4$ or NH_3 [e.g., 5-8]. The abundant terrestrial salt NaCl is probably strongly partitioned into planetary fluid reservoirs, and will therefore be an important constituent in the interiors of icy satellites. However, this salt has received little attention. Early work at room temperature [9] suggested that NaCl had a relatively minor effect on the formation of ice VI, but assumed that the ice phase contained no NaCl. Frank et al. [10] showed that at room temperature, ice VII could contain significant NaCl. However, the system H_2O-NaCl does not appear to have been studied at high temperature.

Methods: Experiments were conducted in a gas-membrane high-temperature diamond-anvil cell fitted with ultra-low-fluorescence diamonds. A 5.5 wt% NaCl solution was used in all experiments. The cell was loaded by placing a 93-μm thick Pt-lined steel gasket with a 150-μm-diameter hole on one of the diamond culets, adding three ruby spheres, and then dispensing a drop of salt solution into the hole with a syringe. The cell was closed immediately, ensuring no H_2O loss by evaporation. The DAC was heated externally; a thermocouple in the gas chamber was constantly monitored, and cell temperature (T) was calculated using a calibration curve.

Phase identifications were made by optical microscopy combined with Raman spectroscopy. Raman spectra were collected using an argon laser (200 mW), Jobin-Yvon/Horiba spectrometer with a Mitutoyo long-working-distance 50x objective, 1800 grating, and 100 μm hole size. Pressure (P) in the cell was calculated using the ruby R_1 frequency shift [11]. Estimated pressure uncertainty is ±0.05 GPa.

Experiments were conducted at 22-150°C and up to 5 GPa by allowing the cell to thermally equilibrate at a given temperature and then varying pressure isothermally while observing phase changes. A key advantage of the gas-membrane DAC for this work is that it maintains nearly constant volume near phase transitions involving the liquid phase, which permits precise determination of liquidus and solidus pressures.

Results and Discussion: The liquidus curves of ice VI and ice VII in a 5.5 wt% NaCl solution were determined at stable and metastable conditions. Significant metastable persistence of each polymorph improved precision of the determinations. Melting was observed at ten discrete temperatures for each polymorph, from 22 to 80°C (ice VI) and from 35 to 150°C (ice VII). A fit to the ice VI data gave $P_m = 0.00415 \bullet \exp(0.0190 T_m)$, where P_m is melting pressure (in GPa), T_m is melting temperature (in Kelvins) and $R = 0.999$; similar fitting of the ice VII data yielded $P_m = 0.234 \bullet \exp(0.00700 T_m)$ ($R = 0.997$). Both curves are steeper than the respective NaCl-free melting curves [12,13], indicating that the freezing-point depression at this bulk composition increases with increasing pressure. At 4.4 GPa, ice VII crystallizes from a 5.5 wt% NaCl solution at 150°C, 90°C below the crystallization temperature of this ice from in the pure H_2O system at 240°C [13]. This effect is significantly greater than is observed for ice Ih at 1 bar.

The intersection of the two liquidus curves indicates that VI-VII-liquid triple point lies at 67±2 °C and 2.57±0.1 GPa at the studied bulk composition. The addition of 1 molal NaCl to H_2O thus results in a shift in the triple point of approximately –13°C and +0.5 GPa relative to the pure H_2O system.

The 5.5 wt% NaCl bulk composition crystallizes completely to a single solid phase of NaCl-bearing ice VI or ice VII solid solution over the investigated temperature range. Raman scattering in the OH-stretching region of both ices shows elevated intensity of the higher frequency components relative to pure H_2O forms. At 22°C, complete crystallization to ice VI_{ss} (where the subscript 'ss' indicates solid solution) was observed at ~1.55 GPa, indicating that ice VI_{ss} coexists with liquid over a ~0.5 GPa interval at this T. As T increases, this P interval decreases significantly, such that at 150°C it is <0.1 GPa.

It proved possible to grow large single crystals of ice VI_{ss} or ice VII_{ss} by slow compression of the cell from near-liquidus conditions to the solidus. Raman

spectra of the last-formed portions of these crystals (grown from NaCl-rich brine) indicated significantly greater scattering in the high-frequency portion of the OH-stretching region than in the cores (grown from ~5.5 wt% NaCl solution). These differences are consistent with zoning in the crystal. The zoning persists for hours to days at 22°C, indicating relatively slow Na^+ and Cl^- diffusivity in the ice structures.

At any temperature, increasing *P* eventually leads to exsolution of a NaCl phase from ice VI_{ss} or ice VII_{ss}. At >30°C, cubic crystals that are not Raman active exsolve from the ice solid solutions. These crystals are interpreted to be halite. At 22 and 30°C, an unidentified Raman-active phase forms at 1.75±0.1 and 1.9±0.1 GPa, respectively, and persists to higher *P*. Raman spectra of the unknown phase yield peaks at positions expected for hydrohalite ($NaCl•2H_2O$). If the phase is hydrohalite, it is stable to higher *P* and *T* than previously inferred [9].

Implications: The large depression of the freezing point in a relatively dilute, 1 molal NaCl solution has important implications for the oceans and interiors of the icy satellites of Jupiter and Saturn. Stabilization of the liquid phase to lower *T* than would be predicted from low-P phase relations means that salt-bearing fluids remain stable to much greater depth expected. This would promote more extensive metamorphism of the silicate interiors due to interaction with mobile fluids. Such fluids would more efficiently strip salts from the silicates and transport them to fluid and ice reservoirs. If this behavior is also characteristic of the other ice polymorphs, it would suppress formation of ices at the bottoms of deep oceans in Titan and the Galilean satellites.

The observation that ice VI and VII form solid solutions with NaCl from 22 to 150°C is also be important. The qualitative inference of low Na^+ and Cl^- diffusivity suggests that compositional gradients could persist over at least modest time scales in these ices. Moreover, the presence of NaCl in ice VI and VII will likely reduce their viscosity and increase electrical conductivity.

References: [1] Kargel J. S. (1991) *Icarus, 94,* 368–390. [2] Khurana K. K. et al. (1998) *Nature, 395,* 777–780. [3] Kivelson M. G. (2000) *Science, 289,* 1340–1343. [4] Zoloatov M. Y. and Shock E. L. (2001) *JGR, 106,* 32815–32827. [5] Grasset O. et al. (1995) *J. Compt. Rend. Acad. Sci., 320,* 249–256. [6] Hogenboom et al. (1995) *Icarus, 115,* 258–277. [7] Hogenboom et al. (1997) *Icarus, 128,* 171–180. [8] Leliwa-Kopynstyski L. et al. (2002). *Icarus, 159,* 518–528. [9] Adams L. H. (1931) *J. Am. Chem. Soc., 53,* 3769–3813. [10] Frank M. R. et al. (2006) *Phys. Earth Planet. Int., 155,* 152–162. [11] Datchi F. et al. (1997) *J. Appl. Phys., 81,* 3333–3339. [12] Choukroun M. and Grasset O. (2007) *J. Chem. Phys., 127,* Article # 124506. [13] Lin J.-F. et al. (2004) *J. Chem Phys, 121,* 8423–8427.

OPTICAL PROPERTIES OF AMORPHOUS AND CRYSTALLINE H_2O-ICES**.** R. M. Mastrapa[1,2], M. P. Bernstein[2], S. A. Sandford[2], T. L. Roush[2], D. P. Cruikshank[2], C. M. Dalle Ore[1,2] [1]SETI Institute (515 N. Whisman Road, Mountain View CA 94043) [2]NASA Ames Research Center (Mail Stop 245-6, Moffett Field, CA 94035, Rachel.M.Mastrapa@nasa.gov).

Introduction: H_2O ice is widespread in the Solar System. The phase of H_2O ice on Solar System objects depends on the pressure and temperature conditions at the time of its formation and its temperature and radiation history. On Solar System objects, H_2O forms a solid that is either in an amorphous phase (Ia) or in one of two crystalline phases: cubic (Ic) or hexagonal (Ih) [1-3]. Amorphous H_2O-ice converts to the cubic crystalline phase in an exothermic reaction near 135 K [4-6]. The cubic phase of H_2O ice is a metastable version of the hexagonal phase that is found in the laboratory at temperatures between 135 and 170 K [6-8]. Above 170 K the phase of H_2O ice is hexagonal. Considering only thermal processes, the presence of amorphous H_2O-ice on a surface might indicate that the surface has been significantly colder than 100 K since formation. The crystallization reaction is irreversible, so once an ice sample crystallizes it stays crystalline even if the temperature is again reduced below 135 K.

Spectroscopy: H_2O ice is detected on Solar System objects by its distinctive infrared absorptions. Although the cubic and hexagonal phases have nearly identical infrared spectra [9], the infrared spectra of amorphous and crystalline H_2O-ices are easily distinguishable [10-15]. In the crystalline phase, the infrared bands are stronger, sharper, and shifted to longer wavelength compared to the amorphous-phase bands [3]. The infrared bands of crystalline H_2O-ice are temperature dependent; they shift to shorter wavelength and decrease in absorption with temperature [9, 11, 14, 16, 17].

Due to the temperature- and phase-dependent variability in position for the H_2O ice bands it is difficult to consistently refer to the same band over a range of temperature by a precise position. For example, the band near 6050 cm^{-1} (1.65 μm) can range in location from 6087 cm^{-1} (1.643 μm) in amorphous H_2O-ice to 6020 cm^{-1} (1.661 μm) in 20 K, crystalline H_2O-ice. We therefore define four spectral band regions and will refer to them as the bands near: 6600 cm^{-1} (1.5 μm), 6400 cm^{-1} (1.56 μm), 6050 cm^{-1} (1.65 μm), and 4900 cm^{-1} (2.0 μm). When we refer to positions of bands at a specific phase and temperature we will refer to the position with the correct and full precision.

Laboratory Measurements: The vacuum system used here has been described previously [18, 19]. To summarize, we collect infrared transmission spectra of ice samples deposited on a window suspended under high vacuum (~10^{-8} mbar) and low cryogenic temperatures (~15 K).

Sample Preparation. To deposit samples we injected H_2O vapor into the vacuum chamber through a narrow inlet tube aimed at the sample window. During deposition, we directly measured the thickness of the samples by monitoring the interference fringes of a He-Ne laser reflected off the sample. The temperature of the sample was adjusted at a rate of ~1K/min and spectra were measured at every 10 K between 20 and 150 K.

Spectral Analysis. We follow the procedure for calculating optical constants described previously [18, 20, 21]. To summarize, we calculate the absorption coefficient α of a plane-parallel absorbing film from:

$$\alpha = \frac{1}{d}\ln\left(\frac{I_0}{I}\right) - \frac{2}{d}\ln\left|\frac{(n_0+n_1)(n_1+n_2)+(n_0-n_1)(n_1-n_2)e^{-2i\delta_1}}{2n_1(n_0+n_2)}\right|$$

where d is the thickness of the ice, I/Io is the transmission spectrum of the ice, n_0 is the index of refraction of vacuum (n_0=1), n_1 is the index of refraction of the sample (1.32 for crystalline H_2O-ice [22], 1.29 for amorphous H_2O-ice [23]), and n_2 is the index of refraction of the sample window (n_{CsI} =1.75, n_{KBr} =1.54, $n_{sapphire}$ = 1.74) and $\delta 1 = 2\pi n_1 \omega d$ where ω is frequency in wavenumbers (cm^{-1}).

We calculate the intrinsic strength of absorption features in cm/molecule, or A-values, following the method of Hudgins, et al. [18]. As with their work, we needed to multiply the integrated areas of our bands by 2.303 to convert from a base 10 logarithm to natural logarithm. The A value is given by:

$$A = N^{-1}\int \tau d\nu$$

where N is the column density of the sample (number of absorbers per unit area), ν is in wavenumbers, and τ is:

$$\tau \equiv \ln(I_0/I)$$

where I is the intensity of light with sample, I_0 is the intensity of light without sample. The column density of the sample is calculated by multiplying the thickness and density of the sample by Avogadro's number, then dividing by the molecular weight of the

material. The densities used are as follows: HDA - 1.1 g/cm^3 [24], LDA - 0.82 g/cm^3 [23], and Ic - 0.931 g/cm^3 [8].

Results: In general, the bands of crystalline H_2O-ice behave similarly to previously reported experiments [16]. The crystalline bands are strongly temperature-dependent: they grow stronger in absorption and shift to longer wavelength with decreasing temperature. However, the bands in our crystalline H_2O-ice spectra have absorptions up to 6% stronger than those published previously. We observed two distinct spectral signatures of amorphous H_2O-ice. Samples that were deposited below 70 K and that have never been heated above that temperature display absorptions that are shifted to shorter wavelength and are weaker than bands in spectra of samples deposited at T > 70 K. For T > 70 K, the bands of the 1.5 and 2 μm bands are stronger and slightly shifted to longer wavelength. Spectra of samples deposited below 70 K and heated above that temperature shifted to look like the higher temperature phase. When re-cooled, the bands remained at the higher temperature phase positions, suggesting that this is an irreversible transition. These different spectra could represent the transition between high-density amorphous H_2O-ice (HDA or I_ah) at low temperature and low density amorphous H_2O-ice (LDA or I_al) at high temperature [4, 23, 24]. The spectral bands of amorphous H_2O-ice show no other changes with temperature.

Applications: The indices of refraction and spectra of pure H_2O ice presented here are directly applicable to modeling spectra of Solar System objects. Calculated mixtures of amorphous and crystalline H_2O-ice predict several changes in the spectrum. As the amorphous content increases, the double band structure seen near 4170 cm^{-1} (2.4 μm) changes to a single broad band, the 4900 cm^{-1} (2.0 μm) and 6600 cm^{-1} (1.5 μm) bands shift to shorter wavelength, and the 6050 cm^{-1} (1.65 μm) and 6400 cm^{-1} (1.56 μm) bands decrease in strength. In the interpretation of the spectra of Solar System objects, the presence of a band near 6050 cm^{-1} (1.65 μm) does not in itself indicate a surface that is 100% crystalline, since the band is clearly present in model spectra with up to 80% amorphous content, Figure 1. Plotting 6050/6600 (1.65/1.5) band ratios, may be a useful diagnostic tool for the characterization of ices. Future studies will examine the effect of grain size on band area ratios by modeling different fractions of amorphous and crystalline H_2O-ice while varying grain size.

References: [1] Cruikshank D. (1998) Earth Moon Planets, 80, p. 3-33. [2] Jenniskens P., et al. 1998 in *Solar System Ices*, p. 139-156. [3] Schmitt B., et al. 1998 in *Solar System Ices*, p. 199-240. [4] Jenniskens P. and Blake D.F. (1994) Science, 265, p. 753-756. [5] Kouchi A., et al. (1994) Astron. Astrophys., 290, p. 1009-1018. [6] Sugisaki M., et al. 1969 in *Physics of Ice*, p. 329-343. [7] Jenniskens P., et al. (1997) J. Chem. Phys., 107, p. 1232-1241. [8] Petrenko V.F. and Whitworth R.W. 1999 *Physics of Ice*. [9] Bertie J.E. and Whalley E. (1967) J. Chem. Phys., 46, p. 1271-1284. [10] Bertie J.E. and Whalley E. (1964) J. Chem. Phys., 40, p. 1637-1645. [11] Hagen W. and Tielens A.G.G.M. (1982) Spectrochim. Acta, 38A, p. 1089-1094. [12] Hagen W. and Tielens A.G.G.M. (1981) J. Chem. Phys., 75, p. 4198-4207. [13] Ockman N. (1958) Adv. Phys., 7, p. 199-220. [14] Smith R.G., et al. (1994) Mon. Not. Roy. Astr. Soc., 271, p. 481-489. [15] Whalley E. (1977) Can. J. Chem., 55, p. 3429-3441. [16] Grundy W.M. and Schmitt B. (1998) J. Geophys. Res., 103, p. 25809-25822. [17] Mastrapa R.M.E. and Brown R.H. (2006) Icarus, 183, p. 207-214. [18] Hudgins D., et al. (1993) Astrophys. J. Suppl. Ser. , 86, p. 713-870. [19] Bernstein M.P., et al. (2006) Icarus, 181, p. 302-308. [20] Heavens O.S. 1991 *Optical Properties of Thin Films*. [21] Bergren M.S., et al. (1978) J. Chem. Phys., 69, p. 3477-3482. [22] Hale G.M. and Querry M.R. (1973) Applied Optics, 12, p. 555-563. [23] Westley M.S., et al. (1998) J. Chem. Phys., 108, p. 3321-3326. [24] Narten A.H., et al. (1976) J. Chem. Phys., 64, p. 1106-1121.

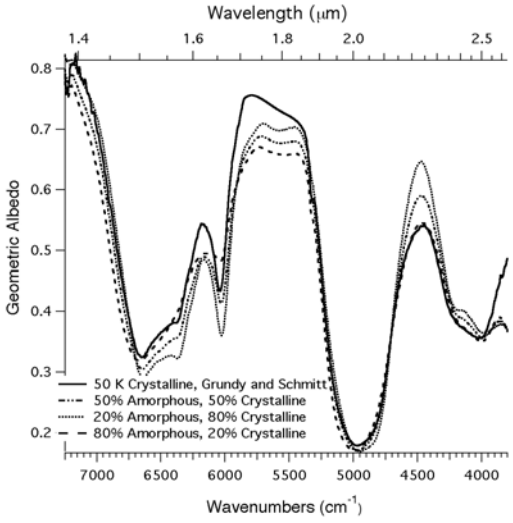

Figure 1. Geometric albedo model spectra of H_2O ice. All spectra were generated using optical constants at 50 K. A model spectrum of crystalline H_2O-ice generated from Grundy and Schmitt (1998) is provided for comparison (solid line). The remaining spectra are of mixtures of amorphous and crystalline H_2O-ice as follows: 80%-20% (long dash, single dot line), 50%-50% (dotted line), 20%-80% (dash, two dot line).

BINDING ENERGIES OF CH_4 AND H_2O-ICE SYSTEMS. R. M. Mastrapa[1,2], T. Cadarette[3], and S. A. Sandford[2]
[1]SETI Institute (515 N. Whisman Road, Mountain View CA 94043) [2]NASA Ames Research Center (Mail Stop 245-6, Moffett Field, CA 94035, Rachel.M.Mastrapa@nasa.gov) [3]Scripps College.

Introduction: Previous results have shown that some volatile species have a higher surface binding energy to H_2O-ice than to themselves, [1-5]. In other words, materials such as CO and CO_2 "stick" to H_2O-ice for longer periods of time then they would "stick" to themselves. The means that these materials may be found stuck to H_2O-ice at temperatures higher than they would normally be stable. CH_4 is a simple organic compound that has been detected on Pluto and Kuiper Belt Objects on the edge of the Solar System. We performed a series of experiments to determine the surface binding energy of CH_4 to H_2O and to itself.

The Experiment: We completed measurements of binding energies of the following systems: CH_4-CH_4, CH_4-H_2O using a cryo-vacuum system and following the methods of Sandford and Allamandola [1, 2]. Briefly, for the CH_4-CH_4 measurements, we monitored the area of relevant infrared features with time at three different temperatures (<50 K) and used the results to estimate sublimation rates. For the mixture H_2O/CH_4 = 20, we carried out a series of experiments in which we deposited the mixtures at increasingly higher temperatures (starting at 15 K) until the infrared features of the more volatile component are no longer seen (usually at > 50 K). We then use the deposition rate of H_2O to estimate the residence time of the more volatile species (CH_4).

Results:

Pure CH_4. For the pure CH_4 experiments, we deposited CH_4 alone at 15 K. We then slowly heated the sample to 36, 37, or 39 K. We then monitored the area of the CH_4 features at 7.7 and 3.3 µm with time.

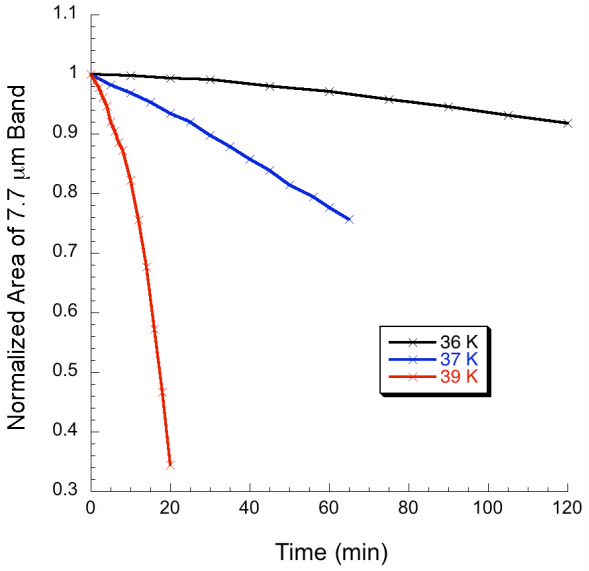

Figure 1 The area of the CH_4 feature at 7.7 µm with time at 36, 37, and 39 K.

H_2O/CH_4=20. We deposited the gas mixture of H_2O/CH_4=20 at a range of temperatures from 15 to 105 K. After each deposition we measured the areas of the H_2O and CH_4 features and noted how their abundance ratio changed with deposition temperature.

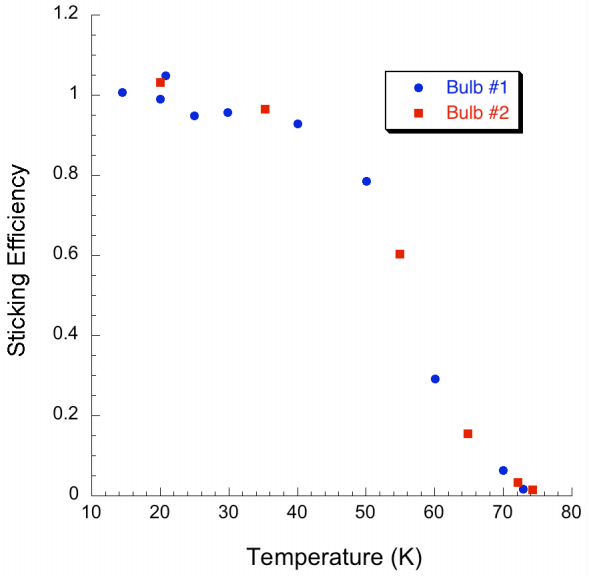

Figure 2 The sticking efficiency of the H_2O/CH_4 system with deposition temperature, calculated by taking the ratio of the molecular abundance of H_2O calculated from the 3 µm feature to that of CH_4

calculated from the 7.7 µm feature then normalized to 20. The scatter in the points at 20 K is from repeated experiments and represents the error in the measurement. The data are presented in circles and squares from two H_2O/CH_4=20 bulbs prepared separately and show good agreement.

CH_4 Residence Times: Note that the small change in binding energy, ~750K, results in a large difference in residence time. Not shown are the values at 10 K since they exceed the lifetime of the universe : CH_4-CH_4 t = 10^{29} yr; CH_4-H_2O t = 10^{60} yr. However, the values quickly become relevant at 20 K where CH_4-CH_4 is stable for a mere 10^4 yr compared to CH_4-H_2O's 10^{20}. These low temperature would be relevant to the interstellar medium and the outskirts of clouds and planetary disks. In the temperature range of Kuiper Belt Objects (40-60 K), the CH_4-H_2O residence times are on the order of years to fractions of a year, while the CH_4-CH_4 stability is 10^5-10^8 times shorter. The relative timescales approach within 10^4 years in the Saturnian system and 10^2 years for the Galilean satellites.

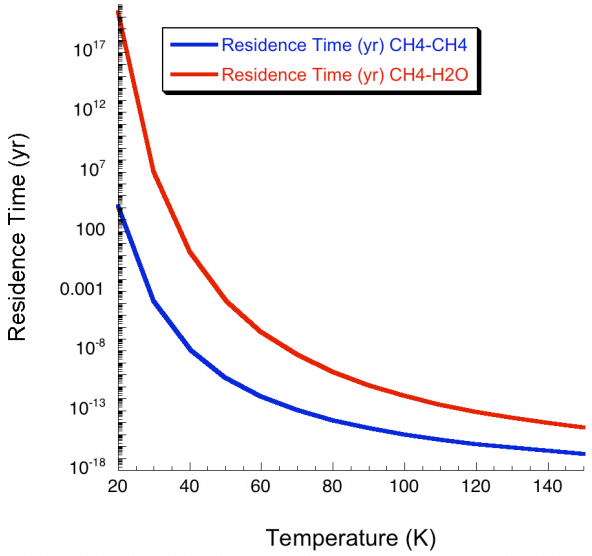

Figure 3 Residence time of CH_4 on CH_4 and CH_4 on H_2O in years. Calculated using the equation $t = \exp(\Delta H_s/kT)/\nu_0$ using values from the results and $\nu_0 = 2.0 \times 10^{12}$ s^{-1}.

Conclusions: The presence of solid H_2O greatly changes the residence time of CH_4 on the surface of objects in the Solar System. Since, H_2O-ice is ubiquitous on satellite surfaces, this greatly changes the possible distribution of CH_4. In other words, the "ice line" for CH_4 could be moved in closer to the sun. This also affects the stability of CH_4 in sub-nebulae that eventually formed the giant planets, depending on the interior temperature distribution.

One must use caution when considering these numbers, because they apply only to the residence time on the surface. It is therefore only applicable to surface condensations or sublimation. However, once the CH_4 is buried, it can be stable for even longer periods of time. Long term stability of CH_4 trapped in amorphous H_2O-ice or enclathrated in crystalline H_2O-ice is not well constrained, but is likely to be longer scale than the surface stability. These numbers must be integrated into atmospheric escape models to fully understand the stability of CH_4.:

References:

[1] Sandford S.A. and Allamandola L. (1990) Icarus, 87, p.
[2] Sandford S.A. and Allamandola L. (1998) Icarus, 76, p. 201-224.
[3] Sandford S.A., et al. (1988) Astrophys. J., 329, p. 498-510.
[4] Sandford S.A. and Allamandola L.J. (1993) Astrophys. J., 417, p. 815-825.
[5] Sandford S.A. and Allamandola L.J. (1993) Icarus, 106, p. 478.

ICE RHEOLOGY AND THE EVOLUTION OF ICY SATELLITES: TEN PROPOSITIONS. William B. McKinnon, Department of Earth and Planetary Sciences and the McDonnell Center for the Space Sciences, Washington University, Saint Louis, MO 63130 (mckinnon@wustl.edu).

Introduction: I propose to defend the following:

1) Realistic and accurate rheology is essential for understanding icy satellites and Kuiper belt objects; agreement between different experimental groups should be sought.

2) Robust numerical methods are necessary for reliable results, with the caveat that models are only as good as the physics behind them.

3) More specifically, the semibrittle regime (poorly enough understood in rock) needs exploration for water ice. This is an important input for localization models, and Beeman's rule could use a revisit as well.

4) Measurement of diffusion creep in ice would be more than just reassuring, it would allow its interplay with grain-boundary sliding to be better understood.

5) Measurement of activation volumes (V^*) in low-stress creep regimes is important.

6) The low-stress (grain-size-sensitive) creep rate for ice III is very important, as it likely an important control on the evolution of larger icy satellites, such as Ganymede.

7) Grain size evolution during creep is no doubt important as well, and could be studied experimentally. Rheologies may be different at small and large strains.

8) Multiple stress and strain systems may couple during creep in couple ways, if at least one of the rheologies is non-Newtonian. The effects may be especially important for tidally flexed satellites, such as Europa and Enceladus.

9) Porosity evolution is important for midsize icy satellites, KBOs, and ice-rich regoliths, but is poorly understood and often neglected. Benchmarking against experiments would be especially valuable.

10) Although strictly speaking not part of this workshop, we should keep our eyes on the properties of "exotic" ices and organic materials, as they are likely important bulk constituents of distant icy satellites and KBOs.

ACTIVITY OF COMETS AT LARGE HELIOCENTRIC DISTANCES. K. J. Meech[1], O. R. Hainaut[2], S. C. Lowry[3], J. Pittichova[1], A. Bar-Nun[4], G. Notesco[4], and D. Laufer[4], [1]Institute for Astronomy, 2680 Woodlawn Drive, Honolulu HI 96822, meech@ifa.hawaii.edu, jana@ifa.hawaii.edu, [2]European Southern Observatory, Casilla 19001, Santiago 19, Chile, ohainaut@eso.org, [3]NASA JPL, 4800 Oak Grove Drive, MS 181-301, Pasadena, CA 91109, sclowry@jpl.nasa.gov, [4]Tel Aviv University, Dept. of Geophysics and Planetary Sciences, Tel Aviv 69978, Israel, akivab@post.tau.acl.il

Introduction: The primary driver of activity in comets close to the sun is sublimation of H_2O-ice. Calculations of gas production for sublimation from a suite of volatiles show that the sublimation rates decrease significantly beyond a specific heliocentric distance; for H_2O-ice this distance is near r=3AU [1]. This has lead to the mis-interpretation that water-driven activity will not continue beyond this distance. However, observations with sensitive detectors are now showing activity in many comets out to large distances, including indications of activity near aphelion for short-period comets [2].

Discussion: Possible mechanisms to explain activity in comets beyond the distance where H_2O-ice sublimation can produce significant coma include the amorphous-to-crystalline ice transition [3-4] or frozen highly volatile materials. However, we know that either there was not a significant amount of these directly frozen gases incorporated into comets, or that evolutionary effects have released these volatiles, because the comets which have been studied in detail do not show significant release of different volatiles at different times, rather they come out in the same proportions over a range of distances regardless of volatility. The amorphous ice transition has been used to explain many cometary phenomena at large heliocentric distances including the comet 1P/Halley outburst near r=13 AU [5], activity in C/1995 O1 [Hale-Bopp], the large outburst in C/Chiron, and the sporadic activity in comet P/Schwassmann-Wachmann 1 [6-8]. New surveys that are targeting short-period comet nuclei [x] near aphelion are finding significant numbers of comets with comae near r=4-5 AU, however, H_2O ice sublimation is sufficient to lift observable dust grains from the surface and can account for the development of a dust coma out to between 5-6 AU [9].

For comets which are active much beyond 9 AU where the equilibrium surface temperatures are lower than the start of the amorphous-to-crystalline ice transition, activity may be due to the perihelion heat wave penetrating into volatile-rich depths in the nucleus. However, discoveries of active dynamically new comets with large perihelion distances, which have never passed into the inner solar system and experienced heating require a different mechanism.

Amorphous ices anneal starting at temperatures near ~37K and lasting until the crystalline phase transition begins. Lab experiments show that gases trapped in amorphous ices are partially released during annealing, and that large ice grains can be liberated during this process [10]. This process is relevant for activity as far out as the Kuiper Belt.

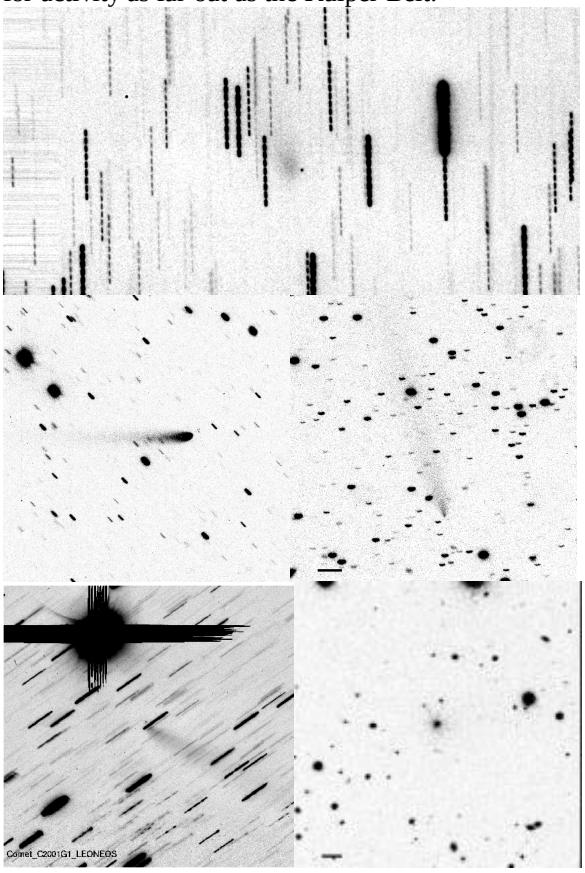

Fig. 1 Images of comets [top] 22P/Kopff at r=4.7 AU; [middle L] C/2003 O1 (LINEAR) at r=6.92 AU; [middle R] C/1999 J2 (Skiff) at r=10.10 AU; [bottom L] C/2001 G1 (LONEOS) at r=11.21 AU; [bottom R] C/2003 A2 (Gleason) at r=11.49 AU. FOV = 3x3 arcmin, N is up and E to the left.

Summary: Deep surveys are discovering fainter distant comets, and targeted observations are now detecting activity on many of these objects. Observations should continue to get both deep coma images suitable for Finson-Probstein dust-dynamical modeling to constrain dust ejection velocities, sizes, and onset of activity, and these can be compared with

thermal models and laboratory experiments to understand the mechanisms for activity. Kuiper belt objects are being observed with a variety of surface compositions, some of which imply outgassing and volatile loss [11]. Amorphous ice annealing provides a mechanism to explain activity inbound at r>9 AU, and is a process which can work even in the Kuiper belt, although searches for activity in these objects have not yet been successful [12].

References: [1] Delsemme A. (1982) in *Comets*, (L. L. Wilkening, ed.), 85. [2] Meech, K. J. and J. Svoren (2004) in *Comets II*, (M. C. Festou *et al*, ed.), 317. [3] Notesco, G., A. Bar-Nun, and T. Owen (2003) *Icarus 162*, 183. [4] Bar-Nun, A. and D. Laufer (2003) *Icarus 161*, 157. [5] Prialnik, D. and A. Bar-Nun (1992*). Astron. Astrophys. 258*, L9, [6] Prialnik, D. (1997) *E&MP 77*, 223. [7] Prialnik, D., N. Brosch and D. Ianovici (1995) *MNRAS 276*, 1148. [8] Jewitt, D. (1990) *ApJ 351*, 277. [9] Fernandez *et al*. (2007) *BAAS 211*, 5602. [10] Laufer, D., I. Pat-El, A. Bar-Nun (2005) *Icarus 178*, 248. [11] Schaller, E. L. and M. E. Brown (2007) *DPS-AAS 39*, 4910. [12] Meech, K. J., O. R. Hainaut, H. Boehnhardt and A. Delsanti (2003) *EM&P 92*, 169.

Acknowledgements: This material is based upon work supported by the National Aeronautics and Space Administration through grant NAG5-12236 and through the NASA Astrobiology Institute under Cooperative Agreement NNA04CC08A issued through the Office of Space Science.

THE RHEOLOGY OF ICE-ROCK MIXTURES – APPLICATION TO THE SATELLITES OF THE OUTER SOLAR SYSTEM. C. A. Middleton[1], P. R. Sammonds[1], P. M. Grindrod[1], A. D. Fortes[1] and L. Vočadlo[1]
[1]Center for Planetary Sciences, Department of Earth Sciences, University College London, Gower Street, London WC1E 6BT (ceri.middleton@ucl.ac.uk).

Introduction: Ice-rock mixtures are likely to occur throughout the solar sytem; understanding of their rheological properties have been based primarily upon studies of terrestrial glaciers and permafrost (e.g. [1,2]). It is likely that there is a large quantity of ice trapped in the Martian subsurface, especially at high latitudes, which may account for features such as patterned ground, polygonal fractures and lobate debris aprons, and be a source of water for exploration [3]. Ice-rock mixtures are also likely to have been, or still be, present in the outer solar system, both in the smaller bodies, such as Kuiper Belt Objects and in the larger satellites of the Gas Giants.

Many of these larger satellites are differentiated, as indicated by the gravitational moment of inertia factor [e.g. 4] but they probably formed from a more homogeneous mixture of rock and ice, which subsequently differentiated. In the case of Callisto, the most likely current structure as calculated from gravitational data is a partially differentiated interior, with an ice-rock core and an overlying ice shell [5]. This means that the thermal evolution of all the large icy satellites has been dominated by the rheology of an ice-rock mixture at some time in the past; the rheology of undifferentiated bodies continue to be controlled by the rheology of ice-rock mixtures to the present day.

Constraining the rheology of these materials is important in understanding the evolution of icy moons, since factors such as the viscosity control differentiation and convection, and hence the spatial distribution of heat-producing radionuclides and the efficiency of heat flow. These factors in turn control the possibility of melting and the formation and long-term stability of subsurface oceans. For example, Durham et al. [6] found that the relative viscosity of a pure ice mixture and an ice-rock mixture varied by up to two orders of magnitude. This increase in viscosity should inhibit convection, increasing the possibility of melting and sub-surface oceans [6].

Previous work: Most of the experimental data for ice-rock mixtures focus on terrestrial environments [1,2] but some experiments have been performed under conditions relevant to the putative permafrost layer on Mars [3]. That study found a brittle/ductile transition in the behaviour of the ice-rock mixtures at a rock volume-fraction of ~0.6. This coincides with the proportions of rock and ice that Nagel et al. [7] used as the packing limit for the concentration of rock in the core of Callisto. However, conditions in the interiors of icy satellites will differ from those described by Mangold et al. [3] since the increased confining pressure should inhibit brittle failure. Hence, rheological parameters obtained in those experiments cannot necessarily be extrapolated easily to different conditions.

The experiments of Durham et al. [6] were carried out at pressures and temperatures relevant to the interiors of large icy satellites. They found that the strength of an ice-rock mixture was greater than that of pure ice, and the viscosity was higher by up to two orders of magnitude. However their results were dependent on the material that constituted the rock fraction, possibly due to the size of the rock particles and associated fabrics in the samples.

The rheological parameters used in models of the thermal and structural evolution of the icy satellites are mostly those of pure ice. For example, McKinnon [8] treats the outer shell of Callisto as ice rather than an ice-rock mixture. Dependent on the mechanism of differentiation the outer shell may be pure ice (in which case using the properties of pure ice is valid), or may contain up to 10 wt% rock [8] (in which case using the properties of pure ice may not be valid). McKinnon [8] then assumes that the change is sufficiently small to not effect the viscosity within the error of the creep law.

There are however some models which consider the introduction of rock into the ices, for instance Nagel et al. [7] include the effect of rock on the viscosity of their ice-rock mixture during differentiation of Callisto, by assuming that the viscosity of the ice-rock mixture is a function of the viscosity of the ice and rock volume fractions. This is a scale invariant relationship, assuming that the dimensions of the particles are not relevant, which may not be a valid assumption, as the results of Durham et al. show [6].

Experiments: We aim to investigate the rheology of ice-rock mixtures at the conditions applicable to the icy satellites, specifically investigating the role of the volume fraction of rock, the grain size of the rock and ice and the grain size ratio, also considering at what volume fraction the rheology becomes dominated by rock rather than the ice.

We will also investigate the effect of the grain size ratio between the ice grains and the rock grains. The role of the grain size ratio was highlighted by [6] showing that finer grained particulates formed a network

around larger ice grains, preventing the formation of a homogeneous mixture.

We will be able to compare our data to that of [6] and increase the amount of data available for the rheology of these materials under conditions likely in icy satellites. The importance of a large data set of rheological experiments on these materials is demonstrated by Durham et al. [6], who found different flow laws for pure ice from different data sets. An increase in data will reduce the ambiguity of the results.

This should also allow us to evaluate the assumption of Nagel et al. [7] that the viscosity is a scale invariant relationship, and also compare results with the results of Friedson and Stevenson [9] based on the viscosity of a suspension.

The first stage in the experiments will be to develop a sample preparation apparatus which will allow the ice grain size, volume fraction of rock and mixing of the sample to be controlled as accurately as possible.

Then experiments on samples of various rock fraction will be conducted at conditions comparable with the literature, with systematic variation in rock fraction, grain sizes and grain size ratio.

We will be using three types of loading cell to investigate the rheological properties of these materials.

Triaxial. The main experiments will be conducted under triaxial conditions; the rig uses nitrogen gas as the confining medium to generate pressures up to 300MPa in the UCL cold room at temperatures as low as 250K, with additional refrigerant on the pressure vessel allowing us to reach ~180K.

Uniaxial. To investigate lower temperature conditions, we will be able to use the uniaxial loading cell with an added cold stage which has a theoretical minimum temperature of ~80K.

True-triaxial. The newly commissioned true-triaxial rig will allow experiments to be carried out in biaxial stress states, relevant to near surface processes in the large satellites up to pressures of 50MPa and temperatures down to 240K.

Application of parameters: The rheological parameters obtained from these experiments will be used to model the structural and thermal evolution of icy satellites, allowing differentiation and convection to be modelled more accurately during the early evolution of these bodies. The results will also be of relevance to the mechanical stability of rock-ice regolith on the Earth and Mars, including possible applications to the mechanical properties, and stability, of clathrate-sediment mixtures in the deep ocean which may have been related to large, rapid global warming events in the past [10].

References: [1] Song et al. (2006) Scripta Materialia, 55, 91-94 [2] Parameswaran and Jones (1981) J. Glaciol., 27, 147-156 [3] Mangold et al. (2002) Plan. Space. Sci., 50, 385-401 [4] Anderson et al. (1996) Nature, 384, 541- 543. [5] Anderson et al. (2001) Icarus, 153, 157-161 [6] Durham et al (1992) JGR, 97, 20883-20897 [7] Nagel et al. (2004) Icarus, 169, 402-412 [8] McKinnon (2006) Icarus, 183, 435-450 [9] Friedson and Stevenson (1981) Icarus, 56, 1-12 [10] Reagan and Moridis (2007), GRL, 34.

LIQUID INTERFACIAL WATER IN PLANETARY ICES: PRESENCE AND CONSEQUENCES

D. Möhlmann, DLR Institut für Planetenforschung, Rutherfordstr. 2, D – 12489 Berlin, Germany (dirk.moehlmann@dlr.de)

Abstract

Microscopic liquid layers of interfacial water can evolve on surfaces of mineral grains, embedded in ice. This is due to the attractive van der Waals forces between mineral surface and water ice, which cause a pressure. That is followed by a freezing point depression, which enables the interfacial water to remain liquid at temperatures of 180 K and less. The properties of interfacial water are analytically and quantitatively described by a sandwich-model of a layer of liquid water between mineral surface layer and ice layer. This model is used to derive an equation to determine the thickness of these layers of liquid interfacial water. This is typically of the order of nanometers, but it increases remarkably near to the frost point temperature. Furthermore, an equation is derived to determine the freezing point depression, i.e. the minimum temperature for water to remain liquid. Also an “Equilibrium moisture content” (EMC)/”Equilibrium Relative Humidity” (ERH) relation for the water content of soil is derived, which relates, for equilibrium conditions, soil water content and atmospheric relative humidity. The undercooled liquid interfacial water may be important for several physical (as rheological), chemical (as photo-catalytic), and biological processes in icy environments.

Examples are discussed for terrestrial ices and other relevant icy bodies in the Solar system. It is shown that the concept of “Planetary Habitability” is to be generalized to keep into account liquid interfacial water.

Formation of Complex Molecules in Planetary Ice Analogs. M. H. Moore[1] and R. L. Hudson[2], [1]NASA's Goddard Space Flight Center, Astrochemistry Laboratory, Greenbelt, MD 20771, marla.h.moore@nasa.gov, [2]Eckerd College, Department of Chemistry, St Petersbury, FL 33711, hudsonrl@eckerd.edu.

Introduction: Molecular ices are known to be part of the composition of many solar system objects, such as planets, satellites, rings, and comets. These ices exist in different radiation environments within the solar system, and are subjected to processing by keV-MeV ions and UV photons. Radiation processing results in changes in the chemical and physical properties of such ices with time. The observed inventory of planetary and satellite ice molecules includes H_2O, CH_4, NH_3, CO, CO_2, SO_2, SO_3, H_2O_2, O_2, O_3, the SO_4^{2-} ion in the form of hydrated sulfuric acid and/or mineral sulfates, hints of complex hydrocarbons, C≡N containing species, and possibly H_2S. Of these, it is generally accepted that H_2O_2, O_2, O_3, and features associated with hydrated sulfuric acid are signatures of energetic processing by the magnetospheric radiation environments of Jupiter and Saturn.

In the Cosmic Ice Laboratory at NASA's Goddard Space Flight Center, we study the photo- and radiation-induced chemistries of ices at 8 – 300 K. We find that radiolysis and photolysis destroy reactant molecules, synthesize new species, cause changes of phase in pure materials, and eject molecules from ices. These observed processes depend on radiation dose, ice temperature, and ice composition. We have examined photo- and radiation chemical changes in H_2O-rich ice mixtures as well as N_2-rich ices more relevant to Triton and Pluto.

Our laboratory radiation results call attention to possible species awaiting future detection. (1) Irradiated H_2O + SO_2 or H_2S ices. Our more-recent work has documented the overall principal chemical trend for sulfur-containing molecular ices as they become oxidized during radiation processing. New radiation products include both anions and cations all with spectral features that make them candidates for possible observation in the Jovian system. (2) Irradiated and thermally processed H_2O + NH_3 ices. Related to surfaces in the outer solar system, we measured changes in the near-IR NH_3 band with composition, formation temperature, and thermal- and radiation processing. These results reveal the difficulty in distinguishing amorphous NH_3 ice mixtures from NH_3 hydrates using a single absorption feature. (3) Irradiated H_2O + CO_2 ices. Irradiated terrains rich in H_2O and CO_2 form carbonic acid, H_2CO_3, which has a unique spectral signature and a volatility less than that of H_2O. Carbonic acid has been tentatively assigned to the weak 3.8-μm band of Europa and Callisto. Irradiated terrains rich in CO_2 lead to a significant production of O_3. New results on the stability of H_2CO_3 and O_3 will be applied to possible future observations. (4) Irradiated N_2 + CO + CH_4 ices. The radiation products expected to form and survive on surfaces such as Triton, Pluto, and KBO's with N_2-rich terrains include anions (OCN^-, CN^-, and possibly N_3^-), and these would be associated with the NH_4^+ cation The distinctive 4.6-μm band of OCN^- has been detected in interstellar and even extragalactic ices and is considered a radiation marker. To date neither OCN^- nor its counterion, NH_4^+ has been detected in planetary ices and so they remain important species for future searches. (5) Irradiated H_2O + CH_3OH ices. Once present in ices, CH_3OH can undergo reactions to form complex organic species such as ethylene glycol, $(CH_2OH)_2$. Ethylene glycol is a good marker of radiation-induced chemistry, is less volatile than H_2O, and has known IR features in both the near- and mid-IR

TIDAL-CONVECTIVE EQUILIBRIUM AT EUROPA AND ENCELADUS. W. B. Moore, *University of California, Los Angeles, Institute of Geophysics and Planetary Physics, BOX 951567, Los Angeles, CA 90095-1567, USA, (bmoore@ess.ucla.edu).*

The thermal evolution of tidally heated bodies such as Europa and Enceladus can be understood in terms of the properties and stability of their thermal equilibrium states. Thermal equilibrium is defined as the point at which a self-consistently derived interior structure (temperature, density, and rheology as a function of radius) transports as much heat to the surface as is generated by tides in the interior. Stable equilibria tend to attract the evolution the system and may trap it either permanently or temporarily. Equilibrium structures are derived using parameterized convection models (and/or conductive solutions) coupled with solutions for the tidal dissipation in the body [1, 2], as illustrated in figure 1.

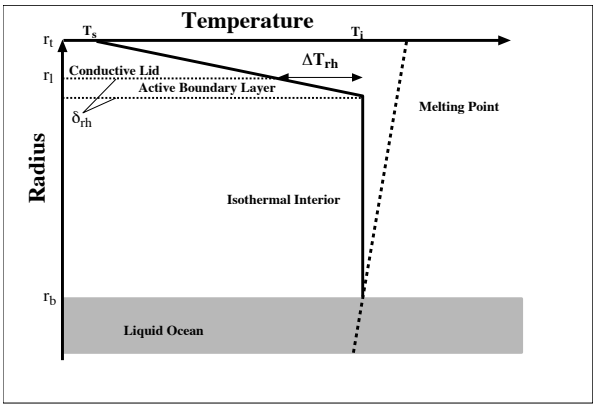

Figure 1: Temperature structure of a convecting ice layer.

The coupling between the heat production and heat transport arises due to the temperature dependence of the viscosity in both ice and rock. It is therefore im-perative that the rheological behavior of ice and rock be modeled as accurately as possible, including the multiplicity of known deformation mechanisms and a self-consistent calculation of the effective rheology. It should be noted that dissipation in liquid layers (oceans or cores) may also be significant (e.g. on Earth) but depends on properties at the interfaces which are at present unknown.

Ice has a complex flow law, but laboratory experiments [3] have established the behavior for some (though not all) of the relevant conditions in icy satellite shells. There are five deformation mechanisms, grain boundary (BD) and grain volume (VD) diffusion, dislocation creep (DC), grain boundary sliding (GBS), and basal slip (BS). Grain boundary sliding and basal slip are mutually accommodating deformation mechanisms effectively forming a single mode of deformation. Dislocation creep and basal slip are grain-size insensitive, but diffusion and grain boundary sliding depend on the grain size, which will therefore be a critical parameter in the remainder of this study. Only the diffusion mechanisms are Newtonian, the others are stress-dependent, dislocation creep most strongly. The full flow law is given by [3]:

$$\dot{\epsilon} = \dot{\epsilon}_{BD} + \dot{\epsilon}_{VD} + \dot{\epsilon}_{DC} + \left(\frac{1}{\dot{\epsilon}_{GBS}} + \frac{1}{\dot{\epsilon}_{BS}} \right)^{-1} \quad (1)$$

where the subscripts indicate the relevant deformation mechanism. The mutual accommodation of grain boundary sliding and basal slip result in strain rate control by the slower of the two mechanisms. While the non-Newtonian deformation mechanisms have been extensively studied in the laboratory, diffusion creep has not been measured due to the low stresses at which it becomes dominant (implying low strain-rates and hence, impractically long experiment durations).

Each of the creep mechanisms follows a law of the form:

$$\dot{\epsilon_x} = A_x \sigma^n h^{-m} \exp\left(-\frac{E_x + PV_x}{RT} \right) \quad (2)$$

where A_x, E_x, V_x, m and n are mechanism dependent parameters, σ is the stress, h the grain-size, P the pressure, R the gas constant, and T the temperature.

Parameterized convection is derived in terms of a simple flow law. Effective values of the flow law parameters may be derived by differentiation of the composite flow law e.g.:

$$m_{eff} = -\frac{d\left(\ln \dot{\epsilon}\right)}{dh} \quad (3)$$

with similar equations for the other parameters E, V, and n.

Rock Rheology: Typically only two deformation mechanisms are used to describe the flow law of rocks: dislocation creep and grain-volume diffusion. The flow law is thus similar to (1) with only the VD and DC terms [4], which have generic flow laws given by (2). Unlike ice, which tends to self-purify through exclusion of impurities, planetary mantle rocks are multi-phase assemblages and can exhibit a range of partially molten states. The rheology of partially molten rocks has been extensively studied in the laboratory, and the effect of melt is to decrease the viscosity exponentially with the volume fraction of melt. Above a certain melt fraction (40-60%), the crystal structure breaks down and the material behaves as a fluid with suspended solids [1]. The effect of water on the rheology of rocks can be profound. In the icy satellites, it seems likely that the rocks are at least somewhat hydrated. "Wet" rheologies [4] are therefore appropriate.

Parameterized Convection For fluids with strongly temperature dependent viscosity, a portion of the upper thermal boundary layer stagnates and transports heat only by conduction. An actively convecting boundary layer exists between the stagnant lid above and the well-mixed interior below. The convection in the interior is essentially isoviscous and is driven by a rheological temperature scale that depends on the temperature dependence of the viscosity η:

$$\Delta T_{rh} = \left| \frac{\eta}{\mathrm{d}\eta/\mathrm{d}T} \right| . \quad (4)$$

In order to incorporate the multiple flow laws, (4) is evaluated numerically from (1).

Since only part of the shell (below the lid) is convecting, we define a Rayleigh number Ra_{rh} for the shell as follows:

$$\mathrm{Ra}_{rh} = \frac{\alpha \rho g \Delta T_{rh} \left(r_l - r_b\right)^{(n+2)/n}}{\kappa^{1/n} \eta \left(T_i, \sigma = 1, h, P\right)^{1/n}} \tag{5}$$

where α is the thermal expansivity, ρ is the density of the ice, g is the gravitational acceleration, r_l and r_b are the radii of the bottom of the lid and bottom of the shell, respectively, and κ is the thermal diffusivity. The viscosity η is evaluated at the mean temperature of the well-mixed interior T_i, the value of the grain size h, and the pressure of the base of the lid $P = \rho g \left(r_t - r_l\right)$, and the stress dependence is removed [see 5, eqs. 20 and 26] by using a stress value of unity.

The heat flux transported convectively by the shell to the base of the lid is therefore:

$$F_{conv} = a_c \frac{k \Delta T_{rh}}{\left(r_l - r_b\right)} \mathrm{Ra}_{rh}^{\beta} \tag{6}$$

where k is the thermal conductivity and $a_c = 0.31 + 0.22 n_{eff}$ and $\beta = n_{eff} / \left(n_{eff} + 2\right)$ are constants [5]. At equilibrium, this flux must balance the production of heat in the shell:

$$F_{conv} = \frac{\rho H r_l}{3} \left(1 - r_b^3 / r_l^3\right) \tag{7}$$

where H is the volumetric heat production rate (assumed constant) that is required for convective equilibrium.

Equilibrium States: These equations are solved for both the mantle and the shell (which is heated from beneath by the mantle and therefore requires a slightly different treatment). Equilibrium states as a function of internal temperature (and grain size, which is a free parameter) may then be mapped out as in figure 2.

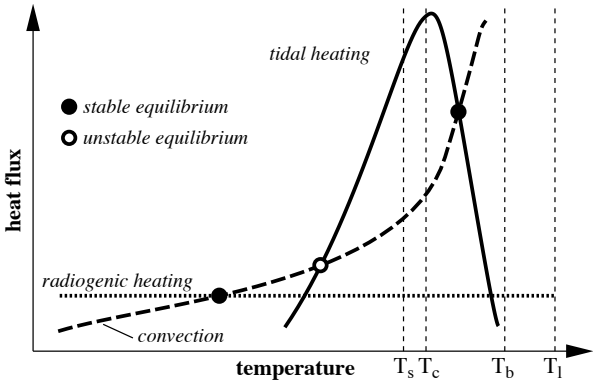

Figure 2: Cartoon depicting equilibrium states for a tidally heated body.

A body that finds itself between unstable and stable equilibria will be driven toward the stable point. Equilibria may merge (for example, if the eccentricity decreases, the high temperature stable and unstable points will merge), or additional equilibria may arise (due to melt-migration heat transport, for example).

New results will be presented for both Europa and Enceladus showing the effect of a new parameterization for layers heated both from below and from within. Grain size remains an important parameter in both ice and rock due to the relatively low stresses involved in rigid-lid convection. A wet rheology is essential for enabling high-temperature states in the silicate; the dry rheology is too stiff to dissipate much energy at tidal periods. Melting, however, tends to dehydrate the mantle, and there is little means for recycling without a process like plate tectonics.

References:

[1] W. B. Moore, *Icarus* **154**, 548 (2001).

[2] W. B. Moore, *Icarus* **180**, 141 (2006).

[3] D. L. Goldsby, D. L. Kohlstedt, *J. Geophys. Res.* **106**, 11017 (2001).

[4] S. Karato, P. Wu, *Science* **260**, 771 (1993).

[5] V. S. Solomatov, L. N. Moresi, *J. Geophys. Res.* **105**, 21795 (2000).

[6] V. S. Solomatov, *Physics of Fluids* **7**, 266 (1995).

[7] C. C. Reese, V. S. Solomatov, J. R. Baumgardner, *Phys. Earth and Planet. Int.* **149**, 361 (2005).

TIDAL DISSIPATION AND FAULTING. F. Nimmo[1], [1]Dept. Earth & Planetary Science, University of California Santa Cruz, CA 95064 (fnimmo@es.ucsc.edu).

Introduction: Planetary bodies typically exhibit a phase lag between an applied stress and a response, leading to dissipation (heating). This phase lag ϕ can be measured at frequencies f from ~1 Hz (seismic attenuation[1]) to ~1nHz (Earth tides [2]), and is described by the dissipation factor Q, where one possible definition is Q^{-1}=tan ϕ [3]. Large values of Q denote small dissipation. Phase lags can also be measured in experimentally-deformed samples [3-5], over a smaller frequency range.

Phase lags and dissipation are central to the evolution of planetary satellites, because they control the rate of rotational despinning [6], orbital circularization [7] and tidal heating [8]. Unfortunately, there is currently a disconnect between orbital treatments of Q and the experimental and observational constraints.

Satellite evolution is typically modelled either assuming that Q is constant [9], or that the satellite behaves as a Maxwell viscoelastic body [10], which in simple cases gives Q~f. (Note that tidal *heating*, as opposed to Q, exhibits a more complex frequency dependence [11]). On the other hand, both experimental [3-4] and observationally-constrained [1-2] values suggest that Q~f^{α}, where α~0.2-0.4. This frequency-dependence can give rise to satellite behaviour differing from conventional results [12].

Part of the disconnect arises from the fact that very different mechanisms may be responsible for dissipation in experimental samples (e.g. dislocation glide [13]) compared with planets (e.g. inertial waves [14]). It is also likely that dissipation in a complex body like a satellite is not well-represented by a simple phase-lag description.

Dissipation: Measurement of phase lags in silicate samples using a torsion apparatus is now relatively straightforward [3-4], but much less work has been done on icy materials [cf. 5]. An advantage of the torsion apparatus is that the periods (~10^5 s) and strain rates (~10^{-10} s^{-1}) appropriate to icy satellites are achievable. Despite the potential pitfalls of relating experimentally-determined Q values to real satellites, **measurement of Q and its frequency-dependence for icy materials would represent a major step forward**. It may also be important to look at the behaviour of partially-molten systems, which tend to exhibit different responses [4].

A factor which complicates ice rheology is its tendency to undergo transient creep [15]. This behaviour may be especially important at the relatively low strains and short timescales characteristic of tidal deformation [Melosh, pers. comm.]. One way of representing this behaviour is with an Andrade model [3], where the strain ε is given by

$$\varepsilon = \sigma\left(\frac{1}{G} + \frac{t}{\eta_{ss}} + \beta t^{n}\right)$$

Here σ is the stress, G the shear modulus, t is time, η_{ss} is the steady-state viscosity and β and n are empirical constants. The three terms on the RHS are, respectively, the elastic, viscous and transient response.

For this model, it may be shown that the corresponding dissipation function Q is given by

$$Q^{-1} = \frac{\frac{f^{n-1}}{\eta} + \beta \sin\frac{n\pi}{2}\Gamma(n+1)}{\frac{f^{n}}{G} + \beta \cos\frac{n\pi}{2}\Gamma(n+1)}$$

where here f is the angular frequency and Γ is a gamma function [3]. If the transient contribution is negligible (β~0) then Q~f, the usual Maxwell response. In the general case, at high frequencies (elastic limit) Q^{-1}~f^{-n} and at low frequencies (viscous) Q^{-1}~f^{n-1}.

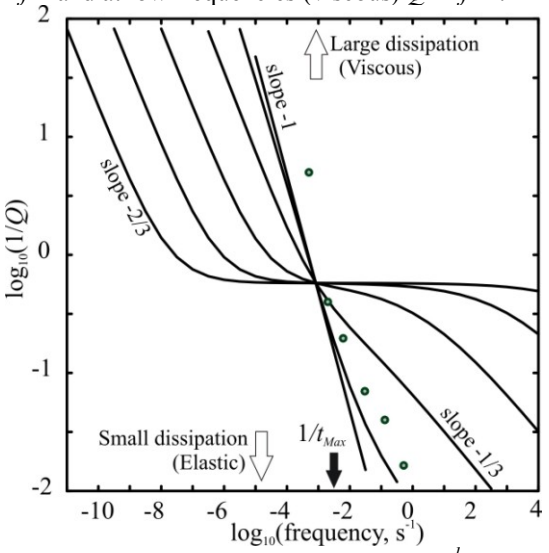

Figure 1. Frequency dependence of Q^{-1} for Andrade rheology. Shear modulus and viscosity are 3 GPa and 10^{12} Pa s, respectively, t_{Max} is the Maxwell time. Andrade model assumes n=1/3 and variable β. For small β, the behaviour is viscoelastic (Q^{-1}~f^{-1}), while at larger β, Q^{-1} shows a shallower frequency-dependence and becomes constant over an intermdiate frequency range. Dots are data for an ice-$MgSO_4$ compression creep test, from [5].

Figure 1 shows how Q changes as a function of the frequency and the strength of the transient component, and also plots the experimentally-determined values of [5]. The Andrade model is attractive because it has some theoretical justification [13], and can also reproduce the observed frequency-dependent behaviour of icy and silicate materials [3,5]. It may therefore become necessary to develop a theory for dissipation in multi-layered Andrade-rheology bodies, as has already been done for viscoelastic bodies [10].

Friction: Although most satellite models assume that dissipation is volumetric and viscoelastic, other mechanisms may also play a role. One such mechanism is frictional heating due to fault motion [16,17]. We will assume that the tidal stresses σ are capable of causing motion on a fault to a depth d, where $d=\sigma/\rho g F$, ρ is the surface density, g is gravity and F is the friction coefficient. In this case, the total heating H is given by

$$H = n^7 e^3 h_2^3 \frac{L_{tot} w \mu'^2 c^3}{2\rho g F G_g^3 \rho_b^3} \qquad (1)$$

where n is the mean motion, e the eccentricity, h_2 the Love number, L_{tot} and w the total fault length and mean separation, μ' an effective modulus, c a constant, G_g the gravitational constant and ρ_b the bulk density. This heating is different from the standard tidal dissipation, which depends on Q^{-1}, e^2 and n^5, and can lead to differing satellite evolution [17]. Heating increases as F decreases because faults can be active at greater depths if friction is lower.

Assuming global tectonic activity (that is, $L_{tot}w \sim$ satellite surface area), the expected mean frictional heat flux on Europa is 2 mWm^{-2} for F=0.3. For Enceladus, the expected value is 5 mWm^{-2} (h_2/0.1) for the same F. This value is larger mainly because of the lower gravity, and for h_2=0.1 represents a total heat flow of 4 GW, comparable to that observed at the South Pole [18]. This heat production is shallow, and does not significantly alter the ice shell temperature structure at depth.

An important factor in equation (1) is the friction coefficient F, which also controls the depth to which brittle faulting is likely to occur. At low strain rates ice demonstrates a constant friction coefficient similar to the behaviour of silicate materials [19]. However, at higher strain rates, more complicated behaviour results [20]. **It may therefore be of interest to more fully characterize the frictional behaviour of ice under the range of conditions appropriate to icy satellites**. It is also important to understand the role of melt in such systems. Melt can reduce the friction coefficient [e.g. 21], potentially giving rise to periodic behaviour in which frictional heating drops dramatically as soon as melt is produced.

References: [1] Anderson D.L. *Theory of the Earth*, Blackwell (1989). [2] Benjamin D. et al., *GJI 165*, 3-16 (2006). [3] Gribb T.T. and R.F. Cooper, *JGR 103*, 27267-27279 (1998). [4] Jackson I. et al., *JGR 109*, B06201 (2004). [5] McCarthy C. et al., *LPS XXXVIII*, Abstract #2429 (2007). [6] Greenberg R. and S.J. Weidenschilling, *Icarus 58*, 186-196 (1984). [7] Goldreich P. and S. Soter, *Icarus 5*, 375-389 (1966). [8] Segatz M. et al., *Icarus 75*, 187-206 (1988). [9] MacDonald G.J.F., *Rev. Geophys. 2*, 467-541 (1964). [10] Tobie G. et al., *Icarus 177*, 534-549 (2005). [11] Ojakangas G.W. and D.J. Stevenson, *Icarus 81*, 220-241 (1989). [12] Efroimsky M. and Lainey V., *JGR 112*, E12003 (2007). [13] Karato *S., Pure Appl. Geophys. 153*, 239-256 (1998). [14] Ogilvie G.I. and D.N.C. Lin, *Ap. J. 610*, 477-509 (2004). [15] Azizi F., *Cold. Reg. Sci. Tech. 16*, 159-165 (1989). [16] Nimmo F. et al., *Nature 447*, 289-291 (2007). [17] Nimmo F., *LPS XXXIX*, Abstract #1311 (2008). [18] Spencer J.R. et al., *Science 311*, 1401-1405 (2006). [19] Beeman M. et al., *JGR 93*, 7625-7633 (1988). [20] Rist M.A. *J. Phys. Chem. B 101*, 6263-6266 (1997). [21] Brodsky E.E. and H. Kanamori, *JGR 106*, 16357-16374 (2001).

ULTRAVIOLET SPECTRA OF ICY SATELLITES. K. S. Noll[1], [1]Space Telescope Science Institute (3700 San Martin Dr., Baltimore, MD 21218; noll@stsci.edu)

Introduction: The ultraviolet (UV) albedos of icy bodies feature unique diagnostics of composition, microphysical structure, and magnetospheric interaction. The ultraviolet opacity of the Earth's atmosphere, the rapidly dropping solar flux at shorter wavelengths, and detector limitations make obtaining high quality UV spectra an observational challenge. In this work I summarize the UV spectra of the satellites of Jupiter, Saturn, and Uranus obtained with the Hubble Space Telescope.

UV Spectra: The Hubble Space Telescope (HST) has obtained spectra of the three icy Galilean satellites of Jupiter [1,2,3], five of Saturn's icy satellites [4], and three satellites of Uranus [5]. A sample of these spectra is shown in Figure 1.

HST's UV satellite observations were made with two different instruments, the Faint Object Spectrograph (FOS) and the Space Telescope Imaging Spectrograph (STIS) between June 1995 and December 2000. The FOS was removed from HST in February 1997 and STIS suffered an electrical failure in August 2004. The Solar Blind Channel (SBC) of the Advanced Camera (ACS) remains in operation, but is only sensitive to wavelengths shorter than 170 nm where there is essentially no reflected flux from these objects. Upon successful completion of the planned servicing mission in 2008, HST will once again have the ability to obtain near UV spectra of icy satellites.

The icy satellite UV spectra obtained with HST come from six different general observer programs, each with somewhat different goals and observing strategies. For most satellites, leading and trailing hemisphere spectra were obtained in order to search for and characterize hemispheric dichotomies that can arise from magnetospheric interactions. For some satellites, there are marked differences between hemispheres, but for others there is little or no distinction. Spectra of objects differ in their wavelength coverage. In some cases, the spectra extend from 200-1000 nm. More frequently, however, only the near-UV and short wavelength visible portions of the spectrum are covered. In these cases, it is desirable to augment the HST spectra with ground-based visible and near-IR spectra when such are available. In Figure 1 the spectra of Rhea and Dione are composites of separately published UV and optical spectra [4,6].

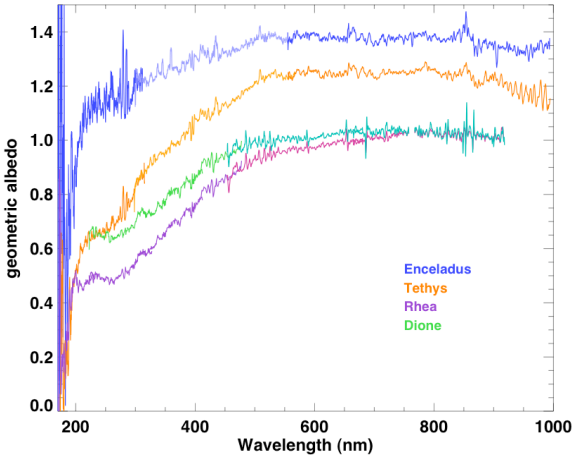

Figure 1. Albedo spectra of four of Saturn's satellites are compared in this figure. Spectra of Enceladus and Tethys were obtained with STIS. Spectra of Dione and Rhea shortward of 450 nm were obtained with the FOS[4], longward of that they are ground-based data[6]. Absolute albedos are calibrated by matching the spectra to albedos measured at low phase angles[7].

Spectral Features: As is evident from Figure 1, the ultraviolet region is not, at first glance, distinctly different from the longer wavelength optical and near-IR spectra of icy bodies. The specrtra can be broadly characterized as having a maximum albedo in the visible and near-IR and a decreasing albedo starting around 500 nm and continuing into the UV. On closer inspection, however, subtle differences can be seen. An absorption band centered at 260 nm is evident in the spectra Rhea and Dione. A weaker version of this band also appears in the spectrum of Tethys, but is not evident in the Enceladus spectrum. This band has been previously identified as possibly due to ozone trapped in ice [2,4]. Enceladus and Tethys spectra reach an apparent maximum albedo at 500 nm while Rhea and Dione albedos continue to increase, gradually, to approximately 700 nm. The cause for this subtle difference in unknown.

Spectral Modelling and Laboratory Data: UV absorption bands present difficulties to modelers for several reasons. UV bands are broad and generally weak so their identification and precise determination of band center in noisy data can be problematic. Band centers are known to shift depending on environmental factors, *e.g.* whether or not a constituent is adsorbed in

water ice and the number of adsorbed constituents that are nearest neighbors. Often this depends on details of the sample preparation which, more frequently than not, are at temperatures and physical conditions that differ significantly from those on satellite surfaces. Simulating the effects of long-term ion irradiation for those satellites that are inside planetary magnetospheres is another challenge for laboratory measurement, yet is an important component of accurate spectral simulations.

References: [1] Noll K. S., Weaver H. A., Gonnella A. M. (1995) *JGR, 100,* 19057. [2] Noll K. S., Johnson R. E., Lane A. L., Domingue D. L., Weaver H. A. (1996) *Science, 273,* 341. [3] Noll K. S., Johnson R. E., McGrath M. A., Caldwell J. J. (1997) *GRL, 24,* 1139. [4] Noll K. S., Roush T. L., Cruikshank D. L., Johnson R. E., Pendleton Y. J. (1997) *Nature, 388,* 45. [5] Roush T. L., Noll K. S., Cruikshank D. P., Pendleton Y. P. (1998) *LPSC XXIX,* 1636R. [6] Buratti B. J., Hicks M. D., Tryka K. A., Sittig M. S., Newburn R. L. (2002) *Icarus, 155,* 375. [7] Verbiscer A., French R., Showalter M., Helfenstein P. (2007) *Science, 315,* 815.

COMBINING NEW LABORATORY STUDIES AND CASSINI CIRS DATA ANALYSIS TO DETERMINE THE COMPOSITION AND TEXTURE OF SATURN'S RINGS. C. R. Nugent[1], M. S. Gudipati[2], L. J. Spilker[2], S. G. Edgington[2], S. H. Pilorz[2], C. Leyrat[2], N. Altobelli[3], C. T. Russell[4]. [1]Department of Earth and Space Sciences, University of California, 595 Charles Young Drive East, Los Angeles, CA 90095 (cnugent@ucla.edu), [2]JPL, 4800 Oak Grove Dr. M/S 230-205, Pasadena, CA 91109, [3]European Space Agency, European Space Astronomy Centre, P.O. Box - Apdo. de correos 50727, Madrid, 28080, Spain, [4]Institute of Geophysics and Planetary Physics, UCLA, 405 Hilgard Ave, Los Angeles, CA 90095.

Introduction: Spectra from Cassini's Composite Infrared Spectrometer (CIRS) is currently being used to investigate the composition and surface texture of Saturn's inner main rings over the wavenumber range of 10 to 600 cm^{-1}. These studies revealed spectral features which have not yet been identified in the laboratory. We present here a combined laboratory and modeling effort to obtain a deeper understanding of the processes that occur on the surfaces of Saturn's inner rings.

Spectral roll off: CIRS observations of Saturn's A, B and C rings have revealed a thermal emission spectral "roll-off" in the far-infrared. Below 50 cm^{-1}, the rings' spectra increasingly deviate from a blackbody curve with decreasing wavenumber (Figure 1). Studies have shown that pure water-ice absorption cannot generate this roll-off [1], and this roll-off has never been observed in a laboratory setting.

Although the cause of this roll-off is unclear, previous studies have hinted that it could be due to a combination of the surface properties of the ice and the presence of impurities.

Ring Composition: Saturn's rings display a variety of colors when seen in visible light, indicating a complex composition (Figure 2). Efforts to isolate spectroscopic signatures due to materials other than water ice are still underway. Cassini's Ion and Neutral Mass Spectrometer has detected molecular and atomic oxygen near the A ring, which are perhaps part of a tenuous ring atmosphere [3]. Results from Cassini's Cosmic Dust Analyzer indicate the E ring is predominantly water ice, with minor contributions from possible combinations of silicates, carbon dioxide, ammonia, molecular nitrogen, hydrocarbons and perhaps carbon monoxide [4].

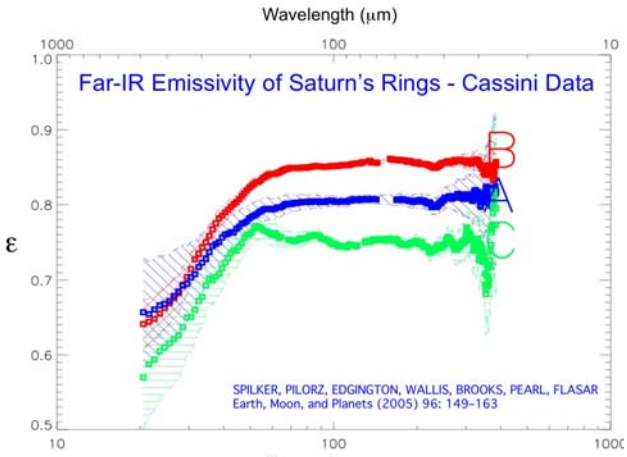

Figure 1: Ring emissivities of the A, B and C rings. Note that each ring system seems to have different spectral characteristics, but all show a roll-off below 50 cm^{-1}[1].

The rings spectra observed by CIRS are a complicated combination of thermal emissions, the effects of scattering from ring particles (over a broad size distribution) and noise. Before the signal can be examined for the faint absorption features, the contributions of scattering and thermal emission must be accounted for and removed using Mie scattering and standard radiative transfer techniques. Since the signatures of the minor ring constituents are very faint, it is important to incorporate the highest quality experimental indices of refraction into the Mie code.

Figure 2: True color inner ring image from Cassini released on October 24, 2007. Color variations reveal the presence of materials other than water ice in the ring particles.

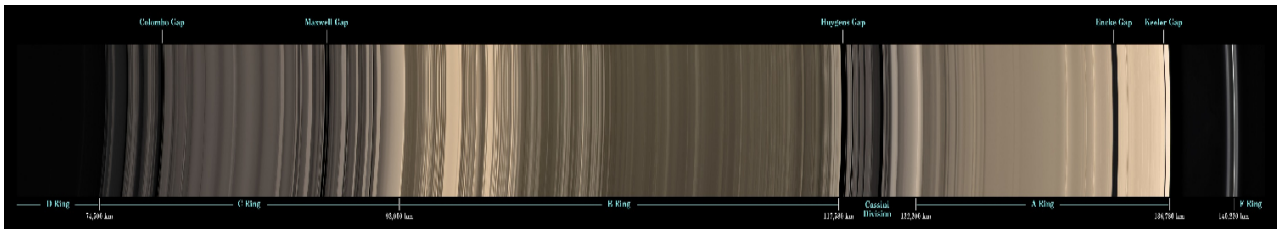

Laboratory Data: Far-infrared laboratory work designed to address these issues will be carried out in Murthy Gudipati's JPL laboratory. We plan to quantify and identify far-infrared (20 – 500 cm^{-1}) spectral features of ices with and without impurities before and after laser and electron sputtering. Sputtering will be used to both simulate Saturn's magnetospheric environment and generate small-grained ice deposits on the surface of the ice. These far infrared spectra will then be correlated with the mid infrared (400 – 4000 cm^{-1}) spectral features, optical constants will be derived, and a community-accessible database will be created.

Need for Further Laboratory Data: As shown in Figure 3, Mie scattering below 100 cm^{-1} is strongly modulated by the ice grain size. Laboratory far-infrared absorption and scattering data is needed for ice grains between 10 microns and a few millimeters in size.

Application to Icy Bodies: Though our focus is on Saturn's rings, it is expected that this new far-infrared data will be useful for studies of other icy solar system objects such as Europa, Enceladus, and Ganymede, as well as icy asteroids such as Ceres. If the experimental work confirms that the spectral roll-off below 50 cm^{-1} is due to a grain size distribution on the surface of the ice, we will have a new method to remotely determine the surface morphology of icy bodies.

References: [1] Spilker, L. J. et al. (2005) *Earth, Moon and Planets*, *96*, 149-163. [2] Cuzzi, J. N. et al., (1984) *IAU Colloquium 75: Planetary Rings*, 73-199. [3] Waite, J. H. et al. (2005) *Science*, *307*, 1260-1262. [4] Hiller, J. K. et al., (2007) *Monthly Notices of the Royal Astronomical Society*, *377*, 1588-1596.

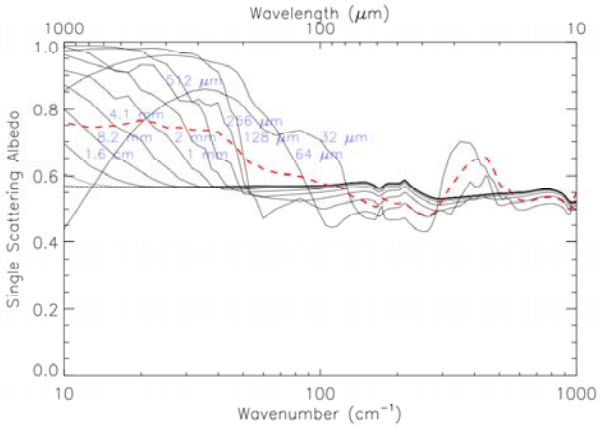

Figure 3: Single scattering albedo of water ice as a function of wavenumber as generated by a Mie scattering code. This plot illustrates the variation of single scattering albedo with particle size (from 32 microns to 1.6 cm). The dashed line displays the single scattering albedo from a weighted average of particle sizes designed to mimic the particle size distribution in Saturn's rings.

THE ROLES OF ENERGY LOCALIZATION AND BURIED INTERFACES IN ELECTRONIC SPUTTERING OF PRISTINE AND MIXED LOW-TEMPRATURE ICES. T. M. Orlando and G. A. Greives, School of Chemistry and Biochemistry and School of Physics, Georiga Institute of Technology, Atlanta, GA 30332-0400 USA (Thomas.Orlando@chemistry.gatech.edu)

Introduction: The radiolysis and sputtering of ice is intimately tied to the electronic structure of condensed water. Throughout the energy regime of 0-100 eV, ice can undergo a number of distinct excitations and/or scattering resonances [1]. These excitations are made mobile by a variety of mechanisms. For example, an exciton can migrate by resonant energy transfer mediated by the hydrogen bond. A "hole" or ion embedded in a highly polar matrix is greatly stabilized due to solvation interactions [2]. This lowers the ionization potential of an embedded molecule by an amount comparable to the ion solvation energy (2-3 eV). Since excitations are mobile in ice, the overall reaction probabilities with adsorbed or embedded inclusions in ice are relatively high. *Hence, excitations that migrate through the ice matrix will preferentially deposit on the organic or embedded "contaminant."*

Approach: Icy grains (i.e. precursors to comet nuclei) can form in many possible ways. In diffuse media, the system is thermally equilibrated to very low temperatures and condensation is limited by encounter frequency. Here, particles will tend to form on surfaces of rocky dust particles, but will accumulate in a relatively uniformly mixed distribution, as depicted below in A. In cooling regions of space, the formation of icy grains follows the sequence of sublimation temperatures as the grains cool. The rocky dust particle is formed at high temperature, and upon cooling first condenses the stickiest molecules (water, methanol etc.) then later cools enough to adsorb volatiles and finally gas molecules, resulting in layered grains shown in B. Later, these grains can begin to coalesce and form larger heterogeneous masses. Thermal cycling of these ordered masses can anneal them and cause spontaneous phase segregation and redistribution of the materials throughout the particle, leading from a situation like B back toward one like A

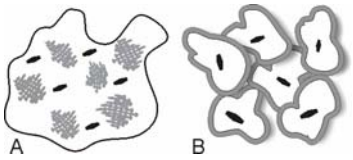

Experimentally, we simulate these two scenarios by controlled deposition. Co-deposition of organics will disperse hydrophilic molecules through the ice, while hydrophobic molecules tend to pool into clusters and pores. Alternatively, organic inclusions can be encased between layers of ice, resembling B. This is shown below where we systematically control the depth of the capping ice layers. We also control the penetration depth of the radiation. The combination allows us to deconvolute the effects of direct irradiation from that of energy migration through the ice.

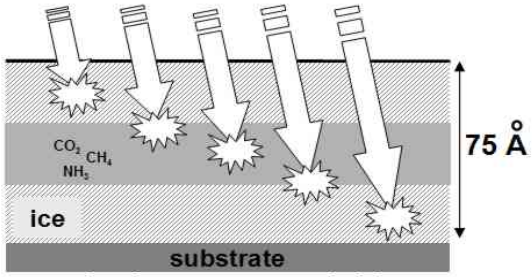

a. ice / precursor sandwich

In addition, there may also be distinct differences in the products of direct irradiation, and those generated by energy delivered through excitation hopping in the ice. Interfaces such as grain boundaries, hollow pores or embedded silicate or carbonaceous dust grain nuclei can also act as alternate points of energy localization within "ices". We have therefore examined the relative importance of pore collapse and grain boundaries on the radiation-induced production and thermal release of gases such as H_2, CO, CO_2 and O_2 from mixed ices containing methane inclusions and from water covered graphite surfaces. These radiation products can be trapped and released at a later time during thermal cycling and pore collapse [3]. Molecules such as H_2 can be released at temperatures up to 50 K, whereas O_2 can be retained within clathrate hydrates until the ice sublimates. We discuss an important link between the physical morphology of ice and the yields of direct and delayed release of molecular fragments from ice and ice covered grains.

References:

[1] R. E. Johnson, P. D. Cooper, T. I. Quickenden, G. A. Greives, and T. M. Orlando, *J. Chem. Phys.* 123, 184715 (2005). [2] J. Herring-Captain, G.A. Grieves, A. Alexandrov, M.T. Sieger, H. Chen and T.M. Orlando, *Phy.l Rev. B.* 72, 035431-1 (2005). [3] G.A. Grieves and T. M. Orlando (2005), *Surf. Sci.* 593, 180-186.

MIXED GUEST CLATHRATES AND PLANETARY DYNAMICS: CONTINUOUS vs. EPISODIC EVENTS. J. P. Osegovic[1] and M. D. Max[2], [1]MDS Research, 1601 3rd St. S, St. Petersburg, FL 33705, josegovic@mdswater.com, [2] MDS Research, 1601 3rd St. S, St. Petersburg, FL 33705, mmax@mdswater.com.

Introduction: Clathrate hydrates may be a ubiquitous form of matter on temperate and cold planetary bodies. Clathrate hydrates are solids composed of a water host structure with caged ("en-clathrated") guests. The guests are typically small, inert gases, but other materials can also particpate [1, 2]. Hydrate has been hypothesized to exist on many planetary bodies including comets, Mars [3], Titan [4, 5], and Enceladus [6, 7].

Hydrate formation and dissociation is dependent on temperature, pressure, and composition. For hydrates that are composed of only one guest, such as biogenic methane hydrate found on Earth, the phase behavior is well described by a single-phase diagram. The behavior of these hydrates is simple to model. Mixed guest hydrates, such as thermogenic natural gas hydrate deposits, have a more complex phase relationship with several degrees of freedom. They are more complicated to model and difficult to interpret.

Hydrate kinetics are controlled by supersaturation and temperature. The higher the supersaturation and temperature, the faster the reaction progresses. Temperature cannot be raised arbitrarily and supersaturation is a function of temperature, amongst other parameters. At cryogenic temperatures, for example the surface of Titan, hydrate may form or dissociate very slowly. There is little experimental data on formation rates at low temperatures [8], but a greater body of work associated with dissociation (for example work see Stern *et al.* [9]). The bulk of these "low temperature" experiments were conducted at ~120 K or higher.

Hydrate was hypothesized to occur naturally on outer system bodies [10] before it was discovered on Earth. Terrestrial hydrate was initially detected by inference, with direct sampling becoming more common. Hydrate is now known to exist on Earth wherever the pressure, temperature, and reactants co-exist. Air, carbon dioxide, and natural gas hydrates occur naturally on Earth.

Hydrate Formation: Hydrate precipitation is a two step process requiring nucleation and growth phases. At low supersaturations, the guest + host phase is metastable and hydrate will not form for extended periods of time. As supersaturation increase, the metastable lifetime decreases. Once the metastable state is broken, nucleation and growth can occur. Nucleation is more sensitive to supersaturation than growth [11], and the initial reaction product is sensitive to the relationship between these two parameters.

Hydrate processes are controlled by heat and mass transfer limitation. In man-made settings, hydrate formation is usually episodic with a sudden pulse of formation that reduces local supersaturation followed by a longer phase where growth is controlled by heat flow. After the initial burst of formation associated with the high supersaturation to break metastablility, the rate of reaction decreases with time until heat transfer out of the formation region equals the rate of heat production by the reaction. Small deviations in heat flow are met with responses in reaction rate and the temperature of the system can be maintained for a considerable period of time.

If the heat flow out of the system exceeds the heat production (perhaps due to limittions of the mass transfer rate), then the system can cool down. The reaction rate will drop with temperature and metastablility may once again be obtained.

Mixed guest hydates add an additional variable. When hydrates form from multiple guest, certain preferred formers may be selectively enclathrated. The composition of the reactants change, which lowers supersaturation as the preferred materials are consumed. When the mixed guest hydrate undergoes dissociation stress, the preferred formers now become preferred dissociators. The resut is a change in the distribution of guests with simultaneous reduction in undersaturation.

Consequences of Episodic/Continuous Behavior: Hydrate formation and dissociation dynamics have different impacts depending on the stage of planetary formation.

Comets and other small bodies. For small bodies, episodic formation is strongly linked to thermal history. Hydrate formation on comets may occur very slowly at temperatures in deep space, but nucleation may be the limiting factor. If there is no initial heat impulse, for instance from internal heat, collision or transects nearer the sun, that will allow the first few crystals to form then growth cannot occur. Hydrate formation in the deep cold of small bodies in trans-Saturn space will be controlled by solid diffusion processes. Hydrate could provide a self-limiting source of gas, allowing comets to be productive for longer periods of time.

Enceladus. The plume from the south pole of Enceladus has been hypothesized to occur due to cyclic dissociation/cooling of clathrates [Kieffer]. The conditions of dissociation have been proposed to be linked

to hydrate → ice + gas reaction, with ice slowly sealing exposed clathrate beds.

With mixed guest hydrates in an open system, the formation composition does not always match the dissociation composition. The formation guest compositions can be calculated based on the measured vapor composition proposed to be produced by hydrates and an assumption of dissociation conditions (Fig. 1) .

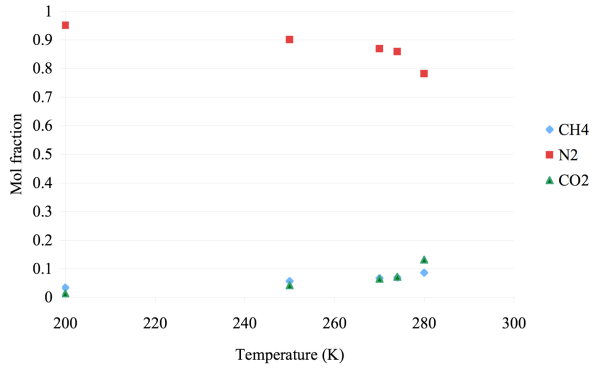

Figure 1. Using the plume gas compstion for Enceladus, the gas composition that formed the potential hydrate deposits can be calculated based on several formation scenarios.

Titan. The surface of Titan is at suitable conditions of pressure, temperature, and composition to form hydrate at high supersaturation [4], but at low absolute temperatures. Hydrate nucleation may be a very strong limiting factor for in-place formation, and may not be directly achievable without introduction of nuclei. The nuclei could be created during an exceptional event, like an impact where heat allows hydrate formation to occur rapidly for a short period of time, or by introduction of nuclei to the surface by cryovulcanism. Hydrate could also be a relict mineral, having been created by conditions in the past and then left in place or transported to the survace actively.

Hydrate produced in an atmosphere by combination of products from the photochemical destruction of organic molecules is technically possible, but likely just a curiosity as, even if enough oxygen is present to produce significant concentrations of water, there is no evidence that the hydrate phase prevents further photochemical degredation.

Conclusions: Hydrate formed from multiple guests must be considered in respect to local environment as a function of history. The thermal history of hydrates may be of primary importance in understanding the role they play in planetary bodies. The rate of hydrate formation is sensitive to heat and mass flows. Certain periods of an object's history may be particularly preferential for formation, which can have long term impacts on the evolution of associated gases. Certain periods of planetary formation may be dominated by heat flows due to hydrate formation or dissociation and hydrate may be a dominate actor in icy body geochemistry.

References: [1] Max, M.D, Johnson, A.H., Dillon, W. P. "Economic Geology of Natural Gas Hydrates", Springer, Dordrecht, 2006.

[2] Sloan, E. D., Koh, C. A. "Clathrate Hydrates of the Natural Gases 3rd Ed." C.R.C. Press, Boca Raton, 2008.

[3] Max, M. D., Clifford, S. M. "The State, Potential Distribution, and Biological Implicatins of Methane in the Martian Crust" *Journal of Geophysical Research* **105(E2)**, 4165-4171 (2000).

[4] Osegovic, J. P., Max. M. D. "Compound Clathrate Hydrates on Titan's Surface" *JGR: Planets* **100**, E08004, doi:10.1029/2005JE002435 (2005).

[5] Thomas, C., Mousis, O., Ballenegger, V. Picaud, S. "Clathrate Hydrates as a Sink of Nobel Gasses in Titan's Atmosphere" *Astronomy and Astrohysics* **474**, L17-L20 (2007).

[6] Kieffer, S.W. *et al.* "A Clathrate Reservoir Hypothesis for Enceladus' South Polar Plume" *Science*, **1764**, 314 (2008).

[7] Fortes, A. D. (2007)"Metasomatic clathrate xenoliths as a possible source for the south polar plumes of Enceladus" *Icarus* **ASAP**, doi:10.1016/j.icarus.2007.06.013.

[8] Hallbrucker, A., Mayer, E. "Unexpectedly Stable Clathrate Hydrates Formed From Microporous Vapor-Deposited Amorphous Solid Water At Low "External" Guest Pressures And Their Astrophysical Implications" *Icarus* **90**, 176-180 (1991).

[9] Stern, L. A., Circone, S., Kirby, S. H., Durham, W. B. (2003) *Can. J. Phys.* **81**, 271–283.

[10] Miller, S. L. (1961) "The Occurrence of Gas Hydrates in the Solar System" *Proc. N. A. S.* **47**, 1798-1808.

[11] Osegovic, J. P., Tatro, S. R., Holman, S. A., Ames, A. L., Max, M. D. (2007) "Growth kinetics of ethane hydrate from a seawater solution at an ethane gas interface" *Journal of Petroleum Science and Engineering* **56**(1-3), 42-46.

RADAR PROPERTIES OF THE ICY SATELLITES OF JUPITER AND SATURN.
S. J. Ostro, 300-233, JPL/Caltech, Pasadena, CA 91109-8099, steven.j.ostro@jpl.nasa.gov).

Introduction: The radar properties of the icy satellites of Jupiter and Saturn are extraordinary, with radar albedos and circular polarization ratios that dwarf values for non-icy solar system targets [1],[2],[3]. These properties are due to coherent backscattering [4], which is a highly efficient kind of multiple scattering from heterogeneities within a nearly transparent medium, in this case water ice, whose electrical loss at radar wavelengths is essentially negligible. The path length for exiting the medium in the backscatter direction is small compared to the absorption path length, the intensity of echoes in the backscatter direction is amplified by phase-coherent interference between waves on identical but time-reversed paths, and the incident sense of circular polarization is preserved [5].

The heterogeneities do not have to be discrete scatterers such as rocks or water-ice blocks; they can include any sort of variation in the dielectric tensor [6]. Because the satellite surfaces have constantly been subject to meteoroid bombardment, their regoliths naturally are structurally heterogeneous. Therefore a reasonably mature regolith of 100% pure water ice would be expected to return radar echoes with high albedos and that preserve the transmitted sense of circular polarization. These unusual signatures, first encountered with Arecibo (2380-MHz, 13-cm) observations of the icy Galilean satellites in 1975-76, had not been seen in any previous radar observations of solar system or terrestrial targets.

Contaminants: Ostro et al. [7] discussed the potential role of contaminants in icy satellite radar albedo variations as follows. "The correlation of our targets' radar and optical albedos [Fig. 1], also seen for groundbased radar observations of the icy Galilean satellites, is most easily understood as involving variations in the concentration of optically dark contaminants in near-surface water ice and the consequent variable attenuation of the high-order multiple scattering responsible for high radar albedos. Plausible candidates for contaminants causing variations in radar albedo include silicates, metal oxides, and polar organics such as nitriles like HCN and possibly acetylene polymers as well as complex tholins.... (In the case of the polar organics, lowering of the visual albedo would be furthered as UV photons or charged particle radiation act on the material.... Extremely small concentrations of impurities can dramatically reduce the microwave transparency of water ice (e.g., [8] and references therein)."

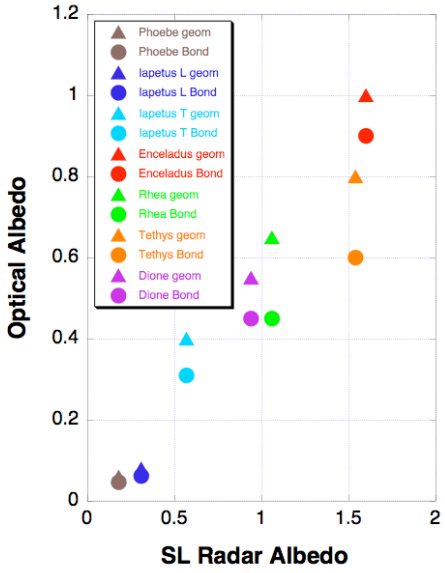

Fig. 1 Optical geometric albedo (triangles) and Bond albedo (circles) plotted vs. Cassini 2.2-cm radar albedos reported by Ostro et al. [7] in their Fig. 4 and Table 1.

The one-way 1/e absorption length in wavelengths of pure, homogeneous water ice at the temperatures of the satellite surfaces is more than 10,000. It can be orders of magnitude lower for water ice contaminated with small percentages of lunar soil, or nonmetallic meteoritic material, or metallic iron, or metallic iron oxides, or complex organics. Therefore any of these candidates might be responsible for the correlated optical and radar albedo variations.

Ammonia: Ammonia would reduce icy surfaces' radar albedos but not their visual albedos, whereas the other candidate contaminants could do both. Lorenz [9] and Lorenz and Shandera [10] explored the electrical properties of water ice containing ammonia along with their dependence on temperature and frequency, and concluded that NH3 concentrations much less than one weight percent can dramatically increase the radar absorption length. They caution that "these measurements are not entirely satisfactory, and absorption cell measurements with good temperature control would be most desirable."

Indeed, very accurate determination of the electrical properties of ammonia containing water ice as a function of concentration, chemical form [11], frequency, and temperature are sorely needed, because the increasing presence of ammonia with depth on Saturn's icy satellites offers an easy hypothetical explanation of the wavelength dependence of these objects' radar albedos: Black et al. [2,3] measured the 13-cm radar albedos of Enceladus, Tethys, Dione, Rhea, and Iapetus, and found that they mostly are lower than the 2.2-cm Cassini values measured by Ostro et al. [7].

However, for Europa, Ganymede, and Callisto, 4-cm and 13-cm albedos are essentially indistinguishable [1]. Ammonia is cosmogonically more likely in the Saturn system than in the Jupiter system, and the upper limits on NH3 from spectroscopic observations of the Saturn satellite system allow the presence of subsurface ammonia. Ostro et al. (2006) argue that "to simultaneously account for its role in affecting the radar properties while being absent from near-infrared spectra requires postulating that ammonia is depleted from the very outermost layer (centimeters or less) to which near-infrared spectra are sensitive, while being preserved at depths to which the radar sounds." "As argued by Lanzerotti et al. [12], a combination of ion erosion and micrometeoroid gardening may have depleted ammonia from the surfaces of Saturn's icy satellites.

"Given the hypersensitivity of water ice's absorption length to ammonia concentration, an increase in ammonia with depth could allow efficient 2.2-cm scattering from within the top one to several decimeters while attenuating 13-cm echoes, which would require a six-fold thicker scattering layer. If so, we would expect each of the icy satellites' average radar albedos to be higher at 2.2 cm than at 13 cm...."

Black et al. [3] agree that their 13-cm albedos "may further support the Ostro et al. [7] suggestion that the effective scattering layers on these moons are determined by an increasing amount of absorber with depth, such that relatively cleaner layers are seen by the 2.2 cm wavelength, while the 13 cm wavelength senses lower, more absorbing layers."

Thorough state-of-the-art measurements of the electrical properties of ammonia-containing water ice as function of concentration, chemical form, frequency, and temperature are needed to provide a firm foundation for realistic interpretation of the inter- and intra-object radar albedo variations in the Saturn system, with important implications for understanding the geologic nature and histories of these objects' surfaces.

References:

[1] Ostro S. J. et al. (1992) J. Geophys. Res., 97, 18227-18244.

[2] Black G. J. et al. (2004) Science, 304, 553.

[3] Black G. J. et al. (2007) Icarus, 191, 702-711.

[4] Hapke B. W. et al. (1993) Science 206, 509–511.

[5] MacKintosh F. C. and John S. (1988) Phys. Rev. B, 37, 1884–1897.

[6] Peters K. J. (1992) Phys. Rev. B, 46, 801-812.

[7] Ostro S. J. et al. (2006) Icarus, 183, 479-490.

[8] Chyba C. F. et al.(1998) Icarus, 134, 292-302.

[9] Lorenz R. D. (1998) Icarus, 136, 344-348.

[10] Lorenz R. D. and Shandera S. E. (2001) Geophys. Res. Lett., 28, 215-218.

[11] Moore M. H. et al. (2007) Icarus, 190, 260–273.

[12] Lanzerotti L. J. et al. (1984) Nature 312, 139-140.

SURFACE WEATHERING IN DIFFERENT RADIATION ENVIRONMENTS. C. Paranicas[1], D. G. Mitchell[1], S. M. Krimgis[1], D. C. Hamilton[2], E. Roussos[3], N. Krupp[3], G. H. Jones[4], R. E. Johnson[5], J. F. Coooper[6], and T. P. Armstrong[7], [1]APL 11100 Johns Hopkins Rd., Laurel, MD 20723, [2]University of Maryland, [3]Max Planck Institut fuer Sonnensystemforschung, [4]MSSL University College London, [5]University of Virginia, [6]NASA Goddard, [7]Fundamental Technologies

Charged particle data have now been returned from orbiters of both Jupiter and Saturn. The Galileo and Cassini spacecraft have made many close flybys of planetary satellites. Data have revealed radiation environments vary greatly in both composition and intensity among the various satellites of these two planets. For example, Europa and Ganymede are both in the Jovian radiation belts, but Ganymede's internal magnetic field shields the surface to a large extent from some charged particles. We will present data summarizing the different radiation environments of the Jovian and Saturnian satellites as well as data showing differential weathering of individual satellites. The main goal of this analysis is to continue to connect differential weathering with changes in surface properties. The work of Khurana et al. [1] has left little doubt that differences in charged particle weathering produces observable differences over satellite surfaces. To the extent possible, we will include new laboratory results to support our work and additionally include recommendations for laboratory experiments that can help us advance the research.

Reference:

[1] Khurana, K. K., R. T. Pappalardo, N. Murphy, and T. Denk (2007), *Icarus*, *191*, 193-202.

IMPACT GARDENING ON EUROPA. Cynthia B. Phillips[1] and Lisa Grossman[1,2], [1]Carl Sagan Center for the Study of Life in the Universe, SETI Institute, 515 N. Whisman Rd, Mountain View CA 94043; phillips@seti.org [2]Department of Astronomy, Cornell University, Ithaca, NY.

Introduction: Remote sensing measurements of Europa and other airless icy bodies are sensitive only to a thin surface veneer of material. Spectroscopic measurements are assumed to apply to the bulk subsurface composition, but in addition to endogenic geological activity, the surface layer is subject to exogenic processes such as sputtering and impact gardening.

Charged-particle interactions with materials at Europa's surface can produce oxidants and simple organics [1-4]. These oxidants and organics, if transported downward through the ice shell to a liquid water layer, could provide a significant amount of energy to sustain a biosphere. However, irradiation also destroys such materials if they remain exposed on Europa's surface [5,6]. Sputtering erosion and surface mixing through impact gardening act to change the preservation depth.

Impact gardening, i.e. mixing of the surface by micrometeorite impacts, can serve to bury surface irradiation products and preserve them from future destruction. It also serves as a physical mixing of the surface remote sensing layer, transporting surface materials to the subsurface as well as subsurface materials to the surface. An investigation of the gardening depth on Europa is relevant to understanding the physical processes at Europa's surface, as well as the physical and chemical state of the remote sensing layer.

Previous Work: An initial survey of gardening vs. sputtering by Chyba [2,3] used an estimate of sputtering at the Europan surface [7] of 0.2 μm yr^{-1}, and a gardening estimate [6], based on a lunar analogy, of 1-10 cm over a mean Europan surface age of ~10 Myr [8,9]. For this case, Chyba [2,3] took the relevant radiation-processed depth at Europa's surface to be ~1 mm, the stopping depth of incident electrons [10,11,4].

However, subsequent estimates [4] suggested that the sputtering rate at Europa was more than an order of magnitude lower, ~0.02 μm yr^{-1}, and that the gardening depth over 10^7 yr was ~1.3 m, rather than 1-10 cm. In this case, oxidants and organics created by irradiation of Europa's surface would be efficiently buried by gardening, and therefore protected. A later estimate by Phillips and Chyba [5] found a gardening depth of 0.67 m. All of these initial estimates depended on extrapolations down from many orders of magnitude.

New Gardening Estimate: We are currently updating the gardening rate for Europa using observations of small craters on Europa by Bierhaus *et al.* [19] combined with the lunar regolith growth studies of Shoemaker *et al.* [14,15] and Gault [16] as summarized in Melosh [17]. This method has the advantage of using actual observations from the Europa system and also requires less extrapolation.

Cumulative crater distributions for Europa and elsewhere in the solar system have a typical form: N_{cum} (>D) = c D^{-b}, where N_{cum} is the cumulative number area density of craters of diameter equal to or greater than D, c is a constant, and b is the exponent in the power law. Using this distribution, we can calculate the fraction f_c of the total area covered by craters with diameters between some value D and the maximum value (we actually integrate up to infinity). Paralleling the Melosh [17] treatment of Shoemaker [14], we can say that:

$$f_c(D,\infty) = -\frac{\pi}{4}\int_D^\infty D^2 \frac{dN_{cum}}{dD}\,dD = \frac{\pi bc}{4(b-2)}\left(\frac{1}{D^{b-2}}\right)$$

At the point where F_c=2, according to Melosh's [17] treatment of Shoemaker [14], the surface is covered twice over with craters in a particular size bin. This is the minimum crater coverage, according to Shoemaker, at which the bottoms of all the craters of this diameter or less are interconnected and therefore form a broken layer [14]. The minimum regolith thickness can therefore be taken to be the depth of a crater whose diameter D_{min} produces a value of F_c=2.

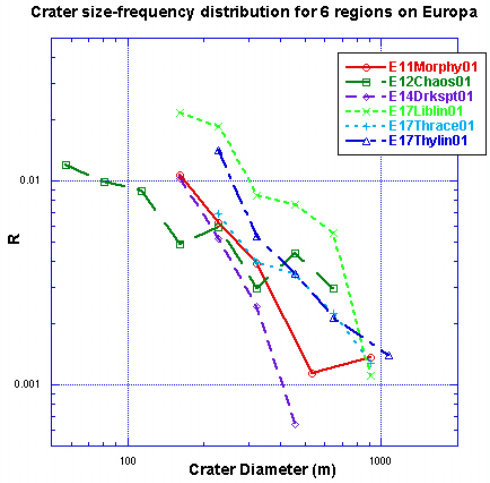

Figure 1: Size-frequency distribution for 6 regions on Europa. Data from Bierhaus et al. [19].

Small Crater Counts: To determine the extent to which the surface was cratered at various crater diameters, we used crater counts from Bierhaus et al. [19,20]. He supplied us with his size-frequency distributions for counts of small craters in six regions on Europa covered by high-resolution Galileo image sequences. The data is shown in R-plot form in Figure 1.

The resolution of the available Galileo images of Europa, which ranged between 10-100 meters per pixel, constrained the minimum measured crater diameter. The smallest crater bin began at 161 meters in diameter for most observations, with only the E12Chaos01 observation going down to 57 meters. Since the surface clearly is not saturated with small craters at these diameters, we had to extrapolate down to smaller craters.

To accomplish this, we took curve fits to the data in Figure 1 and used them to extrapolate down to smaller craters. We continued this extrapolation until we reached a point where cumulative F_c=2, to determine the minimum crater diameter which covered the surface twice over. This crater diameter then gave us the minimum regolith depth. Figure 2 shows our extrapolations. The solid lines are the actual crater counts from Bierhaus et al. [19,20], and the dotted lines are our extrapolation. The horizontal line at the top represents the value F_c=2.

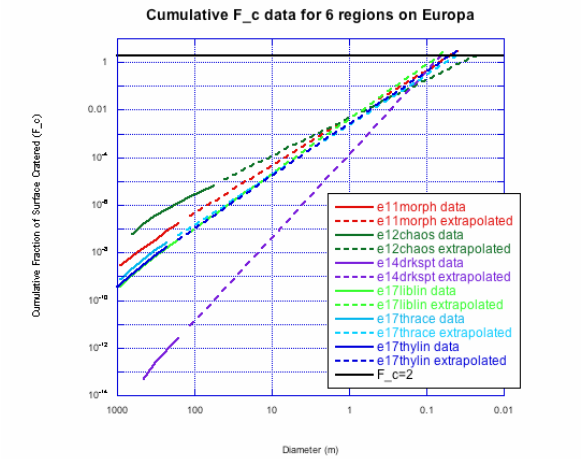

Figure 2: Measured and extrapolated crater data for regions in Figure 1, extrapolated down to a crater diameter at which F_c=2

If we assume a depth/diameter ratio of 1:4, then we can use the intersects of Figure 2 to calculate the regolith thickness for each of the six observed regions. This data is summarized in Table 1.

Observation	Regolith depth (cm)
E11MORPHY01	1.20925
E12CHAOS01	0.55125
E14DRKSPT01	1.598
E17LIBLIN01	1.69425
E17THRACE01	1.00475
E17THYLIN	1.22475

Table 1: Regolith Thicknesses

Our results indicate that the regolith thickness in these six regions varies from a minimum of about 0.5 cm to a maximum of about 1.7 cm, for an average thickness of about 1 cm. We thus suggest that the average regolith thickness on Europa, or the depth to which the surface has been turned over at least once, is about 1 cm. The lowest value of 0.5 cm corresponds to the E12Chaos01 region, which has been suspected of being geologically younger than other parts of Europa [19].

Comparison with Sputtering: For a mean surface age of ~10^7 yr [8,9], Cooper *et al.* [4] suggested that gardening should extend to a depth of 1.3 m. Our new gardening rate suggests that the gardening depth is about 0.01 meters. It thus appears that sputtering may dominate over gardening in most areas of the surface.

Secondary Craters: Bierhaus [19,20] suggests that the majority of the small craters counted in his studies are in fact secondary craters that can be accounted for by the few large primary impact craters on Europa. The presence of secondaries rather than small primary craters does change the process of gardening somewhat. Rather than having a slow, steady accumulation of small impacts spread randomly over the surface, various parts of the surface will instead experience brief showers of small secondary impactors from a particular large impact, interspersed with long periods of very little impact activity.

We believe that the overall mechanics of gardening, in which the surface is mixed once or a number of times down to a particular depth, will remain the same whether the impactor population is made up of small primaries or of secondaries. One possible influence of secondaries may be that their lower impact velocity could result in shallower craters, changing the depth:diameter ratio and therefore the gardening depth estimate. We will be investigating this and other results of secondary craters in the future.

Acknowledgements: Special thanks to Edward Bierhaus for providing data that was used in this study, and to Christopher Chyba for helping initiate this project. CBP was funded by the NASA Astrobiology Institute. LG was funded by the NSF REU program.

References: [1] Chyba C.F. and Phillips C. B. (2001) *PNAS USA*, **98**, 801-804. [2] Chyba C.F. (2000a) *Nature* **403**, 381-382. [3] Chyba C.F. (2000b) *Nature* **406**, 368. [4] Cooper J.F. et al. (2001) *Icarus* **149**, 133-159. [5] Phillips, C.B., and C. F. Chyba (2001) LPSC XXXII, abs. 2111. [6] Varnes E.S. and Jakosky B.M. (1999) *LPSC XXX*, 1082 (CD-ROM). [7] Johnson R.E. et al. (1998) *Geophys. Res. Lett.* **25**, 3257. [8] Zahnle K. et al. (1998) *Icarus* **136**, 202-222. [9] Zahnle K. et al. (1999) *LPSC XXX*, 1776 (CD-ROM). [10] Delitsky M.L. and Lane A.L (1997) *J. Geophys. Res.* **102**, 16,385-16,390. [11] Delitsky M.L. and Lane A.L (1998) *J. Geophys. Res.* **103**, 31,391-31,403. [12] Shoemaker E. M. *et al.* (1982) The Geology of Ganymede, in Satellites of Jupiter, ed. D. Morrison, UA Press, Tucson AZ. [13] Cuzzi J.N. and Estrada P.R. (1998) *Icarus* **132**, 1-35. [14] Shoemaker E. M. et al. (1969) *JGR* **74**, 6081-6119. [15] Shoemaker E.M. et al. (1970) Proc. Apollo 11 Lunar Science Conference, v. 3, 2399-2412. [16] Gault D.E. (1970) *Radio Science* **5**, 273-291. [17] Melosh H. J. (1989) Impact Cratering: A Geologic Process. Oxford University Press. [18] Ip W.-H. et al. (1998) *Geophys. Res. Lett.* **25**, 829-832. [19] Bierhaus E.B. et al. (2001) Icarus 153, 264-276. [20] Bierhaus, E.B. (2004) PhD Thesis, U. Colorado Boulder.

DIFFERENTATION OF GAS-RICH BRINY CRYOMAGMAS IN ICY SATELLITES. SIMULATION EXPERIMENTS AT HIGH PRESSURE O. Prieto-Ballesteros[1], J. S. Kargel[2] J. A. Rodriguez-Manfredi[1], F. Gómez[1] and V. García Baonza[3], [1]Centro de Astrobiología, INTA-CSIC. Ctra. Ajalvir km.4, 28850 Torrejón de Ardoz. Madrid. Spain (prietobo@inta.es), [2]University of Arizona, Tucson, AZ, USA [3]Facultad de CC. Químicas. Universidad Complutense de Madrid, Spain,

Introduction: Evidences of cryomagmatism have been detected in some icy satellites such as Europa, Titan and Enceladus. A typical problem about cryomagmatism is that many aqueous cryomagmas have negative bouyancy relative to a pure water ice crust of an icy body. However, some geochemical models show that crusts of these satellites include other components making the crusts denser, and cryomagmas may contain ammonia or exsolvable gases, making them less dense and potentially causing positive buoyancy [1-3]. Segregated cryomagmatic liquids should have lower compositional or temperature-driven densities than the host materials in order to ascend in the crust. In the case of Europa, salt and sulfuric acid hydrates have been nominated as part of the composition of the surface and the crust suported by spectroscopic observations [4-6]. Although significant amounts of these solids can make the ice crust significantly denser, when dissolved they also make the liquid phase denser. Getting the right combination of low density liquid and high density crust and having it all make cosmochemical and petrological sense has been a long-standard challenge, albeit one with various proposed solutions.

We suggest that the formation of clathrate hydrates from an aqueous magmatic chamber enriched in gasses and dissolved ions will result in the differentiation of the cryomagmas into the icy satellites. Then, distilled aqueous cryomagmas, lacking a heavy load of dissolved salts and containing exsolvable gases, could ascend from the more dense residue, decompress, expand, and erupt explosively. We are testing this hypothesis making a set of experiments in a new high pressure simulation chamber.

The High Pressure Planetary Simulation Chamber (HPPSC): A new equipment for the simulation of different planetary environments at high pressure has been built at Centro de Astrobiolgia in Madrid (Spain). The equipment has two different chambers, one for physico-chemical studies which can reach pressures up to 10000 bar (called MINchamber), and other for biological experiments which has higher volume and can reachs up to 3000 bar (BIOchamber). Both can work in the temperature interval from 123 to 600 K. The heating/cooling system is an integrated circuit of liquid nitrogen and electrical resistance heaters.

Each chamber has four different ports to incorporate several sensors. They are used for making in situ analysis and to be able to monotor the processes ocurring during the changes of pressure and temperature. Currently, a Raman spectromete, and a video camera are installed on two ports using sapphire windows. Other sensors able to be incorporated for specific studies are those to measure magnetic susceptibility, electrical resistivity, and mass spectrometry.

The whole system can be controlled automatically, with data logging of the pressure, the temperature and other parameters while the experiment is running.

Testing hypothesis: clathration as a type of differentiation processes in aqueous cryomagmas. When an aqueous cryomagma with some gasses and salts is cooling, it should fractionally crystallize different minerals, including salt hydrates and clathrate hydrates of the gases. Clathrate hydrate formation should occur as soon as they reach the saturation concentration corresponding to the pressure of the dissociation curve. If the confining pressure is less than that and instead the saturation vapor pressure is attained first, then bubble exolution can occur. If that happens rapidly, and the cryomagma is free to expand (for instance, upon eruption), an explosive eruption may ensue.

On the other hand, sulfates compete with clathrates for the water in the aqueous cryomagma. But the evolution of the process will depend on which is the first hydrate which is formed in the interior of the planetary body. Formation of clathrate hydrates removes water from the original solution. So if the solution also contains salts, there will be a higher concentration in ions as soon as the clathrates are formed. Then, clathration could result in a cryomagmatic differentiation. The formation of clathrates would separate the crystals from the more concentrated brine magma by density. If the destruction of the clathrate layer occurred by any movement or fracturation, clean water ice or gas-enriched ice could ascend through the brine to higher levels. Crystallization of gas hydrates generally would cause expansion of the assemblage if water ice is a crystallizing phase, so that would cause tensional stresses on surrounding ice, and it might also drive fracturing, and then drive expulsion of the liquid.

References:

[1] Croft, S.K., et al., 1988, *Icarus 73*, 279-293. [2] Kargel, J. S. et al. (2000) *Icarus 148*, 226-265. [3] Hogenboom, D. L. et al. (1997) *Icarus 128*, 171-180.

[4] McCord, T. B. et al. (1998) *Science 280,* 1242-1245. [5] McCord, T. B. et al. (1999) *J. Geophys. Res. 104* , 27157-27162. [6] Carlson, R. W:, et al. (2005) *Icarus 177*, 461-471.

Compaction of Porous Solar System Ices by Ion Irradiation: Laboratory Studies U. Raut[1], M. Famá[1], M.J. Loeffler[1] and R.A. Baragiola[1]. [1] Laboratory of Atomic and Surface Physics, University of Virginia, Charlottesville, VA 22904.

Introduction: The surface of objects in various astrophysical environments, such as cold satellites, rings, comets, and TNOs [1] is likely coated with ice formed from accretion of water molecules in vapor phase. For example, water molecules in the sputtered flux or in the ejecta produced by micrometeorite impacts can return to the surface of satellites in gravitationally bound trajectories. The water vapor observed in plumes as seen on Enceladus can coat the surface of grains in the rings of Saturn. Laboratory measurements show that ice grown by accretion from the gas phase is porous with pore dimensions from the sub-nm scale to the mesoscopic scale [2-4]. Porosity determines important properties of ice such as its gas adsorption capacity, thermal conductivity and behavior under stress.

Astrophysical ices exist in radiation environments where they are continually bombarded by energetic photons and ions. The energy deposited by these particles can affect the porosity and, in fact laboratory studies have demonstrated that ion irradiation can compact porous ice films [5, 6]. For instance, we previously observed that irradiation with 100 keV Ar^+ ions to a fluence of ~ 10^{14} ions/cm^2 was sufficient to fully compact an ice film with 26% initial porosity [6]. Though the details of physical processes by which compaction occurs in our ice films are not fully understood, we posit that the energy deposited by the ions causes molecular motion that alters the ice structure to decrease the internal surface energy of the porous film. The compaction process should therefore depend on the energy deposited by the ion per unit path length or stopping power (dE/dx). In this study, we irradiated porous ice films using different ions at different energies. By varying the type and energy of the projectiles we were able to study the dependence of compaction on the stopping power. We analyze the results with theoretical models that have been used to describe amorphization and damage created by fast ions in solid targets. We intend to use these models to extrapolate our results to solar system and interstellar conditions to estimate compaction timescales for porous ice subjected to ion irradiation, including cosmic rays.

Experimental Details: Thin ice films were deposited at 30 K from a collimated vapor source at 45^o incidence onto the polished surface of a gold-coated quartz crystal microbalance. The incidence angle was chosen to produce wholly microporous films with significant porosity [4]. The microbalance measures the areal mass of the films, which is converted to column density in molecules/cm^2 by dividing by the molecular mass. Ices were irradiated at 20^o incidence with different ions at different energies produced from a 300 kV mass-analyzed ion accelerator. Reflectance spectra in the 200-800 nm wavelength range were collected at near-normal incidence using an Ocean Optics CCD spectrometer. The interference fringes in the reflectance spectra were fit using Fresnel equations to obtain the index of refraction and the film thickness *d*, which together with the areal mass of the microbalance, gives the average film density ρ . We derive the average film porosity, $1 - \rho / \rho_c$, using ρ_c = 0.94 g/cm^3 for compact ice.

Preliminary Results: Figure 1 shows the change in porosity of ice films when irradiated with different projectiles at different energies. In all cases, the porosity of the ice films reduces from ~ 0.26 (± 0.02) to 0 (± 0.01) as a result of irradiation. Different projectiles show different fluence dependence of compaction. For instance, 80 keV protons need nearly ten times more fluence to compact the ice film than 150 keV Ar^{++}.

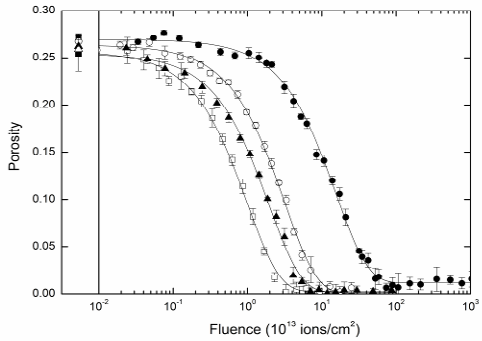

Figure 1 - Fluence dependence of compaction for ice films deposited at 40 K at 45^o incidence for different projectiles at different energies. Symbols: 80 keV H^+ (●), 320 keV He^{++} (○), 150 keV Ne^+ (▲), and 150 keV Ar^{++} (□). The lines are fits to data of the form $\Phi(F) = y_o + \Phi_o \exp(-\sigma_c F)$. The data points shown in the left partition of the plot are the initial porosities of the unirradiated films.

The porosity (Φ) decays exponentially with ion fluence (F) suggesting that the rate of compaction of porous ices due to ion bombardment is proportional to the fraction of voids or pores present in the ice during irradiation. The data is fit with $\Phi(F) = y_o + \Phi_o \exp(-\sigma_c F)$, where y_o is the residual porosity after compaction, Φ_o is the film porosity of the unirradiated ice, and σ_c is the "compaction cross section". We assume that ice compacts in a small cylindrical region around the ion's path (the track), whose radius r_c is given by $(\sigma_c / \pi)^{1/2}$.

Models: There are two theoretical models that predict the how the damage track size, caused by ions traversing through the solid, is related to the the electronic stopping power of the ions: (i) *the modified lattice potential* model [7] where secondary electrons ejected by the ion modify the effective intermolecular lattice potential and transfer sufficient energy to produce motion of nuclei and molecules in the solid in some restricted region around the path of the ion, and (ii) the *thermal spike* model [8] which assumes that the solid is melted in a high-temperature region formed around the track. Both models predict that the track radius is proportional to the square root of the electronic stopping power of the projectile and have been successfully tested in experimental studies of amorphization and radiation damage of solids like quartz and YIG.

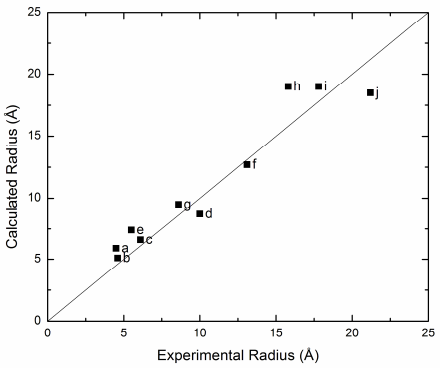

Figure 2 – The calculated radii vs. experimental radii (r_c). The experimental values obtained from fits similar to those shown in Figure 1 for (a) 80 keV H^+, (b) 220 keV H^+, (c) 80 keV He^+, (d) 320 keV He^{++}, (e) 120 keV He^+, (f) 150 keV Ne^+, (g) 400 keV Ne^{++}, (h) 150 keV Ar^+, (i) 150 keV Ar^{++} and (j) 300 keV Ar^{++}. The calculated radii are deduced from the empirical equation discussed in the text.

In Figure 2, we plot the values of calculated radii obtained by using the empirical equation,

$$r\ (\text{calculated}) = \alpha\ (\sqrt{S_e} + \sqrt{S_n})$$

vs. the experimental radii, r_c. Here S_e and S_n are the mean electronic and nuclear stopping power of the different ions in water ice respectively. The coefficient $\alpha \approx 2\ (Å^3/eV)^{1/2}$. In our experiments, the fast light ions such as H^+ and He^+ lose their energy in the ice films mostly through electronic excitations. Their nuclear stopping power is negligible compared to their electronic counterpart. The compaction radius for these fast light ions is proportional to the square root of the electronic stopping power, in agreement with the models. However, for low velocity projectiles like Ar ions, the nuclear stopping power is not negligible, and therefore should contribute to the compaction. For these ions, both electronic and elastic processes induce compaction. We assume that the radius produced from the elastic collisions has a square root dependence on the nuclear stopping power and add its contribution to that obtained for electronic processes.

Further work is in progress to refine this model. Our goal is to estimate timescale for compaction of astrophysical ices, provided we have information regarding radiation environment (particle, energy, flux) that irradiate these ices.

References:

[1] Schmitt, B., C. de Bergh, and M. Festou, *Solar System Ices*. 1998: Dordrecht Kluwer Academic Publisher. [2] Mayer, E. and R. Pletzer, *Astrophysical implications of amorphous ice-a microporous solid.* Nature, 1986. **319**(6051): p. 298-301. [3] Stevenson, K.P., et al., *Controlling the morphology of amorphous solid water.* Science, 1999. **283**(5407): p. 1505-7. [4] Raut, U., et al., *Characterization of porosity in vapor-deposited amorphous solid water from methane adsorption.* The Journal of Chemical Physics, 2007. **127**(20): p. 204713. [5] Palumbo, M.E., *Formation of compact solid water after ion irradiation at 15 K.* Astronomy and Astrophysics, 2006. **453**(3): p. 903-909. [6] Raut, U., et al., *Compaction of microporous amorphous solid water by ion irradiation.* Journal of Chemical Physics, 2007. **126**(24): p. 244511. [7] Tombrello, T.A., *Predicting latent track dimensions.* Nuclear Instruments and Methods in Physics Research Section B: Beam Interactions with Materials and Atoms, 1994. **94**(4): p. 424-428. [8] Szenes, G., *A possible mechanism of formation of radiation defects in amorphous metals bombarded with high-energy heavy ions.* Mat. Sci.Forum, 1992. **97-99**: p. 647-652.

VOLATILE ICES IN THE KUIPER BELT: THEORY AND OBSERVATION. E. L. Schaller and M.E. Brown[1], [1]Division of Geological and Planetary Sciences, Caltech, Pasadena, CA 91125 (schaller@caltech.edu).

Introduction: Unlike Pluto and Eris, the vast majority of Trans-Neptunian objects (TNOs) are too small and hot to retain volatile ices such as CH_4, N_2, and CO on their surfaces to the present day. As a result, their infrared spectra are either dominated by involatile water ice or dark featureless material. To understand the dichotomy between volatile rich and volatile free surfaces in the outer solar system, we constructed a simple model of atmospheric escape of volatile ices over the age of the solar system [1]. A prediction of this model is that (50000) Quaoar, an object about half the size of Pluto but with a perihelion ~12 AU further from the sun, should be just capable of retaining its volatile ices to the present day.

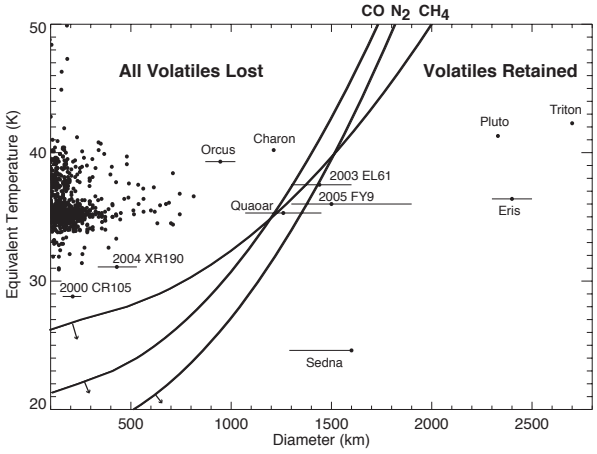

Figure 1: Volatile loss in the outer solar system as a function of object temperature and diameter [1]. The lines correspond to the temperature and diameter at which an object will have lost all of its initial CH_4, N_2 and CO after 4.5 billion years. Volatiles have only been detected on objects on the right side of this phase space. Note that decreasing the assumed initial volatile abundances by an order of magnitude does not appreciably change the positions of the lines (see arrows) as they are controlled mainly by the vapor pressures of the compounds. However, recent laboratory measurements revealing high surface binding energies of volatile ices on water ice [3,4] may shift the positions of these lines in the opposite directions of the arrows, potentially expanding the number of objects on which surface volatiles could presently exist. Further laboratory work on the behavior of volatile ices on water ice surfaces will enhance the predictive capabilities of this model.

Results and Discussion: We observed Quaoar with NIRSPEC on the Keck II telescope in April 2007. We found that its infrared spectrum shows distinct absorption features of crystalline water ice, solid methane, and possibly ethane and other higher order hydrocarbons [2]. The detection of methane on Quaoar means that it is only the fifth TNO on which volatile ices have been detected. The small amount of methane on an otherwise water ice dominated surface suggests that Quaoar is a transition object between the dominant volatile-poor small TNOs and the few volatile-rich large TNOs such as Pluto and Eris [2].

The 1.65-micron crystalline water ice feature is present in the spectrum of Quaoar and on every other TNO with sufficient signal-to-noise on which water ice has been detected [5]. Recent laboratory experiments [6] have shown that thermal recrystallization may dominate over amorphization due to irradiation at 50K thereby allowing crystalline water ice to survive longer than previously assumed. Laboratory experiments are now indicating that recent cryovolcanism is not likely to be required to explain the presence of crystalline water ice on the surfaces of outer solar system bodies. The spectrum of Quaoar is consistent with that of a cold, geologically dead object slowly losing the last of its primordial volatiles by thermal escape [2].

References: [1] Schaller, E.L. & Brown, M.E. (2007a) *ApJL*, 659, L61-64. [2] Schaller, E.L. & Brown M.E. (2007b) *ApJL* 670, L49-51. [3] Mastrapa, R.M. et al. (2007a) *AAS DPS Meeting # 38.06.* [4] Mastrapa, R.M. et al. (2007b) *AGU Fall Meeting #P13G-03.* [5] Barkume, K.M. et al. (2008) *AJ* 135, 55-67. [6] Zheng, W. et al. (2008) arXiv0801.2805Z (submitted).

CRATERING ON ICE – A COLD LABORATORY. P.M. Schenk, Lunar and Planetary Institute, 3600 Bay Area Blvd., Houston, TX 77058 (schenk@lpi.usra.edu).

Introduction: When Voyager first saw the icy satellites of the outer planets it discovered a rich canvas of new and unusual impact landforms. The intervening decades of study, and two major orbital missions, have shown that these landforms are related directly to the fact of icy crustal and lithospheric composition and the thermal structure of these diverse bodies. These studies have shown that impact crater landforms are inherently different on icy bodies, and are also subject to unusually high degrees of post-impact modification. The rolling of time has also shown that our understanding of ice rheology *under planetary conditions* has grown only drudgingly. Although we are on the cusp of physically realistic modeling of impact crater formation and modification on icy worlds, much work remains to be done.

Impact: Impact crater morphology can be a very useful tool for probing planetary interiors, but nowhere in the solar system is a greater variety of crater morphologies observed than on the large icy Galilean satellites Ganymede and Callisto [e. g., 1, 2]. With increasing size, these same craters become less like their counterparts on the rocky planets. Several impact landforms and structures (multiring furrows, palimpsests, and central domes, for example) have no obvious analogs on any other planets. Further, several studies [e.g., 3, 4, 5] have drawn attention to impact landforms on Europa which are unusual, even by Galilean satellite standards, and these may be related to the liquid water ocean possibly lurking beneath a thin warm outer ice shell. As such, large impact structures are important probes of the interior structure of these bodies over time.

Post-Impact: Post-impact creep or relaxation of impact crater topography on icy surfaces allows us to see into the mechanical state and thermal history of large icy satellites such as Ganymede and Callisto [e.g., 1], and smaller satellites such as Enceladus and Dione (ongoing). Relaxation is due to the strong dependence of ice flow on lithospheric temperatures. Recent advances in our understanding of ice rheology [e.g., 6, 7] and the mechanics of lithospheric deformation [8] have sharpened our understanding of the relaxation of topography on large icy satellites.

Future: Understanding of the impact formation and post-impact modification of craters depends critically on our understanding of ice rheology. Issues concern deformation mechanisms, role of non-ice components, porosity, degree of fracturing, and extrapolation from laboratory conditions and time-scales. Major advances have been made in the past 3 decades, but a major question concerns the degree of correlation between experimental insights into ice behavior and the actual physical state of the icy lithospheres of these bodies.

References: [1] Passey, Q., and E. Shoemaker, in *Satellites of Jupiter*, pp. 379 – 434, 1982. [2] Schenk, P., in *Jupiter*, pp. 427 – 456, 2004. [3] Moore J.M. et al., *Icarus*, 151, 93-111, 2001. [4] Turtle, E., and E. Pierazzo, *Science*, 294, 1326-1328, 2002. [5] Schenk, P., *Nature*, 417, 419-421, 2002. [6] Durham W.B. and Stern L.A., *Annu. Rev. Earth Planet Sci.* 29, 295-330, 2001. [7] Goldsby, D.L. and D.L. Kohlstedt, *Scripta Mat., 37*, 1399-1406, 1997. [8] Dombard, A., and W. McKinnon, *J. Geophys. Res.*, 111, E01001, 2006.

FRICTION AND FRACTURE OF ICE Ih. E. M. Schulson, Thayer School of Engineering, Dartmouth College, Hanover NH 03755 U.S.A., (erland.schulson@dartmouth.edu).

When rapidly compressed under low confinement, ice reaches terminal failure through the initiation and growth of microcracks [1]. The cracks interact and lead to the creation of Coulombic (C) shear faults. Fundamental to the process is frictional sliding. Under higher confinement, frictional sliding is suppressed. Terminal failure then occurs through the development of plastic (P) faults [2]. In this presentation we will focus on C-faults and the role of internal friction in their formation. Discussion will be based upon measurements of the coefficient of internal friction, deduced from the slope of failure envelopes for both fresh-water ice [3] and arctic sea ice [4] deformed at -3 °C and -10 °C, and of the coefficient of friction across naturally-formed C-faults, deduced from the resistance to sliding across such features at speeds from ~ 10^{-6} m s^{-1} to 10^{-2} m s^{-1} at temperatures from -3 °C to -40 °C. The two coefficients have similar values. At lower sliding speeds ($<10^{-5}$ m s^{-1}) friction increases with increasing speed; at higher speeds, it decreases [5]. The latter effect imparts strain-rate softening when ice is deformed within the brittle regime.

References: [1] Schulson E. M. (2001) *Engg. Fracture Mech., 68*, 1839-1888. [2] Schulson E. M. (2002) *Acta Mater., 50*, 3415-3424. [3] Schulson E. M. et al. (2006) *Acta Mater.*, 5415, 3923-3932. [4] Schulson E. M. et al. (2006) *JGR 111(C11S25)*: doi: 10.1029/2005JC003234186. [5] Fortt A. L. and Schulson E.M. (2007) *Acta Mater., 55*, 2253-2264.

ON FROZEN VOLATILES IN COMETS, AND THEIR SUBLIMATION. Rita Schulz, ESA Research and Scientific Support Department, ESTEC, Postbus 299, 2200 AG Noordwijk, The Netherlands, rschulz@rssd.esa.int.

Introduction: A comet approaching the Sun can be considered an excellent planetary laboratory in which the sublimation of ice-dust mixtures into vacuum can be studied without any obstructing boundaries. The development of cometary activity is undoubtedly related to most complex physico-chemical processes in the surface layer of the nucleus and in the inner coma. These processes form the atoms, molecules and ions making up the composition of the gas coma as we know it from decades of remote-sensing observations. Great effort has been put into trying to infer the composition of the comet nucleus from that of the coma by chemical modeling, starting with simple gas chemistry and later introducing more complex hydrodynamic-chemical models [1]. A number of processes were identified that are capable of altering the initial composition of volatile material sublimating from the nucleus surface and/or subsurface. However, we do not know enough yet to draw any conclusions, which would allow confirming or discarding one of these mechanisms or unambiguously inferring the physico-chemical nature of a comet nucleus. For this we need measurements, at least for one comet nucleus and its near-nucleus environment. Key information is expected from the Rosetta rendezvous mission with Jupiter-family comet 67P/Churyumov-Gerasimenko. Hence, we need to exploit this mission to find the clues required for determining the properties of cometary nuclei from coma observations. Ideas how this can be achieved from parallel measurements will be presented.

Comet Nucleus Composition: The key to the origin of comets and possibly to the formation and evolution of the solar system is the composition of the comet nuclei. Although no ground-truth measurements of this composition exist, much could be inferred from spectroscopic observations of active comets mainly at infrared and radio wavelengths. Of the about 45 molecules, radicals or ions identified as coma species, about 25 are likely to have sublimated from nucleus ices [2]. To date only very few direct measurements exist from comet fly-by missions. However, the availability of very large telescopes in combination with advanced new instrument technology, particularly in the infrared, provides nowadays the opportunity to attempt direct measurements of the surface composition of cometary nuclei also from ground. Spectroscopic observations in the near-infrared region between 1.4 μm and 2.5 μm are sensitive to absorption bands of water and hydrocarbon ices. A number of searches for spectral signatures diagnostic of surface ices have already been conducted for minor bodies in the outer solar system, in particular for Centaurs and TNOs. The results are rather promising with a number of frozen volatiles detected [3]. A few near-infrared spectra of comet nuclei have also been published opening the opportunity to take a glimpse at the surface a comet from ground [4] [5]. However, owing to the faintness of a bare comet nucleus the observations merely allow to derive the nucleus reflectance spectrum. A near-infrared spectrum of a comet nucleus can only be compositionally diagnostic if the reflected light from the nucleus is measured with a high enough signal-to-noise to render a clear distinction between absorption bands and noise patterns. Therefore, to ensure the correct interpretation of such data it is essential to compare them with the results of space missions. There is an infrared spectrometer on Rosetta, which will obtain spectra of the nucleus of comet 67P/Churyumov-Gerasimenko from the orbiting spacecraft [6]. These spectra will serve as a reference to what spectroscopic features would in principle be observable in this comet from ground if there were no constraints in sensitivity. In practice it is however rather unlikely that a diagnostic infrared spectrum of the comet will be obtained by ground-based telescopes in the near future. The infrared spectra obtained by Rosetta should therefore be used for comparison with ground-based spectra of bright comet nuclei, which will undoubtedly be available at the time of the Rosetta encounter.

Water Ice: The measured water production rates in comets suggest that water ice is the most abundant frozen volatile of a comet nucleus. Nevertheless, water ice deposits on the nucleus surface have up to now been directly detected only once, on the surface of comet 9P/Tempel by the infrared spectrometer on board the Deep Impact mission [7]. The Stardust mission to comet 81P/Wild 2 did not carry an instrument capable of searching for water ice and the infrared spectrometers on board the Vega and Deep Space 1 missions were searching for, but did not find any evidence for absorption bands of water ice in comet 1P/Halley or 19P/Borrelly. This is very surprising, not only because water ice must be present in every comet nucleus and was expected to be detected, but also because water ice grains were detected in the coma of comets at large heliocentric distances (beyond 2.8 AU) by infrared spectroscopy [8-10]. The presence of an icy grain halo around a comet nucleus at such large distances would support that these ice grains were

dragged from the surface or at least from very close to the surface by gentle sublimation of volatiles, which in turn would support the presence of deposits of icy grains on the nucleus surface that may be made up of either pure water ice or be a mixture of water ice and non-volatile or less volatile species. Closer to the Sun icy grains are extremely difficult detect, because inside 2 AU the icy component sublimates within 1-2 hours forming a secondary source for water and its decay products. Nevertheless, when produced under non-steady state conditions icy grains can be detected; and indeed the observations of the fresh coma material ejected from the nucleus of comet 9P/Tempel within the first 1.5 hours after the impact led to the detection of disintegrating icy grains [11]. It was demonstrated that the mass loss during and immediately after the impact was probably not in form of gentle water sublimation [12] and the detection of disintegrating icy grains proved the long standing assumption that the water in comets does not exclusively sublimate directly from the comet nucleus, but is also ejected in form of small icy grains at least during outbursts [11]. The only way to find clear evidence that can solve the question on how water ice is deposited in comet nuclei (at least close to the surface) and how it is released under different conditions is to focus certain measurements of the Rosetta mission on this topic. The nucleus activity of the target comet has to be monitored along the orbit from the onset of the nucleus activity to perihelion and also during outbursts that may occur along its path. Details will be given on the capabilities of the Rosetta payload to tackle the question of water ice deposits as well as the release and characterisation of icy grains.

Evidence from coma observations: The monitoring of the Rosetta target comet will include parallel compositional measurements in the coma by various instruments opening the opportunity to cross-correlate the values obtained by the different measurement techniques. The remote-sensing instruments on board the Rosetta orbiter work on the same principle as respective telescope instrumentation. The results can therefore further be correlated with parallel measurements from ground or the HST. The OH abundance and its relation to the water production will be of particular interest, as OH is regarded as a direct daughter product of water the most reliable measure for the overall activity of a comet from ground. However, the spacecraft measurements will also identify parent molecules other than water and provide quantitative information on chemical reaction chains in the near-nucleus region by which the daughter species accessible from ground are eventually produced. A link between the coma chemistry uncovered by the space mission and the abundance of daughter species observed from ground can therefore be established if parallel ground-based monitoring is available. This will be of utmost importance for being able to transfer what we learn from Rosetta also to other comets.

Conclusions: A complete characterization of a comet will only be possible if cold samples of the surface and the interior of the nucleus are brought back to Earth for detailed analysis. As this will definitely not be the case in the foreseeable future, the physical properties and composition of comet material has to be disclosed by other means. Rosetta will conduct a great number of important measurements which should provide major pieces to the puzzle. However, only if the results of all measurements can be put into mutual context will we be able to draw a consistent picture of the physico-chemistry of cometary matter and its relation to the solar nebula at the time of comet formation. It is therefore crucial to develop theoretical and experimental methods by which the results of measurements can be explained on the basis of the rules of physics, chemistry and mineralogy. Laboratory experiments have already become of growing importance for the interpretation of astronomical data and the preparation of space missions. The investigations include production, processing and analysis of cometary analogues [13][14] as well as experimental and theoretical techniques for studying photochemical reactions [15] and infrared signatures of mineralogical compounds [16]. The interpretation of experimental results on cometary analogue material by theoretical investigations helps to prepare us for what to expect from the data we are about to collect. Once the spacecraft data are available the picture will reverse in that the knowledge gained from the space missions will bear refined theories and trigger further experiments that will help to secure even more pieces to the puzzle.

References: [1] Rodgers et al. (2005) in Comets II, Univ. Ariz. Press, 505-522. [2] Crovisier (2005) in ACM, Cambridge Univ. Press, 133-152. [3] Barucci and Peixinho (2005) ACM, Cambridge Univ. Press, 171-190. [4] Licandro et al. (2003) A&A 398, L45-L48. [5] Abell et al. (2005) Icarus 179, 174-194. [6] Coradini et al. (2007) SSR 128, 529-559. [7] Sunshine et al. (2006) *Science, 311*, 1453–1455. [8] Davies et al. (1997) Icarus 127, 238- [9] Lellouch et al. (1998) A&A 339, L9- [10] Kawakita et al. (2004) ApJ 601, L191-L194. [11] Schulz et al. (2006) A&A 448, L53-L56. [12] Hughes (2006) MNRAS 365, 673-676. [13] Colangeli et al. (1999) SSR 90, 341-354. [14] Strazzulla (1999) SSR 90, 269-274. [15] Jackson (2002) EMP 89, 197-220. [16] Wooden (2002) EMP 89, 247-287.

LABORATORY MEASUREMENTS ON WATER ICE UNDER SIMULATED MARS' CONDITIONS. D.W.G. Sears[1,2,*], V. Chevrier[1], R. Ulrich[1,3], L.A. Roe[1,4], K. Bryson[1], [1]Arkansas Center for Space and Planetary Sciences and W. M. Keck Laboratory for Space Simulation. [2]Department of Chemistry and Biochemistry. [3]Department of Chemical Engineering. [4]Department of Mechanical Engineering. All at the University of Arkansas, Fayetteville, Arkansas, 72701. (dsears@uark.edu).

Introduction: Ice plays a potentially critical role in determining the water cycle on Mars. It is widespread at relatively shallow depths, even at mid latitudes, and comes to the surface at the poles. It serves as a major reservoir that could be tapped for natural geological, climatological and biological processes, and for human planetary exploration. We have been measuring the properties of exposed ice in the presence of winds of various intensities and under various layers of unconsolidated regolith [1-7]. The main properties of interest are the diffusion of water vapor through the layers, and the adsorption and desorption of water vapor on the regolith particles. From such data it is possible to evaluate the ability of the regolith to act as a depository for atmospheric water vapor and the timescale on which adsorption and desorption occurs, which is important in understanding the role of the regolith on the diurnal cycle of water vapor in the atmosphere as it condenses in response to the diurnal atmospheric, surface and subsurface thermal cycle [8]. Such data also enable the determination of the effectiveness of regolith in stabilizing ice that may have formed during the last obliquity change.

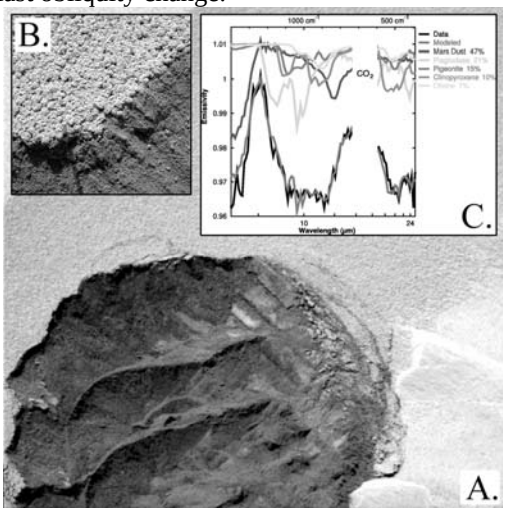

Fig. 1. A scuff mark caused by MER Spirit displays the very thin lighter dust layer on top of a darker regolith with grain sizes similar to those used in our experiments. In this case, the regolith is basaltic in composition. Wheel marks of the MERs, abundant dust devils, and global dust storms suggest that most of the surface of Mars is fine-grained unconsolidated material. [Images 2P132756681 EFF1957P2352L2M1 and 2M132842058EFF2000P2977 M2M1, refs. 9,10].

The present paper reviews our recent work on these topics. While our experiments have been performed in an effort to understand the environment of Mars, simple modifications to our procedures would allow us to gain data relevant to other solar system bodies.

Experimental: Our planetary chamber is a 0.61 m diameter 2.08 m high stainless steel vacuum chamber with cooling coils, heating cables, pressure gauges, hygrometers, and several ports for observation. Measurements are made by evacuating the chamber to less than 0.09 mbar, filling with dry CO_2 gas to 1 bar, and cooling to the desired temperature. The chamber was then opened, the sample placed on a top-loading balance, and the chamber evacuated to 7 mbar. The temperatures of the chamber are maintained $\leq$ 0°C to prevent melting of the ice. For experiments into the effect of wind, calibrated fans were installed in the chamber that produced velocities up to 11.4 m/s, typical of values observed by Viking. For the dust layer experiments we used blankets of mock regolith appropriate to Mars (Fig. 1); the JSC Mars simulant Mars-1 emulates the weathered volcanic dust (palagonite) abundant on Mars, montmorillonite clay mimics places on Mars where spectral data suggest clays to be important, and basalt represents that large amounts of Mars' surface covered with this third major component of the planet's surface. These samples were baked for one day at 102 to 104ºC and 35 mbar to eliminate adsorbed water. These experiments lasted 2 to 8 hours and, where necessary, the humidity was controlled by bleeding dry CO_2 into the atmosphere while pumping.

Discussion: If our experiments replicate Mars conditions, or can correctly be scaled to Mars, we can make the following observations.

Exposed ice: Like pure liquid water, and liquid brines, the evaporation rates of exposed ice under our experimental conditions exactly match those predicted by semi-empirical equations based on suitably modified forms of Fick's law for water vapor diffusing through a CO_2 atmosphere [11-13]. In fact, changes in evaporation rate associated with the melting and freezing of water over short time scales can be observed and reflect our high level of precision and accuracy in our experiments and the reliability of the theoretical treatments [12]. At the triple point of water, evaporation rates for water on Mars are 0.8 mm h^{-1} for the liquid and about half this much for ice.

Exposed ice affected by winds: At –15°C, and for relative humidities around 1%, sublimation rates in-

crease with wind velocity in a manner described by [14]:

$$E_S = 0.68 + 0.025\ V$$

Where E_S is the sublimation rate in mm h^{-1}, and V is the wind velocity in m s^{-1}. In high relative humidity atmospheres (30-35%), wind has an almost negligible effect on sublimation rate which remains nearly constant at 0.33 ± 0.04 mm h^{-1}. Pure forced convection theory [e.g. 15] fails to explain the data, so a new semi-empirical expression for the sublimation rate that combines free and forced convection was developed by ref. [14, their equation 22] using analogy with heat transfer models. Using this expression, sublimation rates of ice as a function of wind velocity for any temperature can be calculated. In general, temperature is more important than wind speed in determining the rate of sublimation of ice on Mars.

Ice covered with unconsolidated dust layers: The transport of water through a regolith layer is a complex process but one which can be quantified by laboratory measurements. In the absence of an external energy source such as solar insolation and a geothermal gradient, transport of water vapor is governed by diffusion through the dust layer (and the atmosphere at regolith depths <10 mm) and by adsorption and desorption of water on the grains[16-18].

In agreement with earlier work, we have found that diffusion of water vapor through these unconsolidated dust layers is rapid, with D values 1-4 x 10^{-4} m^2s^{-1}. Thus diffusion alone does not present a significant barrier in communication with the atmosphere at shallow depth. Therefore, only temperature controls the distribution of ice, which is most probably at equilibrium with the atmopshere. Adsorption does not play a significant role at long timescales, but can strongly affect the water diurnal cycle. It is the rate of adsorption and desorption that is important, and whether the regolith has the capacity to store sufficient condensed water vapor.

Adsorption and desorption of water vapor on basalt appear to be rapid enough for the regolith to respond to the diurnal cycle, and the amount of water vapor that can be adsorbed is sufficient to account for the diurnal cycle in water vapor in the atmosphere. Depths of a few centimeters of basalt powder are generally required to account for the variation in atmospheric humidity. Such depth are very easily reached due to high diffusion coefficients. Alternativley, while clays can store large amounts of water vapor, their kinetics of adsoprtion is much slower than basalt.

These laboratory derived kinetic data can be used to estimate the lifetime for water ice as a function of burial depth and temperature. For all three of the regolith materials investigated in our work to date ice would survive at mind-latitudes through years under several tens of centimeters of regolith, and under several meters would survive several times 10^5 years, that is since the time of the last major change in Mars' obliquity. However, temperature remains the most important parameter in determining the behavior and stability of ice under unconsolidated dust layers.

Conclusions: While the processes governing the behaviour of ice on Mars have been treated theoretically for some time, relatively few experimental studies existed prior to the present work and the required input parameters were poorly known. The data are still not complete for some materials, but a generally internally consistent picture is emerging. Diffusion of vapor through the dusty regolith resembling those observed on Mars (Fig. 1) is rapid and independent of mineralogy. Whether the regolith can be an important reservoir for water vapor and whether the condensation in the regolith explains the diurnal cycle depends on adsorption and desorption rates and storage capacity. The experimental work suggests that these mock regolith samples have the required properties to explain the diurnal cycle in water vapor. Subsurface ice is stable on Mars, especially under a meter or more of regolith, so that ice formed at the last major obliquity change can still persist. However, it should be stressed that main factor in determining the lifetime of surface and subsurface ice is temperature.

References: [1] Fanale F.P. & Cannon W.A. (1971) *Nature* **230**, 502-504. [2] Farmer C.B. (1976) *Icarus* **28**, 279-289. [3] Jakosky B.M. (1985) *Space Sci. Rev.* **41,** 131-200. [4] Smoluchowski R. (1968) *Science* **159**, 1348-1350 [5] Zent A.P. and Quinn R.C. (1997) *JGR* **102**, 9085-9095. [6] Schorghofer N. & Aharonson O. (2005) *JGR* **110**, doi:10.1029/2004JE002350, E05003. [7] Ulrich R. (2008) *Icarus* (sub.). [8] R. Ulrich, T. Kral, V. Chevrier, R. Pilgrim, & L. Roe (2008) *Icarus* (sub). [9] Herkenhoff K. E. & 22 others (2004) *Science* **305**, 824-826. [10] Christensen P.R. and 25 others (2004) *Science* **305**, 837-842. [11] Sears D.W.G. & Moore S.R. (2005) *GRL* **32**, doi:10.1029/2005GL023443, L16202. [12] Moore S.R. & Sears D.W.G. (2006) *Astrobiology* **6**, 644-650. [13] Sears D.W.G. & Chittenden J.D. (2005) *GRL* **32**, doi: 10.1029/2005 GL024154, L23203. [14] Chittenden J.D., Chevrier V., Roe L.A., Bryson K., Pilgrim R., and Sears D.W.G. (2008) *Icarus* (in press). [15] Hecht M.H. (2002) *Icarus*. **156,** 373-386. [16] Chevrier V., Sears D.W.G., Chittenden J.D., Roe L.A., Ulrich R., Bryson K., Billingsley L., & Hanley J., (2007). *GRL* **34**, doi:10.1029/2006GL028401, L02203. [17] Chevrier V., Ostrowski D.R. & Sears D.W.G. (2008). *Icarus* (sub.). [18] Bryson K. L., Chevrier V., Sears D.W.G. & Ulrich R. (2008) *Icarus* (in press).

Ion Irradiation Induced Electrostatic Charging Effects on Solar Ices. J. Shi[1], M. Famá[1] and R. A. Baragiola[1], [1]University of Virginia, Laboratory for Atomic and Surface Physics, Thornton Hall, Charlottesville, VA 22904-4238 (Contact email: raul@virginia.edu)

Introduction: Water ice is abundant on the surfaces of many objects in the outer solar system, where they are exposed to UV photons, solar wind, cosmic rays and energetic charged particles trapped by the planetary magnetic fields. Radiation effects induced by energetic ions in ice such as sputtering, secondary ion emission, amorphization of crystalline ice, compaction of microporous amorphous ice, and chemical radiolysis (molecular decomposition and synthesis) have been extensively studied in laboratory conditions [1-4]. In comparison, electrostatic charging effects on ice induced by ion irradiation have been barely studied and consequently the level of charging on icy astrophysical surfaces is relatively unknown. So far, no mission has landed on any icy object in space, and therefore there is no information on surface electric fields. For example, electrostatic charging of ice could be important for charged small ice particles in planetary rings because these particles are so small that electrostatic forces could be comparable to gravitation [5, 6].

The process of charge trapping starts with the creation of electron/hole pairs from the ionizing energy deposited by an incoming particle. Electrons that do not immediately recombine are much more mobile than holes. They can be trapped in the solid contributing to a negative charging, or can escape from the film (in times typically ~1 ps) resulting in secondary electron emission. They also can drain through the substrate and leave an excess of positive charges in the film. The holes are relatively immobile and can be easily trapped by localized defects or long-lived trapping levels (energy states located between the valence and conduction bands) resulting in an effective positive polarization. The electric field produced by the trapped charges is limited to the value at which dielectric breakdown occurs, as long as potentials are high enough to allow for cascade multiplication of electrons. The presence of an internal electric field can affect the energy and trajectory of ejected species such as secondary electrons and ions. One must also consider the hypothesis of a net electrical polarization of ice during condensation (ferroelectricity) [7]. However, should ferroelectricity exist in solar ices, it could be masked by charging effects induced by particle or UV irradiation.

Condensed gases are a convenient group of insulators to study charging effects; they are simple in composition (usually one type of molecule), can be easily vapor deposited to form thin films, and most of their physical properties can be measured with appropriate spectroscopy tools. Electrostatic charging effects in solidified noble gases caused by ion bombardment have been previously studied in our laboratory [8,9].

Here we propose a different approach to study charging effects on ice induced by ion bombardment, which is the measurement of the energies of ejected secondary ions. We bombarded ice films with 100 keV Ar^+ and measured the kinetic energy of secondary H_3O^+ sputtered from the surface for different film thicknesses and ion fluxes. The energy of the sputtered ions results a direct measurement of the ice surface potential induced by electrostatic charging.

Experiments: The experiments were conducted in a cryopumped ultra high vacuum chamber with a base pressure of ~10^{-10} Torr. Using a microcapillary array doser, 0.2 to 7 μm ice films were vapor deposited at 80K onto a Liquid Helium cooled gold-coated quartz crystal microbalance, which measures the mass column density of the films [10]. Mass analyzed ion beams of 100 keV Ar^+ were scanned uniformly over the sample. Secondary ions emitted at 45° from the surface where analyzed with a Hiden EQS 300 sector field electrostatic energy analyzer and quadrupole mass spectrometer. As soon as the ion beam is turned on, we observe a build up of the kinetic energy of secondary ions sputtered from the ice which eventually saturates. All measurements were taken at saturation conditions.

Results: [I] *Thickness Dependence*. Fig. 1 shows the dependence of the kinetic energy of the ionized protonated water molecule on film thickness. A typical energy scan for H_3O^+ is shown in the lower-right inset of this figure.

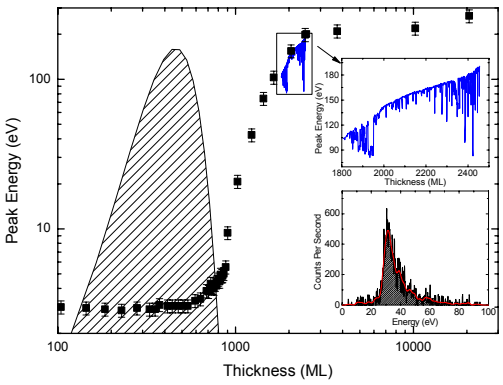

Figure 1 *Peak H_3O^+ energy vs. ice film thickness. Films were grown at 80K and the ion energy was measured using a flux of 7.8x10^{11} $Ar^+cm^{-2}s^{-1}$. The shaded area is the range distribution of the projectiles calculated with TRIM. The lower-right inset shows a typical energy distribution scan. The energy of secondary ions abruptly decreases when dielectric breakdown occurs, shown in the upper-right inset.*

For thicknesses below the maximum range of the projectiles ~600 monolayers (ML), the kinetic energy of the emitted ions is relatively constant and between 4~5 eV. We assume this is the intrinsic kinetic energy value for the secondary H_3O ions due to sputtering. For film thicknesses larger than the maximum projectile range, the kinetic energy of the secondary ions rises sharply up to hundreds of eVs, saturating for thicknesses greater than 1800ML. Above this thickness the surface potential reaches ~150 V and the corresponding internal electric field a value of ~2.5 MV/cm, similar to the dielectric strength of ice, and dielectric breakdown occurs as shown in the upper-right inset. Between 600ML and 1800ML, the peak energy increases linearly with a slope of ~0.05 eV/ML.

[II] *Discharging*. When the beam is turned off the ice starts to discharge through self-drifting of the charges to the substrate due to the electric field they generate. We measured the H_3O^+ kinetic energy as a function of time since the beam was turned off, but using an ultra low flux of 100 KeV Ar ions to avoid additional charging up of the films. An example of discharging is shown in Figure 2.

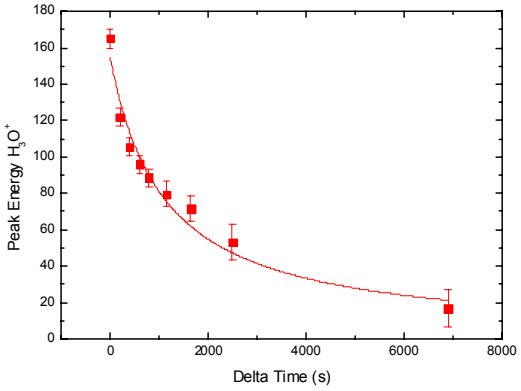

Figure 2 *Discharging of saturated charged ice films by ion irradiation.*

[III] *Temperature Effects*. We studied the temperature dependence of the kinetic energy of secondary ions by changing the ice temperature from 20 to 140 K and vice versa. For ices grown and measured at 130K (crystalline phase) the secondary ions are sputtered at energies corresponding to their intrinsic values (~4 to 5 eV), as seen in Figure 3. Cooling these ices down to 20K increases the kinetic energy of secondary ions up to ~20 eV. By increasing the ice temperature back to 130-140K the secondary ion energies return to their original values. Using a different approach, we repeated these measurements for films grown at 80K and annealed up to 130K. The results are not reversible as shown in the inset of Figure 3.

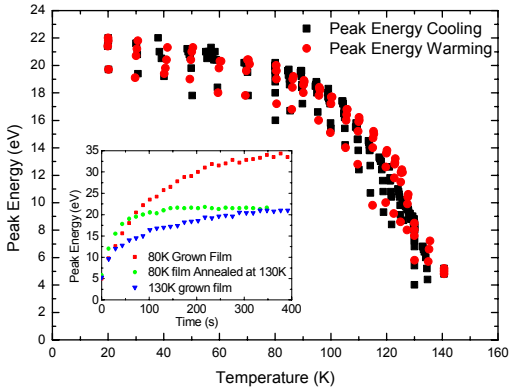

Figure 3 *Temperature dependence for peak energy of H_3O^+. Inset: Time dependence of charging of films grown at 80 K before and after annealing at 130K.*

[IV] *Ferroelectricity*. To test the ferroelectric properties of vapor deposited ice, we examined the charging up curves of 2500ML films grown at 40K, at very low ion fluxes. We found that the initials scans of the secondary ion energies do not show a secondary ion signal immediately; but require an incubation time. An extrapolation of the peak energy to zero fluences gives a negative initial offset for the potential of the ice surface. This value is similar to those found in ferroelectricity studies [11].

Discussion: Icy surfaces in the solar system are susceptible to charging effects due to energetic particle irradiation. The voltage created at the surface is limited by the drifting of charges due to the internal electric field they generate.

References: [1] Baragiola, R.A. (2003) *Planet. Sp. Sci. 51,* 953-961. [2] Orlando, T.M. and Sieger, M.T. (2003) *Surf. Sci., 529,* 1. [3] Raut, U. et al. (2007) *J. Chem. Phys., 126,* 244511. [4] Famá, M. et al. (2008) *Surf. Sci., 602,* 156. [5] Jurac, S. et al. (1995) *J. Geophys. Res. 100,* 14821 [6] Mitchell, C.J. et al. (2006) *Science, 311,* 1587. [7] Su, X. et al. (1998) *Phys. Rev. Lett. 80,* 1533. [8] Baragiola, R.A. et al. (1998) *Phys. Rev. B 58*, 13212. [9] Grosjean, D.E. et al. (1999) *Nucl. Instr. Meth. B, 157,* 116. [10] Bahr, D. et al. (2001) *J. Geo. Res., 106,* 332865. [11] Iedema, M.J. et al. (1998) *J. Phys. Chem. 102,* 9203.

ABRASION SUSCEPTIBLITY OF ULTRA-COLD WATER ICE: PRELIMINARY MEASUREMENTS OF ABRASION RATE, TENSILE STRENGTH AND ELASTIC MODULUS.

Leonard S. Sklar[1], Peter Polito[1], Beth Zygielbaum[1], and Geoffrey C. Collins[2], [1]Dept. of Geosciences, San Francisco State University, San Francisco CA 94132, [2]Physics and Astronomy Dept., Wheaton College, Norton MA 02766. leonard@sfsu.edu

Introduction: Images of the surface of Titan obtained by the Cassini mission have revealed a remarkably earth-like surface morphology, with branching channel networks, meandering river valleys, and finely-dissected ridge and valley topography [1-3]. Fluvial erosional processes likely play a major role in modifying Titan's surface, raising the question of whether we can apply process models developed for fluvial bedrock incision on earth to ultra-cold conditions on Titan, where liquid methane is cutting into water ice.

The saltation-abrasion bedrock incision model, developed by *Sklar and Dietrich* [4] is sufficiently explicit in its representation of the physics of rock detachment by low-velocity sediment impacts to be scaled to Titan considitions [5]. The model treats erosion as proportional to the flux of kinetic impact energy delivered to the river bed by saltating bedload sediments. Wear of brittle-elastic materials by repeated low-veocity impacts occurs by the growth and intersection of a network of fractures. The energy required to detach a unit volume of rock (ε_v) is proportional to the material strain energy, which depends on tensile strength (σ_T) and the modulus of elasticity (E)

$$\varepsilon_v = K_v \frac{\sigma_T^2}{2E} \qquad (1)$$

where the constant of proportionality (K_v) is a dimensionless abrasion susceptibility coefficient. *Sklar and Dietrich* [6] established experimentally that for a wide variety of terrestrial rock, K_v is a constant ~10^6 to first order, but varies somewhat depending on the relative strength and surface geometry of the bedrock and impacting sediment particles.

Impact tests on sea ice [7] have shown that the erosion rate of water ice is also proportional to impact energy, suggesting that ultra-cold water ice can be modeled with equation 1. To estimate the value of K_v for water ice under Titan conditions, *Collins* [5] conducted simple drop tests with ice samples cooled with liquid nitrogen, and found K_v to be ~10^4, suggesting that water ice is roughly 100 times more erodible than rock of similar strength. However, these tests were not conclusive, in part because we lack measurements of σ_T and E measured at ultra-cold temperatures, far from the melting point of ice.

Here we report preliminary results of an experimental program to measure rates of water-ice erosion by ice sediment impacts, as well as water-ice material properties, from near melting point down to the ~90 °K conditions that prevail on Titan.

Making and testing water-ice "bedrock": To create consistent, poly-crystalline ice, we freeze clear blocks from boiled-distilled water, which we then crush and sieve to obtain uniform-sized seed crystals ranging from 1 to 4 mm. The seed crystals are packed into cylindrical and disk-shaped molds, which are then filled with near-freezing water. The molds have copper bottoms and insulated sides and tops, to force the water to freeze from the bottom up, preventing any bubbles and large fractures from forming.

We use the 50mm-diameter cylinders for "Brazilian" tensile-splitting strength tests [6], in which samples are loaded on a line parallel to the cylinder axis to cause tensile failure. Ice cylinders are also loaded in axial compression for measurements of elastic modulus. We use dry ice and liquid nitrogen to control sample temperature, and have conducted tests both in air and submerged in ethanol; we will submerge samples in liquid nitrogen to reach the coldest temperatures.

To reproduce the sediment particle impacts that drive fluvial incision, we have constructed an apparatus for repeatedly dropping an ice clast from a known height onto an ice disk target. The 20cm-diameter, 10cm-thick disks are placed in the bottom of a cylinder, which is encased in a

larger cylinder that can hold dry ice or liquid nitrogen (figure 1). We use balloons as molds to make spheroidal ice sediment clasts, and position lead weights suspended from Kevlar strings in the balloon center before adding ice seed crystals and water in a freezer. In the test apparatus, the string is used to raise the clasts to a known height before releasing, while the lead weights allow control of the buoyant density of the ice clasts for submerged drop tests. We will conduct drop tests in air and submerged in ethanol and liquid nitrogen. After a sequence of drops from a fixed height, any liquid is drained off, eroded fragments are vacuumed from the disk surface, and the disk is weighed from a suspended balance. Volume eroded per impact energy can be calculated from the change in disk mass and the clast mass, and impact velocity.

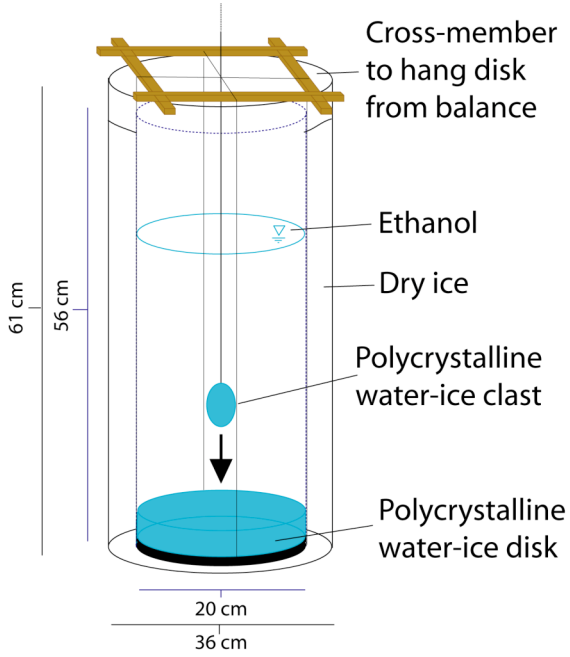

Figure 1. Schematic of drop test apparatus for measuring erosion of ice disks due to multiple impacts of water ice sediment clasts.

Preliminary experimental results: To date we have obtained measurements of ice tensile strength over temperatures ranging from -5 to -75 °C, for two grain-size ranges, in both air and submerged in ethanol (figure 2). These preliminary data suggest a linear increase in tensile strength down to about -50 °C, below which strength may become insensitive to further reductions in temperature.

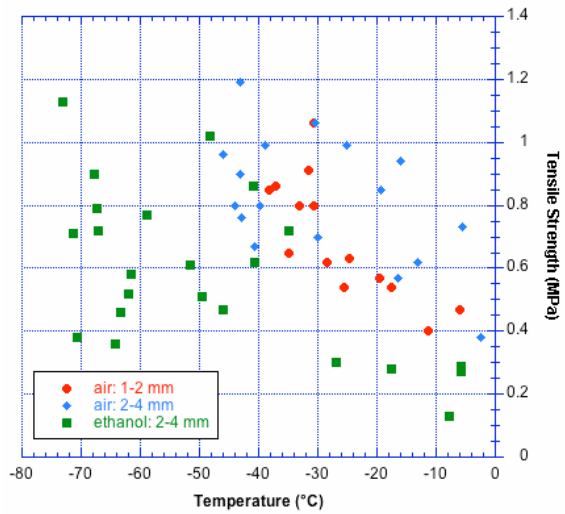

Figure 2: Preliminary measurements of variation in ice tensile strength with temperature.

Applications to planetary geomorphology: Understanding the controls on ice strength and abrasion susceptibility will not only help parameterize the saltation-abrasion fluvial incision model for application to Titan, but will be useful for interpreting many other geomorphic processes and features on Titan as well as on Mars. For example, the efficiency of fluvial erosion by suspended particles, and erosion by aeolian processes, should depend on abrasion susceptibility. The width and sinuosity of bedrock channels on earth are sensitive to rock strength, as is the rate of knickpoint propagation [8]. Strength also plays a role in the debate over the importance of sapping in creating amphitheater headed valleys [9].

References: [1] Lorenz et al. (2006) *Science* 312, 724-727; [2] Tomasko et al. (2005) *Nature* 438, 765-778; [3] Elachi et al. (2005) *Science* 308, 970-974; [4] Sklar and Dietrich (2004) *Water Resour. Res.* 40, W06301; [5] Collins (2005) *Geophys. Res. Lett.* 32, L22202; Collins et al. (2008) this meeting; [6] Sklar and Dietrich (2001) *Geology* 29, 1087-1090; [7] Timco and Frederking (1993) *Cold Regions Sci. Tech.* 22, 77-97; [8] Whipple et al. (2000) *GSA Bull.* 112, 490-503; [9] Lamb et al. (2006) J. Geophys. Res. 111, JE002663.

Acknowledgements: This work is supported by grant NNX07AL26G from the Outer Planets Research Program.

CONVECTION IN ICY SATELLITES: MODELS AND CONSTRAINTS FROM LABORATORY EXPERIMENTS. C. Sotin[1], G. Tobie[2], P. Duval[3], [1]Jet Propulsion Laboratory and California Institute of Technology, Pasadena, USA, [2]Laboratoire de Planétologie et Géodynamique, Université de Nantes, Nantes, France. [3]Laboratoire de Glaciologie et Géophysique de l'Environnement, UMR-CNRS 5138, Saint Martin d'Hères, France. [Christophe.Sotin@jpl.nasa.gov]

Introduction: The question of subsolidus convection in the outer icy shell of the icy satellites is important for the understanding of their internal structure, their evolution, and the relationships between a possible liquid layer (ocean) and the surface. Heat transfert by convection is controlled by viscosity of ice I. The value of this parameter has been determined by observations of terrestrial glaciers and by laboratory experiments. It depends on a number of parameters including temperature, deviatoric stress, grain size and the presence of impurities. For the last 20 years, progresses in the modelling of thermal convection have lead to a better understanding of this process.

Description of the convection process: The Galileo mission returned data that suggest that an ocean is present at depth below the outer ice I layer of the icy Galilean satellites Europa, Ganymede and Callisto. In addition, the moment of inertia of both Europa and Ganymede suggest that they are fully differentiated (Figure 1).

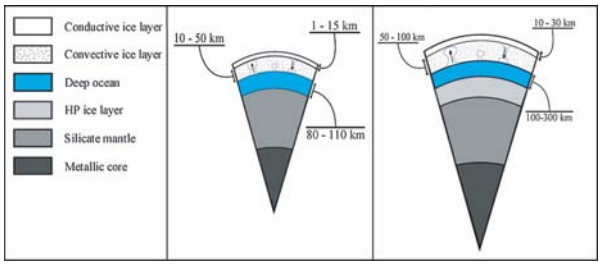

Figure 1: Internal structure of Europa (left) and Ganymede (right). Figure from [1].

It is believed that, after the accretion, the large icy satellites differentiated into a rocky core and an outer H_2O layer which was composed of an outer ice I layer, a liquid layer and a solid layer of high-pressure phases of ice. This structure is dictated by the phase diagram of water ice (Fig. 2). Because the ice I layer is cooled from above with a temperature at the ice/liquid interface equal to the freezing temperature, this layer may become unstable to convection [e.g. 2] with hot plumes forming at the hot thermal boundary layer (Fig. 3). Because viscosity of ice is very strongly temperature dependent, convection is in the so-called 'conductive lid regime': the convective interior is overlaid by a conductive layer where most of the temperature variations take place. The presence of this conductive lid limits the amount of heat that can be removed through the ice layer. Once stationary state is achieved, the hot thermal boundary layer is quite thin.

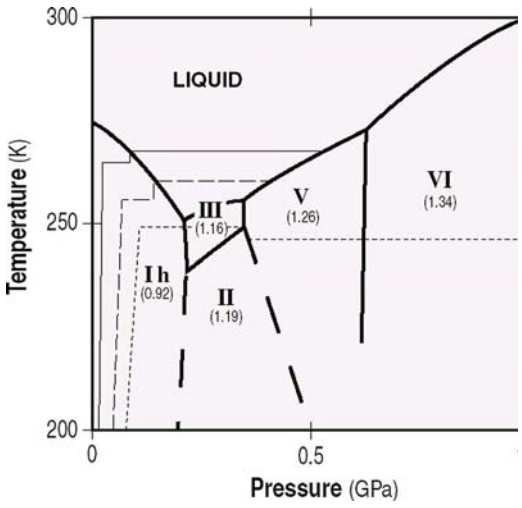

Figure 2: Phase diagram of water ice with temperature profiles to illustrate the structure described in Fig. 1.

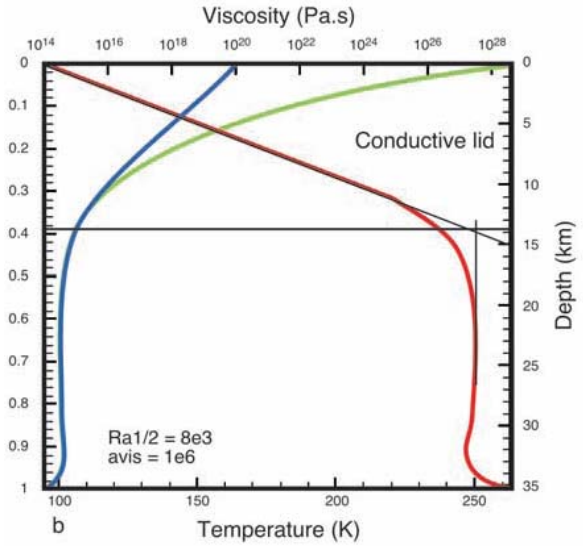

Figure 3: Example of a temperature profile and viscosity profile in Ice Ih (cf Fig. 2).

Amount of heat transferred by convection: The total amount of heat that can be removed by convection must be compared with the difference heating sources of heating. For example the decay of the long-lived radiogenic elements can be estimated (Figure 4)

based on the total amount of silicates. Other heating sources include the cooling of the satellite and the latent heat when liquid water freezes due to global cooling.

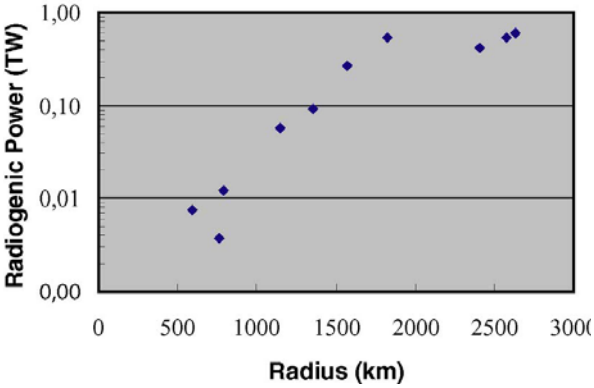

Figure 4: Radiogenic power versus size of the satellite for the mid-sized saturnian satellites and the large icy satellites.

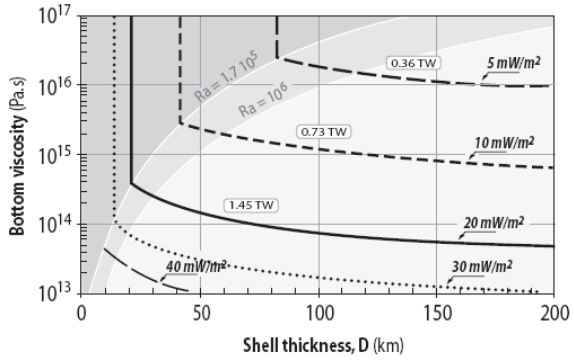

Figure 5: Amount of power that can be transferred by convection as a function of the shell thickness and the viscosity at the solid/liquid interface (numbers are for Callisto).

The comparison between Figure 4 and Figure 5 shows that if the viscosity of ice at its melting point is lower than 10^{15} Pa.s, then convection can transfer more heat than that produced by the decay of the radiogenic elements. In this case, the difference between the heat that is transferred and the radiogenic heat gives the cooling rate. For a viscosity of 10^{14} Pa.s, it takes some 100s of My for the ocean to freeze.

But the viscosity at the melting point can vary if impurities are present in the liquid phase (ammonia for example) and an equilibrium thickness can be reached [3].

An additional heat source can be tidal heating for icy satellites that have (or had) eccentric orbits. Titan has still a large eccentricity (on the order of 3%) but is far from Saturn. Europa has a smaller eccentricity but is closer to Jupiter and tidal heating is the largest among the icy satellites (Figure 6). If viscosity is optimum, the amount of heat can be more than one order of magnitude larger than radiogenic heating.

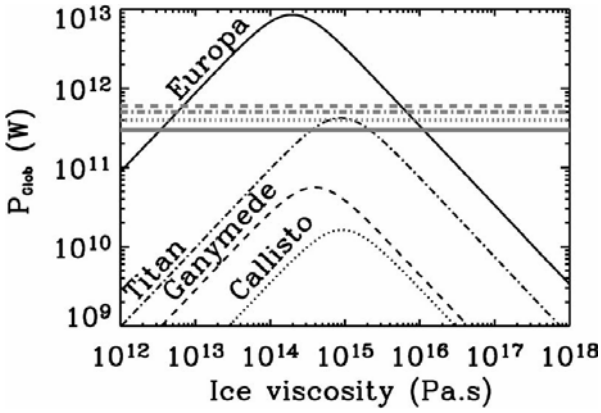

Figure 6: Tidal heating versus ice viscosity for the largest icy satellites.

Tidal heating depends very strongly on viscosity. If viscosity is too small, friction does not provide a lot of heat. If viscosity is too large, deformation is very limited and little heat can be produced. There is an optimum viscosity which is on the order of the viscosity of ice at its melting point according to glacier measurements. One important aspect of tidal deformation is to understand the attenuation process in the ice as it undergoes cycling stresses during the orbit of the satellite around the giant planet. Is the viscous process identical to that operating for convection and how convection stresses and tidal stresses interact to control properties such as dislocation densities and grain size.

Tidal heating is internal heating. Models of convection with homogeneous volumetric heating suggest that convection is controlled by the formation of cold plumes at the cold thermal boundary layer. However, tidal heating is not homogeneous because it depends on viscosity. It can locally produce partial melt. Because liquid water is denser than ice, the melt would migrate downward, replenishing the liquid reservoir. This process may have important implications for the evolution of Enceladus and Europa.

Conclusion and Perspectives: Viscosity of ice is a key parameter that controls the internal dynamics and evolution of icy satellites. Laboratory experiments are necessary to provide the parameters that will be included into models of the internal dynamics of icy satellites in order to explain observations made by missions to the outer planets.

Bibliography : **[1]** Sotin C. and TobieG. (2004), CRAS-Physique, 5, 769. et al (2003), *Icarus, 164, 461*. **[2]** Barr A. et al. (2004), JGR, 109. **[3]** Deschamps F. and Sotin C. (2001), JGR, 106. **[4]** Sotin C. et al. (2002), GRL, 29.

GANYMEDE'S IMPACT CRATER MELKART: AN EXAMPLE FOR A COMBINATION OF HIGH-RESOLUTION SPECTRAL AND GEOLOGICAL ANALYSES IN THE OUTER SOLAR SYSTEM. K. Stephan[1], R. Wagner[1], C.A. Hibbitts[2], G.B. Hansen[3], R. Jaumann[1], [1] DLR, Inst. for Planet. Res. Rutherfordstrasse 2, 12489 Berlin, Germany, [2]Applied Physics Laboratory, Laurel, MD, USA, [3] Planetary Science Institute, 22 Fiddler's Rd., Winthrop WA 98862-0667, USA (Katrin.Stephan@dlr.de).

Introduction: Despite the identification of the spectral, i.e. the chemical and physical properties of an icy satellite's surface it is essential to know their spatial distribution in order to identify the source of specific compounds or physical properties. Since the Galileo mission hyperspectral mapping spectrometers have been produced so-called "image cubes" that relate individual spectra to specific areas on the planetary surface in the outer solar system with sufficient pixel ground resolution. They allow attributing surface properties to specific points on the planetary surface e.g. geological and morphological surface features.

The Jovian satellite Ganymede is a unique object to study relationships between chemical and physical surface properties and geological and/or morphological surface features. Esp. geological features like impact craters of various surface composition, sizes, morphologies and crater retention ages as well as tectonic surface features (e.g. Sulci) are of special interest. Additionally, Ganymede's magnetic field offers the exclusive opportunity to study the effects of incoming energetic particles from Jupiters' magnetosphere upon the surface properties.

However, spatial highly-resolved spectral (and imaging) data are very rare and concentrated more or less completely on the anti-Jovian hemisphere up to now. Only two local regions were simultaneously observed by the Near Infrared Mapping spectrometer (NIMS) [1], acquiring spectra between 0.7 and 5.2 µm, and the Galileo Solid State Imaging (SSI) camera [2] with relatively high spatial resolution. We chose the NIMS observation of the impact crater Melkart at 10°S/ 186°W, illustrating the potential to combine high resolution data to investigate its spectral properties as well as the stratigraphic position, morphology, and relative and absolute crater retention age.

Geological and spectral characteristics of Melkart: Melkart is one of Ganymede's central dome craters with a diameter of 105 km. It is partly located within the dark ancient cratered terrain of Marius Regio and within the younger bright grooved and smoothed terrain (small area extending from southern Sippar Sulcus). A linear tectonic feature characterizes the transition between the two different substrates across the crater area. Figures 1 and 2 show results of analyzing the NIMS observation G8GNMELKART (spatial resolution of ~5 km per pixel) with respect to the simultaneously acquired Galileo SSI image (global context is provided by Voyager images). In general, the NIMS spectra of the crater deposits show a mixture of water ice and rocky non-ice contaminant (including the absorption of CO_2 at 4.25µm. Two spectral endmembers could be defined in the observed area. Spectra with a relatively high amount of water ice and weak absorptions of CO_2 (band depth of about 10%) characterizes the impact crater itself and the region of the bright grooved and smoothed terrain, whereas Marius Regio exhibits a distinct higher spectral influence of the dark rocky contaminant(s) and a deeper CO_2 absorption (band depth of max. 26%). No spectral variations occur that distinctly separate the impact crater itself from its substrate (i.e. the bright grooved terrain). This is consistent with Melkart's relatively high crater retention age of max. 3.77 Gyr (3.85 Gyr on the crater floor) [3, 4]. This corresponds to the crater retention age derived for the grooved and smoothed terrain in general of about 3.6 - 3.9 Gyr [5] and an advanced equalization of the spectral properties between impact crater and substrate due to space weathering processes including impacts of micrometeoroids and thermal sublimation processes.

In addition, there are no variations between the crater material and the dome material. Only towards the crater rim which is located within Marius Regio the abundance of water ice is decreasing. However, this does not correspond exactly with the tectonic border between the younger bright grooved and the ancient dark terrain. Darker material within the impact crater is supposed to be the result of later mass wasting processes of darker material originating in Marius Regio into the crater area rather than of the impact itself. This indicates that in deeper regions (<10km) no distinct variations between the two major terrain types of Ganymede occur supporting the results of [6] that the dark material only represents a thin veneer of dark material over an icy crust.

Sizes of the water ice particles do not vary distinctly within the entire observed region. All spectra exhibit particle radii of ~ 200 µm distinctly larger than measured for fresh impact craters (~10µm) [7]. Melkart's particle radii correspond to the global distribution of particle radii derived for the anti-Jovian hemisphere at latitudes of ~ 10°S [7] and are supposed to be caused by sublimation processes that dominate the equatorial region of Ganymede.

Conclusions: The impact crater Melkart represents an example for the combined analysis of high-resolution spectra and imaging data. These data make it possible to map spectral variations not only of the impact crater correlation to the specific substrate but

also within the impact crater itself. Comparable data of impact craters on Ganymede could give more inside into the impact process itself. Especially, observations of fresh impact craters could reveal the source of volatiles in the surface material on Ganymede like CO_2.

References: [1] Carlson, R. W. et al., *SSR*., 60, 457-502, 1992; [2] Belton, M. J. S. et al., *SSR*, 60, 413-455, 1992, [3] Stephan, K. et al., *LPSC XXXIV*, abstract No. 1687, 2003; [4] Wagner, R. et al., *LPSC XXIX*, abstract No. 1818, 1999; [5] Neukum, G. et al., *LPSC XXX*, abstract No. 1742, 1998; [6] Stephan, K. et al., *LPSC XXXVI*, abstract No. 2061, 2005 [7] Prockter, L. M. et al., *Icarus*, 135, 317-344, 1998.

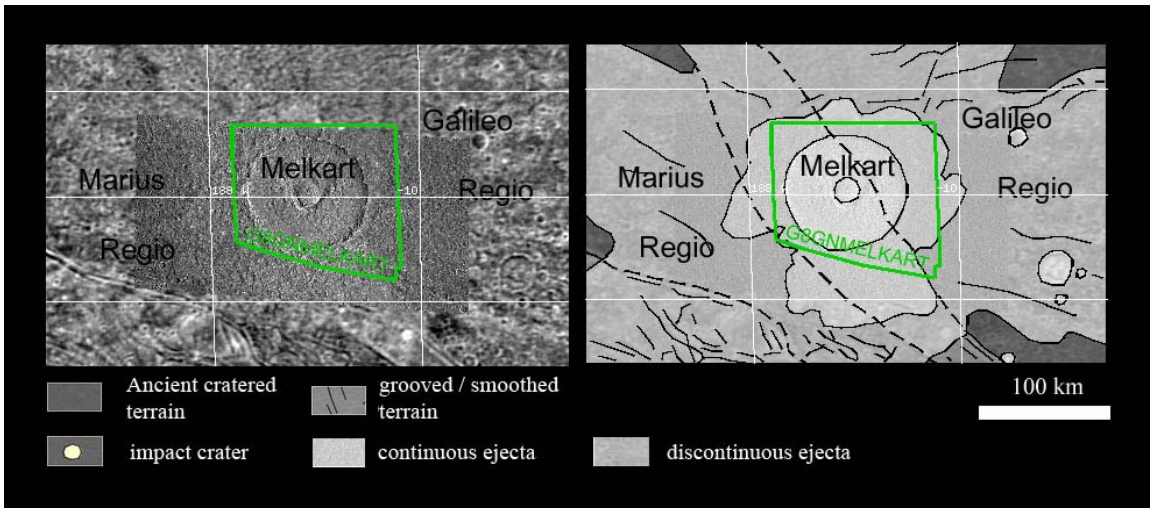

Figure 1: Geological context of the NIMS observation G8GNMELKART

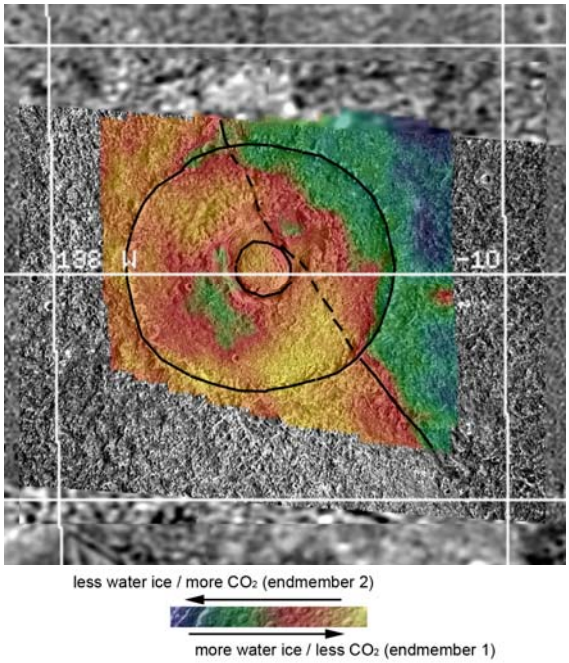

Figure 2: Distribution of the two spectral endmembers (see text) in the observed region.

WHAT WE WANT TO KNOW ABOUT ICES FOR UNDERSTANDING THE STRUCTURE AND EVOLUTION OF ICE-RICH BODIES. D. J. Stevenson[1], [1]Division of Geological and Planetary Sciences, California Institute of Technology, Pasadena, CA, Email: djs@caltech.edu.

I will discuss the three kinds of material properties that we need to model the interiors of ice-rich bodies: Thermodynamics, transport properties, and kinetics (to the extent that this is not already implicit in transport properties). The most important thermodynamic issues that remain imperfectly understood concern phase equilibria of impure ices (including partial melting). The most important transport properties are thermal conductivity and rheology (i.e viscosity). However, these depend in turn on kinetics (e.g., what determines grain size?). One cannot necessarily write the effective viscosity merely as a function of temperature and stress. A prime example of a challenge is the response of ice to periodic loading on tidal time scales (i.e the complex Love number as a function of everything) since this figures prominently in our understanding of Europa, Enceladus and probably many other bodies.

ADVANCES IN MODELING COLLISIONS ON ICY BODIES. S. T. Stewart and L. E. Senft. Department of Earth and Planetary Sciences, Harvard University, 20 Oxford Street, Cambridge, MA 02138 (sstewart@eps.harvard.edu).

Introduction: Impact cratering is one of the major geologic processes on the icy planets and satellites in the outer solar system. The outcome of impact calculations have been used to suggest the presence of transient liquid water after cratering events [1-4] and to infer the thickness of brittle crusts [5]. These studies rely heavily on the accuracy of (1) the model equation of state of H_2O to infer the post-impact temperature field and the occurrence of phase changes and (2) the constitutive model to describe the shear and tensile strengths and the degradation of strength with damage. Here, we summarize recent advances in the quality of equation of state and constitutive models for H_2O and implications for collisional processes on icy bodies.

Equation of State Models: Because of the complexity of the H_2O phase diagram, most equation of state (EOS) models used in hydrocode calculations have been tailored to specific phases with little or no ability to extend calculations to broad regions of the phase diagram. In general the phase diagram is simplified, with one solid phase, liquid, and vapor (with simplified dissociation). Recent development includes an ANEOS-based multiphase equation of state that includes all of the stable solid phases [6].

We have developed a new tabular equation of state for H_2O [7]. The table includes three solid phases (ices Ih, VI, and VII), liquid, and vapor. The EOS of the phases and phase boundaries are experimentally determined. The liquid and vapor are described by the International Association for the Properties of Water and Steam (IAPWS) [8]. The equation of state of ice Ih is given by [9]. The equation of state of ices VI and VII are taken from [10], and the phase boundaries are given by [8, 11]. The model shock Hugoniots are compared with experimental Hugoniots in Fig. 1.

A crucial experimental data set that has been lacking for equation of state model validation is shock temperature measurements starting in the ice phase (shock temperatures in liquid water has been measured by [12, 13]). In the Shock Compression Laboratory at Harvard, we have new peak-shock and post-shock temperature measurements in polycrystalline ice Ih in the peak shock pressure range of 8 to 14 GPa [14]. Peak shock temperatures range from 650 to 1000 K.

The post-shock temperature provides direct information about the onset and kinetics of shock-induced phase changes. Upon release from shock pressures of 8 to 14 GPa, the continuum temperature of ice is 373 to 550 K.

Our tabular EOS is in excellent agreement with all of the shock and post-shock temperature data on liquid water and ice Ih.

Strength Model: The strength model describes the response of a material to deviatoric stresses; we develop new strength parameters for H_2O based on laboratory data. We use the strength model developed by [15] and implemented into the CTH shock physics code by [16]. In this model, shear strength is linearly degraded from an intact strength value (strength controlled by the creation of new fractures) to a fragmented (strength controlled by dry friction) value. A dimensionless scalar variable (damage) is introduced to track this degradation; damage ranges from zero (completely intact) to one (completely fragemented). Thus, shear strength is a function of damage, temperature, and pressure, and tensile strength is a function of damage.

Strength parameters are chosen by fitting to quasi-static laboratory test data. We use uniaxial compressive strength temperature dependence data from [18], friction data from [19], dynamic tensile strength data from [20], and triaxial shear strength data from [21]. Fig. 2 shows the shear strength data of intact (non-damaged) ice from [21] (circles) and the shear strength data of fragmented (damaged) ice from [19] (triangles). Note that the strength of ice has a strong temperature dependence. We fit a temperature degradation function to uniaxial compression data from [18] and use this to calculate the strengths at other temperatures. For example, the intact and damaged shear strength curves at 210 K are shown. The method outlined above assumes that the temperature dependence for uniaxial compressive strength is the same as the temperature dependence at higher pressures and that intact and fragmented ice have the same temperature dependences. In reality, this is not true; for instance, the coefficient of friction of ice is not significantly temperature dependent until very close to the melting point, and also depends upon a number of other neglected factors (such as strain rate).

Measurements of fresh complex craters on the icy satellites show that these craters are in general much shallower than their lunar counterparts [25, 26], which is expected as a result of the very low coefficient of friction of ice (~0.2 for cold ice, 77 K) as compared to rock (~0.6). It has been shown that icy layers can significantly shallow depth to diameter ratios [7, 27]. Furthermore, crater collapse may be aided by frictional melting processes [28]. At a temperature of -10° C, the coefficient of friction of ice approaches 0.001 as the sliding velocity along the fault approaches 1 m/s. Note that the friction coefficient also depends on temperature, but there is a lack of data for high sliding velocities and low temperatures; thus, it is unclear how much heating needs to occur for frictional melting to play a role in crater collapse on icy bodies. An alternative approach is to model crater collapse on icy bodies using acoustic fluidization [29].

Summary: We have developed a new multi-phase equation of state for water. We have also developed strength parameters to model ice over a wide range of conditions. With these advances, we are now able to model collisions throughout the solar system with much better accuracy.

References: [1] Artemieva, N. and J.I. Lunine (2005) *Icarus* **175**(2), 522-533. [2] Artemieva, N. and J. Lunine (2003) *Icarus* **164**(2), 471-480. [3] Pierazzo, E., N.A. Artemieva, and B.A. Ivanov (2005) *Geological Society of America Special Paper* **384**, 443-457. [4] Stewart, S.T., J.D. O'Keefe, and T.J. Ahrens (2004) *Shock Compression of Condensed Matter -- 2003*, American Institute of Physics: Melville, NY, p. 1484-1487. [5] Turtle, E.P. and E. Pierazzo (2001) *Science* **294**(5545), 1326-1328. [6] Ivanov, B.A. (2005) *LPSC* **36**, Abs. 1232. [7] Senft, L.E. and S.T. Stewart (submitted) *Meteoritics & Planetary Science*. [8] Wagner, W. and A. Pruss (2002) *Journal of Physical and Chemical Reference Data* **31**(2), 387-535. [9] Feistel, R. and W. Wagner (2006) *Journal of Physical and Chemical Reference Data* **35**(2), 1021-1047. [10] Stewart, S.T. and T.J. Ahrens (2005) *JGR* **110**, E03005. [11] Frank, M.R., Y.W. Fei, and J.Z. Hu (2004) *Geochimica et Cosmochimica Acta* **68**(13), 2781-2790. [12] Kormer, S.B. (1968) *Soviet Physics USPEKHI* **11**(2), 229-254. [13] Lyzenga, G.A., et al. (1982) *Journal of Chemical Physics* **76**(12), 6282-6286. [14] Stewart, S.T., A. Seifter, and A.W. Obst (2008) *LPSC* **39**, Abs. 2301. [15] Collins, G.S., H.J. Melosh, and B.A. Ivanov (2004) *Meteoritics and Planetary Science* **39**(2), 217-231. [16] Senft, L.E. and S.T. Stewart (2007) *Journal of Geophysical Research* **112**(E11), doi: 10.1029/2007JE002894. [17] Cohn, S.N. and T.J. Ahrens (1981) *Journal of Geophysical Research* **86**(B3), 1794-1802. [18] Arakawa, M. and N. Maeno (1997) *Cold Regions Science and Technology* **26**, 215-229. [19] Beeman, M., W.B. Durham, and S.H. Kirby (1988) *Journal of Geophysical Research* **93**(B7), 7625-7633. [20] Lange, M.A. and T.J. Ahrens (1983) *Journal of Geophysical Research* **88**(B2), 1197-1208. [21] Sammonds, P.R., S.A.F. Murrell, and M.A. Rist (1998) *Journal of Geophysical Research* **103**(C10), 21,795-21,816. [22] Griffith, A.A. (1920) *Philosophical Transactions of the Royal Society of London A* **34**, 137-154. [23] Housen, K.R. and K.A. Holsapple (1990) *Icarus* **84**, 226-253. [24] Housen, K.R. and K.A. Holsapple (1999) *Icarus* **142**, 21-23. [25] Schenk, P.M. (2002) *Nature* **417**, 419-421. [26] Schenk, P.M. (2007) *Ices, Oceans, and Fire: Satellite of the Outer Solar System Conference*, Abs. 6025 [27] Senft, L.E. and S. T. Stewart (2007) *Workshop on Impact Cratering II*, Abs. 8008 [28] Senft, L.E. and S. T. Stewart (2008) *LPSC* **39**, Abs. 1417 [29] Bray, V.J., G.S. Collins, J.V. Morgan, and P.M Schenk (2007) *Workshop on Impact Crater II*, Abs. 8056.

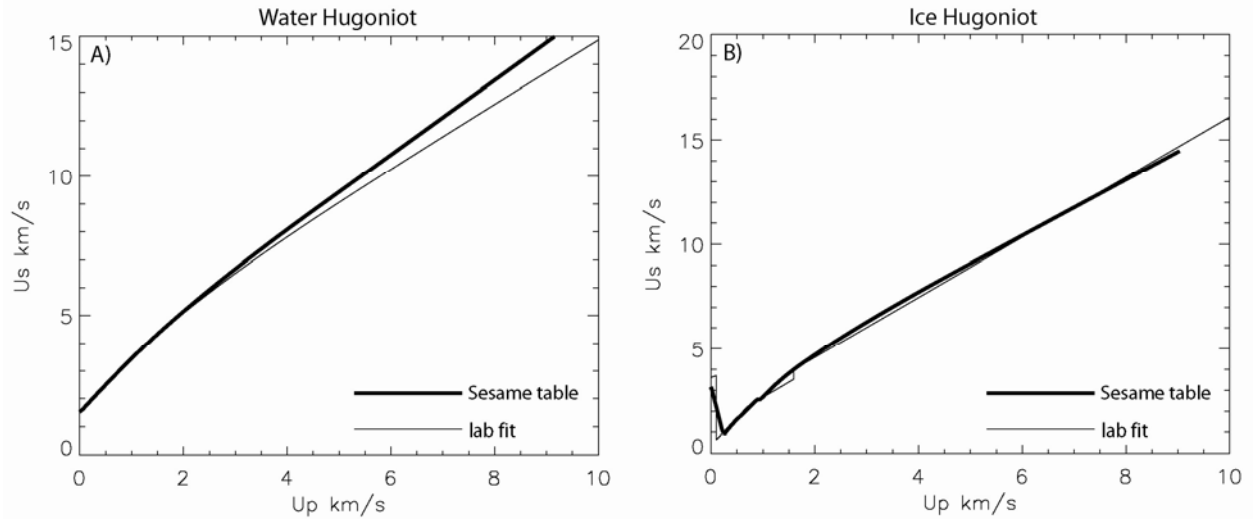

Fig. 1. Hugoniots for water (A; initial temperature of 300 K) and ice (B; initial temperature of 250-263 K) calculated from our Sesame table for H_2O (thick lines) compared to lab hugoniots (thin lines) from [10]. U_s is shock velocity, U_p is particle velocity.

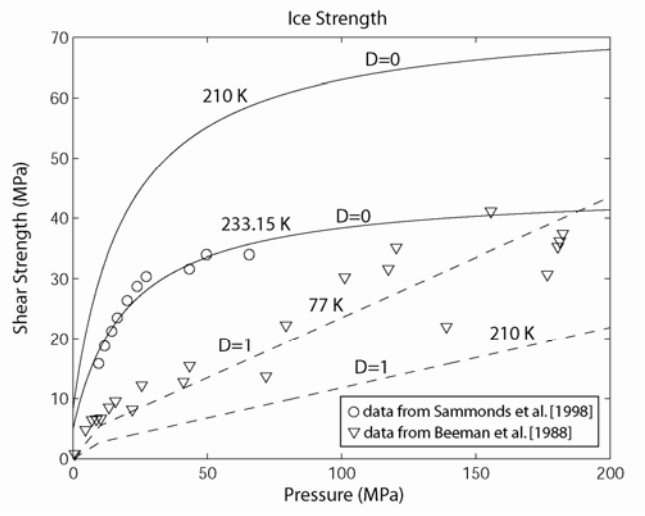

Fig. 2. Shear strength (in terms of the square root of the second invariant of the deviatoric stress tensor, $\sqrt{J_2}$) for fragmented ice (i.e. ice-on-ice friction; dashed lines) and intact ice (solid lines). Circles are data at 233.15 K from [21], and triangles are data at 77 K from [19]. Also shown are strength curves at 210 K, appropriate for models of cratering on Mars.

ION IMPLANTATION AND THE ORIGIN OF MINOR SPECIES ON THE SURFACES OF ICY SATELLITES. G. Strazzulla, INAF-Osservatorio Astrofisico di Catania, Italy, (gianni@oact.inaf.it).

The surfaces of icy satellites are continuously irradiated by energetic ions mostly in the keV-MeV energy range. Being the penetration depth of the incoming ions much lower than the thickness of the target, they are stopped (implanted) into the ice. A complex "hot" chemistry is induced and molecules different from the original ones can be produced.. Reactive ions (e.g., H, C, N, O, S) induce all of the effects of any other ion, but in addition have a chance to form new species containing the projectile. An ongoing research program performed at our laboratory has the aim to investigate ion implantation of reactive ions in many relevant ice mixtures. Among the recent results:

- The production of CO_2 after C implantation in water ice (figure 1). The measured yield (CO_2 molecules formed per impinging ion) has been measured to be 0.47 for implantation at 16 K and 4.2 at 77 K [1].
- The formation of sulfuric acid dissolved in water ice after S implantation in water ice (Figure 2). The measured yield is Y=0.65 equivalent sulfuric acid molecules per impinging 200 keV sulfur ion [2].
- H implantation in sulfur dioxide produces poly-SO_3 [3].

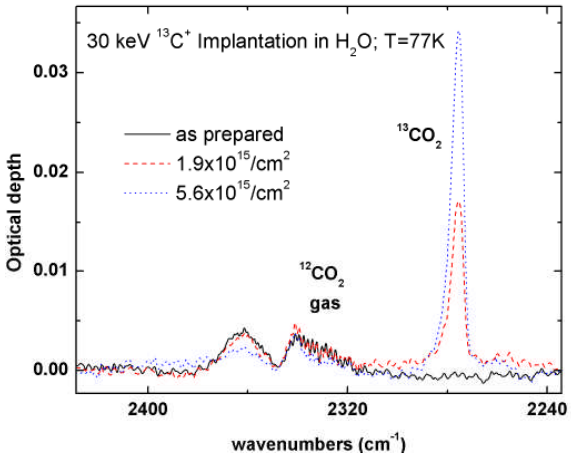

Figure 1: IR spectra (2430-2230 cm^{-1}) showing the formation of CO_2 after implantation of 30 keV carbon ions in water ice at 77 K.

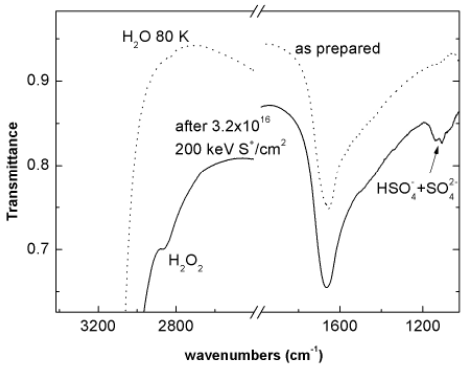

Figure 2: IR spectra (3420-1020 cm^{-1}) of a water ice target before and after implantation of 200 keV sulfur ions at 80 K. The features observed after implantation testify to the formation of hydrogen peroxide and sulfuric acid dissolved in the ice.

In this talk I would like to stimulate a discussion between observers, modelers and experimentalists on the following question: are some of the minor species (e.g. CO_2, SO_2, O_3) observed as contaminants of icy moons, formed after implantation of reactive ions from planetary magnetospheres?

[The experimental work in Catania has been performed in the last years by the LASP Team and coworkers (G.A. Baratta, R. Brunetto, D. Fulvio, M. Garozzo, O. Gomis, S. Ioppolo, G. Leto, M.E. Palumbo, F. Spinella). This Research has been supported by Italian Space Agency contract n. I/015/07/0 (Studi di Esplorazione Sistema Solare)]

References:

[1] Strazzulla G. et al. (2003) Icarus, 164, 163-169. [2] Strazzulla G. et al. (2007) Icarus, 192, 623-628. [3] Garozzo et al. (2008) Pl Sp Sci submitted.

PHASE PROPERTIES AND TYPE OF EARTH'S WATER ICE AND SPACE ICES

Thakur K. Praveen[1] and A. Velumurgan[1],
[1]Indian Institute of Remote Sensing, Dehradun, Uttarakhand, India
Corresponding author: praveen@iirs.gov.in

Introduction: Ice is the name given to any one of the 15 known crystalline solid phases of water. In non-scientific contexts, it usually describes ice I_h, which is the most abundant of these phases. It can appear transparent or an opaque bluish-white color depending on the presence of impurities such as air. The addition of other materials such as soil may further alter appearance [1]. The most common phase transition to ice I_h occurs when liquid water is cooled below 0 °C (273.15 K, 32 °F) at standard atmospheric pressure. It can also deposit from a vapor with no intervening liquid phase, such as in the formation of frost. Ice appears in nature in varied forms such as hail and glaciers. Amorphous ice is more common in outer space whereas hexagonal crystalline ice is extremely rare, which is predominant on Earth [6].

Phase properties of Earth's Water Ice: The main physical nature and phases of water ice are given in the table 1. The figure 1 a) and b) shows the phase diagram of water and different ice types.

Table 1: Phases and characteristics of Water Ice [6]

Phase	Characteristics
Amorphous ice	Amorphous ice as an ice which does not have crystal structure. This ice occurs in three forms; low density (LDA) formed at atmospheric pressure, or below, high density (HDA) and very high density amorphous ice (VHDA), forming at higher pressures. LDA forms by extremely quick cooling of liquid water ("hyperquenched glassy water", HGW), by depositing water vapour on very cold substrates ("amorphous solid water", ASW) or by heating high density forms of ice at ambient pressure.
Ice I_h	Normal hexagonal crystalline ice. Almost all ice in the Earth's biosphere is ice I_h with small amount of I_c
Ice I_c	Metastable cubic crystalline variant of ice. The oxygen atoms are arranged in a diamond structure, made at 130-150 K, and is stable upto 200K, when it transform to ice I_h. It is sometimes present in the upper atmosphere.
Ice 2	A rhombohedral crystalline form with highly ordered structure. Formed from ice I_h by compressing it at temperature of 190-210 K. When heated it undergoes transformation to ice 3.
Ice 3	A tetragonal crystalline ice, formed by cooling water down to 250 K a 300 MPa, least dense of the high pressure phases and denser than the water.
Ice 4	Metastable rhombohedral phase. Does not easily form without a nucleating agent.
Ice 5	A monoclinic crystalline phase, formed by cooling water to 253 K at 500 MPa. Most complicated structure of all.
Ice 6	A tetragonal crystalline phase, formed by cooling water to 270 K at 1.1 GPa, shows Debye relaxation.
Ice 7	A cubic phase. The hydrogen atom's position is disordered, the material shows Debye relaxation. The hydrogen bonds from two interpenetrating lattices.
Ice 8	A more ordered version of Ice 7, where the hydrogen atoms assume fixed positions, formed from ice 7 by cooling it beyond 5°C.
Ice 9	A tetragonal metastable phase, formed gradually from ice 3 by cooling it from 208 K to 165 K, stable below 140 K and pressures between 200 and 400 MPa. It has density of 1.16 g/cm³, slightly higher than ordinary ice.
Ice 10	Proton ordered symmetric ice, forms at about 70 GPa.
Ice 11	An orthorhombic low temperature equilibrium form of hexagonal ice, which is ferroelectric.
Ice 12	A tetragonal metastable dense crystalline phase. it is observed in the phase space of ice V and ice VI. It can be prepared by heating high-density amorphous ice from 77 K to about 183 K at 810 MPa
Ice 13	A monoclinic crystalline phase, formed by cooling water below 130 K at 500 MPa. The proton-ordered from of ice 5.
Ice 14	An orthorhombic crystalline phase, formed below 118 K at 1.2 GPa. The proton-ordered from of ice 12.
Ice 15	The predicted but no proven proton ordered form of ice 6, thought to be formed by cooling water to around 108-80 K at 1.1 Gpa

Space Ice: The solid-vapor curve becomes very low (fig. 1a) [3] as pressures and temperatures decreases and by -90°C the vapor pressure of ice is about 10^{-4} mb. At the temperatures of the outer solar system, the vapor pressure of ice is so low that ice remains for geologically long times even in a vacuum. In Space, instead of pure water

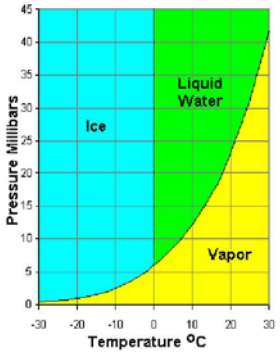

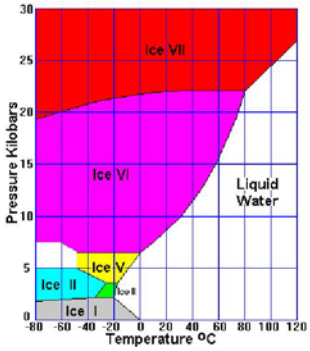

Fig. 1a): Phase diagram of water and **Fig. 1b):** Phase diagram of Ice (source: Steven Dutch)

ice, we find *Clathrate Hydrates,* which were first discovered in 1810 by Sir Humphrey Davy, they are crystalline water based solids physically resembling ice, in which small non polar molecules are trapped inside *cages* of hydrogen bonded water molecules. These gases includes O_2, H_2, N_2, CO_2, CH_4, H_2S, Ar, Kr, and Xe as well as some higher hydrocarbons and freons which forms hydrates at suitable temperatures and pressures [6].

Fig. 2a): Glacier's Dense Black Ice (source: Praveen Thakur)

Fig. 2b): White Ice, Snow & Water (source: Praveen Thakur)

Fig. 2c): Blue Ice, Snow at Antarctica (source: Bangor Uv.)

The fig.2 a), 2b) and 2c) shows the Earth's Black glacier ice, lake white ice, snow, water and blue ice of Antarctica. The absorbance spectra of the 3, 6 and 12-µm features of amorphous and crystalline H_2O ice between 10 and 140 K has shown that the ice undergoes an amorphous-to-crystalline phase transition in the 110–120 K range [5].

Remote Sensing of Water Ice and Space Ice: The ice in space may occurs in form of dry ice at Mars polar caps [2] [7], clathrate hydrate, Earth moon poles, Europa, and Triton are other examples where ice is found and has been studied using remote sensing based observations. The CO_2, SO_2, and H_2S, other than the water ice, have been detected on the surface of Europa by spectroscopic sensors. These substances might occur as pure crystalline ices, as vitreous mixtures, or as clathrate hydrate phases, depending on the system conditions and the history of the material [4]. Similar ice types are found on the Saturn's icy moons by Cassini Team [8].

References: [1] Bogorodski V.V. (1971), The physics of ice. 17-51. [2] Clifford SM et al. (2000), Icarus, 144: 210-242. [3] http://www.uwgb.edu/dutchs/PETROLGY/Ice%20Structure.HTM. [4] Olga Prieto *et al*(2005), Icarus 177(2): 491-505. [5] Marco M. Maldoni et al (1998). in Monthly Notices of the Royal Astronomical Society 298 (1), 251–258. [6] wiki enclyclopidia 2008. [7] Thakur and Prasad (2006), Abstarct 8018, In Fourth Mars Polar Science Conference at Davos. [8] Carolyn Porco *et al* (2005), *Science* **307:** 1237-1242.

AMMONIA HYDRATE ON TETHYS' TRAILING HEMISPHERE. A. J. Verbiscer[1], D. E. Peterson[1], M. F. Skrutskie[1], M. Cushing[2], P. Helfenstein[3], M. J. Nelson[1], J.D. Smith[2], J. C. Wilson[1], [1]University of Virginia (P.O. Box 400325 Charlottesville VA 22904-4325 verbiscer@virginia.edu), [2]Steward Observatory (University of Arizona, Tucson AZ 87512), Cornell University (Ithaca NY 14853).

Introduction: The detection of ammonia hydrate on the surface of any body in the Solar System is of particular interest because its presence enables geologic activity. The melting temperature of ammonia hydrate at 1 bar is ~194 K [1], considerably lower than that of pure water ice. On a saturnian satellite, photolysis would deplete a 10-μm layer of ammonia-rich ice in only 100 years [2], and sputtering would deplete the uppermost surface layer of any ammonia molecules on time scales of less than 10^6 years. [3]. Therefore, the presence of ammonia hydrate on the surface of an icy satellite implies recent emplacement, possibly by cryovolcanic activity. Such activity has been invoked to explain the presence of ammonia hydrate on Pluto's satellite Charon [4-6].

In an effort to search for any non-water ice components such as ammonia hydrate, we obtained near-infrared spectra 0.8 – 2.5 μm of Tethys' trailing hemisphere (latitude -26° S, longitude 250° W) with the CorMASS spectrograph [7] on the 1.8 m Vatican Advanced Technology Telescope (VATT) at the Mt. Graham International Observatory. The spectral resolution ($R = \lambda/\Delta\lambda$) of these CorMASS data (R ~ 300) is comparable to but nevertheless higher than that of Cassini's Visual and Infrared Mapping Spectrometer (VIMS) (R = 225). Previous analyses of high resolution (R ~ 800) near-infrared spectra of Tethys' trailing hemisphere [8-9] did not report the detection of any non-water ice components.

Our spectrum of Tethys' trailing hemisphere (black line in Fig. 1) is dominated by the absorption bands of water ice at 1.04, 1.25, 1.52, 2.02 μm. A narrow water ice band at 1.65 μm and a weaker one at 1.31 μm are strongly temperature dependent, increasing in depth with decreasing temperature [10]. A weak band at 2.21 μm matches that of ammonia hydrate (1% $NH_3{\cdot}H_2O$) (Fig. 3). The spectrum is normalized to the albedo of Tethys' trailing hemisphere at 0.9 μm [11].

Spectral Modeling: We model the spectrum of Tethys using a Hapke [12] spectrophotometric mixture model in the same manner in which spectra of Enceladus obtained with the same telescope and instrument were analyzed [13]. We find that spectral models (red line in Fig. 1) which include as much as 80% by weight of ammonia hydrate (1% $NH_3{\cdot}H_2O$) intimately mixed with water ice at 60 K covering 30% of the illuminated surface area fit the observed spectrum.

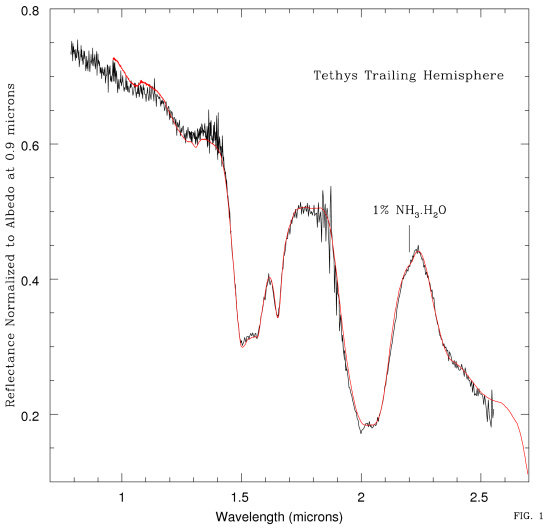

FIG. 1

Comparison with Enceladus: We compare this spectrum with that of the trailing hemisphere of Enceladus [13] in Fig. 2. Enceladus has a pronounced blue spectral slope, particularly in the region 0.8 – 1.3 μm, relative to Tethys. The relatively weaker water ice absorption bands in Tethys' spectrum indicate that, in general, particles on its trailing hemisphere are smaller than those on Enceladus. Close examination of the water ice band at 1.52 μm reveals that its arcuate shape is also more pronounced on Enceladus. The difference in the relative shapes of this band suggest that Tethys either has more amorphous water ice on its surface and/or there is ammonia hydrate present. In addition, the shape of the peak at 1.7 μm in Tethys' spectrum is consistent with amorphous water ice and/or ammonia hydrate. The absorption at 2.21 μm, however, cannot be due to amorphous water ice and indicates the presence of ammonia hydrate on Tethys.

Future work: Optical constants for all hydration states of ammonia at temperatures between 50 – 100 K are not currently available. New laboratory measurements would significantly enhance our ability to model the near-infrared spectra of all icy bodies in the Solar System on which ammonia hydrate has been found.

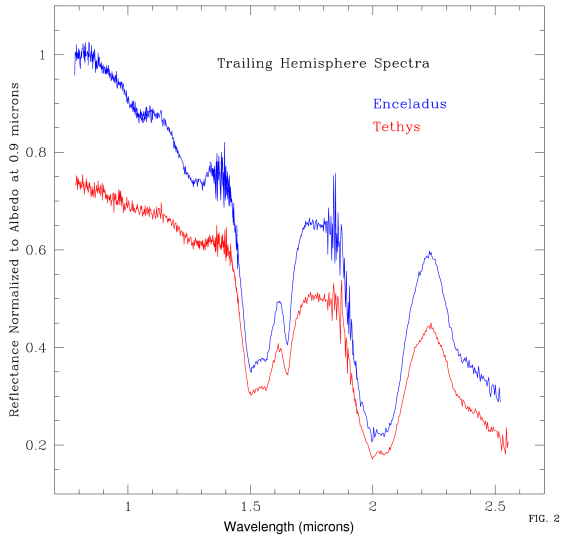

Figure 3 (below) [13] illustrates model spectra of (a) pure water ice at 70 K and (b) 1% ammonia hydrate at 77 K calculated using optical constants derived from laboratory spectra [14, 15]. Grain sizes from top to bottom are 50, 100, 250, 500, and 1000 µm. All bands strengthen with increasing particle size until they reach saturation. Spectral slopes increase with particle size as does the width of the 2 µm band. Correspondingly, the peaks centered at 1.8 and 2.25 µm narrow with increasing particle size.

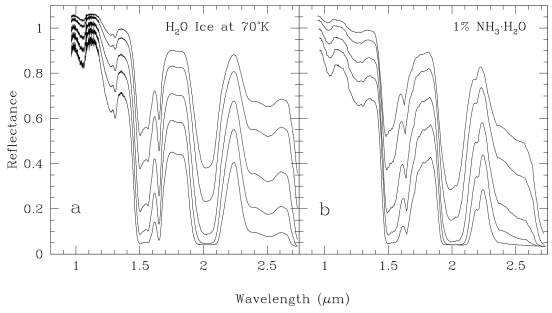

References: [1] Croft, S. K. et al. (1988) *Icarus 73,* 279–293. [2] Consolmagno, G. and Lewis, J. (1978) *Icarus 34,* 280-293. [3] Lanzerotti, L. et al. (1984) *Nature 312,* 139-140. [4] Brown, M. E. and Calvin, W. (2000) *Science 287*, 107-109. [5] Cook J. et al. (2007) *Ap. J. 663*, 1406-1419. [6] Verbiscer, A. J. et al. (2007) Workshop on Ices, Oceans, and Fire: Satellites of the Outer Solar System. *LPI Contribution* #1357. [7] Wilson, J. C. et al. (2001) *PASP 113,* 227-239. [8] Emery, J. et al. (2005) *Astron. Astrophys. 435*, 353-362. [9] Cruikshank, D. P. et al. (2005) *Icarus 175*, 268-283. [10] Grundy, W. et al. (1999) *Icarus 142*, 536-549. [11] Buratti, B. J. et al. (1998) *Icarus 136*, 223-231. [12] Hapke, B. (1993) *Theory of Reflectance and Emittance Spectroscopy*, Cambridge Univ. Press, New York. [13] Verbiscer, A. J. et al. (2006) *Icarus 182*, 211-223. [14] Grundy, W., Schmitt, B. (1998) *JGR 103*, 25809-25822. [15] Brown, R. H. et al. (1988) *Icarus 74*, 262-271.

Acknowledgements: We thank Drs. Will Grundy and Ted Roush for generously providing the optical constants for water ice and ammonia hydrate, respectively.

EROSIONAL PROCESSES ON CALLISTO: GALILEO SSI RESULTS, OPEN QUESTIONS, AND REQUIREMENTS FOR NEW CAMERA DATA. R. J. Wagner[1] and G. Neukum[2], [1]Inst. of Planetary Research, German Aerospace Center (DLR), Rutherfordstrasse 2, D-12489 Berlin, Germany, e-mail: roland.wagner@dlr.de; [2]Inst. of Geosciences, Freie Universitaet Berlin (FUB), D-12249 Berlin, Germany.

Introduction: The second-largest satellite of Jupiter, Callisto, is characterized by a unique surface geology almost entirely dominated by impact and erosional processes [1, 2]. This puts Callisto in strong contrast to the Jovian satellite Ganymede whose surface was shaped not only by impacts, but also by tectonic forces [3, and ref's therein]. One common feature of these two largest Galilean satellites is the similarity in impact crater forms [1][4] which implies a similar subsurface structure of their outer icy crusts [1][3][4]. At high-resolution, Callisto's surface is characterized by landforms inferring erosion and degradation. These landforms are bright massifs and knobs several tens of meters high, embayed by a smooth, dark, globally abundant blanket [1][2][5]. In this work, we (1) present the characteristics of these erosional and degradational landforms, (2) use measurements of crater distributions and cratering model ages to derive the erosional history of Callisto's surface, (3) discuss open questions and (4) suggest requirements for remote sensing data in an upcoming mission to Jupiter and its satellites.

Image data base: Between 1996 and 2003, Callisto was imaged by the Galileo SSI camera at various resolutions [6][7]. Global coverage for Callisto at resolutions of 1-2 km/pxl is more or less complete, combining imagery from both the Voyager and Galileo SSI cameras [1][7]. However, due to the technical problems of Galileo [7], only a small number of areas on Callisto's surface could be imaged at regional (100 – 500 m/pxl) and especially at high resolution (10 – 50 m/pxl) [1].

Procedure: We used regional- and high-resolution images of the Galileo SSI camera to identify and map landforms on Callisto indicative of erosion and degradation. Where possible, anaglyph images were created to support morphologic mapping. Unfortunately, stereo image coverage of Callisto by Galileo SSI was very limited. Second, crater size distributions were measured on mapped units, and relative ages extracted from cumulative frequencies at a given reference diameter (generally 1 km). Also, the shape of crater distributions could be used to constrain resurfacing processes. To derive absolute time-scales of surface processes, we used two cratering chronology models: one by Neukum et al. [8] with a lunar-like time dependence of the cratering rate, based on the preferential impact by asteroidal bodies, and the model by Zahnle et al. [9], based on a constant cratering rate preferentially by cometary bodies.

Brief summary of crater distributions on Callisto: It has been widely assumed that Callisto's heavily cratered surface is saturated with craters [e.g. 9]. Our measurements show, however, that this is not the case, except for some areas where crater distributions show the characteristic -2 slope in cumulative diagrams indicative of an equilibrium distribution, at least at smaller crater sizes [10][11][2]. Even the most densely cratered plains on Callisto show production distributions [11]. Also, we did not find evidence for any apex-antapex asymmetry of craters on Callisto [2]. Therefore, Callisto was impacted preferentially by projectiles in planetocentric orbits [12]. An alternative, but less likely explanation, is a non-synchronous rotation of Callisto.

Results: Erosion and degradation affected all high-standing landforms [1][2][13]. Such landforms comprise rims of impact craters, ridges and scarps involved with multi-ring basins, and palimpsests. Although tectonism was never as pervasive on Callisto as on Ganymede, Callisto has experienced early tectonic stress outside large impact structures [2, and ref's therein]. These stresses created zones of weaknesses along which the bright high-standing material degraded (***Fig. 1***). The source material is thought to consist of a mixture of ice/non-ice constituents [1]. The material evolved into massifs, hummocks, and knobs, or groups of massifs, most likely by processes of sublimation degradation and separation of highly volatile substances from less volatile material [1, and ref's therein]. These processes eventually formed a globally abundant layer of dark material [1]. Hummocks and massifs are surrounded by debris aprons. While the massifs degraded with time, dark material was accumulated in the aprons. Eventually, the massifs disappeared, and aprons of former massifs merged to create a uniform blanket of dark material that embayed the most resistent hummocks and massifs. Therefore, it is apparent that dark material formed *in situ*. While an exotic transportation process such as electrostatic levitation [e.g. 14] cannot be ruled out, it is actually not needed to explain the emplacement of the global blanket of dark material, despite its "mobile" appearance. At present time, the dominant geologic processes active on Callisto are (1) occasional impacts, (2) erosion and degradation, possibly at very slow rates, and (3)

continuous outgassing of CO_2, creating a tenuous atmosphere around Callisto [15]. In addition, the Jovian magnetosphere is constantly bombarding the trailing hemisphere of Callisto, there creating a very thin deposit of CO_2 on the surface [16].

Open questions: Several issues of Callisto's geologic properties and processes remain unsolved and should be addressed in future missions. (1) The thickness of the dark blanket and its spatial variability is not known. (2) The relative proportions of volatile abundances in the bright host materials and in the dark blanket are not known. (3) The time-scales of erosion and deposition of the dark blanket are not known also. Application of the two cratering chronologies yields large differences in model ages. In the lunar-like asteroidal chronology model [8], the dark blanket has an average model age of 3.5 Gyr while in the cometary constant-cratering rate model [9] ages of this unit are on the order of only 500 Myr. (4) The thermal inertia of the surface materials on Callisto is not known. Measuring the thermal inertia could constrain erosional and degradational rates and help to constrain time-scales for processes of erosion and degradation.

Requirements for future missions: Global image coverage of Callisto should be completed in a future mission, especially at resolutions 100 – 300 m/pxl. Also, high-resolution coverage at resolutions of about 10 m/pxl should be carried out over a much larger surface area, including observations at resolutions less than 10 m/pxl in closest encounters. To provide enough image context, it is mandatory to implement a narrow angle as well as a wide angle camera. Also, color filters should range from the ultraviolet to the near-infrared to account for hemispherical asymmetries in the global color distribution, also of local color and compositional differences.

References: [1] Moore J. M. et al., in: *Jupiter* (eds. F. Bagenal et al.), p. 397- 426, Cambridge Univ. Press, Cambridge/UK, 2004. [2] Wagner, R. J., *PhD Dissertation* (in german), Free Univ. Berlin, Germany, http://www.diss.fu-berlin.de/2007/806. [3] Pappalardo R. T. et al., in: *Jupiter* (eds. F. Bagenal et al.), p. 363-396, Cambridge Univ. Press, Cambridge/UK, 2004. [4] Schenk P. M. et al., in: *Jupiter* (eds. F. Bagenal et al.), p. 427 - 456, Cambridge Univ. Press, Cambridge/UK, 2004. [5] Basilevsky A. T., *LPSC XXXIII*, abstr. No. 1014, 2002. [6] Belton M. J. S. et al., *Space Sci. Rev. 60*, 413 – 455, 1992. [7] Carr M. H. et al., *J. Geophys. Res. 100*, 18,935 – 18,956, 1995. [8] Neukum G. et al., *LPSC XXIX*, abstr. No. 1742, 1998. [9] Zahnle K. et al., *Icarus 136*, 202 – 222, 1998. [10] Neukum G. and H. Dietzel, *Earth Planet. Sci. Lett. 12*, 59 – 66, 1971. [11] Wagner R. et al., *1st International Conference on Impact Cratering in the Solar System*, ESA/ESTEC, Noordwijk, NL, abstr. book 235, 2006. [12] Horedt G. P. and G. Neukum, *J. Geophys. Res. 89*, 10,405 – 10,410, 1984. [13] Wagner R. et al., *LPSC XXXII*, abstr. No. 1838, 2001. [14] Klemaszewski J. et al., *Ann. Geophys. 16* (suppl. III), C992, 1998. [15] Carlson R. W., *Science 283*, 820 – 821, 1999. [16] Hibbitts C. A. et al., *J. Geophys. Res. 105*, 22,541 – 22,557, 2000.

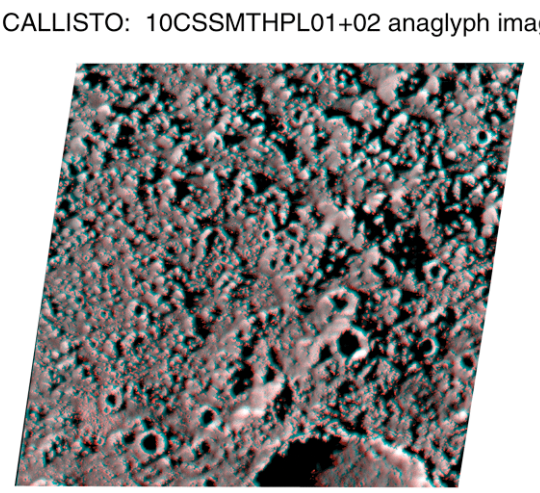

Figure 1: Anaglyph image created with Galileo SSI data from orbit C10, observations 10CSSMTHPL01 (68 m/pxl) and 10CSSMTHPL02 (270 m/pxl). The images cover an old, now heavily degraded palimpsest [2][4][13].

Gas Inclusion, Adsorption, and Diffusion in Ices

C. Wittig, H. Reisler, S. Malyk, and O. Rebolledo
Department of Chemistry
University of Southern California
Los Angeles, CA 90089
wittig@usc.edu

Our understanding of molecular transport in amorphous solid water (ASW) in the temperature range 90-160 K will be reviewed. This phase of water exists below ~ 160 K, at which temperature ASW changes irreversibly to crystalline ice. Several experimental groups have reported phenomena that take place throughout the amorphous regime (including a so-called glassy regime), as well as at the temperature where the system undergoes its transition from ASW to crystalline ice. Dramatic effects can be observed as a consequence of this transition, for example, volcano like behavior in which the thermally driven agitations of the host material that lead to the phase transition result in the explosive release of trapped gas. In the amorphous regime, significant morphological changes can be monitored through the introduction and monitoring (via mass spectroscopy and Fourier transform IR) of small dopant atoms and molecules. This has enabled qualitative features such as large changes in dopant uptake to be determined, as well as revealing some details of site-specific bonding of guest molecules. Experimental results from several research groups will be summarized and discussed. A unique theoretical model of such phenomena is, at this point, difficult to establish. Implications of the various experimental results on viable models will be discussed.

CO_2 in Comets Beyond 5 AU. L. M. Woodney[1], Y. R. Fernandez[2] and C. M. Lisse[3]. [1]California State University, San Bernardino (5500 University Pkwy, San Bernardino CA 92407), [2]University of Central Florida (4000 Central Florida Blvd., Orlando, FL 32816), [3]Johns Hopkins University (APL/SD/SRE, MP-3, 7707 Montpelier Road, W-155, Laurel, MD 20723).

There is debate about the cause of cometary activity at heliocentric distances (r) too far and too cold for significant water sublimation. Observations that would shed light on the driver of activity -- e.g. direct detections of gas in comets beyond $r \sim 3$ AU -- are rare, and can be challenging to accomplish with ground-based observations. Some active comets have likely not been close enough to the Sun recently enough (or ever) to have significant water ice sublimation, so their activity could be driven by sublimation of CO and/or CO_2, which are believed to be the next most common volatiles in comets. We have used the high-resolution mode of the IRS instrument aboard the Spitzer Space Telescope to search for evidence of CO_2 outgassing in two active Centaurs and one long-period comet whose perihelia are all at r>5 AU. Spitzer can observe the 15-μm band of CO_2 and IRS's high-resolution mode minimizes the diluting flux per spectral bin from the dust coma's thermal emission. We will show Spitzer spectra of 29P/Schwassmann-Wachmann 1, 95P/Chiron, and C/2003 O1 (LINEAR). No gas emission was detected from any of these objects, and we will present upper limits to the CO_2 production rate of each. The data provide us with an estimate of dust production rate as well and so we will also present constraints on the gas-to-dust ratio in comparison to those of Jupiter-family, Halley-family, and long-period comets.

Near Infrared Spectroscopy on The Outburst Comet 17P/Holmes

Bin Yang, David Jewitt and Schelte J. Bus

Institute for Astronomy, University of Hawaii, Honolulu, HI 96822

The Jupiter family comet 17P/Holmes underwent a remarkable outburst on October 24, 2007 UT. It was reported that the comet's brightness increased abruptly with its apparent magnitude rising from 17 to 1.5 in just a few hours. Shortly after the outburst, we performed near-infrared (0.8- to 4.2-μm) spectroscopy on 17P with the 3.0-m NASA Infrared Telescope Facility (IRTF) on Oct. 27, 28 and 31, 2007 UT.

Two broad absorption bands were found at 2-μm and 3-μm, respectively, in the reflectance spectra of the comet. These features are consistent with abundant water ice grains in the central coma. A thermal emission excess was detected in all the comet's spectra at wavelengths beyond 3-μm. Our thermal model suggested the color temperature at the time of observation of 17P is about 290K. The overall continuum from 0.9- to 4.0-μm appeared negatively sloped after the removal of thermal emission. Furthermore, the negative slope grew steeper with the time further apart from the initial outburst. Linear and non-linear mixture models were applied, which suggested the coma of 17P was dominated by submicron-sized fine grains.

EXPERIMENTAL STUDY ON THE RHEOLOGY OF ICE-SILICA BEADS MIXTURES: EFFECTS OF SILICA CONTENT AND TEMPERATURE ON THE FLOW LAW. Minami Yasui and Masahiko Arakawa, Graduate School of Environmental Studies, Nagoya University (Furo-cho, Chikusa-ku, Nagoya, 464-8601, Japan. e-mail:yasui@eps.nagoya-u.ac.jp)

Introduction: Planetary explorations revealed various flow features on Mars and icy satellites related to water ice mixed with silicate materials. For example, polar layered deposits on Mars include exposed sequence alternating dark dust and bright ice, so each layer is expected to contain various ratios of water ice and dust [1-4]. Also, the surface on Ganymede consists of two colored areas, bright area and dark area, and it is expected that these areas have different ratios of ice and rock. Many topographic features related to ice-solid particle mixtures are found on these surfaces. Therefore, rheology of ice-solid particle mixtures is important to study the formation condition of these topographic features. Furthermore, the surface temperatures of these bodies are very low: it is -60°C on Mars, and -160°C on Galilean satellites (except for Io) in the average. So, we must examine the temperature dependence of the rheology of ice-solid paricle mixtures.

Thus, we focused our attention on the flow law, and carried out deformation experiments of the ice-solid particles mixtures. At the temperature on the surface of icy satellites, the deformation type of ice could not be ductile and change to brittle. In the case of pure water ice, the brittle-ductile boundary is on the line expressed by the following equation, $d\varepsilon/dt[s^{-1}] = 1.6\times10^{6}\exp(-42.6[kJ/mol]/RT)$, where $d\varepsilon/dt$ is strain rate [5]. This boundary could be affected by the silica inclusion. So, we examined the brittle-ductile boundary of the mixtures.

Experimental methods: The sample was prepared by mixing ice particles (0.3-1mm in the diameter) with silica beads having the diameter of 1μm. The silica contents are from 1 to 80wt.%, and at the temperature below -15°C, they are 30, 50, and 80wt.%. We made the samples by following method. The sample was made of ice grains, beads and liquid water. The ice particles were mixed with beads homogeneously. This mixed grains were put into a cylindrical mold and pore space was filled with cold water (0°C). We call the sample prepared by this method frozen sample (f.s.). We used other method to prepare f.s. with the silica content higher than 50wt.%: the suspention of silica beads was frozen at -10°C. We also prepared pure ice sample for the comparison with the mixtures. The samples removed from the cylindrical mold were kept in a cold room at the temperature of –10°C for one day. The sample has a cylindrical shape with the diameter of 30mm and the length of 60mm.

We made the uniaxial compression tests under constant strain rates from 2.9×10^{-3} to 8.6×10^{-7} s^{-1} in a cold room at -10, -15, -20, and -25°C.

Results: We used the flow law expressed by the relationship between the applied strain rate $d\varepsilon/dt$ and the maximum stress σ_{max} on the stress-strain curve, $d\varepsilon/dt=A_0\exp(-Q/RT)\sigma_{max}^{n}$, where Q is activation energy, R is gas constant (8.314 $JK^{-1}mol^{-1}$), T is absolute temperature, and A_0 and n are constants dependent on silica content. This equation is equivalent to a flow law derived from creep tests [6].

Effect of silica content. The relationship between strain rate and maximum stress for various silica contents at the constant temperature of -10°C is shown in Fig.1. At the silica contents up to 10wt.%, the maximum stresses become almost a constant with increasing the strain. However, at the silica contents from 10 to 80wt.%, the maximum stress becomes larger as the silica content increases. At the temperature of -10°C, the deformation type is ductile deformation. So, we examined the flow parameters, A and n, for various silica contents. Here, we defined the parameter $A\equiv A_0\exp(-Q/RT)$. Firstly, the A exponentially decreases with increasing the silica content and can be fitted by the exponential equation, $A=9.7\times10^{-6}\exp(-8.4\times10^{-2}C)$, where C is the silica content in wt.%. Secondly, the n is almost constant of n=3-4 at the silica contents up to 10wt.%. However, it becomes 6-7 at the silica contents from 30 to 80wt.%.

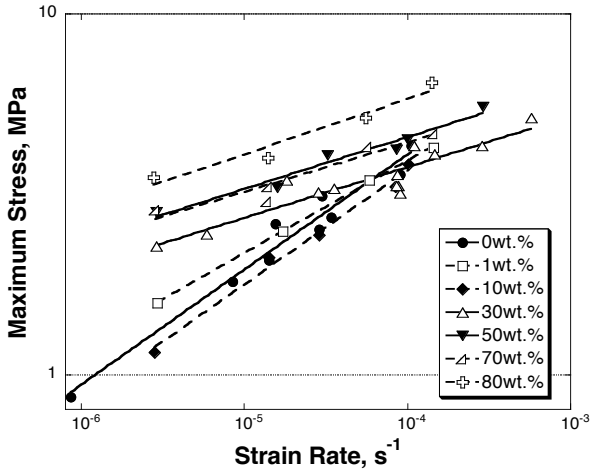

Figure 1. Maximum stress vs. strain rate with various silica contents at the temperature of -10°C

Effect of temperature. The relationships between strain rate and maximum stress for 30 and 50wt.% samples at various temperatures are shown in Fig.2a and 2b, respectively. In the case of 30wt.%, the maximum stress becomes larger, but the slopes of fitting lines do not change when the temperature becomes lower. On the other hand, in the case of 50wt.%, the deformation type changes from ductile deformation to brittle failure below -20°C. Furthermore, the maximum stress is almost constant when the deformation type shows brittle failure. The similar behavior is found in the case of 80wt.%. So, we examine brittle-ductile boundary of 50 and 80wt.% samples. Figure 3 shows a deformation map, which is written by T and $d\varepsilon/dt$, obtained by the experiments for 50 and 80wt.% samples. As a result, the temperature of brittle-ductile boundary of the mixtures is 40-60°C higher than that of pure ice at the same strain rate [5]. Thus, we found that the mixtures of 50 and 80wt.% samples could break easily in comparison with pure ice. Next, we examine the flow parameters in the region of ductile samples (at higher than -15°C for 50 and 80wt.%). As a result, the n is found not to change for the samples with the same silica contents at any temperatures. We suppose that the deformation mechanism does not change with the decrease of the temperature. It is well known that the parameter A depends on the temperature. So, we examine the activation energy, Q, of 30wt.% sample because all of the 30wt.% samples show ductile deformation. As a result, the Q is about 130 kJ/mol and is close to that of pure ice at the temperature higher than -8°C [7]. From this previous work, we know that the deformation mechanism of pure ice at higher than -8°C is grain boundary sliding (gbs) of ice crystals. So, the deformation mechanism of 30wt.% sample might be also gbs at the temperature lower than -10°C. The silica beads distributed among ice grains could be responsible for this deformation mechanism.

References: [1] Cutts J. A. et al. (1979) *JGR, 84,* 2975–2994. [2] Squyres S. W. (1979) *Icarus, 40,* 244-261. [3] Toon O. B. et al. (1980) *Icarus, 44,* 552–607. [4] Milkovich S. M. and Head J. W. (2005) *JGR, 110,* E01005. [5] Arakawa M. and Maeno. N. (1997) *Cold regions science and technology, 26,* 215-229. [6] Mellor M. and Cole D. M. (1982) *Cold regions science and technology, 5,* 201-219. [7] Barnes P. et al. (1971) *Proc. Roy. Soc. London, A324,* 127-155.

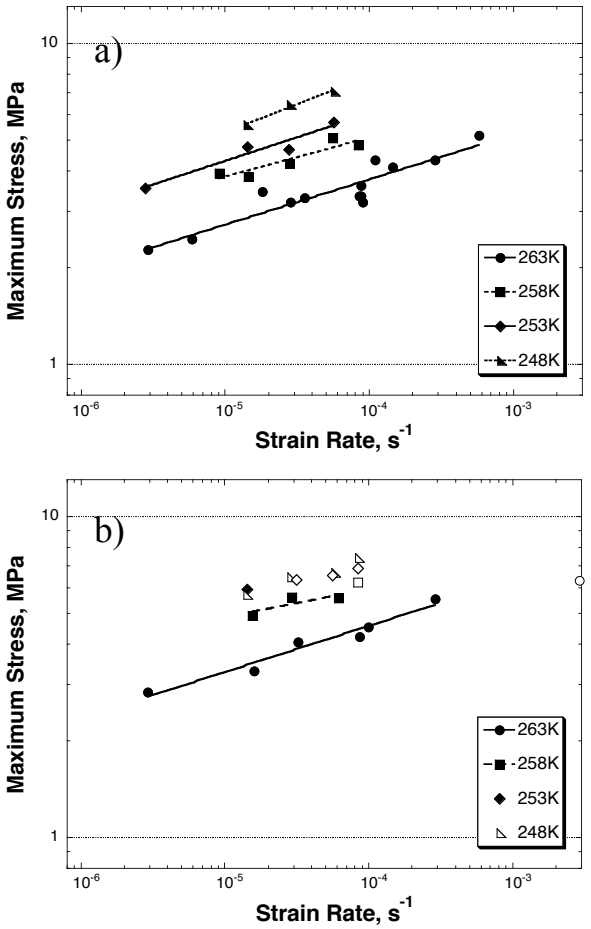

Figure 2. Maximum stress vs. strain rate at various temperatures. The open symbol means that the deformation type is brittle failure.
a) 30wt.% b) 50wt.%.

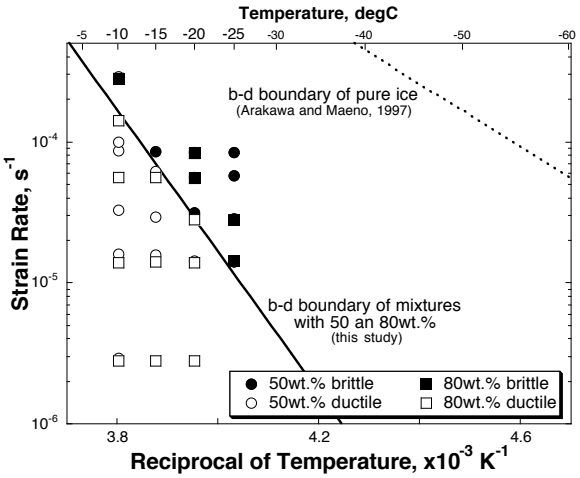

Figure 3. Deformation types of mixtures for 50 and 80wt.% samples. The brittle-ductile bound -ary of pure ice is referred to the retults of Arakawa and Maeno [5].

SPATIAL DISTRIBUTION AND EVOLUTION OF NITROGEN ICE ON TRITON. L. A. Young[1], W. M. Grundy[2], J. A. Stansberry[3], M. W. Buie[2], [1]Southwest Research Institute, 1050 Walnut St., Boulder CO 80302; layoung@boulder.swri.edu, [2]Lowell Observatory, 1400 W. Mars Hill Rd., Flagstaff AZ 86001; W.Grundy@lowell.edu and buie@lowell.edu, [3]Steward Observatory, Univ. of Arizona, 933 N. Cherry Ave., Tucson AZ 87721; jstansberry@as.arizona.edu

Introduction: Because Triton's surface is in vapor-pressure equilibrium with its primarily N_2 atmosphere, large changes in atmospheric pressure are caused by small changes in the surface temperature, which in turn can arise from changes in Triton's sub-solar latitude and the distributions of the surface frosts. After the Voyager encounter with Triton in 1989, various models tried to explain both the observed surface pressure and the albedo patterns, namely the bright southern (summer) hemisphere, in terms of volatile transport and vapor-pressure equilibrium (e.g., [1]). However, these models depended on the identification of bright terrains with N_2 frost, an assumption that could not be tested with Voyager, which did not fly a near-IR spectrograph.

We have a program to monitor Triton spectroscopically with SpeX at the Infrared Telescope Facility. We report here on 45 nights of data spanning 0.8 to 2.4 micron. This wavelength range includes absorption bands of the surface ices N_2, CH_4, H_2O, CO, and CO_2 (Fig. 1)

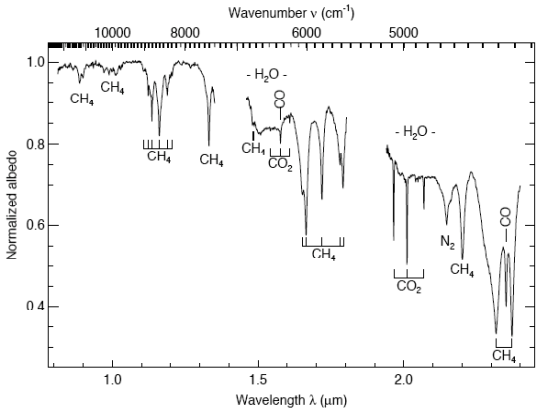

Fig. 1.— Average IRTF/SpeX spectrum of Triton, with specific ice absorptions marked. Gaps coincide with high atmospheric opacity.

Spatial distribution: In 2002, we observed Triton over a complete rotation, and reported on the variation of the depth of the N_2 band at 2.15 micron [2]. Data from subsequent years confirm that the N_2 absorption is nearly twice as deep on the sub-Neptune hemisphere as the Neptune-facing hemisphere (Fig. 2)

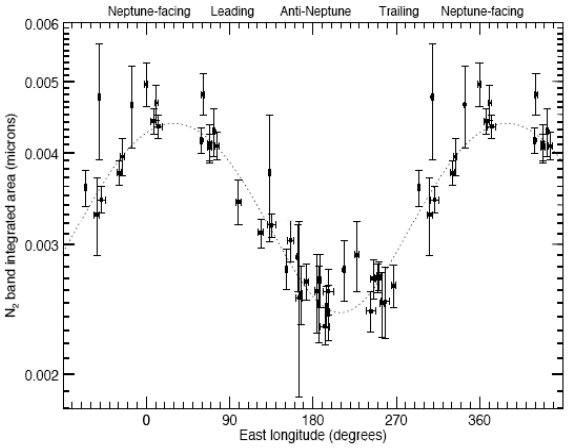

Fig. 2.— Integrated area of the 2.15 micron N_2 ice absorption band as a function of sub-solar longitude on Triton.

The clear longitudinal dependence of the N_2 band depth shows that simply associating bright terrains with N_2 frost is too simplistic. During our observations, Triton's sub-solar latitude was near −50°, so most of Triton's southern cap is visible at all rotational phases. If high southern latitudes were covered with N_2 frost, the amplitude of the N_2 band depth variation would be much more muted than we observed with SpeX during 2000-2007. In [2], we used the geologic units identified in the Voyager maps, and showed that unit 5, making up the bulk of the southern cap, could explain our SpeX observations if Triton's southern pole had been devolatilized to a latitude of -31° latitude. More recently, we are investigating models based on energy balance (Fig 3), which also have a devolatilized south pole.

Evolution: One of the more successful models of volatile transfer on Triton postulated very high thermal inertia, and predicted a perennial southern N_2 cap and pressures that increased in the decades following the Voyager encounter [1]. This model gained support with a series of stellar occultations in the 1990's, which detected an increase of a factor of two in Triton's atmosphere between 1989 and 1997 [3]. However, we see evidence for changes in the distribution of N_2 as a function of time, with N_2 subliming from the longitudes of deepest N_2 absorption. This suggests that N_2 is actively subliming from the sub-Neptune hemisphere, in contrast to the static models. The longitudinal varia-

tion in N_2 band depth, the observed change in atmospheric pressure, and the changes in the N_2 distribution together give powerful new constraints on models of volatile transport and surface-atmosphere interaction.

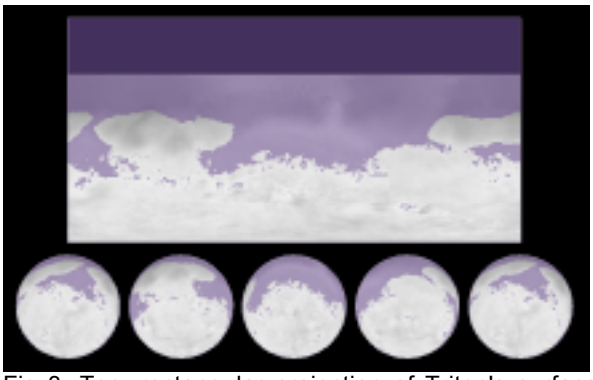

Fig 3. Top: rectangular projection of Triton's surface and a thermophysical model for N_2 frost distribution, centered on 0° longitude. The brightness of the map indicates Triton's bond albedo, as seen by the Voyager 2 spacecraft in 1989 [4]. The purplish shading shows the regions where the combination of high albedo and low solar incidence angle would lead to stable N_2 frost. Bottom: the observed projection of Triton's disk at a sub-observer latitude of -50° and sub-observer longitudes of -180°, -90°, 0°, 90°, and 180°. These show that the projected area of N_2 frost (purple) near 0° is twice that at 180°, consistent with our SpeX observations (Fig 2).

Laboratory data: Further understanding of the behavior, distribution, and evolution of Triton's volatile ices relies on knowledge of their spectral thermophysical properties. These include: emissivity, far IR optical constants, sticking coefficients, annealing rates, and thermal inertia. It is also important to know the effects of solutions of CO or CH_4 in N_2. What are the thermophysical effects described in the CH_4-N_2 phase diagram? The spectrum of pure CH_4 differs from CH_4 in N_2; is the spectrum affected for CH_4 in an N_2:CO solid solution? What are their diffusion rates, and do the foreign molecules migrate to defects and accumulate there? What do the contaminants do to the far-IR optical constants? What are the equilibrium vapor pressures for CH_4:CO:N_2 mixtures?

References: [1] Moore J. M. and Spencer J. R. (1990) *GRL, 17,* 1757-1760. [2] Grundy W. M. and Young L. A. (2004) *Icarus, 172,* 455-465. [3] Elliot, J. L. et al., (2000) *Icarus*, *148*, 347-369. [4] Stanberry et al., (1992) *Icarus*, *99*, 242-260.

Additional Information: This work was funded by NSF grants AST-0407214 and AST-0085614 and by NASA grants NAG5-4210, NAG5-10497, NAG5-12516, and NNG04G172G.

NEW TECHNIQUE FOR MEASURING THERMAL CONDUCTIVITY OF ICY MATERIALS UNDER PRESSURE. F. Zhong[1], M. Barmatz[1], H. Englehardt[2], [1]Jet Propulsion Laboratory, California Institute of Technology, M/S 79-24, 4800 Oak Grove Drive, Pasadena, CA, 91109, E-mail: Fang.Zhong@jpl.nasa.gov, [2]Department of Geology and Planetary Sciences, California Institute of Technology, MC 100-23, Pasadena, CA, 91125.

Introduction: Thermal conductivity plays an important role in geological and geophysical modeling of planetary objects. This is especially the case for outer planet satellites whose material thermal conductivity can vary by up to two orders of magnitude depending on temperature, composition, structure, and pressure. Because of lack of experimental measurements, earlier models have been forced to use the published data for ordinary ice Ih. The more recent Galileo mission to Jupiter and Cassini mission to Saturn have been able to obtain spectral information of icy satellite surfaces that suggest the surfaces are composed of impure ice compositions. Candidate compositions include salt hydrates, clathrate hydrates, and ammonia water compounds. We plan to perform thermal conductivity measurements on relevant icy satellite analogs that can be used in models to obtain a better understanding of the geological development of these satellites.

Experimental technique: We have developed a method for measuring the thermal conductivity of icy compositions over a broad range of cryogenic temperatures and elevated pressures along the same heat flow direction. The innovation of this measurement approach is that it has been coupled with a high precision Instron Materials Measurement System to permit the simultaneous measurement of thermal conductivity during various compression (higher pressure) studies (Young's modulus, creep, and relaxation). A cryogenic chamber was incorporated around the Instron compression platens to permit measurements over the temperature range 90 – 270 K. With this system, we can directly measure the thermal conductivity of a given sample over the entire temperature range or can perform measurements on a sample at a given temperature, before and during various axial compression studies that may ultimately lead to the sample destruction.

For compression studies, a cylindrical sample is placed between two platens. The bottom platen is fixed while the top platen can be moved down to produce a given stress or stress rate, or a given strain or strain rate. We have mounted a calibrated silicon diode thermometer and heater on each platen that allow us to control the temperature of either platen to within ± 0.004 K. A schematic of the inside of the chamber is shown in Fig. 1. The samples were 2.54 cm in diameter by 0.63 cm long. They were grown and characterized in the Mars Simulation and Ice Laboratory at Caltech. Using a single crystal seed, the water was frozen from the bottom to the top of a cylindric mold in a cold room at -15 ºC at a rate slower than 10^{-6} m/s with air constantly flowing at a slow rate in the remaining water. This method excludes bubbles and cracks during freezing and leads to the production of perfect single ice crystals.

The sample thermal conductivity is determined by increasing the bottom platen temperature by a known amount, ΔT_{bot}. This temperature change causes the PID temperature control of the top platen to change its control heat power, $\dot{Q}_{top}$, to maintain its same initial temperature. The foam insulator ensures that the sample sidewall heat loss is reduced. It also minimizes any heat transfer between the platens via the surrounding nitrogen gas. The Instron rods just outside the cryo-chamber and the copper shield are controlled at constant temperatures. Because these temperature differences remain the same between the top platen and its surroundings, the measured $\Delta\dot{Q}_{top}$ is the heat current that comes directly from the sample. Knowing ΔT_{bot} and $\Delta\dot{Q}_{top}$, the sample thermal conductivity can ideally be calculated.

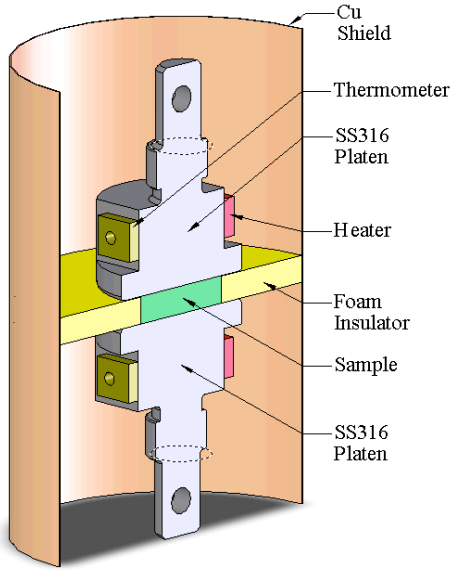

Fig. 1. The thermal conductivity experimental setup. The ice sample was 2.54 cm in diameter and 0.63 cm high. The remaining items in the drawing are scaled to the sample size.

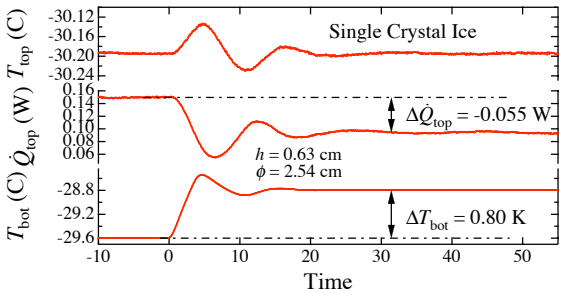

Fig. 2. Measurement of the thermal conductivity of single crystal ice at ~ -29.7 C.

Thermal conductivity measurements: At this time, we are evaluating this technique using single crystal ice samples. Figure 2 shows the temporal profiles of temperatures and heat current measurements with 40 N load force applied on the sample. With the system in thermal equilibrium, the temperature of the bottom platen was increased by 0.8 °C (at time t = 0). The system reached equilibrium after ~ 33 minutes. Given the change in heat current at the top platen, the total thermal resistance including the contribution by the platens is calculated to be 14.5 K/W. By replacing the ice sample with a pure copper disk of identical geometry and repeating the same procedure as outlined above, the thermal resistance just due to the platens was determined to be 3.33 K/W. Thus, we obtained 1.11 W/m-K for the ice sample thermal conductivity by subtracting the platen resistance from the total thermal resistance. The thermal conductivity of single crystal ice has been measured previously [1-6]. Our newly measured value is smaller than the most recent study by Waite *et al*. [6]. The difference between the two is outside the uncertainties in the measurements. We are in the process of determining the source of this inconsistency.

One of the unique capability of this approach is that it can measure the heat flux through a sample as a function of an applied stress while keeping a constant temperature gradient. These measurements are a sensitive indicator of structural defect changes within the sample. Figure 3 shows the temporal profiles of the control heat powers during the creep of the same ice sample under constant loads. Since T_{top} = -30.2 C and T_{bot} = -28.8 C remained constant, the heat exchanges from the platens to the surroundings should remain unchanged. Thus, the non-zero net heat power change $\Delta\dot{Q}$ shown in Fig. 3 directly indicates the change in thermal conductivity. The response of the control heat power and thus the thermal conductivity to the sample creep was found to be linear as shown in Fig. 4.

Once this technique is validated using single crystal ice samples, it will be used to study other important icy

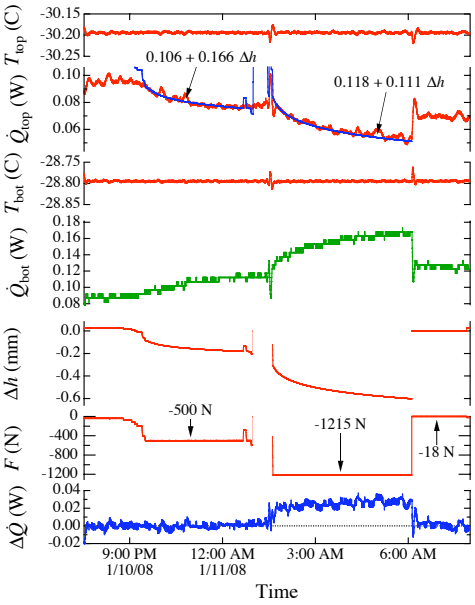

Fig. 3. Responses of the control heat powers to the ice sample creep.

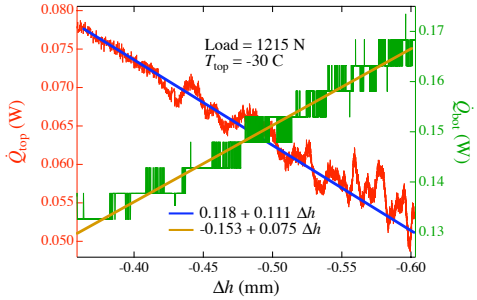

Fig. 4. Measured control heat powers versus ice sample creep. The dependence is linear.

compositions simultaneously with Instron compression studies.

Acknowledgement: This work was performed at the Jet Propulsion Laboratory – California Institute of Technology under contract to NASA. Copyright 2008 California Institute of Technology. Government sponsorship acknowledged.

References: [1] R.G Ross, P. Andersson, and G. Backstrom (1978) *J. Chem. Phys.*, **68**, 3967–3971. [2] V.J. Lunardini (1981) *Heat Transfer in Cold Climates*, Norstrand Reinhold Company, New York, P. 309. [3] J.G. Cook and D.G. Leaist (1983) *Geophys. Res. Letts.*, **10**, *397-399*. [4] U.S. Army Corps of Engineers (1996) *Engineering and Design – Ice Engineering: Manual* No. 1110-2-1612, Washington D.C., p. 2-2. [5] E.D. Sloan Jr. (1998) *Clathrate Hydrates of Natural Gases* (2nd ed.): Marcel Dekker, Inc. New York [6] W.F. Waite, L.Y. Gilbert, W.J. Winters, and D.H. Mason (2006) *Rev. Sci. Instru.* **77**, 044904.

NOTES

BEST POSTER RECOGNITION
(Voluntary)

The Science of Solar System Ices: A Cross Disciplinary Workshop

Colleagues,

At the end of the poster session on the second day, please pass on this sheet with your ranking of the best 5 posters.

In order to create a vibrant poster session environment and show colleagues that presenting a poster can be a rewarding experience, we strongly encourage all the participants to take poster sessions seriously, spend the fully allotted time to visit and discuss as many posters as you can, and enjoy the refreshments provided during the poster session.

Welcome to ScSSI,

Murthy Gudipati
Bob Pappalardo
Julie Castillo

Your Name (optional): _____

Rank	First Author	Title (optional)
#1		
#2		
#3		
#4		
#5		